DISSERTATION

Odor representation in mouse olfactory cortex during food intake

Geruchsrepräsentation im olfaktorischen Cortex der Maus während der Nahrungsaufnahme

zur Erlangung des akademischen Grades
Doctor of Philosophy (PhD)

vorgelegt der Medizinischen Fakultät
Charité – Universitätsmedizin Berlin

von

Hung Lo

Erstbetreuung: PD Dr. Friedrich Johenning

Datum der Promotion: 28.02.2025

Table of Contents

List of Tables

List of Figures

List of Abbreviations

OSN	Olfactory sensory neurons
(a/p)PC	(anterior/posterior) Piriform cortex
OB	Olfactory bulb
LOT	Lateral olfactory tract
GC	Gustatory cortex
AON	Anterior olfactory nucleus
cNTS	Caudal nucleus of the solitary tract
GCG	Glucagon
AgRP	Agouti-related peptide
POMC	Pro-opiomelanocortin
(v)DMH	(ventral) Dorsomedial hypothalamus
VMH	Ventromedial hypothalamus
ARC	Arcuate nucleus of the hypothalamus
DA	Dopamine
5HT	Serotonin
PV	Parvalbumin
SST	Somatostatin
VIP	Vasoactive intestinal polypeptide
MCPO	Magnocellular preoptic nucleus
HDB	Horizontal limb of the diagonal band
SI	Substantia innominata
PVT	Paraventricular nucleus of the thalamus
ZI	Zona incerta
ARC	Arcuate nucleus of the hypothalamus
PAG	Periaqueductal gray
VP	Ventral pallidum
PFA	Paraformaldehyde
vHPC	Ventral hippocampal formation
TN	Hypothalamic tuberal nucleus
mPFC	Medial prefrontal cortex
BLA	Basolateral amygdala

vSub	Ventral subiculum
CA1	Cornu Ammonis 1
NAc	Nucleus Accumbens
PVH	Paraventricular nucleus of the hypothalamus
α-MSH	α-Melanotropin or α-Melanocyte-Stimulating Hormone
GABA	γ-Aminobutyric acid
NPY	Neuropeptide Y
MC4R	Melanocortin 4 receptor
ChR2	Channelrhodopsin-2
Oxtr	Oxytocin receptor
HFD	High-fat diet
OSN	Olfactory sensory neuron
NMDA	N-methyl-D-aspartate
(m/l) ENT	(medial/lateral) Entorhinal cortex
STFP	Social transmission of food preference
CB1R	Cannabinoid receptor 1
LH	Lateral hypothalamus
CCK	Cholecystokinin
TMT	2,4,5-trimethyl thiazole
2PE	2-phenyl ethanol
TMA	Trimethylamine
IGF-1R	Insulin-like growth factor 1 receptor
Kv1.3	Voltage-gated potassium ion channel 1.3
auROC	Area Under the Receiver Operating Characteristics Curve
s.e.m.	Standard error of the mean
EPSC	Excitatory post-synaptic current
CEA	Central nucleus of the amygdala
LPS	Lipopolysaccharide
PKCδ	Protein kinase Cδ
Pnoc	Prepronociceptin
PVT	Paraventricular nucleus of the thalamus
NE	Norepinephrine / Noradrenaline
NAcc	Nucleus Accumbens

Abstract

Smell, or olfaction, is a crucial element in the flavor perception of food. One often experiences altered flavor perception and appetite when our olfactory system is not fully functional (e.g. having a stuffy nose or loss of smell due to COVID-19 infection). However, little is known about how food odor is represented in the olfactory system during food intake. Additionally, increased eating speed, also known as binge eating, commonly leads to overeating, despite the exact underlying mechanism also being unclear. In this thesis, I studied how food flavor is represented in the mouse anterior olfactory (piriform) cortex (aPC) using a miniaturized microscope (miniscope) to perform *in vivo* Ca^{2+} imaging in freely moving mice during food intake. With collaborative efforts, we established a liquid food delivery system to deliver food to mice with different feeding rates. During slow feeding, a clear food-activated neuronal ensemble is observed. Surprisingly, once the mice switched from slow feeding to binge feeding, the aPC neurons were globally suppressed, even for the food-activated aPC neurons during slow feeding. This binge feeding-induced suppression is not observed in the gustatory cortex (GC) and the olfactory bulb (OB), suggesting the binge feeding-induced suppression is mostly limited to the aPC and is not inherited from the input or modulated by the gustatory system. I further verified that the binge-induced suppression is not mediated by the local GABAergic aPC neurons or by long-range serotonergic or dopaminergic modulation. Food consumption can be predicted by the magnitude of aPC suppression during binge feeding but not for slow feeding. Such appetite-correlated neuronal modulation is not preserved under anosmia or fasting, suggesting that it is perceptual- and metabolic-state-dependent. I further confirmed that binge feeding-induced aPC suppression is functional- suppressing aPC with closed-loop optogenetics experiments increases appetite. In summary, the aPC representation of food constitutes a negative feedback control to orexigenic circuits and is blunted by binge feeding to reduce satiation, which promotes overeating. My results demonstrate a novel cortical mechanism of appetite control in a rapid time scale, adding new insights into the understanding of the feeding and satiety circuits.

Zusammenfassung

Der Geruchssinn ist ein entscheidend für die Geschmackswahrnehmung von Lebensmitteln. Wenn unser Geruchssystem nicht voll funktionsfähig ist (z. B. bei verstopfter Nase oder Geruchsverlust aufgrund einer COVID-19-Infektion), sind Geschmackswahrnehmung und Appetit oft beeinträchtigt. Es ist jedoch unklar, wie der Geruch von Lebensmitteln während der Nahrungsaufnahme im Geruchssystem repräsentiert wird. Außerdem führt eine erhöhte Essgeschwindigkeit, auch bekannt als Binge Eating, häufig zu übermäßigem Essen, obwohl der zugrunde liegende Mechanismusunklar ist. In dieser Arbeit untersuchte ich, wie der Geschmack von Nahrungsmitteln im anterioren olfaktorischen (piriformen) Kortex (aPC) der Maus repräsentiert wird, indem ich ein miniaturisiertes Mikroskop (Miniskop) benutzte, um in vivo Ca^{2+}-Bildgebung bei frei beweglichen Mäusen während der Nahrungsaufnahme durchzuführen. Wir haben ein System zur Verabreichung von Flüssignahrung entwickelt, um die Fressgeschwindigkeit der Mäuse steuern zu können. Während der langsamen Fressgeschwindigkeit beobachten wir ein spezifisches nahrungsaktiviertes neuronales Ensemble. obald die Mäuse jedoch von der langsamen zur schnellen Fressgeschwindigkeit übergehen, beobachten wir eine globale Hemmung der Neurone im aPC. Diese Hemmung schließt auch die Neurone mit ein, die vorher bei langsamer Fressgeschwindigkeit aktiviert wurden. Diese globale neuronale Hemmung durch die hohe Fressgeschwindigkeit wird im gustatorischen Kortex (GC) und im Riechkolben (OB) nicht beobachtet. Somit wird die durch hohe Fressgeschwindigkeit hervorgerufene globale Hemmung der neuronalen Aktivität im aPC weder von vorgelagerten sensorischen Eingängen aus dem olfakto Darüber hinaus konnte ich nachweisen, dass die durch hohe Fressgeschwindigkeit hervorgerufene globale Hemmung der neuronalen Aktivität weder durch lokale inhibitorische GABAerge Schaltkreise noch durch serotonerge oder dopaminerge Modulation vermittelt wird. Die Menge der Nahrungsaufnahme korreliert mit der durch hohe Fressgeschwindigkeit hervorgerufenen globalen Hemmung der neuronalen Aktivität im aPC. Eine solche appetitkorrelierte neuronale Modulation bleibt bei Anosmie oder Fasten nicht erhalten, was darauf hindeutet, dass sie wahrnehmungs- und stoffwechselabhängig ist. Darüber hinaus konnte ich bestätigen, dass die durch hohe Fressgeschwindigkeit ausgelöste Hemmung des aPC funktionell relevant ist; optogenetische Hemmung des aPC während der

Nahrungsaufnahme führt zu erhöhter Einfuhr. Zusammenfassend lässt sich sagen, dass die aPC-Repräsentation von Nahrung eine negative Rückkopplung auf orexigene Schaltkreise vermittelt, die durch schnelle Nahrungsaufnahme unterdrückt wird. Der so durch sensorische Hemmung unterdrückte Sättigungsprozess induziert übermäßiges Essen. Meine Ergebnisse zeigen einen neuartigen kortikalen Mechanismus der Appetitkontrolle auf einer schnellen Zeitskala, der neue Einblicke in die Nahrungsaufnahme- und Sättigungsschaltkreise ermöglicht.

1. Introduction

Sensory inputs are crucial for organisms to receive information from the environment. Understanding how our brains interpret these signals is the key to decoding the outside world (Lange et al., 2023). Smell, or olfaction, is one of the most important sensations for living organisms to interact with the external world, and is evolutionarily conserved due to its significance for survival. Underlying foraging, flavor, mating, and predator avoidance, olfaction is essential in many aspects of life. The importance of olfaction can also be observed in many strong innate preferences for certain smells, e.g. preferring the smell associated with palatable food and avoiding the smell of rotten food. Some innate olfaction-driven behaviors also aid in avoiding predator encounters - for instance, the innate fear responses in rodents when exposed to the smell of fox urine (Rosen et al., 2015) and the courtship vocalizations of adult male mice when the female mice's odors are presented (Egnor and Seagraves, 2016).

Olfaction is also important for flavor perception, combining taste, temperature, tactility, sound, and vision; these senses constitute the full experience of food flavors, which contributes to our appetite for food items (Shepherd, 2006). While it is known from our daily experiences that alterations in the ability to smell (e.g. having a cold or COVID-induced anosmia (Hannum et al., 2020; Lechien et al., 2020; Parma et al., 2020)) greatly affect how we perceive food flavors and our appetites, our understanding of olfaction in flavor perception during food consumption is very limited.

Senses do not arise from only passively receiving external stimuli; in fact, senses are mostly accompanied by a movement, given that smell can be accompanied by a deep inhale or a fluffy tactile sensation from petting a dog. In the past 4 years, several important studies have shed light on the fact that the neuronal activities in most sensory brain regions are heavily influenced by the corresponding behaviors (Musall et al., 2019; Steinmetz et al., 2019; Stringer et al., 2019), but there was a contrary study where this was not observed in the monkey visual cortex (Talluri et al., 2023)), while the sensory neuroscience field has mostly observed sensory responses in the brain passively without acknowledging the behavioral output related effects on sensations (Hubel and Wiesel, 1962; Illig and Haberly, 2003; Poo and Isaacson, 2009; Poo and Isaacson, 2011;

Rennaker et al., 2007; Stettler and Axel, 2009; Stiebler et al., 1997; Vestergaard et al., 2023; Yamamoto et al., 1985). New perspectives in the system neuroscience field have emphasized that neuronal dynamics only make sense when we consider the behaviors in the equation (Buzsáki, 2019).

In this thesis, I aimed to focus on discovering the neuronal dynamics of olfactory flavor representation in the olfactory cortex during food intake and how the speed of eating affects flavor perception. In the following sections, I will introduce the current knowledge of the olfactory system and neuronal circuits of feeding. Furthermore, I will elaborate on the interactions between the olfactory system, feeding behaviors, and metabolism.

1.1. Olfactory system

Olfaction is a chemical sensation that requires a physical interaction between chemicals (odor molecules) and chemical receptors (odorant receptors). The olfactory system is the neuronal system that supports, computes, and processes this physical interaction (Figure 1). In this section, I will introduce the olfactory system in rodents, emphasizing the piriform cortex.

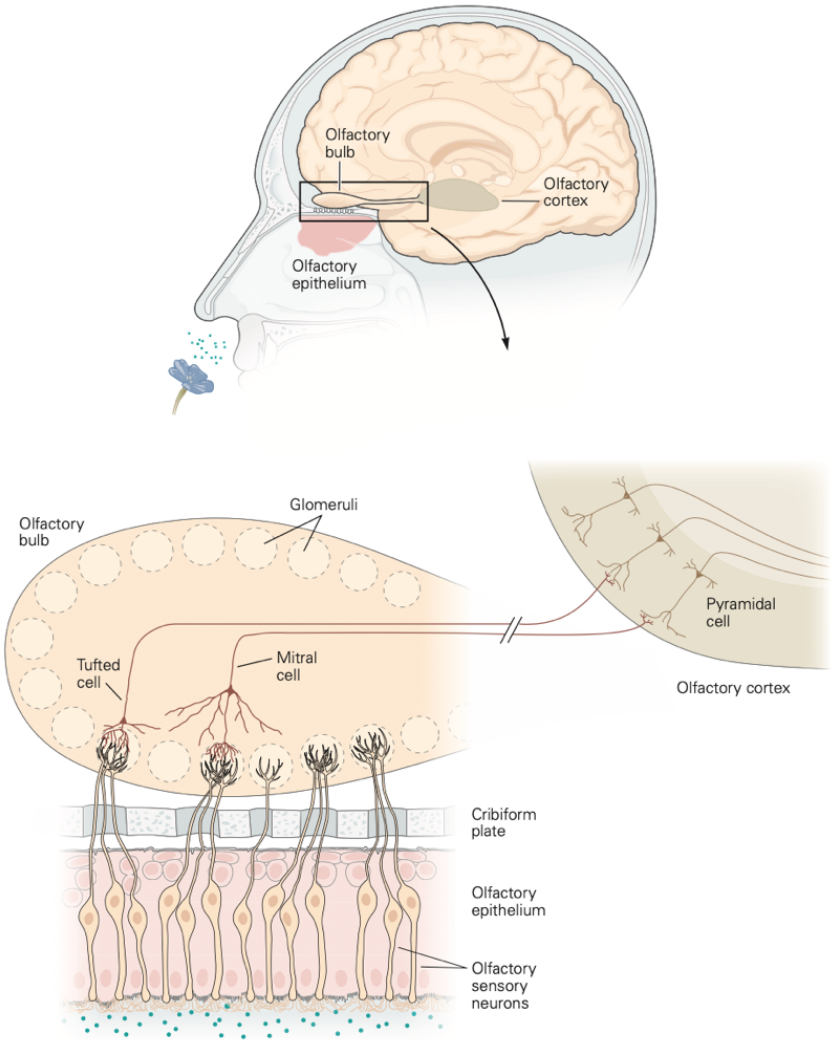

Figure 1. ***The olfactory system.*** *Illustration of how odor molecules are sensed by olfactory sensory neurons in the nostril and odor information is transferred to the olfactory bulb and then transferred to the olfactory cortex. Figure adapted from (Kandel, 2013).*

1.1.1. From the Nose to the Brain: An Anatomical Overview

From an anatomical perspective, the olfactory sensory pathway is distinct from other senses. Most sensory systems receive physical inputs from peripheral receptors expressing neurons (e.g. photoreceptor-expressing cone cells in the retina, mechanical sensor-expressing hair cells in the cochlea, chemical receptor-expressing taste receptor cells in the taste buds, etc.). These sensory signals travel through pathways including the cranial nerves and brainstem circuits, which arrive at the different subregions of the thalamus, and then relay to other cortical (e.g. primary sensory cortices, etc.) and subcortical areas (e.g. amygdala, hypothalamus, etc.) for higher-order processing. In the case of olfaction, the odorant receptor-expressing olfactory sensory neurons (OSNs) in the periphery (the nostril epithelium) transmit the sensory signals to the olfactory bulb, and then the sensory cues are directly delivered to primary olfactory cortical regions (e.g. the piriform cortex [PC], the anterior olfactory nucleus [AON], etc.) without traveling through thalamic nuclei (Blazing and Franks, 2020; Kay and Sherman, 2007), making the olfactory pathway distinct from other senses (Figure 1).

Odor molecules, odorant receptors, and olfactory sensory neurons

Olfaction starts in the nose, where odor molecules bind to the odorant receptors and transmit the interaction to the nervous system. Odor molecules are chemical compounds that have a smell, usually containing distinct functional groups that interact with the odorant receptors. The odorant receptors are chemoreceptors expressed in the cell membrane of the olfactory sensory neurons (OSNs) in the nostril. The OSNs are specialized epithelium cells that express odorant receptors on their processes (cilia) facing the nostril cavity. In each OSN, only one type of odorant receptor is expressed, allowing an early combinatorial source separation of mixed scents. However, the binding between odor molecules and odorant receptors is not exclusive, meaning a single odorant receptor can bind with different odor molecules with different affinities, and a single odor molecule can also bind with several odorant receptors, creating a complex image for individual odors (Murthy, 2011). Odor molecules do not function alone; in fact, almost all scents we experience in daily life are mixtures of many odor molecules with varied concentrations and properties. This complexity enriches the odor features that can be

carried by the odor mixtures and requires a flexible computational capacity for the brain to perceive the odors. Importantly, the olfactory senses produced by OSNs are not static. OSNs adapt their odorant receptor expression levels after short exposure (~2 hours) to a novel odor environment (Tsukahara et al., 2021), making olfaction an adaptive dynamic sensory system.

Notably, the interaction between odor molecules and odorant receptors is not as a 1-to-1 matching pair; a single odorant receptor can bind to different odor molecules, and a single odor molecule can bind to different odor receptors, which indicates that even with simple odors, olfactory information consists of a combination of activated odorant receptors/OSNs. The binding affinity between odor molecules and odorant receptors also differs, making the transmission of odor information not limited to just the odor identity but also the chemical affinity.

The basis of odor sensation lies in the chemical structures of odor molecules, such as functional groups and chemical bonds; however, mapping the odor molecular structure to the odor perception has been a key challenge in the olfactory field. Recently, researchers utilized graph neural networks to generate a principal odor map that captures the perceptual relationships and molecular properties (Lee et al., 2023). The network generates odor profiles that are closely matched with human perceptions and enable odor quality prediction for uncharacterized odor molecules, allowing the possibility of digitizing odors for future research with advanced computational power.

Since the odor sensation is based on the interaction between odor molecules and odorant receptors, it is intuitive to assume that olfactory performance (odor discrimination and detection) is tightly linked to the number of odorant receptors; the more receptors one has, the more capability to detect and distinguish different odors. For instance, rodents have around 1200 odorant receptor genes which are around 5% of the encoding genes in their genome, contributing to their extraordinary olfactory ability. In comparison, human beings only have around 400 genes encoding odorant receptors. This has led to the canonical conclusion that humans mostly rely on perceptions in other sensory domains (e.g. vision and hearing) (Buck and Axel, 1991; Godfrey et al., 2004; Niimura, 2009). However, a recent study has estimated that human beings are capable of perceiving more than 1 trillion odor stimuli (Bushdid et al., 2014). This result suggests that flexible higher-

order computations in the human olfactory system beyond the genetic variety of odor receptors support the ability to discriminate a wide range of odors (McGann, 2017).

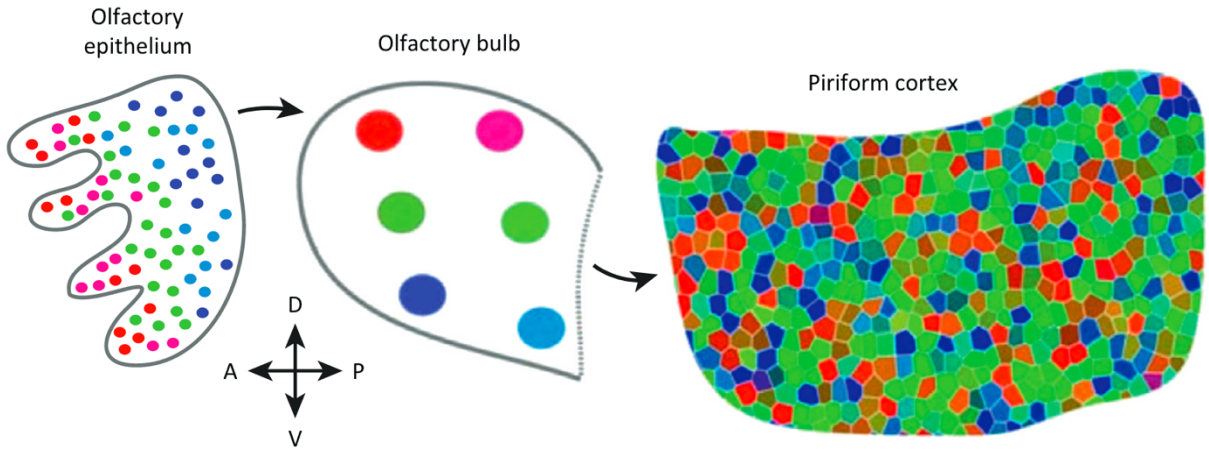

Figure 2. ***Odor representation along the olfactory pathway.*** *Each color represents the same olfactory receptor expressed by the olfactory sensory neurons. The spatial organization of olfactory receptors in the olfactory bulb is scrambled and distributed in the piriform cortex. Figure adapted from (Bekkers and Suzuki, 2013).*

Olfactory Bulb

The OSNs project to the olfactory bulb (OB), the first brain region in the olfactory system, via the first cranial nerve. The axons from the same odorant receptor-expressing OSNs converge into one (or two when counting both hemispheres) glomeruli (a small ball-shaped structure of neuropil) in the OB glomerular layer, forming the odotopic map (Mombaerts et al., 1996), meaning that the chemical similarities of odor molecules are spatial localized in the OB (Burton et al., 2022) (Figure 2). When an odor is presented to the nose, a few glomeruli are activated to encode this odor with different temporal dynamics (Burton et al., 2022). The sequential temporal dynamics of OB glomeruli activation are crucial for odor perception; when jittering the temporal dynamics of the same sets of OB glomeruli, mice tend to perceive the altered patterns as a distinct odor (Chong et al., 2020). Additionally, concentrations of odor stimuli also affect the activated OB glomeruli, in both their identities and their temporal dynamics (Burton et al., 2022). A recent study also suggested that when the odor concentration became too intense, a strong distortion of OB glomeruli activation occurred due to the transmission failure from OSN axons to the OB (Conway et al., 2023). Activation of OB glomeruli is sufficient to introduce olfactory sensation in the mice, even with novel spatial and temporal dynamics

of OB glomeruli that have not been experienced, or are even theoretically non-existent (Chong et al., 2020), suggesting a generalizable sensory capacity of the olfactory system. The glomeruli are not only structured in an odorant receptor-specific manner, but also their spatial arrangement is stereotyped and mirrored on both hemispheres. The glomeruli that are activated by a given odor are likely to be located on roughly the same anterior-posterior and medial-lateral axis across different mice and mirrored across the midline (Burton et al., 2022) (Figure 3), suggesting that OSN axons are guided and pruned during development in an odorant receptor-specific manner consistent with genetically determined hardwiring (Cho et al., 2009).

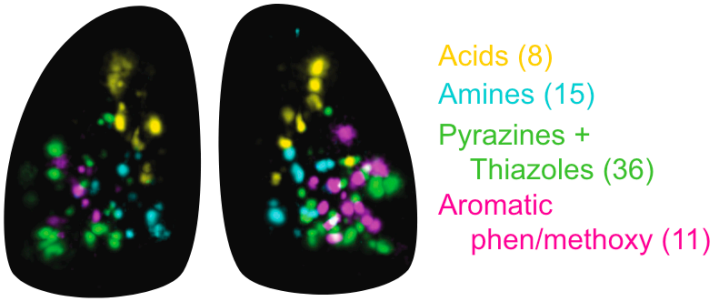

Figure 3. ***Topographic mapping of odors in the olfactory bulb.*** *Chemically similar odors are clustered in closer spatial locations in the olfactory bulb. Figure adapted and modified from (Burton et al., 2022).*

After the odor signals converge in the glomeruli via OSN axon projections, the axons form glomerular synapses that subsequently activate the two OB output neurons, the mitral cells, and the tufted cells. These two neuron types differentially carry the odor information to the higher-order olfactory systems, including the olfactory cortex. The mitral cells project more densely to the anterior and posterior piriform cortex (aPC, pPC). In contrast, the tufted cells project more to the anterior olfactory nucleus (AON) and the olfactory tubercle (OT) (Chen et al., 2022) (Figure 4). Despite a clear separation of the odotopic map in the OB, the spatial organization of odors is not preserved in the PC, rather, a distributed representation of odors is formed (see the following paragraphs on the coding principle of the piriform cortex). Acute odor adaptation also appears at the OB level; on repeated exposure to the same odor 3-4 times, both OB mitral cells and tufted cells show only ~70% of the evoked responses compared to the first exposure, while the OSN axons in the OB glomeruli respond to the odor similarly (Storace and Cohen, 2021). This indicates a different temporal structure of odor adaptation at the level of OSN and the OB output neurons, where the former takes place hours after the odor exposure, and the

latter adapts within tens of seconds, allowing a flexible input-output logic for odor processing at early stages.

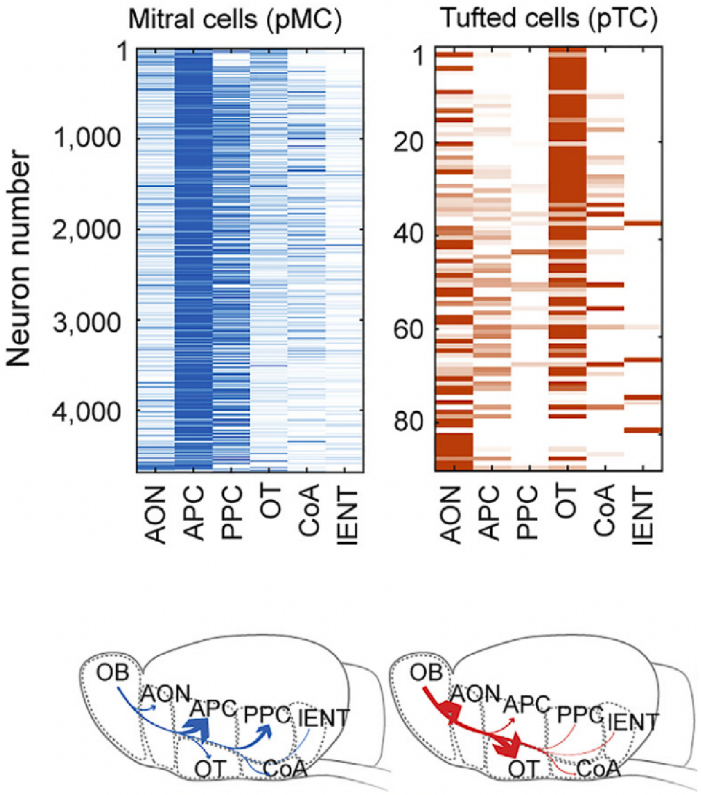

Figure 4. ***OB mitral and tufted cells projection to higher olfactory regions.*** *Mitral cells project mostly to the piriform cortex, while the tufted cells preferentially project to the anterior olfactory nucleus and olfactory tubercle. Figure adapted and modified from (Chen et al., 2022).*

Piriform cortex

Structure and cell types

The mitral and tufted cell axons form the lateral olfactory tract (LOT), which transmits odor information processed in the olfactory bulb next to the olfactory cortex. Among other structures, the piriform cortex (PC) is the largest cortical region that directly receives synaptic inputs from the OB output neurons. This is also a unique feature of the olfactory system. Unlike other sensory systems, olfactory processing does not involve a thalamic relay, positioning the olfactory cortex, or PC, only two synapses away from the external world, the shortest route to a sensory cortex from the peripheral sensory organs. This

early cortex-reaching structure is conserved throughout species, suggesting that this feature may arise from the evolutionary importance of computing odor or chemical signals.

The PC is a paleocortex, an ancient brain structure similar to the archicortex (consisting of the hippocampus and the dentate gyrus), with a simple 3-layer structure along the dorsal-ventral axis. This structure is different from the typical neocortex structure, which is commonly known as a 6-layer structure with column-specific neuronal projection principles (Kandel, 2013).

In all sensory cortices but the piriform cortex, sensory inputs relayed from the thalamus arrive mainly at layer 4 stellate neurons, and to a lesser degree at layer 5 pyramidal neurons. The processed signals from layer 4 neurons are then transmitted vertically upwards to layer 2/3 pyramidal neurons within the same cortical column, which in turn project downwardly to layer 5 pyramidal neurons as a form of sensory gain control. The layer 5 pyramidal neurons are the main output neurons that project broadly outside the cortical column, including other cortical and non-cortical areas (Moberg and Takahashi, 2022).

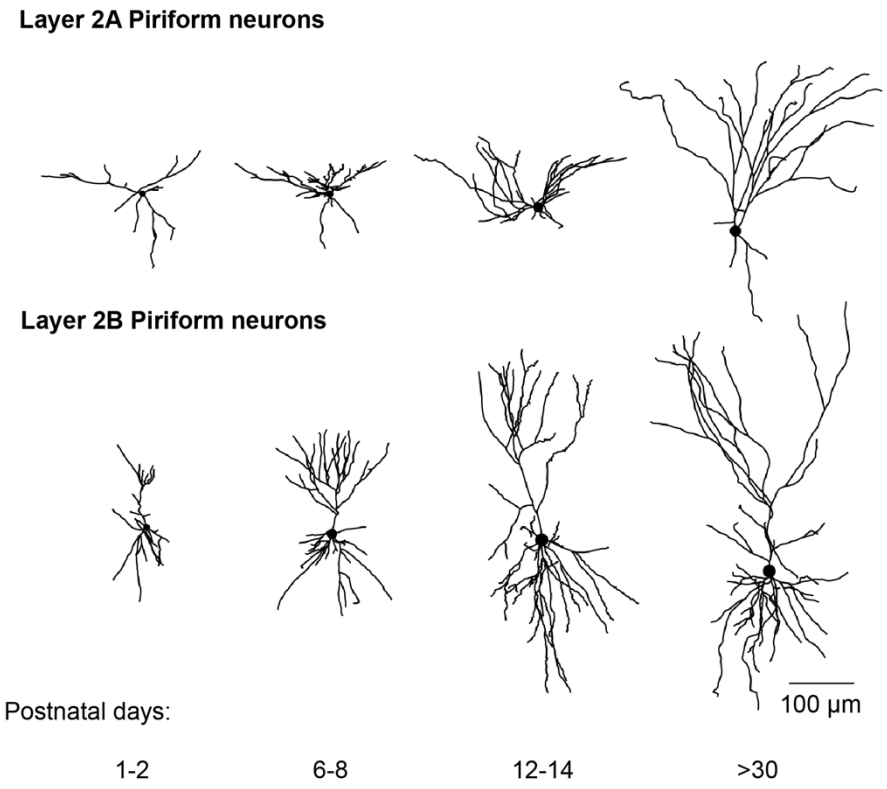

Figure 5. ***Two distinct cell types in the anterior piriform cortex across postnatal development.*** *Layer 2A neurons are the semilunar neurons, exhibiting early branching and lack of basal dendrites. Layer 2B neurons are the pyramidal neurons, showing a long apical dendrite stem from the soma. Figure adapted and modified from (Moreno-Velasquez et al., 2020).*

In the PC, we observe a completely different schema. Most excitatory neurons are located in layer 2, transitioning into a lower density in layer 3, with almost no excitatory neurons in layer 1. The excitatory neurons in layer 2 can further be distinguished into 2 types - the semilunar neurons occupying the upper one-third of layer 2 and the superficial pyramidal neurons in the lower two-thirds of layer 2 (Moreno-Velasquez et al., 2020). Structurally, the semilunar and pyramidal neurons are quite distinctive; the semilunar neurons' apical dendrites split right after exiting the cell body, whereas the pyramidal neurons show a long apical dendritic stem before branching out (Figure 5). In layer 3, deep pyramidal neurons can be found, sharing similar pyramidal morphology. These 3 types of excitatory PC neurons all extend their dendrites in layer 1 of the PC, where the distal portion (layer 1a) receives direct sensory (afferent) inputs from the OB axon bundles (the lateral olfactory tract, LOT), and the more proximal portion (layer 1b) mostly receive recurrent (associational) inputs from the excitatory aPC neurons. The layer 2 semilunar neurons mostly receive sensory inputs from the OB, and the layer 2 and 3 pyramidal neurons

receive both sensory inputs and recurrent inputs (Suzuki and Bekkers, 2011; Wiegand et al., 2011). Along with other research groups, my colleagues and I have shown that these structural differences already arise during development and affect their computational properties, whereby NMDA (N-methyl-D-aspartate) receptor-mediated supralinear dendritic spikes are only found in the pyramidal neurons and not in the semilunar neurons (Kumar et al., 2021; Kumar et al., 2018; Moreno-Velasquez et al., 2020) (Figure 6).

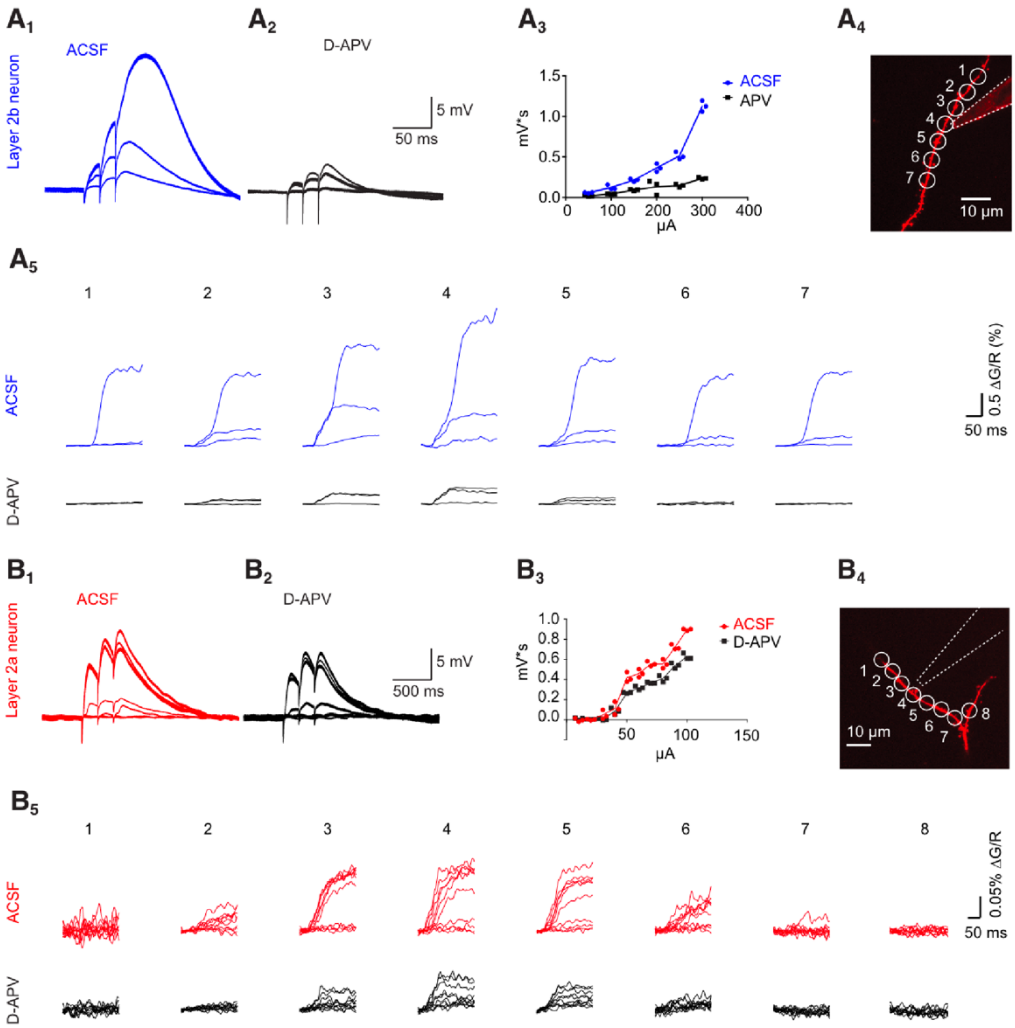

Figure 6. ***Dendritic properties of two types of aPC excitatory neurons.*** *Dendritic/NMDA spike is only observed in the layer 2b (pyramidal) neurons and not in layer 2a (semilunar) neurons in the anterior piriform cortex. Figure adapted from (Moreno-Velasquez et al., 2020), contributed by the author.*

The projecting neurons in PC also have different downstream targets, roughly based on their anatomical location (Diodato et al., 2016) (Figure 7). The centrifugal OB-projecting PC neurons are marked with molecular marker Cux1 and are mostly located in layer 2b and layer 3, suggesting they are the superficial and deep pyramidal PC neurons. A

spatially overlapping population of pyramidal PC neurons in layer 2b and layer 3 are projecting to the medial prefrontal cortex (mPFC), sharing gene expression of Cux1 and Ctip2. The cortical amygdaloid nucleus (CoA)- and lateral entorhinal cortex (lEnt)-projecting PC neurons can be labeled with Reelin and Fezf2, and are located in layer 2a, suggesting most of these neurons are semilunar PC neurons.

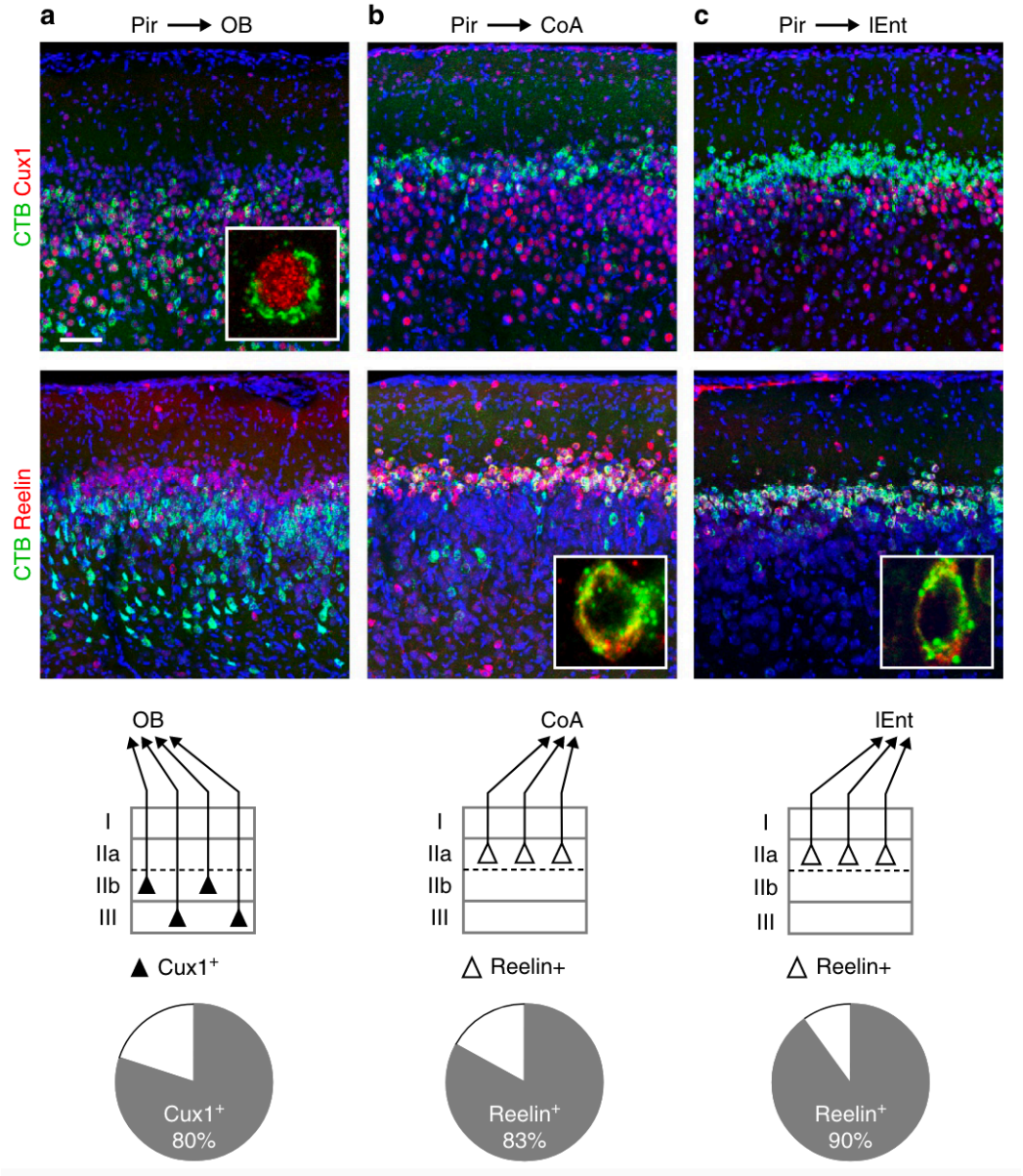

Figure 7. ***Molecular signatures of neural connectivity in the piriform cortex.*** *The PC neurons projecting to the OB express Cux1 and those projecting to the CoA and lEnt express Reelin. Figure adapted from (Diodato et al., 2016).*

The PC is not only organized along the DV axis but can also be divided into the anterior and posterior parts. The anterior PC (aPC) receives more olfactory inputs and the posterior PC (pPC) is more connected with other brain regions including the hippocampus, the lateral entorhinal cortex, and the basolateral amygdala, indicating a potential mixed functionality along the AP axis (Wang et al., 2020b). The aPC projects to pPC extensively, while projection in the opposite direction from pPC to aPC is negligible (Hagiwara et al., 2012). While both parts of the PC respond to odors, the pPC neurons are more associative, meaning that they are capable of changing their responses to the odor cues after learning (Calu et al., 2007).

The odor representation in the PC, unlike the odotopic map in the OB, is not organized chemotopically - the receptive fields from individual glomeruli overlap and are broadly distributed in the aPC in rodents (Illig and Haberly, 2003; Rennaker et al., 2007; Roland et al., 2017; Sosulski et al., 2011; Stettler and Axel, 2009). While some projection principles from the OB to the PC along the anterior-posterior axis have been reported (Chen et al., 2022), the overall topographic map of odor representation in the OB is nearly completely reformatted, or in other words, scrambled, in the entire PC; meaning there is no clear spatial separation based on the chemical properties of odor molecules for rodents (Illig and Haberly, 2003; Rennaker et al., 2007; Roland et al., 2017; Stettler and Axel, 2009) and humans (Howard et al., 2009; Sagar et al., 2023). Furthermore, *in vivo* electrophysiology recordings in rodent PC neurons also support the same notion, i.e., that individual PC neurons respond broadly to many different, often chemically distinct, odors (Miura et al., 2012; Poo and Isaacson, 2009; Poo and Isaacson, 2011; Zhan and Luo, 2010), indicating that PC neurons are not tuned for the chemical properties of odors. Instead, the evidence supports PC neurons as encoding perceptually similar odors more similarly (generalization or categorization of similar odors, e.g. the smell of orange and lemon both belong to the citrus category), regardless of their chemical relationships (Pashkovski et al., 2020), implicating the role of the PC in odor perception.

The distribution coding of odor representation and the strong recurrent network in the PC provide flexible computing power and functionalities. In the next section, I will introduce several known functions of PCs, including odor discrimination, concentration coding, and many other functional roles of PCs beyond just odor processing.

1.1.2. Multifaceted functionality of piriform cortex

Odor processing: discrimination, concentration coding, and representational drift

Odor coding can be divided into two parts: identity and intensity (molecular concentration). In the following paragraphs, I will introduce how odors are identified and how odor intensity is encoded in the olfactory system.

Identification of odors starts in the nostrils; as mentioned above, different odorants are captured by different sets of odorant receptors on the cilia or dendrites of OSN neurons (Buck and Axel, 1991). The OSN neurons transfer the odor-evoked signals to OB glomeruli in an odorant receptor-specific manner (Mombaerts et al., 1996), allowing the separation of different odors at the first olfactory brain region (Murthy, 2011). Odor-evoked responses in the OB output neurons, the mitral and tufted cells, are then relayed to the olfactory cortices, the largest of which is the PC, in addition to the anterior olfactory nucleus, the olfactory tubercle, the cortical nucleus of the amygdala, and the lateral entorhinal cortex (Miyamichi et al., 2011; Sosulski et al., 2011). These OB mitral and tufted cells' projections to PC neurons are diffuse and overlapping, permitting individual PC neurons to integrate different combinations of glomeruli inputs, meaning that each PC neuron is not specifically tailored to one given odor. Cortical neuronal representations of odors in the PC are not sparse (Bolding and Franks, 2017; Miura et al., 2012; Poo and Isaacson, 2009; Poo and Isaacson, 2011; Rennaker et al., 2007; Stettler and Axel, 2009; Tantirigama et al., 2017; Zhan and Luo, 2010), and each odor presentation activates ~5-20% of PC neurons. PC representations for different odorants overlap, regardless of the chemical similarities between odor molecules. When presenting a mixture of 2 odors, the odor representation of this odor mixture is not simply the combination of the odor representation of these odors, but rather a subset of those neurons is activated, with additional neurons participating in the ensemble (Bolding and Franks, 2017), and each odor or odor mixture is represented in a unique PC neuron population code (Stettler and Axel, 2009).

Intensity coding of odor concentrations also begins in the nostril; odorant receptors on the OSNs bind odorant molecules at different affinities, which limits the detection

threshold of given odors (Araneda et al., 2000; Hallem et al., 2004; Malnic et al., 1999; Saito et al., 2009). The increment of odor concentrations within the OB can be represented in three forms, 1) enhanced neuronal activities within glomeruli, including the mitral and tufted cells (Arneodo et al., 2018; Junek et al., 2010; Margrie and Schaefer, 2003; Spors and Grinvald, 2002), 2) faster recruitment of glomeruli (Arneodo et al., 2018; Junek et al., 2010; Spors and Grinvald, 2002), and 3) recruitment of additional OB glomeruli (Arneodo et al., 2018; Burton et al., 2022; Spors and Grinvald, 2002), except for when the increased concentration breaks perceptual constancy (Conway et al., 2023). This underlies rate coding (encoding with neuronal firing rates) and time coding (encoding with neuronal firing time) encoding concentrations through different neuronal firing rates in the OB output neurons. However, PC appears to be odor concentration invariant (Blazing and Franks, 2020; Bolding and Franks, 2018; Bolding and Franks, 2017; Stettler and Axel, 2009), meaning that PC neurons do not exhibit obvious higher activity when experiencing higher odor concentrations (Bolding and Franks, 2018). This invariance of concentration coding in PC is mediated by the local feedback inhibitory circuit (Bolding and Franks, 2018). The percentage of activated PC neurons is also stable across concentrations, despite the inhibited PC neurons increasing slightly in percentage (Bolding and Franks, 2017). While rate coding is unlikely to contribute to concentration coding in the PC neurons, time coding of different concentrations seems a more probable mechanism in PC neurons; when exposed to higher concentrations of odors, PC neurons fire closer in time, meaning they are more synchronized, followed by a strong inhibition. This is also supported by the upstream inputs. OB mitral and tufted cells also exhibit shorter spiking latency when the odor concentration increases (Arneodo et al., 2018; Junek et al., 2010; Margrie and Schaefer, 2003; Spors and Grinvald, 2002). However, odor concentration coding by temporal filtering in PC tends to result in a lower accuracy compared to odor identity coding (Bolding and Franks, 2017). In summary, these results suggest the PC encodes odor identity in different ensembles, and encodes odor intensity, despite being less accurate, in ensemble latency and synchrony. In other olfactory cortices, functionalities in odor concentration appear to be more prominent. For instance, the lateral entorhinal cortex (lENT) also encodes odor concentration with a temporal coding (Bitzenhofer et al., 2022), suggesting the concentration coding of odors may mostly occur outside PC.

Identification of a given odor relies on the reactivation of a majority of certain PC representations. This motivates the thinking that stable cortical representations are a prerequisite for optimal neuronal processing for odor identification. However, while the representation of PC odor coding is stable at a short-term time scale (~ 4 days) (Wang et al., 2020c), the odor representation of a given odor is unstable at a longer time scale (~ 1 month), with only ~6% of odor responding PC neurons still responding to the same odor (Schoonover et al., 2021). Changes in the neuronal representation of external variables, also called representational drift, are reported in other brain regions including the hippocampus CA1 (Kentros et al., 2004; Lee et al., 2020b; Mankin et al., 2012; Rubin et al., 2015; Ziv et al., 2013), the motor cortex (Rokni et al., 2007), and posterior parietal cortex (Driscoll et al., 2017), and have been proposed to aid continual learning for separating and relating memories across times (Driscoll et al., 2022). Representations of basic senses are very robust and stable in most sensory cortices, meaning there is little difference in the neuronal ensembles for sensory stimuli across time (Clark et al., 1988; Gilbert and Wiesel, 1992; Kato et al., 2015; Margolis et al., 2012; Mayrhofer et al., 2015; Rose et al., 2016; Weinberger et al., 1993), however, a recent study reported that the naturalistic visual representation in the primary visual cortex also drifts (Marks and Goard, 2021). The gradual and rather fast drifting in the PC of representations of basic odors illustrates that the drifting is a special feature, which may contribute to its function as both a primary sensory area and an associative area for learning and memories (Calu et al., 2007; Chapuis and Wilson, 2012; Li et al., 2008; Roesch et al., 2007; Shakhawat et al., 2014). Repeated exposure to a given odor slows down the representational drift, while on discontinuing the exposure, the drift rate increases again, and the PC ensembles are not stabilized by pairing an odor with foot shock, despite animal behaviors demonstrating that the memory of conditioned odor is stable (Schoonover et al., 2021). The exact mechanism of the representational drift in the PC remains unclear, while the synaptic plasticity of OB mitral and tufted cells' axonal terminals as well as local synaptic and circuit plasticity in the PC recurrent network may explain the highly malleable PC representation. In a different study, the authors suggest that the encoding of task-relevant odors may be more stable across time in the PC (Berners-Lee et al., 2023). They showed that in the pPC, task-relevant odors are represented differently from the non-target odors. After (over-) training, pPC neurons encode task-relevant odors more selectively and improve performance on difficult trials. This data suggests that pPC is a robust system to optimize task performance even when the performance demands are not high. This result

illustrates the selectivity of representational drift, in that when the animals need to actively distinguish a given odor, the odor representation of this odor may be more stable across time, meaning less drifting. However, in these two studies, the respective recordings were performed in the aPC (Schoonover et al., 2021) and the pPC (Berners-Lee et al., 2023), which may indicate different representation coding mechanisms in different parts of the PC. The latter study also does not record from the same pPC neurons across days, so the neuronal selectivity of task-relevant odors may be contributed to by different neurons over time.

Odor adaptation and temporal filter

Detecting odors from the surrounding environment is not trivial; when new odors are mixed into the current odor environment, how does the olfactory system detect new odors from the already existent odors (e.g. appearance of a predator smell in a familiar environment)? One way to solve this figure-ground separation problem is through odor adaptation, also known as olfactory fatigue, which decreases the odor sensitivity to already-existing odors and allows new odors to be perceived without a masking effect from the old odors. Odor adaptation has been reported at many levels of the olfactory pathway. In the OSNs, odor adaptation takes place via 2 distinct pathways: 1) a fast adapting, cAMP and Ca^{2+}-activating negative feedback within seconds (Kurahashi and Menini, 1997; Lowe and Gold, 1993; Reisert and Matthews, 1999) and 2) a slow adaptation to environmental smells by altering expressions of odorant receptors in hours (Tsukahara et al., 2021). In the OB, a few repeated odor stimuli also lead to a reduction of odor-evoked responses of mitral and tufted cells (Storace and Cohen, 2021). Repeated odor presentation also leads to reduced odor-evoked responses in the PC, likely via metabotropic glutamate receptor-mediated pre-synaptic depression at the afferent fibers from the OB (Best and Wilson, 2004; Wilson, 1998). An additional filtering mechanism is presented in the aPC, in that odor-evoked responses in PC are rapidly suppressed after the initial responses by feedback inhibition via recurrent cortical circuits (Bolding and Franks, 2018; Wilson, 1998). This means that only the earliest OB inputs are captured by the aPC, which represent the most odorant-specific and concentration-invariant features of the odor.

Additional feedback from the olfactory cortices back to the OB inhibitory granular cells also introduces a secondary filtering mechanism for increasing the signal-to-noise ratio of more prominent odors in the environment (Boyd et al., 2012; Davis and Macrides, 1981; Markopoulos et al., 2012). These mechanisms of odor adaptation provide the capability of the olfactory system to robustly detect novel odors in odor environments.

Pattern completion, separation, and associative learning

While odors can be separated from the background by a mechanism like the abovementioned adaptation, sometimes the opposite is necessary, namely the recognition of an odor based on a degraded input. PC representations of odor mixtures are flexible and robust, meaning they can reactivate a complete neuronal representation with similar odor mixtures or the same but with degraded odor inputs. Recent research has found that despite the bulbar odor inputs being degraded by mild anesthesia, neuronal representation of odors in the PC remains robust, meaning that with less informative odor input, the complete odor image can still be recapitulated in the PC pyramidal neurons (Bolding et al., 2019). When blocking the recurrent circuits in the PC with tetanus toxin (TeLC) expression in the excitatory PC neurons, the cross-state (wake vs. anesthetized) odor representations drop to a similar level as the odor representation of OB neurons, suggesting the recurrent circuits are required to stabilize PC odor representations.

Another study suggested that the PC odor representation matches well with the perceptions of the odors (Chapuis and Wilson, 2012). Rats are trained to learn an odor-reward association task, where an odor mixture of 10 odors is used as the cue (referred to as 10c in the following). After learning, the olfactory cue is changed in 2 ways: 1) keeping the same odors but taking out one odor (10c-1); 2) the same as 1), but the removed odor is replaced by a new odor (10cR1). The neuronal responses for 10c and 10c-1 are mostly similar in the PC, whereas the response similarity drops quite a lot comparing 10c to 10cR1, suggesting that 10cR1 is likely to be perceived as a different odor. Notably, the odor representations for 10c-1 in the OB are fairly different from 10c, suggesting that the PC receives the reduced odor input (10c-1) and completes the neuronal pattern that is close to the full odor image (10c). This response similarity matches well with the rats behaviors. When switching the olfactory cue from 10c to 10c-

1, rats still consider this odor to be associated with reward. Conversely, rats do not perform as well when the 10cR1 is presented, which matches with the PC odor representations.

Interestingly, while natively PC odor representation promotes pattern completion, the PC odor representation is also plastic and can support pattern separation. Via learning, both the separation of similar odors and the completion ("grouping") of distinct odors can be achieved (Chapuis and Wilson, 2012). When rats are trained to discriminate similar odors, like the previously mentioned 10c and 10c-1, the rats can learn to differentiate these 2 odors in a few days and the corresponding PC odor representations diverge. Conversely, when rats learn to group the rather distinct odors 10c and 10cR1 into one category and distinguish them from a completely different odor, the odor representations in PC for 10c and 10cR1 also become similar.

The PC drives learning not just under artificial conditioning experimental settings, but also in ethologically relevant behaviors, for instance, the social transmission of food preference (STFP) (Galef and Wigmore, 1983; Kogan et al., 1997; Strupp and Levitsky, 1984). An observer mouse exposed to a demonstrator mouse fed with scented food (e.g. cumin-flavored food) will learn to prefer the exposed food odor over the innate preference for food odors (e.g. thyme-flavored food). When blocking the prefrontal-projecting PC neurons with chemogenetics during social interaction or food preference tests, the observer mice no longer prefer the learned odor (Loureiro et al., 2019), suggesting that the odor representation in the PC is necessary for identifying the learned odor in this food preference learning. The synaptic potentiation induced by STFP is also essential for STFP expression; after optogenetically depressing the synaptic transmission of the PC-to-prefrontal cortex circuit right before the food preference test, the mice no longer prefer the learned odor. These studies reveal a robust and flexible network in the PC that performs pattern completion, pattern separation, and social interaction-based odor learning.

Spatial encoding

Olfaction is an important sense for animals during certain behaviors, including foraging and navigation, especially in a given environment associated with a certain smell. While

spatial encoding ability is mostly attributed to the hippocampal formation circuits including the place cells in the hippocampus CA1 (O'Keefe et al., 1978) and grid cells in the medial entorhinal cortex (Hafting et al., 2005), recent studies have also revealed that PC has roles in spatial coding. Electrophysiological (Poo et al., 2021) and optical recordings (Mena et al., 2023) in the PC reported that PC neurons also encode the spatial location of the animals, and surprisingly, more PC neurons encode for location (~40%) over odor identity (~29%) (Poo et al., 2021). Decoding accuracy for odor and location in the PC are both robust, where the location decoding is at a similar level as hippocampus CA1 neurons. PC neurons encode the location of the animal regardless of the heading direction, contrasting with the lateral entorhinal cortex (lENT) neurons that encode direction-specific positions (Mena et al., 2023), which indicate differential encoding of spatial information.

In summary, the PC is mostly involved in odor discrimination and is capable of flexibly categorizing odors into the same or distinct groups via associative learning. Odor representation in the PC matches with one’s perceptual experience of given odors as distinct (pattern separation) or similar (pattern completion). Temporal filtering of odor representations results in concentration-invariant coding of odor intensity in the PC. Additionally, spatial information is also encoded in the PC, indicating its role in odor-space association and guiding olfactory-cued spatial navigation. Despite the close relationship between olfaction and flavor perception during feeding, the role of the PC in representing flavors currently remains unclear. In the next sections, I will introduce the neurocircuits involved in food intake and the reciprocal interaction between olfaction and metabolism.

1.2. Neurocircuits of food intake and metabolism

Eating, or feeding behavior, is the main way for organisms to obtain energy and nutrients to reach homeostasis, the steady state of energy balance (Andermann and Lowell, 2017). Eating can also take place beyond homeostatic needs, which is known as non-homeostatic eating or hedonic eating, meaning the drive for eating is not aiming for reaching homeostasis but the pleasantness of eating the food (Andermann and Lowell, 2017; De Araujo et al., 2020; Liu and Kanoski, 2018). In the following sections, I will focus on the brain regions, specific neuronal types, and neurotransmitters and receptors involved in homeostatic eating, which is controlled by the hunger and satiation states.

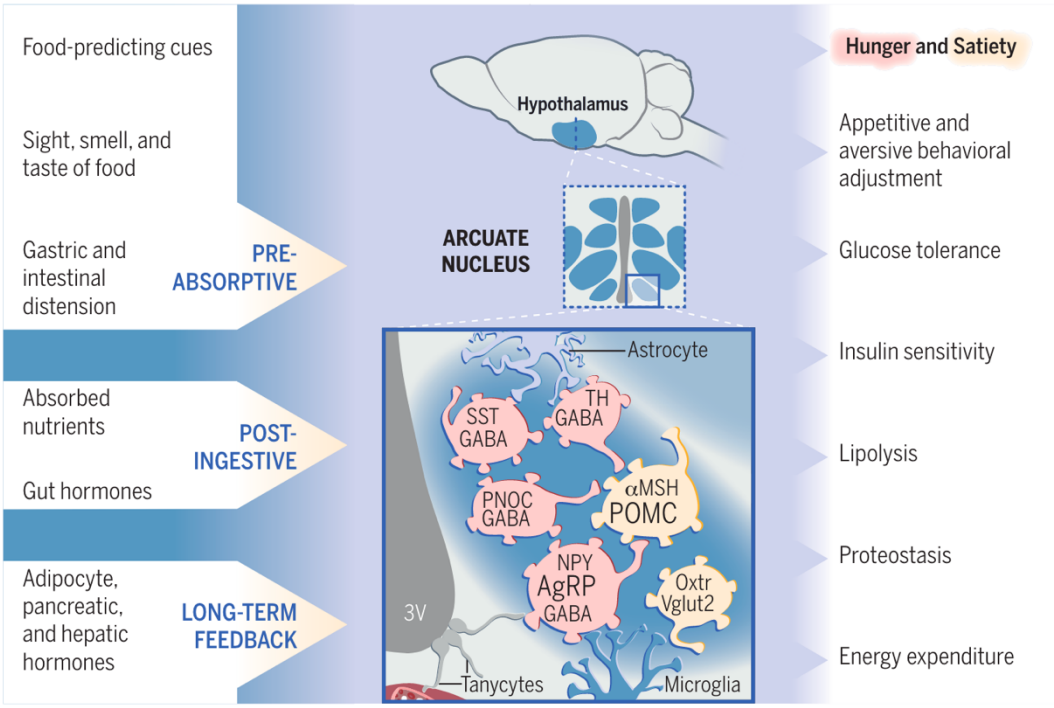

Figure 8. ***Feeding behavior is regulated by the different neurons in the ARC.*** *Figure adapted from (Brüning and Fenselau, 2023).*

1.2.1. Hunger and satiation circuits in the arcuate nucleus of the hypothalamus

The arcuate nucleus of the hypothalamus (ARC) has an important role in controlling feeding behaviors (Brüning and Fenselau, 2023) (Figure 8). Two main neuronal types within the ARC are the agouti-related peptide (AgRP) neurons and the pro-

opiomelanocortin (POMC) neurons, which respond to hunger and satiety states, respectively.

Hunger drives AgRP neurons' activity through the hunger hormone Ghelin, which is produced by the enteroendocrine cells of the gastrointestinal tract. The role of AgRP neurons is tightly linked to promoting feeding as ablation of AgRP neurons causes starvation (Luquet et al., 2005; Tan et al., 2014; Wu et al., 2008a; Wu et al., 2008b), but the contrary finding has also been presented recently (Cai et al., 2023). When bypassing the Ghrelin stimulation with direct optogenetic stimulation, AgRP neurons can introduce a hunger-like state in mice which rapidly promotes food intake (in minutes to hours) (Aponte et al., 2011; Krashes et al., 2011; Krashes et al., 2013). The hunger-like state driven by AgRP neurons signals negative valence in mice, suggesting that the hunger state is unpleasant for individuals, encouraging them to do something (e.g. foraging and feeding) to counter the unpleasantness (Betley et al., 2015). The fast-acting function of the AgRP neurons is mostly through the release of inhibitory neurotransmitters (γ-Amino-butyric acid (GABA)) and neuropeptides (Neuropeptide Y (NPY)), instead of the slow-acting AgRP peptide, an antagonist for the melanocortin 4 receptor (MC4R) that suppresses feeding (Atasoy et al., 2012; Garfield et al., 2015; Krashes et al., 2013).

Conversely, the POMC neurons are activated by the satiety hormone Leptin, a peptide hormone released from adipose tissue, which also inhibits AgRP neurons (Beutler et al., 2017; Cowley et al., 2001; Williams et al., 2010). The main function of POMC neurons was proposed to be terminating meals, since POMC deficiency or ablation of POMC neurons leads to overeating and obesity in humans and mice (Krude et al., 1998; Xu et al., 2005; Yaswen et al., 1999; Zhan et al., 2013). The tight link between the opposite neuronal activities of AgRP and POMC neurons motivates a robust model of feeding control (Sternson and Eiselt, 2017). The main effector of the POMC neurons is caused by releasing POMC-derived peptide α-Melanotropin (α-Melanocyte-Stimulating Hormone, or α-MSH) to the MC4R-expressing paraventricular nucleus of the hypothalamus (PVH) neurons, which is the main satiety center antagonized by the AgRP peptide (Loos and Yeo, 2022). Yet, acute optogenetic activation of POMC neurons has limited effects on reducing food intake and body weight. This only occurs under long-term activation, for example, more than 4-hour stimulation of GLP-1R-expressing POMC neurons (Biglari et al., 2021), 24-hour ChR2 stimulation of generic POMC neurons (Aponte et al., 2011), and

days of chemogenetics activation of POMC neurons (Zhan et al., 2013), suggesting that the satiety effects from POMC neurons function on a slower time scale than AgRP neurons' GABAergic- and NPY-ergic-mediated fast feeding promotion (Atasoy et al., 2012; Garfield et al., 2015; Krashes et al., 2013). So far, and only under energy deficit conditions, optogenetically stimulating POMC neurons in fasted mice can reduce feeding in a 30-minute feeding window (Wei et al., 2018). Acute chemogenetic activation of POMC neurons, unexpectedly, promotes cannabinoid-induced feeding via activating the cannabinoid receptor 1 (CB1R) on a subset of POMC neurons and selectively increases the release of orexigenic β-endorphin (Koch et al., 2015).

Interestingly, while the AgRP neurons strongly inhibit the POMC neurons through GABAergic synaptic transmission within the ARC (Cone, 2005), AgRP to POMC inhibition is not required for food intake. On shutting down POMC neurons alone with chemogenetics, mice did not eat more food. Simultaneously activating both AgRP and POMC neurons with optogenetics still promotes feeding, indicating that the feeding promotion led by AgRP neuronal activity mostly acts outside the ARC and that POMC neurons are not the direct functional downstream targets of the AgRP neuron-driven rapid feeding behavior (Atasoy et al., 2012). Several downstream brain regions of AgRP neurons outside the ARC have functions in the regulation of feeding behaviors (Betley et al., 2013), among these regions, the PVH is the most prominent region. The inhibitory long-range projection from AgRP to the PVH is sufficient and necessary for promoting feeding (Atasoy et al., 2012; Betley et al., 2013). Directly inhibiting PVH through chemogenetics can recapitulate the AgRP-mediated feeding promotion. When co-activating AgRP and PVH^{SIM} neurons, the feeding behavior is successfully blocked, demonstrating a causal link to this AgRP -| PVH circuitry being the backbone of the feeding promotion (Atasoy et al., 2012).

Subsequently, fast-acting satiating neurons in the ARC were discovered; a different subpopulation of Oxytocin receptor (Oxtr)-expressing ARC glutamatergic neurons form excitatory connections to the MC4R-expressing PVH, suppressing feeding more rapidly (in 1-2 hours) (Fenselau et al., 2017). These Oxtr-expressing ARC neurons' axons converge onto mostly the same MC4R-expressing PVH neurons that are targeted by the AgRP neurons. In addition, the POMC-releasing α-MSH postsynaptically potentiates the

excitatory synapses from the Oxtr-expressing ARC to the MC4R-expressing PVH neurons, strengthening the satiety effects of the ARC-PVH melanocortin circuit.

Here, I have summarized that neurons in the ARC nucleus have important roles in regulating food intake upon different metabolic states (sated and hunger) as well as their functional roles in regulating feeding behaviors in rapid (minutes) and long-term (hours) conditions.

1.2.2. Circuit dynamics during feeding

In the last section, I described the ARC AgRP and POMC neurons' function in regulating feeding via modulating PVH activity. While bodily hormones representing the hunger and satiety states (Ghrelin and Leptin) modulate AgRP and POMC neurons' activities reflecting the energy homeostasis, the neuronal dynamics of AgRP and POMC neurons during feeding and after ingestion were not demonstrated until the last few years. The technical advances for neuronal recordings (both electrophysiological and optical) in deep brain regions with molecule-specificity targeted cell types have gradually matured in the last decade (Chen et al., 2013; Cohen et al., 2012; Cui et al., 2013; Gunaydin et al., 2014; Ziv et al., 2013), allowing researchers to investigate specific neuronal dynamics throughout feeding bouts.

While one would expect a gradual change in the ARC AgRP and POMC neurons' activities throughout a meal mediated by hormones like Ghrelin and Leptin, surprising findings have been reported of extremely rapid modulations of both AgRP and POMC neurons upon feeding or even just the sensory detection of food items (Betley et al., 2015; Chen et al., 2015; Mandelblat-Cerf et al., 2015). The AgRP neurons are rapidly suppressed even before feeding onsets (Betley et al., 2015; Chen et al., 2015; Mandelblat-Cerf et al., 2015). The suppression magnitudes are gradually decreased across feeding bouts (Betley et al., 2015) and are correlated with food palatability (peanut butter vs. regular mouse chow or fasted vs. fed) and the accessibility of food (freely accessed vs. caged vs. hidden food) (Chen et al., 2015). The AgRP suppression also depends on learning; when a cue is paired with a food reward, the cue is sufficient to suppress AgRP neurons' activities (Betley et al., 2015), suggesting that the anticipatory

aspect of feeding is sufficient to drive this rapid modulation. The POMC neurons are also rapidly activated by sensory detection of food items, at a similar timescale as the AgRP neurons (Chen et al., 2015; Mandelblat-Cerf et al., 2015). The magnitude of activation of POMC neurons is also scaled with food palatability and food accessibility (Chen et al., 2015). These 3 studies all support the new role of ARC AgRP and POMC neurons in foraging control (driving food discovery via negative valence), instead of the putative model of feeding controls under hunger and satiety (Andermann and Lowell, 2017; Chen and Knight, 2016).

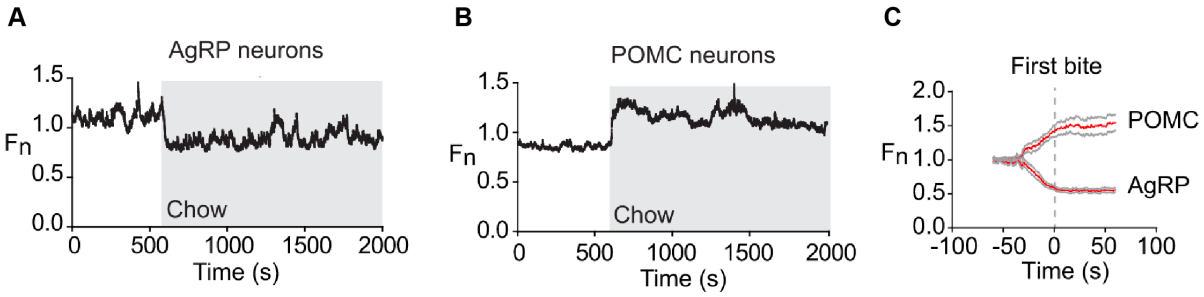

Figure 9. ***ARC AgRP and POMC neurons are rapidly modulated by feeding or the sensory detection of food.*** *(**A**) Fiber photometry recording of AgRP neurons shows reduced activity upon food presentation. (**B**) Fiber photometry recording of POMC neurons shows increased activity upon food presentation. (**C**) Neuronal activities of AgRP and POMC neurons are modulated before the first bite, suggesting sensory detection of food items is sufficient to modulate these two types of ARC neurons. Figure adapted and modified from (Chen et al., 2015).*

The food cue-driven rapid suppression in AgRP neurons is mediated by the lateral hypothalamic glutamatergic (LH^{Vglut2}) neurons (Berrios et al., 2021) onto the ventral compartment of the dorsomedial nucleus of the hypothalamus leptin receptor-expressing ($vDMH^{LepR}$) GABAergic neurons (Garfield et al., 2016), then targeting the ARC AgRP neurons. Both LH^{Vglut2} neurons and $vDMH^{LepR}$ neurons respond similarly to food cues as the rapid suppression in AgRP neurons and acute inhibition of either LH^{Vglut2} neurons or $vDMH^{LepR}$ neurons are sufficient, but not necessary, to inhibit the homeostatic feeding (Berrios et al., 2021; Garfield et al., 2016) at a similar level as inhibiting AgRP neurons directly (Stachniak et al., 2014; Vardy et al., 2015). While this circuit provides a clear inhibitory mechanism of AgRP modulation upon food cues, it is still unclear how sensory information (e.g. visual and olfactory inputs of food) is integrated into the hypothalamic circuits.

In addition to the rapid food cue modulation of AgRP and POMC neurons, there are also slower and long-lasting modulations from the nutrient responses in the gut and the restoration of energy balance (satiety) (Beutler et al., 2017; Su et al., 2017). The AgRP neuronal activity suppression upon feeding is suggested to promote learned associations between food flavors and nutrient contents postprandially (Betley et al., 2015); however, blunting AgRP suppression does not prevent, but rather potentiates, flavor-nutrient learning in a sex-dependent manner (Nyema et al., 2023). Other studies have suggested brain regions and the nervous system outside the brain are involved in flavor-nutrient learning, including the sugar-sensing cholecystokinin-expressing epithelial enteroendocrine cells (CCK-expressing EECs) in the small intestine (Bai et al., 2022; Buchanan et al., 2022), the vagal nerve nodose ganglia (Han et al., 2018; Tan et al., 2020) and the cNTS (Han et al., 2018; Tan et al., 2020; Williams et al., 2016) for food reward preference (De Araujo et al., 2020; Holman, 1975; Sclafani, 2001). Conversely, the serotonin- and substance P-expressing EECs in the small intestine (Bai et al., 2022), the insular cortex (Wu et al., 2020), and the amygdala (Zimmerman et al., 2023) are suggested for learning aversive food avoidance (Carter et al., 2015; Garb and Stunkard, 1974; Garcia et al., 1955; Garcia and Koelling, 1966; Revusky and Bedarf, 1967; Xie et al., 2022; Zhang et al., 2021a). Given the limited direct connectivity (Wang et al., 2020b), the question of whether the learning signal from AgRP neurons is directly linked to the abovementioned vesical feedback from the gut to the brain still requires more validation.

1.3. Interactions between olfaction and metabolism

Due to the close relationship between odor, food, nutrient contents, and physiological needs, olfaction and metabolic states are tightly connected. While the olfactory system also affects physiology via pheromones, I will exclusively focus on the olfaction of regular volatile odors and their relationship with energy metabolism (Jovanovic and Riera, 2022).

1.3.1. Effects of metabolic states on olfaction

It is a common heuristic experience of people that when hungry, one becomes very aware of food smells around them. Studies also support this, in that after fasting or Ghrelin injection, there is increased olfactory performance in terms of detection threshold, and discrimination in both rodents (Aimé et al., 2007; Aimé et al., 2012; Freeman, 1960; Julliard et al., 2007; Prud'homme et al., 2009; Soria-Gómez et al., 2014; Tong et al., 2011) and humans (Albrecht et al., 2009; Cameron et al., 2012; Iravani et al., 2024). In rodents, the AgRP -| PVT circuit mediates the hunger-driven olfactory enhancement, specifically with the NPY-NPY5R receptor signaling pathway (Horio and Liberles, 2021).

Food items themselves, especially ones with high nutrient contents, can also have a direct impact on the olfactory system. A high-fat diet (HFD) is a commonly used food regimen for inducing overeating and obesity in laboratory rodents for hyperlipidemia and hyperglycemia studies. Consuming an HFD affects olfactory performance in rodents (Thiebaud et al., 2014), even in the absence of obesity (Takase et al., 2016).

Under disruption of energy intake and expenditure, such as obesity, olfactory function is also affected. Poor olfactory function is associated with increased body weight (Fernández-Aranda et al., 2016; Han et al., 2021; Peng et al., 2019; Richardson et al., 2004) and visceral fat (Fernandez-Garcia et al., 2017). Interestingly, despite a generally poorer olfactory function in obese patients, they are more sensitive to food-related smells (Han et al., 2021; Stafford and Whittle, 2015) and there is a greater food odor-evoked brain activation in reward-processing areas (Han et al., 2021). This olfactory alteration may be caused by altered bodily hormones in obesity, due to the expression of receptors of Ghrelin, Leptin, IGF-1, and Insulin in the olfactory system (Baskin et al., 1983; Elmquist

et al., 1998; Gupta et al., 1992; Hill et al., 1986; Russo et al., 2018; Tong et al., 2011). However, currently, there is no clear consensus in the field on the olfactory modulatory effects of leptin (Fernández-Aranda et al., 2016; Fernandez-Garcia et al., 2017; Poessel et al., 2020a; Sun et al., 2019; Uygun et al., 2019) or insulin (Edwin Thanarajah et al., 2019; Poessel et al., 2020b).

1.3.2. Effects of olfactory experience and alterations on metabolism and physiology

The interaction between metabolic states and olfaction is not one-directional - olfaction also has direct impacts on metabolism. Smelling food odors can increase appetite tailored to the specific nutrient content in humans (Zoon et al., 2016), which is hypothesized to prepare the body for digesting the upcoming nutrients. Briefly experiencing certain non-aversive non-food odors (e.g. Osmanthus fragrans (fragrant tea olive)) can decrease appetite by decreasing the expression of orexigenic hormones and increasing the anorexigenic hormones in rodents (Yamamoto et al., 2013), while some food-odors (e.g. milk) can increase expression of orexigenic hormones and decrease anorexigenic hormones. Food odors can also affect metabolism; smelling familiar food odors is sufficient to increase lipolysis in the adipose tissues and elevate serum-free fatty acids (Tsuneki et al., 2022). Notably, a recent counter study in rodents suggested that the food smell of an HFD does not promote appetite for normal food items, nor is it required for HFD-induced obesity (Boone et al., 2021), indicating that the relationship between food odors and appetite is more indirect.

Aversive odors can have negative effects on appetite, even though this is not simply due to feeding suppression. One example is the fear-inducing 2,4,5-trimethyl thiazole (TMT, red fox urine odor), a predator odor for rodents, which increases metabolic rate and reduces diet-induced obesity with minimal alteration of food intake and locomotion (Genné-Bacon et al., 2016). The mechanism is contributed to by elevated neuronal circuits of the dorsomedial hypothalamus (DMH) -> ARC POMC neurons (Genné-Bacon et al., 2016; Lee et al., 2020a) and increased release of corticotropin-releasing hormone neurons, indicating a state of chronic stress. Interestingly, this odor-induced chronic stress can also be blocked by combining different odors like the smell of rose (2-phenyl

ethanol, 2PE) and fish (trimethylamine, TMA), activating the inhibitory neurons in the ventromedial nucleus (VMH) (Lee et al., 2022). These studies reveal that certain odors (and odor mixtures) have impacts on feeding behaviors and metabolism, regardless of the nutrient contents and valence values of these odors.

Modulations of odor perception also affect metabolism (Jovanovic and Riera, 2022); chronically decreased olfactory perception by ablation of OSN reduces body weight in mice and protects against high-fat diet-induced obesity, and conversely, increased olfactory sensitivity by Insulin-like growth factor 1 receptor (IGF-1R) knockout leads to obesity, accompanied with an elevated level of insulin resistance and more visceral fat (Riera et al., 2017). Different studies showed that super-smeller mice (voltage-gated potassium ion channel 1.3, Kv1.3, knockout) (Fadool et al., 2004) are resistant to diet-induced obesity and this resistance depends on olfactory perception (Thiebaud et al., 2014; Tucker et al., 2012), suggesting that the directionality between olfactory perception and metabolism is not solely linear. While these studies provided insights into the effects of chronic olfactory alterations on metabolism, the acute olfactory sensation during feeding remains poorly understood.

1.4. Effects of eating speed on metabolism

Feeding behavior is the main approach for organisms to obtain energy to reach homeostasis, and the feeding behavior itself is surprisingly complicated. One aspect of feeding is how fast the food is consumed, i.e., the eating speed. Eating rapidly in a short time, commonly known as binge eating, can reduce satiation (the process that leads to satiety, the satisfied feeling of being full after eating) and lead to overeating (Andrade et al., 2008; Bolhuis et al., 2013; Teo et al., 2020; Teo et al., 2021; Zeng et al., 2018).

People with an inherently higher eating speed are more likely to develop overweight and obesity (Hurst and Fukuda, 2018). In the same direction, reducing eating speed by smaller sip size or longer oral residence duration (Bolhuis et al., 2014b), or increased food hardness (Bolhuis et al., 2014a) is an effective measure for reducing food consumption and promoting weight loss.

One example of the relationship between eating speed and satiation is the “soup paradox”. Drinking energy-dense liquids, like apple juice, provides less long-term satiety compared to isocaloric solid counterparts, such as apples. However, interestingly, when eating the same food item in soup form (apple soup), the food intake rate is slowed down with spoon feeding, and the satiety effect is comparable to the solid food again and influences a stronger satiety effect in 24 hours (Mattes, 2005). The canonical explanation for reduced satiation by binge eating is suggested by the delayed negative visceral feedback from the gastrointestinal tract to the brain (Grove et al., 2022; Samakidou et al., 2023; Slyper, 2021). While visceral satiation from ingestion and absorption is uncontested, some studies have revealed that the satiation signals can also be mediated solely by flavor perception (Betley et al., 2015; Cecil et al., 1999; Chen et al., 2015; Mandelblat-Cerf et al., 2015).

The abovementioned studies demonstrated that oral exposure time is positively associated with satiety, suggesting that eating speed affects the flavor perception of food, which may in turn influence satiation. Till now, however, no study has investigated whether altering flavor perception during feeding is sufficient to reduce sensory satiation.

1.5. Aims of the study

Olfactory perception of food is crucial for feeding, and metabolic states can affect olfaction drastically. However, there is to date no knowledge of the neuronal dynamics of the olfactory system are during food intake, and how feeding speed modulates the olfactory system. In this thesis, I aimed to answer these questions:

1) What are the neuronal dynamics of the olfactory cortex during food intake?
2) How do different feeding rates affect the cortical flavor representation, and what are the potential mechanisms of the modulation?
3) How does the cortical flavor representation interact under sensory deprivation and metabolic needs?
4) Is the olfactory representation of food is functionally linked to feeding behaviors?

To probe these questions, I combined mouse genetics, stereotactic viral injections, and an *in vivo* optical recording technology (miniaturized microscope or “miniscope”) in freely moving mice to measure specific neuronal activity in real-time during feeding. Immunostaining and imaging were performed to verify cell types, viral expression efficacy, and optical implant locations. With collaborators, we built a liquid food delivery system that controled the food flavors and feeding rates. To manipulate specific neuronal populations during feeding, a closed-loop optogenetics system was employed to trigger light stimulation during feeding. I also measured neuromodulator dynamics *in vivo* during feeding by using specific neuromodulator sensors. Temporal anosmia and overnight fasting were used to alter sensory perception and metabolic states. With support from colleagues, additional *in vitro* slice electrophysiological recordings were used to verify molecular constructs and neuromodulators’ effects. To analyze neuronal activities and feeding behaviors, custom-made scripts in Python, MATLAB, and R were written to assist in data visualization and to perform statistical testing.

2. Methods

2.1. Animals

All experimental mice were housed at the animal facility (Forschungseinrichtungen für experimentelle Medizin, FEM) of the Charité. The mice were kept under a regular 12/12 hour light-dark cycle. All animal experiments were approved by the ethics committee and by the local authorities (Landesamt für Gesundheit und Soziales, LaGeSo Berlin, license numbers G0313/16, G0278/16, and G0156/20).

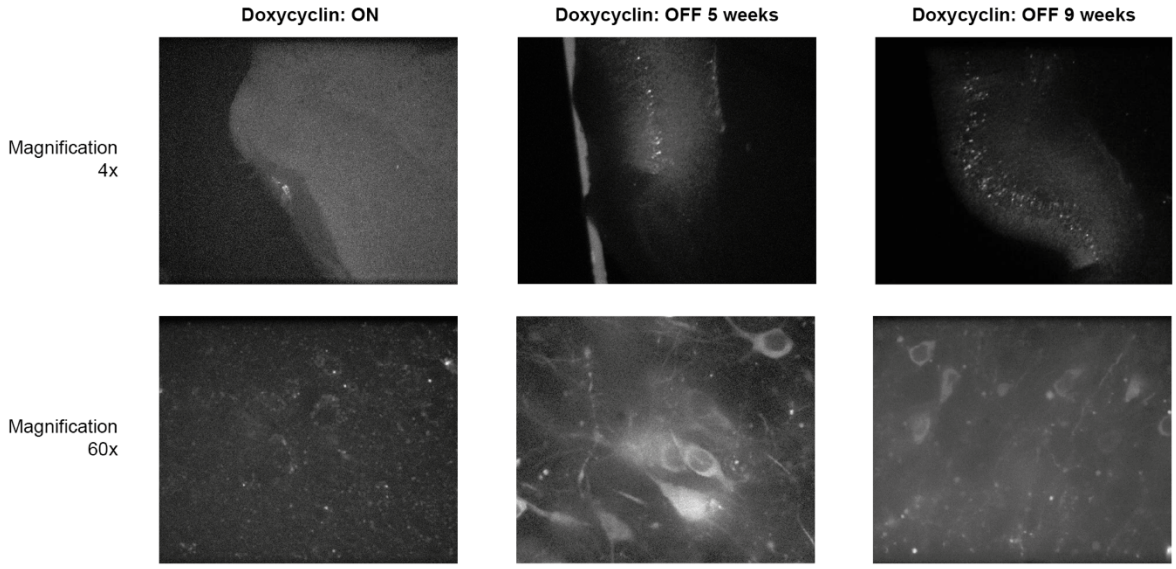

Figure 10. ***Effects of Doxycycline suppression of GCaMP6f expression.*** *When doxycycline is fed to the mice, no GCaMP6f expression is observed in the Ai93D; CaMK2-Cre; Rosa-tTA mice. After removing doxycycline-containing food, GCaMP6f expression can be observed in a few weeks.*

To perform Ca^{2+} imaging in the excitatory neurons in the aPC, I cross-bred Ai93D (TITL-GCaMP6f) mice, CaMK2-Cre mice, and Rosa-tTA mice to specifically express the Ca^{2+} indicator (GCaMP6f) in the excitatory neurons. Early expression of GCaMP during development can lead to aberrant neuronal activities such as epileptic-like events in the mouse brain (Steinmetz et al., 2017). To prevent such events, I fed the breeding pairs and the offspring with doxycycline-containing food to suppress the expression of GCaMP6f until at least 3 weeks old (Figure 10). The abovementioned transgenic mice are suitable for Ca^{2+} imaging in the aPC, but the GCaMP6f expressions in the insular

areas including the gustatory cortex (GC) are suboptimal (Figure 11). Instead, the AAV virus carrying hSyn-Cre was injected in the GC of Ai148D (TIT2L-GC6f-ICL-tTA2) mice to express GCaMP6f in the GC. To record from aPC GABAergic neurons, I virally injected the Cre-dependent Ca^{2+} indicator (hSyn-floxed-GCaMP6f) in the PV-Cre or SST-Cre mice. To image dopamine and serotonin dynamics in the aPC, I injected the dLight1.3b (Patriarchi et al., 2018) and iSeroSnFR (Unger et al., 2020) in the aPC in C57BL/6N (wildtype) mice. To monitor breathing, we attached the head bar on two C57BL/6N mice and monitored the breathing with a piezo sensor on the chest or a video track of the movement of the chest via DeepLabCut tracking (Mathis et al., 2018). For optogenetic suppression experiments, a Cre-dependent eOPN3 virus or a Cre-dependent tdTomato expressing virus was injected in the aPC in CaMK2-Cre mice. All behavioral experiments were performed between 9 a.m. and 6 p.m., including Ca^{2+} imaging and optogenetics, under regular light conditions.

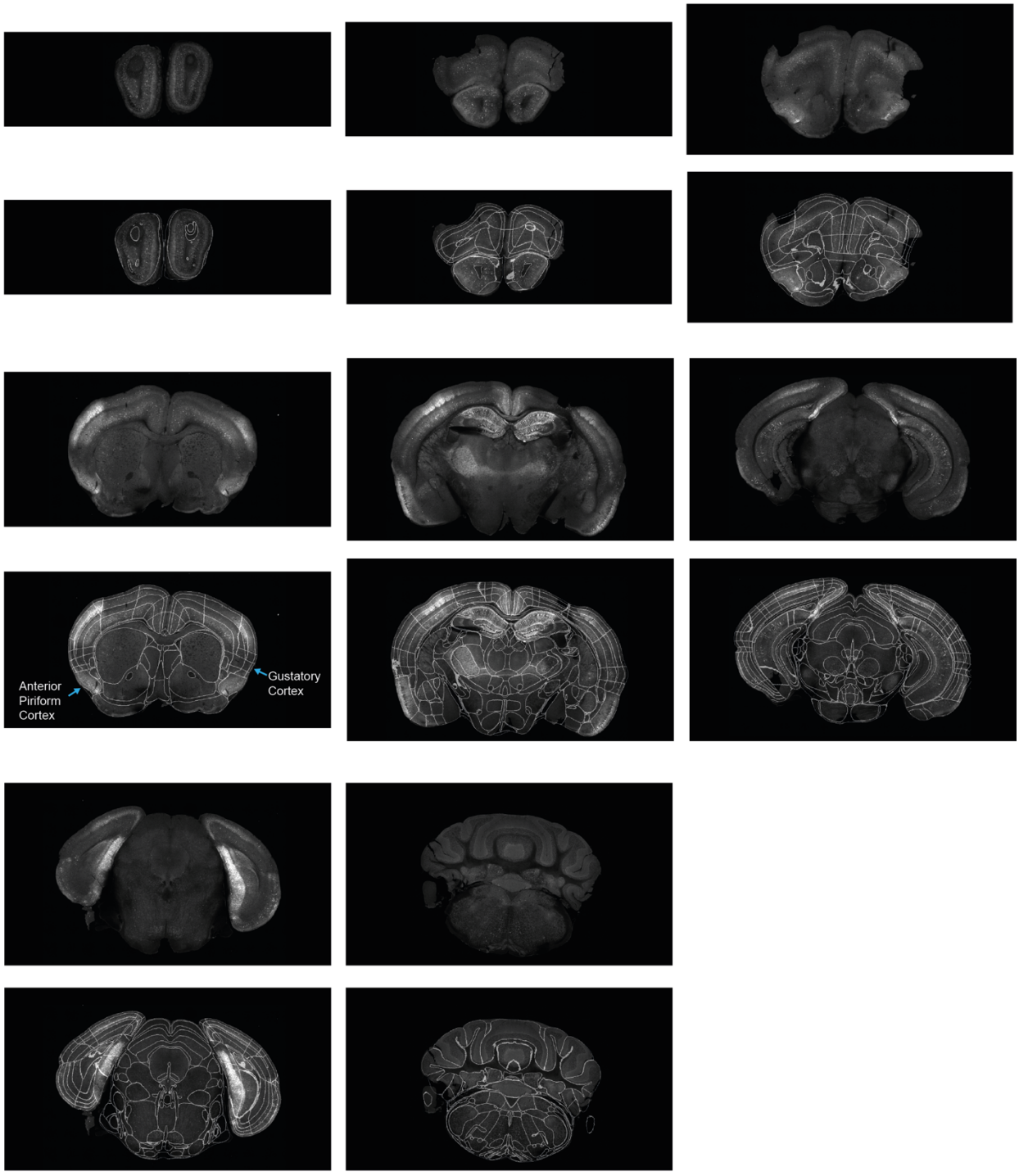

Figure 11. ***Expression of GCaMP6f in the Ai93D; CaMK2-Cre; Rosa-tTA mice.*** *Clear GCaMP6f expression can be found in the aPC, but a limited expression is observed in the GC. For each row, the upper ones are the raw images acquired with Brainsaw, and the lower ones are the same images registered to the Allen Institute Mouse Brain Atlas by BrainReg (Tyson et al., 2022).*

2.2. Liquid food delivery system

To ameliorate stress, all behavioral experiments were performed inside the mice's home cages. I modified the cages to allow the lick spout to protrude into the cage (product from Phenosys, Berlin, Germany). Each behavioral protocol started with a 5-minute baseline, and after the baseline period, the motorized lick spouts were inserted in the home cage and scheduled for liquid food or water delivery for 2 min, with intervals (1 minute) between each lick spout presentation. During intervals, the lick spouts were retracted. To isolate potential odor contaminations before feeding onsets, the lick spout was located inside a glass tube, which contains an opening for mice to reach the lick spout. An air suction was connected to the glass tube, so I could limit olfactory responses before the mice interacted with the lick spout. To monitor licking behavior, the lick spouts were equipped with piezo sensors. Each lick event triggered an activation of electrical peristaltic pumps (~400 ms for each delivery event), which resulted in pumping ~1.8 µL of liquid food (Ensure, an energy-dense artificial milkshake, made by Abbott Laboratories. In this study, both strawberry and chocolate-flavored Ensure were used) or water. After each pump delivery, a refractory delay period is introduced (for slow feeding: 4 sec, for binge feeding: 400 ms). For slow feeding rounds, Ensure and water were delivered at a ratio of 7 to 3, and the ordering was pseudorandomized. In each behavioral protocol, three binge feeding rounds and four slow feeding rounds were pseudorandomly swapped (Figure 12). All mice were fed *ad libitum* (or food presentation was withheld for up to four hours), except that once per week the mice were overnight fasted to measure neuronal responses under homeostatic deficiency.

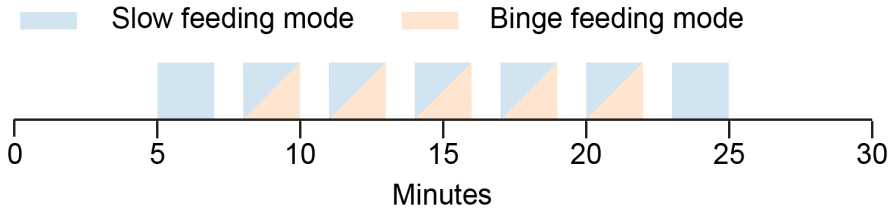

Figure 12. ***Illustration of the behavioral protocol.*** *The duration of each round of lick spout presentation is 2 mins, and the interval between each lick spout presentation is 1 min. Except for the first and the last rounds of presentation being always in slow feeding mode, the other 5 presentation blocks can be slow feeding or binge feeding mode. The sequence of the feeding mode is different in every recording session, with 3 presentations are for binge feeding mode.*

2.3. Surgery procedures

2.3.1. Stereotactic injection

For anesthesia, mice were anesthetized with isoflurane via inhalation (for induction: 4-5%, then tuned to ~1-2%. Air flow was driven by oxygen gas, with a flow rate between 0.5 to 1 L/min). Local anesthesia (1-2% Lidocaine) was injected subcutaneously. A craniotomy was operated over the stereotactically targeted regions (Table 1) using a Neurostar stereotactic apparatus (Neurostar, Tübingen, Germany). I used a 10 µL-Hamilton syringe to inject viruses (typically 0.4 to 1 µL). Operative pain was alleviated by a subcutaneous injection of Carprofen (5 mg/Kg) before the operation. Additionally, Carprofen was injected in the following 3 days after surgeries. The mice were left to recover for at least two weeks after the surgery. In some experiments, the viral injection was performed right before the implantation of the prism-attached GRIN lens or the optic fiber. For *in vivo* Ca^{2+} imaging experiments, AAVs containing floxed-GCaMP or Cre recombinase were injected into the desired brain regions (Table 3). For *in vivo* neuromodulator imaging (serotonin and dopamine), the sensors for serotonin (iSeroSnFR) or dopamine (dLight) were injected in the aPC (Table 3). For *in vivo* closed-loop optogenetics, AAVs containing eOPN3 or mCherry were bilaterally injected in the aPC (Table 3).

Table 1. Coordinates for viral injection and GRIN lens and prism implantation.

Brain regions	*Coordinates (AP/ML/DV) (mm)*	*Notes*
aPC	0.32/-3.5/5.5	For viral injection
	0.32/-3.0/5.5	For implantation, the bottom right corner of the prism as the reference
GC	0.26/-3.6/4.0	For viral injection
	0.26/-3.0/4.1	For implantation, the bottom right corner of the prism as the reference
OB	4.3 - 4.6 / ±0.6 / 0.3	For viral injection

2.3.2. GRIN lens and optical fiber implantation

The anesthesia procedure was the same as described above in the stereotactic injection (**Methods 2.3.1**). For craniotomy, a square of ~1.2 mm side length was used to fit the prism GRIN lens (1 mm diameter) (coordinates are listed in Table 1). Some brain tissues were removed by aspiration to pave the insertion tract until ~1 mm above the image site of the microscope. I used a sharp needle to perform the aspiration (23G), which was connected to a vacuum. The aspiration procedure was performed twice to ensure a sufficient removal of brain tissues. The microendoscopic GRIN lens attached with a prism (~9.1 or ~4.3 mm long based on the imaging site, 1 mm diameter, Inscopix) was inserted into the desired image plane at a rate of 100 μm/min with 10˚ angles in coronal axis (the top of the implant was tilted to the medial part and the bottom of the implant was tilted to the lateral part of the brain). I used adjusted implantation coordinates that aligned with the bottom right corner of the prism; the exact coordinates are listed in Table 1. The microendoscopic lenses attached with the baseplates (Inscopix) were fixed to the skull with an adhesive (VetBond, 3M or TRUGLUE, TRUSETAL) and dental cement (Super-Bond C&B, SUNMEDICAL). The optical surface was protected from contamination by a plastic cap (Inscopix baseplate cover). For optical fiber implants, a similar procedure was performed with a few modifications: 1) two optical fibers were implanted bilaterally with a vertical angle (no tilting), 2) the insertion speed was set to 1 mm/min, 3) one fiber (usually the left ones) was inserted first and fixed with minimal dental cement and then a second optical fiber was inserted, 4) an additional headpost was attached to the back of the skull surface with dental cement for more accessible handling of the animals, and 5) the optical fibers were protected with a plastic cap which also blocked potential pre-experimental activation of optogenetic constructs. To deal with post-surgery pain, I injected Carprofen (5 mg/Kg) subcutaneously right before the surgery, along with additional daily Carprofen injections in the three days after the surgical procedure. In some mice, the microendoscopic lenses were not pre-fixed with the baseplates (materials compatible with the early version of the Inscopix miniscope). The optical surfaces of the microendoscopic lenses were secured with a silicone cap. A follow-up surgery attaching the baseplate for the miniscope was performed in 3-4 weeks after the GRIN lens/prism implantation.

2.3.3. Cranial window for olfactory bulb imaging

This part of the surgical procedure was performed collaboratively with the Larkum lab (Humboldt-Universität zu Berlin) and Judkewitz lab (Charité – Universitätsmedizin Berlin). We anesthetized wild-type mice (C57BL/6, <P40) with inhalation isoflurane (4-5% for induction, 1-2% for maintenance with oxygen gas, flow rate 0.5-1 l/min). We injected subcutaneously 1-2% Lidocaine for local anesthesia. We first removed the scalp and periosteum and created a 3 mm craniotomy on top of the two olfactory bulb hemispheres. We used an injection micropipette (tip diameter ~10–20 µm) for viral injection, which was filled with AAVs containing the construct of the non-Cre-dependent Ca^{2+} indicator GCaMP7s (Table 3). We injected 100 nL of virus in each bulb hemisphere with a 50 nL/min rate (Table 1). We then placed a semi-circular <3 mm stack of two glass coverslips (these two coverslips were glued using optical adhesive) into the craniotomy. The craniotomy was then sealed with dental cement. We further attached a headpost to the skull with adhesives (light-curing RelyX, 3M) for head-fixed 3-photon imaging. We injected subcutaneously Buprenorphine (0.1 mg/Kg) mixed with Carprofen (5 mg/Kg) right before surgery to manage surgical pain. Additional Carprofen (5 mg/Kg) injections were performed daily for three days after the surgery. We started habituation of the head fixation three weeks after the surgery.

2.4. *in vivo* Ca^{2+} imaging

2.4.1. Habituation

For freely moving recordings, I habituated the mice in their home cage with licking from the lick spout with 10% sucrose solution before the actual imaging sessions. In each habituation protocol, mice were exposed to a slow feeding mode paradigm where the lick spout was presented to the mice for 40 minutes after the 5-minute baseline. In the second week of habituation, I placed the glass tube (which was connected to an air suction device) around the lick spout. In the third week, I mounted the dummy scope on the mice so they could get used to the weight of the miniscope and handling before the imaging sessions.

For head-fixed recordings (in collaboration with the Larkum lab at Humboldt-Universität zu Berlin) and Judkewitz lab at Charité – Universitätsmedizin Berlin), we habituated mice for head-fixation five days before the imaging sessions. We gradually increased the head-fixation duration from five minutes to one hour from the first day to the last day before the imaging session. We also presented Ensure in a lick spout to the mice in the later habituation days so that the mice had already learned how to use the lick spout before the imaging sessions.

2.4.2. *In vivo* miniscope imaging

I mounted the miniaturized microscope (nVista 2 or nVista 3 miniscope, Inscopix, CA, USA) to the implanted mice without anesthesia. Mice could rest in the home cage for a few minutes before the recording session started. The recording session started with a baseline period in which the lick spout was not presented to the mice (5 min), and then the lick spout was inserted into the home cage to present the slow feeding and binge feeding paradigms (Figure 12). For individual mice, the Ca^{2+} or neuromodulator imaging settings (including LED intensity, imaging gain, focus of the imaging panels, field of views, etc.) were separately tuned to aim for a common level of brightness of the imaged fluorescence (around 50-60 A.U. for the mean values in the fluorescence histogram panel in the Inscopix acquisition software). For all recordings, the sampling rate was kept at 20 Hz with a single focal plane, regardless of whether the recordings were for Ca^{2+} imaging or neuromodulator imaging. To save storage space, around 90% of the imaging sessions were spatially down-sampled (4x) online during data acquisition, which still provided good imaging quality for further extraction of the region of interest (ROIs were for both individual cells or areas with neuromodulator sensor expression). I coupled the behavioral system (Phenosys, Berlin) to the Inscopix imaging system by synchronizing the pump delivery TTL pulses. I imaged each mouse for up to twenty-five sessions across five weeks. I performed overnight fasting (~20 hours) once per week for the implanted mice to measure neuronal dynamics under metabolic needs.

2.4.3. *In vivo* 3-Photon imaging

This part of the experimental procedure was performed collaboratively with the Larkum lab (Humboldt-Universität zu Berlin) and Judkewitz lab (Charité – Universitätsmedizin Berlin). Mice were head-fixed in a home-built 3-photon microscope to perform Ca^{2+} imaging in the olfactory bulb. Light pulses (wavelength at 1300 nm) were delivered from a laser (Opera-F, pumped by Monaco, Coherent). We used a repetition rate at 1MHz for excitation of the Ca^{2+} indicator jGCaMP7s. The laser output passed a four-pass prism pulse compressor for dispersion compensation. We adjusted the laser power via a motorized half-wave plate and a polarizing beam splitter. The output power from the objective (Nikon 25x/1.1) was lower than 20 mW. We used dual linear galvanometers to acquire images at a ~10 Hz frame rate. We synchronized the image acquisition with the laser pulses and controlled the acquisition with LSMAQ (https://github.com/danionella/lsmaq). Image stacks (time-series movies, 200 x 200 pixel size) were recorded at depths of ~ 200-300 µm below pia, to aim for the olfactory bulb mitral cell layer.

2.5. Triton X-100 application

It was previously reported that nasal lavage with 0.5% Triton X-100 solution (in 0.1M PBS) can induce temporal anosmia in rodents for up to 3 weeks (Cummings et al., 2000). Here, with support from Dr. Friedrich Johenning and Anke Schönherr, we perform the nasal lavage procedure to temporally block olfactory sensation in mice. Mice were anesthetized with an intraperitoneal injection of Ketamine (100 mg/Kg), Xylazine (20 mg/Kg), and Acepromazine (3 mg/Kg). Additional analgesia is delivered by subcutaneous injection of Caprofen (5mg/Kg) right before the nasal lavage and the day after. We performed two groups of experiments with different solutions - the Triton X-100 (experimental group) or PBS (control group) applications. We injected ~40 µL of 0.5% Triton X-100 solution to each nostril, via a gel loading pipette tip, which was protruded 2-3 mm into the nostril. We slowly applied the Triton X-100 solution with a micropump (Narishige, Japan), and the overall procedure took several minutes for each nostril. Between applications on each nostril, we allowed a 5-minute interval. We indicated whether a procedure was successful by observing foams building up at the nostril opening. Mice were kept on an inclined plane throughout the operation and until they woke up so that their nostrils were below their

trachea and lungs to prevent excessive solution from entering the air track. All procedures were performed in a heated chamber to maintain body temperature.

2.6. Buried food test

To verify whether the Triton X-100 application in the nostril indeed induced anosmia, Dr. Friedrich Johenning, Anke Schönherr, and I examined the ability of anosmic mice to find a buried food pellet (sucrose pellet, TestDiet, 181125, 5TUT) located 1 cm underneath the bedding materials in the cage. To motivate mice to search for the hidden food pellet, mice were overnight food-deprived and habituated to the experimental cage (~5 minutes) before the experiment started. Mice were removed from the experimental cage, and we then buried the food pellet in the experimental cage. Mice were then transferred back into the experimental cage. The latency to find the pellet was measured by an experimenter with a stopwatch. The mice were allowed to find the food pellet for up to 15 minutes; if they failed to find it, the session was stopped. The same task was applied to the control mice that underwent the same nasal lavage procedure with 0.1M PBS. We repeated the buried food tests weekly to monitor the mice's olfactory capability and ensure that the mice remained anosmic throughout the imaging sessions.

2.7. Respiration monitoring

To monitor the respiration of mice during feeding, I built a head-fixed setup where mice could drink from a lick spout. A camera facing the mice monitors on the side and a piezo sensor is attached to the mice's chest. The mice are habituated with the head fixation and lick spout for 5 days before the recording. The movie is then processed with DeepLabCut (Mathis et al., 2018) to mark body parts including eye, nose, chest_1, chest_2, chest_3, chest_4, and back. The movement from the chest is used as a proxy for respiration. The extracted pixel movement is filtered with Hilbert-Huang transform (PyHHT, Python) to remove the general movement from the mice's body position.

2.8. Closed-loop optogenetics

Like the Ca^{2+} imaging experiments, I habituated the implanted mice to the lick spout that delivers 10% sucrose solution for 4-5 days before starting the closed-loop optogenetics experiments using Ensure. Mice were habituated firstly without mounting the optical fibers for one day and then on the following days with mounting fibers. They needed to reach the criteria that they could successfully trigger sham closed-loop triggers (at least 3 pump events with a maximum of 1.5 seconds inter-delivery interval) in one habituation session (~15-20 minutes) so that I would considered that they had learned how to use the lick spout. Before the optogenetics experiment, I mounted a splitter patchcord (200 µm diameter, NA 0.57, Doric) to the optical fiber cannulas on the implanted mice. The patch-cord was connected to a mono fiber optic patchcord (480 µm diameter, NA 0.63, Doric). Mice were then returned to their home cage and allowed to explore for a few minutes. The light was emitted from a light source (Ce:YAG, Doric), with an intensity of ~8 mW at the tip of the fibers. Mice had free access to the lick spout throughout the 1-hour experiments (except for the first five minutes of baseline). When a binge feeding bout was detected (defined here as 3 pump deliveries with a maximum of a 1.5 s inter-delivery interval), a light stimulation was activated (one pulse of 500 ms light, white light) on the "LED on" days (even sessions). After the light stimulus was delivered, I introduced a refractory period (10 seconds) to halt binge bout detection and subsequent LED activation. Binge bout detection was back online after the refractory period. The overall procedures were the same on "LED off" days (odd sessions), except that the light source was decoupled with the binge feeding bout detection so that no light was triggered. The LED off and on days were repeated for 6 sessions for each condition (12 days total).

2.9. Imaging processing

I temporally down-sampled the Ca^{2+} videos obtained from the *in vivo* miniscope recordings to 10 Hz (recommended for the *CNMFe* detection algorithm). A quick $\Delta F/F$ movie was generated and I produced a maximum-projected image of the movie to obtain a rough spatial distribution of the active cells. The image was used to outline the field of view (FoV) where the active Ca^{2+} transients were visible. The rest of the image outside this FoV was then cropped out to save computing time for the following movie processing steps. The same cropping parameters were used for the same mice on different experimental dates to obtain consistent FoV in processed outputs. Before cell detection, videos

were first spatially bandpassed (low cutoff = 0.005, high cutoff = 0.500, computed in Inscopix IDPS) and then motion corrected (the first frame of the video or the mean image of the video was used as a reference frame for alignment, max_translation = 20, computed in Inscopix IDPS). I then used *CNMFe* (Giovannucci et al., 2019; Zhou et al., 2018) to detect active neurons in the FoV. The parameters were fed into the algorithm (Cell diameter=10 px, PNR=10 for excitatory cells and 20 for GABAergic cells, Corr=0.8) and this algorithm is implemented in the Inscopix IDPS. Ca^{2+} traces from individual extracted neurons were then manually curated with the predefined selection criteria (i.e., the peak amplitude of trace >80 A.U., drifting in trace baseline was no larger than 20% of peak values, clear shapes, position in distance to nearby blood vessels, minimal motion artifacts of the given cells). For neuromodulator imaging (iSeroSnFR and dLight 1.3b), the raw images were also downsampled to 10 Hz. Importantly, the spatial filter was not applied, as due to the slow kinetics of neuromodulators and the corresponding sensors, the filter would have removed the actual dynamics. Motion correction and calculation of the difference in fluorescence signals ($\Delta F/F$) were performed, and an ROI was drawn to capture the FoV where the patch has the strongest fluorescence. Additional detrending of the extract fluorescence traces was applied to remove the potential bleaching (Python, BaselineRemoval package).

Movies acquired from the head-fixed 3P imaging were processed with Suite2P (Pachitariu et al., 2016) for the following actions; motion correction, segmentation of region-of-interests (ROIs), and extraction of Ca^{2+} traces. The following processed images were used to aid the manual curation of the putative OB mitral cells; the ‘mean img’, the ‘correlation map’, and the ‘max projection’ views of the given movie in Suite2P. I analyzed the extracted Ca^{2+} traces in Python. I removed neuropil signals to reduce background contamination from other neurons. If a certain frame had higher motion artifacts (based on the post-registration x and y shifts at individual frames), I excluded those time points and interpolated the missing value from the nearest time points. An additional filtering criterion was when the phase correlation was below 50% of the maximum phase correlation between the reference frame and individual frames. The processed Ca^{2+} traces were used to calculate $\Delta F/F$ and the z-scored time series (see processing scripts in the GitHub repository for details).

2.10. Data analysis, statistical analysis, and data point illustration

I wrote customized scripts to analyze and perform statistical analysis on the acquired data; the scripts were mostly in Python (Numpy, Scipy, Dabest, etc.), with additional ones in R (Lmer, Emmeans) and MATLAB (image registration). A table of all statistical tests performed in individual figure panels can be found in the statistical summary (Table 6), with sample size (e.g. number of cells, number of sessions, number of animals, etc.) and statistical results (e.g. correlation coefficient and P values of Pearson's r, linear mixed models, effect sizes…etc.). I plotted most figures in Python (matplotlib, seaborn) and some in R (ggplot). The figures were then imported into Illustrator (Adobe) to adjust their appearance (including text font, size, legend alignment, etc). To increase the accessibility for common forms of color blindness, I chose the Okabe-Ito color palette (Ichihara et al., 2008) for visualizing categorical data.

2.10.1. Data synchronization

I coupled the miniscope system with the behavioral rig and with the BNC cables so that I could synchronize these two systems by aligning the time stamps of TTL pulses generated by each pump activation. An additional camera was synchronized via miniscope triggers so that the overall behaviors were recorded at 20 Hz, synchronized with the Ca^{2+} data.

2.10.2. Identification of binge feeding bout detection and slow feeding processing

I defined a binge feeding bout with the following parameters: the inter-pump interval was shorter than three seconds, and each bout contained at least three pump activations. If the above two criteria were not met, the feeding events were discarded.

To ensure that the neuronal responses I measured were linked to the feeding behaviors, each pump event in the slow feeding paradigm was excluded if no further lick event following the pump delivery, meaning no active licking after the food was delivered. I did not perform additional exclusion on binge feeding bouts, since due to the nature of the

behavior, binge feeding bouts were guaranteed to have active feeding/licking events during the feeding bouts. Initial motor artifacts in the lick events caused by the physical lick spout movements were excluded from the lick events.

2.10.3. Area Under the Receiver Operating Characteristics Curve (auROC)

I employed the auROC analysis to cluster neurons based on their responses to food and water deliveries. For individual neurons, I compared the distribution of Ca^{2+} fluorescence values during baseline activity (-1 to 0 seconds before food delivery) to the distribution of Ca^{2+} fluorescence values in each time bin (100 ms) across all trials (from -1 to 5 seconds). For each time bin, a ROC curve was calculated by a moving threshold from the pooled minimal to the maximal Ca^{2+} fluorescence values from both the baseline distribution and the distribution from a given time bin. The probability of Ca^{2+} fluorescence values larger than the threshold from the given time bin (p(time_bin)>threshold) was plotted against the baseline probability (p(baseline)>threshold), which produced the ROC curve for this time bin. The area under the ROC curve was measured and produced an auROC value (range from 0 to 1, and the midpoint 0.5 means no specific response on this time bin). The same process was applied for all the time bins to generate an auROC trace for each neuron. To classify neurons that have positive responses to food, auROC values from the first 2 seconds after delivery onset were compared with the baseline auROC values, and if at least four consecutive time bin values were greater than mean plus 2 S.D. of baseline values, this neuron was considered a food/water activated neuron.

2.10.4. Effect size calculation

For the effect size of feeding-induced modulation, I utilized bootstrap-based estimation statistics (DABEST, Python). The mean difference between binge feeding and slow feeding was bootstrapped (resampled with replacement, meaning the same data points can be resampled again) 5000 times so that I could generate a distribution of the mean difference of these two conditions (illustrated as a violin plot in the figures). To present values in units of Cohen's d, the distribution was divided by the pooled S.D. of both conditions (Dabest.cohens_d, Python). To calculate P values, I used the permutation test (Dabest.PermutationTest, Python)

2.10.5. Q value calculation

To compare two neuronal time series data across the temporal axis, I used the Q values to represent the significantly different time bins. The Q values were calculated from the P values obtained from the Student's t-test (scipy.stats.ttest_ind, Python) and then adjusted with the false discovery rate (statsmodels.stats.multitest.fdrcorrection, Python). For visualization, different Q values were plotted with different thicknesses on top of each time series data (thin, Q<0.05, medium, Q<0.01, thick, Q<0.001).

2.10.6. Linear Mixed Models

My neuronal and behavioral data were highly nested (multiple cells/sessions from one mouse), so treating each observation as independent units might have largely overestimated the statistical power of the data. To consider the internal difference in each mouse (e.g. the magnitude of modulation on different feeding trials, sex, body weight, the general preference for liquid food etc.), I employed the linear mixed model (also called mixed effect model, lmer, R) to estimate the true contribution of a given factor among other factors while adjusting different intercepts and slopes for individual mice. A full model [1] was fitted including all potential factors (and the appropriate interaction between them), and a reduced model [2] lacking a given factor (e.g. the interaction of virus types (tdTomato vs. eOPN3) and LED states (with vs. without light stimulation)) was also fitted in the same way. I then compared these two models to estimate the contribution of the given factor (the interaction of virus types and LED states) to the whole model, where I could measure the P values of the given predictor. A contrast comparison was also performed to compare the differences between groups using marginal means/contrasts with multi-testing corrections (Emmeans, R). Representative fitted models were structured as follows:

Full model

$$Food.consumption \sim 1 + Body.weight + Baseline.time + Sex + Optogenetic.actuator + LED.state + Optogenetic.actuator \times LED.state + (1 \mid Mouse.id) \quad [1]$$

Reduced model (without the interaction)

$$Food.consumption \sim 1 + Body.weight + Baseline.time + Sex + Optogenetic.actuator + LED.state + (1 \mid Mouse.id) \quad [2]$$

2.10.7. Statistical analysis

To report statistical measurements, the mean and standard error of the mean (s.e.m.) and the 95% confidence interval, unless indicated otherwise, were used in the thesis. For the box plot, the center line indicates the median of the data, the box itself represents the 1st and 3rd quartiles of the data, the whiskers show the 1.5x interquartile range from 1st and 3rd quartiles, and the individual points outside the whiskers represent the outliers. Applied statistical tests and the sample size for each statistical analysis are listed in the statistical summary table (Table 6). For null hypothesis testing, I used a significance level of $P < 0.05$ to reject the null hypothesis. Sample sizes were not predetermined. Blinding was not applied, since all experiments (viral injection, implant surgeries, animal behaviors. Etc.) were performed by myself. Therefore, it was challenging to blind myself from the mice I had already worked on (with the presence of visible earmarks). I performed statistical analysis in both Python (linear model, t-test, permutation test, etc.) and R (linear mixed model, marginal means, etc.). All analysis scripts and source data for figures and tests can be found in my GitHub repository (https://github.com/hung-lo/BingeFeeding_2023).

2.11. Slice preparation for *in vitro* electrophysiology

Acute mouse brain slices were prepared from C57BL/6N mice for dopamine modulation experiments, and from CaMK2-Cre mice for the *in vitro* validation of viral injected flox-eOPN3. Both sexes of mice were used, and for the dopamine modulation experiments the mice were around P28-35, while for the optogenetics experiments the mice were around 2-3 months old by the time of experiments, which is 3-4 weeks after the viral injection. Brains were sliced in coronal orientation, with a slight angle to preserve dendritic structures (Moreno-Velasquez et al., 2020). Brains were harvested in ice-cold artificial CSF containing sucrose (sucrose ACSF; pH 7.4). Brains were sliced coronally at 300-µm

thickness and incubated at 34˚C for 30 minutes. The brain slices were then transferred to the standard ACSF solution at room temperature. After another 30 minutes of incubation, the slices were ready for electrophysiological recordings.

Sucrose ACSF

Reagents	Concentration (mM)
NaCl	87
$NaHCO_3$	26
glucose	10
KCl	2.5
$MgCl_2$	3
NaH_2PO_4	1.25
$CaCl_2$	0.5
sucrose	50

Standard ACSF

Reagents	Concentration (mM)
NaCl	119
$NaHCO_3$	26
glucose	10
KCl	2.5
$MgCl_2$	1.3
NaH_2PO_4	1
$CaCl_2$	2.5

2.12. *In vitro* electrophysiology

All experiments, including whole-cell current and voltage clamp, were conducted at 32–34°C. An Axon Multiclamp 700B amplifier (Molecular Devices) was used for the electrophysiological recordings. I filtered the signals with at 2 kHz and digitized the signal at a 20 kHz sampling rate (BNC-2090, National Instruments Corporation). I filled the glass pipettes (resistance 3–6 MΩ) with an intracellular solution. I did not correct for liquid junction potential. In the current clamp, I compensated the bridge balance. If a cell had a resting membrane potential above -60 mV or if the series resistance was larger than 30 MΩ, the cell was discarded. No holding current was applied for the dopamine modulation experiments, and cells for the eOPN3 experiment were held at -60 mV, with a maximal 200 pA injected current. For both experiments, layer 2b (superficial pyramidal) aPC neurons, except for 1 interneuron, were patched based on their morphology and location in the aPC. For the dopamine experiments, 10 µM of dopamine was applied in the bath and incubated for 5 minutes before starting recording. For current inject protocols, the injected current was tuned in the range of 80-150 pA to aim for triggering ~3-5 action

potentials for baseline conditions, and each current stimulation was repeated 6 times under both baseline and dopamine wash-in conditions. For the voltage clamp experiments, the strength of layer 1b recurrent fiber stimuli was tuned to aim for robust EPSC (~200-600 pA) being able to observed. A paired-pulse protocol with a 40 ms inter-pulse interval is used. For optogenetics light stimulation, a single flash of 550/580 nm LED light for 500 ms is shined onto the brain slice with ~10 mW/mm^2 intensity.

Intracellular solution

Reagents	Concentration (mM)
K-gluconate	135
KCl	6
HEPES	10
EGTA	0.2
$MgCl_2$	2
Na-ATP	2
Na-GTP	0.5
phosphocreatine Na (pH 7.3)	5
biocytine	0.2%

2.13. Histology, immunostaining, and imaging

Before perfusion, mice were anesthetized with intraperitoneal injection of Ketamine (100 mg/Kg) and Xylazine (15 mg/Kg) and perfused in the heart with 0.1 M PBS (pH 7.4) followed by 4% paraformaldehyde (PFA). Brains were harvested and stored in 4% PFA at 4˚C overnight and transferred to 0.1M PBS for long-term storage. For implanted mice, the brains were kept in the skull in PFA at 4˚C overnight and then for at least 1 day in 0.1M PBS at 4˚C before removing from the skull. This prevents damaging the brain before fixation takes place. For immunostaining, brains were embedded in 4% agar-agar and sliced coronally or sagittally at 100-150 µm thickness with a vibrating microtome (Leica Microsystems, VT 1200S). Brain sections were washed with 0.1M PBS for 5 minutes, repeated 3 times, and incubated with a blocking solution containing 5% NGS (Biozol), 1% Triton-X100 (Sigma-Aldrich), and PBS for 1-2 hours at room temperature with gentle shaking. I diluted the primary antibodies (all antibodies are listed in Table 2) in a similar

blocking solution (2.5% NGS, 1% Triton-X100, PBS). The incubation time for primary antibodies was around 48-72 hours at 4˚C with gentle shaking. Before applying the secondary antibodies, sections were washed 2-3 times, for 10-20 minutes each in 0.1 M PBS at room temperature with gentle shaking. The secondary antibodies were diluted in the 0.5% Triton PBS solution (dilution factors are listed in Table 2) and sections were incubated in the solution at room temperature for 2-3 hours with gentle shaking. Brain sections were then washed with PBS 3 times, for 10 minutes in 0.1 M PBS at room temperature with gentle shaking. Finally, the brain sections were mounted on the glass slides in the mounting medium without or with DAPI staining (Mowiol or NucBlue, Molecular Probes).

Mounted sections were imaged by with an upright epifluorescence microscope (Leica DMi8) or an upright confocal microscope (confocal microscope, Leica SP5). The following laser lines were used to illuminate fluorescent samples through a 20x or 40x immersion objective (0.7 NA; Leica Microsystems): 405 nm (diode), 488 nm (Argon laser), 568 nm (solid state), and 633 nm (Helium, Neon). For cell counting, 25 µm stacks were taken with a 0.64 µm z step size. For each mouse, at least 3 brain sections were imaged with at least 2 field-of-views. The acquired image stack was then maximum projected at the z-axis. The acquired images were then manually aligned to the mouse brain atlas (Paxinos and Keith B. J. Franklin, 2007) for registering the implant path of the GRIN lens/prism or the fiber optic cannula.

Table 2. Antibodies used in this thesis.

1˚ Antibodies	*Species*	*Dilution*	*Supplier, catalog*
GFP	Chicken polyclonal	1:1000	Abcam, ab13970
Tbr1	Chicken polyclonal	1:100	Millipore, AB2261
2˚ Antibodies	Species	Dilution	Supplier, catalog
Alexa 488	Goat anti chicken	1:1000	Invitrogen
Alexa 647	Goat anti chicken	1:500	Invitrogen

2.14. Serial 2-Photon tomography (Brainsaw)

Some fixed mice brains were simultaneously sliced and imaged by serial 2P tomography, which can image the whole brain structures with cellular resolutions (Ragan et al., 2012). A custom-made 2P microscope (COSYS, UK) was controlled with the BakingTray software built in our laboratory (ScanImage & BakingTray, MATLAB, https://bakingtray.mouse.vision/). For each imaging round, an automatic vibratome cut off a 40 μm thick brain section, and a tile of images was acquired with the 2P microscope at 5-8 optical depths. The acquired images were stitched into one tiff file for each optical section (StitchIt, MATLAB). I then aligned the image stacks to the Allen mouse brain atlas CCFv3 with 10 to 25 μm resolution (BrainReg, Python), detected fluorescent protein-expressing (e.g. GFP, GCaMP…etc) cells (Cellfinder, Python), and visualized them with napari (Python).

2.15. Fluorescence image processing: cell counting

To count cells that are positively stained with given antibodies or genetically expressed fluorescent proteins, I imported the z-projected images into CellPose (Stringer et al., 2021) and trained the software to identify positive neurons. After successfully identifying cells, an output cell mask image would be generated. To load the output cell mask into ImageJ/FIJI, I used the LabelToRois tools, a plug-in tool in the ImageJ/FIJI, which enabled me to convert the mask image into ROIs and import them into the ROI manager in ImageJ/FIJI for identifying the overlapping cells (script adapted from (Waisman et al., 2021)). To better visualize the outcome, auto coloring and boundary drawing were

performed with the “Label to RGB” function and the “Label to boundary” function in the MorphoLabJ toolset (Legland et al., 2016).

2.16. Materials/reagents/software/packages

2.16.1. Virus and construct

Table 3. Virus and DNA constructs used in this thesis.

Reagent or resource	*Source*	*Identifier (RRID)*
AAV1 *pAAV.Syn.Flex.GCaMP6f.WPRE.SV40*	Virus: Addgene	100833-AAV1 RRID:Addgene_100833
AAV8 *pAAV-Syn-iCre-RFP-WPRE*	Plasmid: Charité viral core Virus: Charité viral core	ID: BA-48c
AAV1 *pGP-AAV-syn-jGCaMP7s-WPRE*	Virus: Addgene	104487-AAV1 RRID:Addgene_104487
AAVrg *pGP-AAV-syn-FLEX-jGCaMP7f-WPRE*	Virus: Addgene	104492-AAVrg RRID:Addgene_104492
AAVrg *pAAV-Syn-iCre-RFP-WPRE*	Plasmid: Charité viral core Virus: Charité viral core	ID: BA-48i
Rabies virus *Switch-Cre*	Plasmid: Charité viral core Virus: Charité viral core	Charité viral core id: BRV-14a
Rabies virus *Switch-Flpo*	Plasmid: Charité viral core Virus: Charité viral core	Charité viral core id: BRV-29
HSV *hEF1α-LS1L-GCaMP6f*	Virus: Massachusetts General Hospital, Gene delivery technology core	MGH core id: RN-506
AAVrg *pAAV-Syn-ChR2(H134R)-GFP*	Virus: Addgene (courtesy of AG Larkum)	58880-AAVrg RRID:Addgene_58880
AAV9 *pAAV-hSyn-Flex-OPN3-mScarlet-minWPRE*	Plasmid: Charité viral core Virus: Charité viral core	Charité viral core id: BA-575b
AAV9 *hSyn-flox-tdTomato*	Plasmid: Charité viral core Virus: Charité viral core	Charité viral core id: BA-234a
AAV9	Plasmid: Addgene	RRID:Addgene_128485

pAAV-CAG-iSeroSnFR-Nlgn AAV9	Virus: Charité viral core	BA677a
	Plasmid: Addgene	RRID:Addgene_128486
pAAV-CAG.FLEx.iSeroSnFR-PDGFR AAV9	Virus: Charité viral core	BA678a
	Plasmid: Addgene	RRID:RRID:Addgene_125560
pAAV-CAG-dLight1.3b	Virus: Addgene (courtesy of AG Larkum)	Addgene viral prep # 125560-AAV9

2.16.2. Mouse line

Table 4. Mouse lines used in this thesis.

Reagent or resource	*Source*	*Identifier (RRID)*
C57BL/6N	Charité Central Animal Facility	N/A
Ai93D *Ai93(TITL-GCaMP6f)-D*	JAX	RRID:IMSR_JAX:024103
Rosa-tTA	JAX	RRID:IMSR_JAX:011008
Ai148D *Ai148(TIT2L-GC6f-ICL-tTA2)-D*	JAX	RRID:IMSR_JAX:030328
Ai210 *Ai210(TITL-GC7f-ICF-IRES-tTA2)*	JAX	RRID:IMSR_JAX:037378
CaMKII-CreT29	JAX	RRID:IMSR_JAX:005359
PV-Cre	JAX	RRID:IMSR_JAX:008069
SST-Cre	JAX	RRID:IMSR_JAX:013044

2.16.3. Software

Table 5. Software used in this thesis.

Software	*Source*	*Identifier (RRID)*
FIJI/ImageJ	(Schindelin et al., 2012; Schneider et al., 2012)	RRID:SCR_002285 Version: 2.14.0/1.54f
Python	Python Software Foundation (van Rossum and de Boer, 1991)	RRID:SCR_008394 Version: 3.9
Numpy	(Harris et al., 2020)	NumPy, RRID:SCR_008633 Version: 1.21.5
Matplotlib	(Hunter, 2007)	MatPlotLib, RRID:SCR_008624 Version: 3.5.1
Seaborn	(Waskom, 2021)	seaborn, RRID:SCR_018132 0.12.2
Scikit-learn	(Pedregosa et al.)	scikit-learn, RRID:SCR_002577 Version: 1.1.1
Statsmodels	(Seabold and Perktold, 2010)	statsmodel, RRID:SCR_016074 Version: 0.13.5
Scipy	(Virtanen et al., 2020)	SciPy, RRID:SCR_008058 Version: 1.8.0
Dabest	(Ho et al., 2019)	Version: 0.3.1
CNMFe/CaImAn	(Giovannucci et al., 2019; Zhou et al., 2018)	Calcium Imaging data Analysis, RRID:SCR_021533 Git forked version: https://github.com/flatironinstitute/CaImAn.git @7dc5b42ab06c6a6b86ff1520dfc5b2334f335a78
Inscopix CNMFe wrapper		https://github.com/inscopix/isx-cnmfe-wrapper@v1.2
Inscopix CNMFe	Inscopix	https://github.com/inscopix/inscopix-cnmfe
Inscopix python API	Inscopix	

Software	*Source*	*Identifier (RRID)*
Inscopix Data Processing Software v1.31, v1.6.0, v1.8.0	Inscopix	
Inscopix Data Acquisition System	Inscopix	Version: 1.3.1
Bonsai	(Lopes et al., 2015)	Bonsai, RRID:SCR_021512 Version: 2.4.0
FlyCapture2		Version: 2.11.3.425
Pyanpple	(Viejo et al., 2023)	Version: 0.3.1
LSMAQ		https://github.com/danionella/lsmaq
Suite2P	(Pachitariu et al., 2016)	https://github.com/MouseLand/suite2p RRID:SCR_016434
StichIt		https://github.com/SainsburyWellcomeCentre/StitchIt
BrainReg	(Tyson et al., 2022)	https://github.com/brainglobe/brainreg
Cellfinder	(Tyson et al., 2021)	https://github.com/brainglobe/cellfinder
BackingTray		https://github.com/SainsburyWellcomeCentre/BakingTray
R	(Team, 2022)	Version: 4.2.2 RRID:SCR_001905
Rstudio	(Team, 2020)	Version: 2022.12.0+353 RRID:SCR_000432
lme4	(Bates et al., 2015)	Version: 1.1.31 RRID:SCR_015654
Illustrator	Adobe	v27.4.1, 2023 RRID:SCR_010279
Cellpose	(Stringer et al., 2021)	https://www.nature.com/articles/s41592-020-01018-x
LabelsToRois	(Waisman et al., 2021)	https://www.nature.com/articles/s41598-021-91191-6
MorphoLibJ	(Legland et al., 2016)	https://imagej.net/plugins/morpholibj
Deeplabcut	(Mathis et al., 2018)	RRID:SCR_021391
HHT-EMD		https://pyhht.readthedocs.io/en/latest/index.html
Baseline removal		https://github.com/StatguyUser/BaselineRemoval

2.16.4. Statistical summary

Table 6. Statistical summary for all figures

Figure Panel	*description*	*Sample size cell/trial/session*	*mouse*	*statistical test*	*statical values*
13D	Cumulative pump/food deliveries Slow feeding Binge feeding	trials: 481 241	8	Independent t-test	t=4.0411 P=5.8911e-05
13H	Cumulative lick events Slow feeding Binge feeding	trials: 481 241	8	Independent t-test	t=46.3075 P=4.4030e-218
22E (left column)	aPC binge-slow all neuron food neuron non-selective neuron water neuron other neuron	cell: 2975 312 61 410 2192	8	non-parametric two-sided approximate permutation t-test	P values: P<0.0001 P<0.0001 P=0.0132 P=0.0596 P<0.0001
22E (right column)	GC binge-slow all neuron food neuron non-selective neuron water neuron other neuron	cell: 1203 137 51 156 859	3	non-parametric two-sided approximate permutation t-test	P values: P=0.4214 P=0.5394 P=0.34 P=0.7688 P=0.2564
22F (left column)	aPC food neuron correlation	cell: 312	8	Pearson's correlation coefficient	r=-0.0647 P=0.2538
22F (right column)	GC food neuron correlation	cell: 137	3	Pearson's correlation coefficient	r=0.4332 P=1.2354e-07
22G	Cumulative distribution of ∆zs-∆F/F of aPC and GC Food neurons	cell: 312/137	8/3	Kolmogorov-Smirnov test	KS_stats=0.1879 P=0.0020

Figure Panel	*description*	*Sample size cell/trial/session*	*mouse*	*statistical test*	*statical values*
24A	aPC CaMK2 all neuron correlation	cell: 2975	8	Pearson's correlation coefficient	r=0.1220 P=2.4028e-11
24A	aPC CaMK2 non-selective neuron correlation	cell: 61	8	Pearson's correlation coefficient	r=0.2600 P=0.0429
24A	aPC CaMK2 water neuron correlation	cell: 410	8	Pearson's correlation coefficient	r=0.1292 P=0.0087
24A	aPC CaMK2 other neuron correlation	cell: 2192	8	Pearson's correlation coefficient	r=0.1522 P=7.7431e-13
24A	GC all neuron correlation	cell: 1203	3	Pearson's correlation coefficient	r=0.2811 P=2.7104e-23
24A	GC non-selective neuron correlation	cell: 51	3	Pearson's correlation coefficient	r=-0.0757 P=0.5972
24A	GC water neuron correlation	cell: 156	3	Pearson's correlation coefficient	r=0.1966 P=0.0138
24A	GC other neuron correlation	cell: 859	3	Pearson's correlation coefficient	r=0.2634 P=4.1829e-15
24B	ΔΔF/F distribution between aPC CaMK2 and GC all neuron	cells: aPC=2975 GC=1203	aPC=8 GC=3	Kolmogorov-Smirnov test	KS_stats=0.0701 P=0.0004
24B	ΔΔF/F distribution between aPC CaMK2 and GC non-selective neuron	cells: aPC=61 GC=51	aPC=8 GC=3	Kolmogorov-Smirnov test	KS_stats=0.1295 P=0.6757

Figure Panel	*description*	*Sample size cell/trial/session*	*mouse*	*statistical test*	*statical values*
24B	ΔΔF/F distribution between aPC CaMK2 and GC water neuron	cells: aPC=410 GC=156	aPC=8 GC=3	Kolmogorov-Smirnov test	KS_stats=0.0748 P=0.5212
24B	ΔΔF/F distribution between aPC CaMK2 and GC other neuron	cells: aPC=2192 GC=859	aPC=8 GC=3	Kolmogorov-Smirnov test	KS_stats=0.0756 P=0.0016
27B	OB all neuron correlation	cells: 752	4	Pearson's correlation coefficient	r=0.6411 P=2.7096e-88
29A	cell types: aPC CaMK2 aPC PV aPC SST GC OB	cell: 2975 684 675 1203 752	8 3 3 3 4	non-parametric two-sided approximate permutation t-test	P values: P<0.0001 P<0.0001 P<0.0001 P=0.4214 P=0.1646
31A (left column)	aPC PV binge-slow all neuron Ensure neuron non-selective neuron water neuron other neuron	cell: 716 67 36 144 469	3	non-parametric two-sided approximate permutation t-test	P values: P<0.0001 P=0.0002 P=0.0006 P<0.0001 P<0.0001
31A (right column)	aPC SST binge-slow all neuron Ensure neuron non-selective neuron water neuron other neuron	cell: 683 89 21 87 486	3	non-parametric two-sided approximate permutation t-test	P values: P<0.0001 P<0.0001 P=0.0274 P=0.1504 P<0.0001
31B	aPC PV all neuron correlation	cell: 716	3	Pearson's correlation coefficient	r=0.3784 P=8.4564e-26

Figure Panel	*description*	*Sample size cell/trial/session*	*mouse*	*statistical test*	*statical values*
31B	aPC PV food neuron correlation	cell: 67	3	Pearson's correlation coefficient	r=0.4517 P=0.0001
31B	aPC PV non-selective neuron correlation	cell: 36	3	Pearson's correlation coefficient	r=0.3460 P=0.0387
31B	aPC PV water neuron correlation	cell: 144	3	Pearson's correlation coefficient	r=0.1959 P=0.0185
31B	aPC PV other neuron correlation	cell: 469	3	Pearson's correlation coefficient	r=0.4023 P=1.1198e-19
31B	aPC SST all neuron correlation	cell: 683	3	Pearson's correlation coefficient	r=0.2693 P=8.1516e-13
31B	aPC SST food neuron correlation	cell: 89	3	Pearson's correlation coefficient	r=0.2259 P=0.0332
31B	aPC SST non-selective neuron correlation	cell: 21	3	Pearson's correlation coefficient	r=0.0944 P=0.6838
31B	aPC SST water neuron correlation	cell: 87	3	Pearson's correlation coefficient	r=0.4534 P=1.0313e-05
31B	aPC SST other neuron correlation	cell: 486	3	Pearson's correlation coefficient	r=0.2705 P=1.3375e-09
31C	ΔΔF/F distribution between aPC PV and aPC SST all neuron	cell: aPC_PV=716 aPC_SST=683	aPC_PV=3 aPC_SST=3	Kolmogorov-Smirnov test	KS_stats=0.1763 P=5.5506e-10
31C	ΔΔF/F distribution between aPC PV and aPC	cell: aPC_PV=67 aPC_SST=89	aPC_PV=3 aPC_SST=3	Kolmogorov-Smirnov test	KS_stats=0.1549 P=0.2804

Figure Panel	*description*	*Sample size cell/trial/session*	*mouse*	*statistical test*	*statical values*
	SST food neuron				
31C	ΔΔF/F distribution between aPC PV and aPC SST non-selective neuron	cell: aPC_PV=36 aPC_SST=21	aPC_PV=3 aPC_SST=3	Kolmogorov-Smirnov test	KS_stats=0.2460 P=0.3364
31C	ΔΔF/F distribution between aPC PV and aPC SST water neuron	cell: aPC_PV=144 aPC_SST=87	aPC_PV=3 aPC_SST=3	Kolmogorov-Smirnov test	KS_stats=0.2224 P=0.0075
31C	ΔΔF/F distribution between aPC PV and aPC SST other neuron	cell: aPC_PV=469 aPC_SST=486	aPC_PV=3 aPC_SST=3	Kolmogorov-Smirnov test	KS_stats=0.1950 P=1.9739e-08
34B	DA effects on aPC neurons	cell: 15	3	Permutation test	P = 0.0158
36	Food consumption in different recording sessions	sessions: all sessions=244	all mice = 19	Pearson's correlation coefficient	r=0.2094 P=0.0009
37B				Linear Mixed Model: contribution of Cohen's d on Ensure consumption	χ2(1) = 2.0315 P=0.1541
	aPC CaMK2 slow feeding vs Ensure consumption	sessions: 103	8	Linear Mixed Model: Fixed effects:	βinteraction = -36.306 ± 25.239 (standard errors)

Figure Panel	*description*	*Sample size cell/trial/session*	*mouse*	*statistical test*	*statical values*
				intercept, recording session, Cohen's d Random effects: Mouse ID Testing for contribution of Cohen's d on Ensure intake	
37B	aPC CaMK2 binge feeding vs Ensure consumption	sessions: 84	8	Linear Mixed Model: contribution of Cohen's d on Ensure consumption Linear Mixed Model: Fixed effects: intercept, recording session, Cohen's d Random effects: Mouse ID Testing for contribution of Cohen's d on Ensure intake	χ2(1) = 11.546 P=0.0006791 βinteraction = -116.462 ± 32.730 (standard errors)
38B	Neuron numbers after anosmia Pre-OP Anosmia	sessions: 21 15	 3 3	Independent t-test	t = 5.0681 P=4.3876e-06
39A	Buried food test Treatment:			Independent t-test	t=-5.1403 P=0.0003

Figure Panel	*description*	*Sample size cell/trial/session*	*mouse*	*statistical test*	*statical values*
	PBS Triton	10 3	10 3		
39B (left column)	aPC CaMK2 Pre-OP Cohen's d vs food consumption	sessions: 21	3 (same mice)	Pearson's correlation coefficient	r=-0.504 P=0.02
39B (right column)	aPC CaMK2 Anosmic Cohen's d vs food consumption	sessions: 15	3 (same mice)	Pearson's correlation coefficient	r=-0.210 P=0.45
39C	aPC CaMK2 Cohen's d in Pre-Op and Anosmic	sessions: 21/15	3 (same mice)	Independent t-test	T = 0.4990 P=0.6209
40B	aPC CaMK2 Ad libitum Cohen's d vs food consumption	sessions: 84	8	Pearson's correlation coefficient	r=-0.4345 P=3.6201e-05
40B	aPC CaMK2 Fasted Cohen's d vs food consumption	sessions: 18	5 (in 3 mice fasting protocol was not implemented)	Pearson's correlation coefficient	r=0.1178 P=0.6414
40C	aPC CaMK2 Cohen's d in Ad libitum and Fasted	sessions: 84/18	8/5	Independent t-test	T=2.7569 P=0.0069
40C	GC Cohen's d in Ad libitum and Fasted	sessions: 32/11	3/3	Independent t-test	T=2.8284 P=0.0072
41 (top left)	Binge feeding responses of cell	sessions: 32	3	Pearson's correlation coefficient	r=-0.1938 P=0.2878

Figure Panel	*description*	*Sample size cell/trial/session*	*mouse*	*statistical test*	*statical values*
	types in ad libitum in GC				
41 (top middle)	Binge feeding responses of cell types in ad libitum in aPC PV	sessions: 54	3	Pearson's correlation coefficient	r=-0.3884 P=0.0037
41 (top right)	Binge feeding responses of cell types in ad libitum in aPC SST	sessions: 40	3	Pearson's correlation coefficient	r=0.0005 P=0.9971
41 (bottom left)	Binge feeding responses of cell types in fasted in GC	sessions: 11	3	Pearson's correlation coefficient	r=-0.2369 P=0.4828
41 (bottom middle)	Binge feeding responses of cell types in fasted in aPC PV	sessions: 5	3	Pearson's correlation coefficient	r=-0.0895 P=0.8860
41 (bottom right)	Binge feeding responses of cell types in fasted in aPC SST	sessions: 10	3	Pearson's correlation coefficient	r=0.4095 P=0.2398
46C	aPC optogenetic suppression vs food intake tdTomato eOPN3	sessions: 24(LED off)/24(LED on) 24(LED off)/24(LED on) 6/6 sessions for each mouse	4 4	Linear Mixed Model: Fixed effects: intercept, recording session, body weight, baseline feeding time, sex, virus type, LED state, virus type*LED state Random effects: Mouse ID	χ2(1) = 11.631 P=0.0006488 βinteraction = 70.7777 ± 20.0774 (standard errors)

Figure Panel	*description*	*Sample size cell/trial/session*	*mouse*	*statistical test*	*statical values*
				Testing for contribution of interaction of virus type and light stimulation on Ensure intake	
46D	aPC optogenetic suppression vs Feeding duration tdTomato eOPN3	sessions: 24(LED off)/24(LED on) 24(LED off)/24(LED on) 6/6 sessions for each mouse	4 4	Linear Mixed Model: Fixed effects: intercept, recording session, body weight, baseline feeding time, sex, virus type, LED state, virus type*LED state Random effects: Mouse ID Testing for contribution of interaction of virus type and light stimulation on Feeding duraiton	χ2(1) = 5.1898 P=0.02272 βinteraction = 47.23888 ± 20.43307 (standard errors)
46E	aPC optogenetic suppression vs feeding bout duration tdTomato eOPN3	sessions: 24(LED off)/24(LED on) 24(LED off)/24(LED on) 6/6 sessions for each mouse	4 4	Linear Mixed Model: Fixed effects: intercept, recording session, body weight, baseline feeding time, sex, virus type, LED state, virus type*LED	χ2(1) = 10.882 P=0.0009711 βinteraction = 4.112 ± 1.245 (standard errors)

Figure Panel	*description*	*Sample size cell/trial/session*	*mouse*	*statistical test*	*statical values*
				state Random effects: Mouse ID Testing for contribution of the interaction of virus type and light stimulation on duration of individual feeding bout	
46F	aPC optogenetic suppression vs number of feeding bout tdTomato eOPN3	sessions: 24(LED off)/24(LED on) 24(LED off)/24(LED on) 6/6 sessions for each mouse	4 4	Linear Mixed Model: Fixed effects: intercept, recording session, body weight, baseline feeding time, sex, virus type, LED state, virus type*LED state Random effects: Mouse ID Testing for contribution of interaction of virus type and light stimulation on numbers of feeding bouts	χ2(1) = 0.0495 P=0.824 βinteraction = -0.4337 ± 1.9494 (standard errors)

2.17. Data and code availability

Source data and code generated and used in this thesis can be found in the GitHub repository (https://github.com/hung-lo/BingeFeeding_2023), including the source data for plotting individual figure panels and the code for plotting individual panels. Processed data and raw data are stored in the Schmitz lab data server (BCCN server, smb://alzheimerfs.home.bccn-berlin.de/alzheimer/hung/inscopix_data) with daily backup. All code for data processing and analysis will be deposited to the same GitHub repository upon acceptance of the accompanying manuscript (Lo et al., 2023).

3. Results

3.1. Establishment of a liquid food delivery system and feeding paradigm

To precisely control the feeding rates of mice, I and collaborators built a liquid food delivery system so that mice can voluntarily trigger the lick spout by licking, getting a droplet (~1.8 µL) of food (Ensure, an artificial energy-dense flavored nutrient solution) or water as rewards. The food delivery system allows me to implement different refractory periods for the delivery pump, i.e., 0.4 seconds for the binge feeding mode and 4 seconds for the slow feeding mode. Therefore, mice can consume more food during binge feeding mode whereas mice have to wait for longer to receive the reward in the slow feeding mode. A typical recording session is set to 30 minutes and the mice have access to the lick spout for a total duration of 14 minutes, with a pseudorandom order of 2 minutes long slow and binge feeding modes. In general, mice consumed more food and more lick events were presented during binge feeding compared to slow feeding (Figure 13), indicating a clear separation of slow feeding and binge feeding behaviors. Notably, the difference in food deliveries was much larger than the lick rate difference (Figure 13), suggesting a similarity in the licking aspect of the feeding behavior.

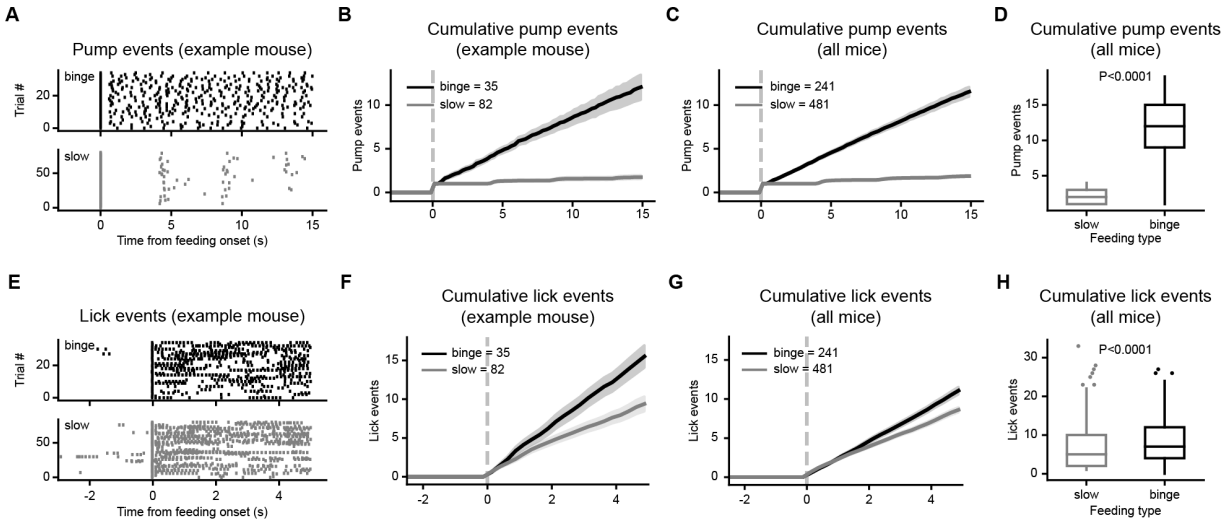

Figure 13. ***Characterization of behavioral signatures across different feeding rates.*** *(**A**) Food or water delivery events (activation of the pump) for slow feeding and binge feeding from an example mouse. (**B**) Cumulative food or water delivery events for slow feeding and binge feeding from the same example mouse (same as in **A**). (**C**) Cumulative food or water delivery events for all aPC CaMK2^{+} mice that I recorded (n= 481 for slow feeding trials and 241 for binge feeding trials in 8 mice). (**D**) Quantification of cumulative food or water delivery events, from feeding bout onset to fifteen seconds after. Unpaired Student's t-test was used for testing the difference between two groups (n is the same as in **C**). (**E**) Lick events for slow feeding and binge feeding from an example mouse (same as in **A**). (**F**) Cumulative lick events for slow feeding and binge feeding from the same example mouse (same as in **E**). (**G**) Cumulative lick events for all aPC CaMK2^{+} mice that I took recordings from (n is the same as in **C**). (**H**) Quantification of cumulative lick events in 4 s after the onset of feeding bouts. Unpaired Student's t-test was used for testing the difference between two groups (n is the same as in **C**).*

3.2. *In vivo* Ca^{2+} imaging in the anterior piriform cortex

To record neuronal activity in the aPC during feeding behavior, I employed an endomicroscopic method for Ca^{2+} imaging and combined it with a head-mounted miniscope to enable the mouse to move around the experimental arena freely and access the food source of its own volition (Figure 14). My colleague and I established a prism-GRIN lens implantation surgical procedure to stably record aPC neuronal activity throughout the 5 weeks of behavioral experiments (Figure 15D, average = 140 ± 72.19 neurons). Implant coordinates were verified with *post hoc* histology (Figure 15A-C). To image a specific population of neurons in the aPC, I crossed the Ai93D mice with CaMK2-Cre mice and Rosa-tTA mice to obtain triple transgenic mice which only express GCaMP6f, a genetic encoded Ca^{2+} indicator, in the excitatory neurons (both the semilunar cells and pyramidal cells) in the aPC (Figure 16).

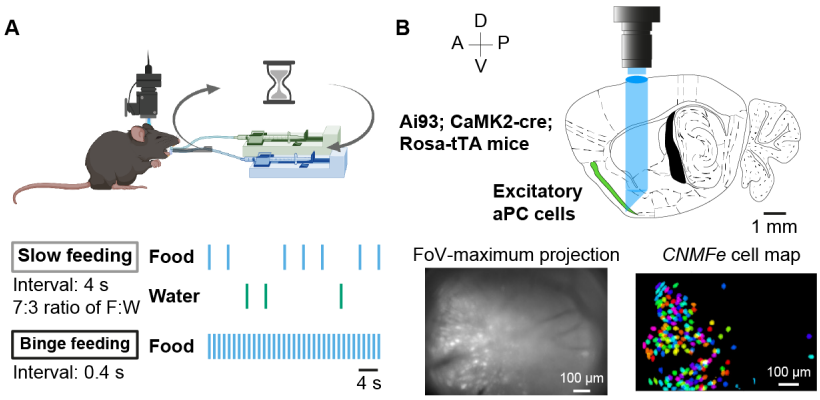

Figure 14. ***Illustration of experimental design and methods.*** *(**A**) Top: Schematics of in vivo Ca^{2+} imaging with a miniscope recording in the aPC and the behavioral setup for delivery of food and water. Bottom: Schematics of behavioral protocol for slow feeding (70% of deliveries are food, the remaining 30% are water) and binge feeding (all deliveries are food). (**B**) Top: Schematics of miniscope implants (GRIN lens attached with a prism, colored in blue in the aPC (green structure)). Bottom: Field-of-view of miniscope Ca^{2+} imaging recordings and the extracted cell identified by the constrained non-negative matrix factorization (CNMFe).*

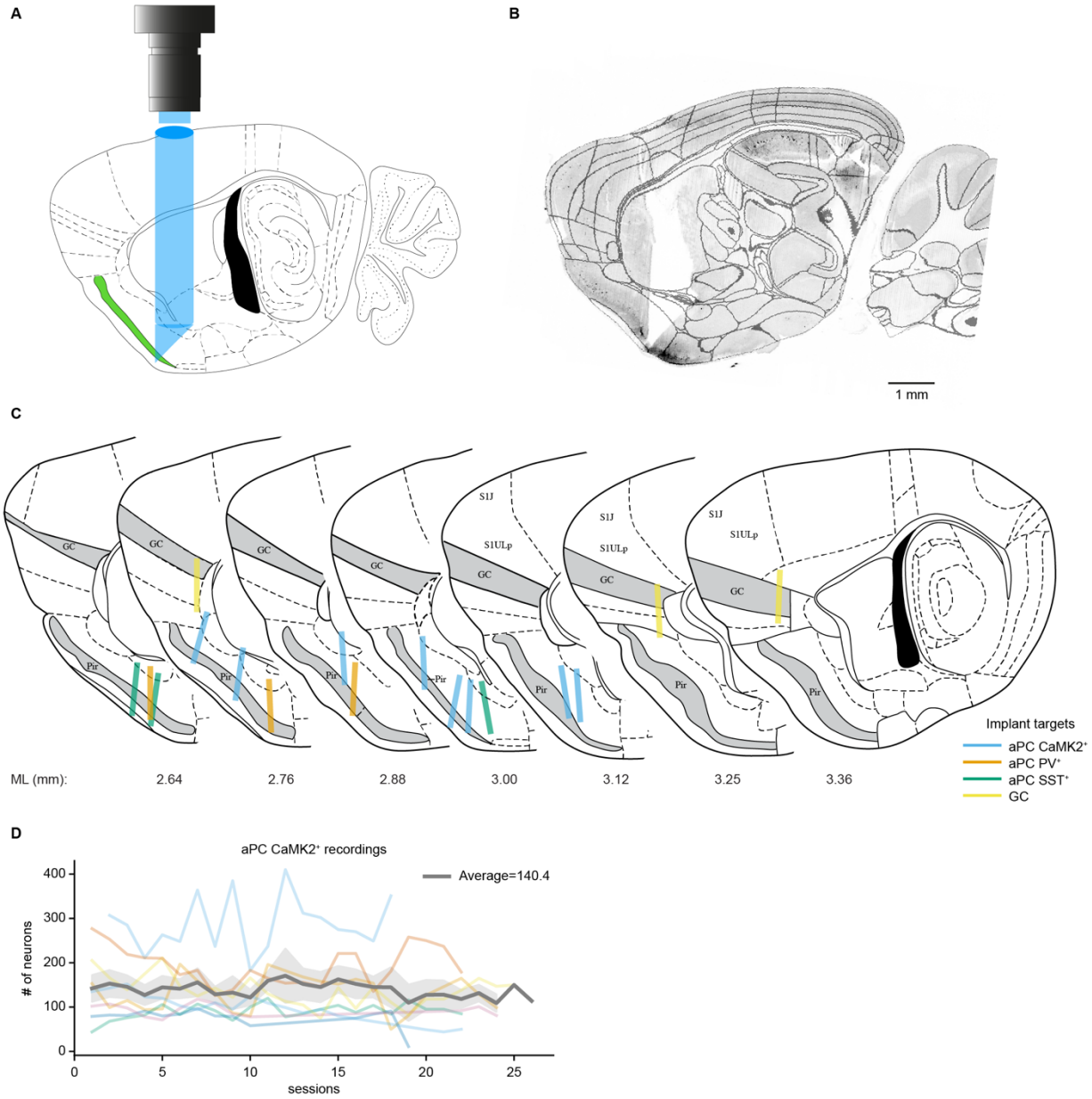

Figure 15. ***Implant coordinates and detected active neurons across experimental dates.*** *(**A**) Schematic of implant coordination in the aPC. (**B**) Path of GRIN lens attached with prism and GCaMP6f expression in the excitatory neurons in the aPC from an example mouse. (**C**) Reconstructed imaging panel of the prism surface in different neuronal types in the aPC (**Results 3.3, 3.7**) and the GC (**Results 3.4**). (**D**) Numbers of detected active aPC CaMK2⁺ neurons extracted with CNMFe algorithm on different recording sessions (n=8 mice).*

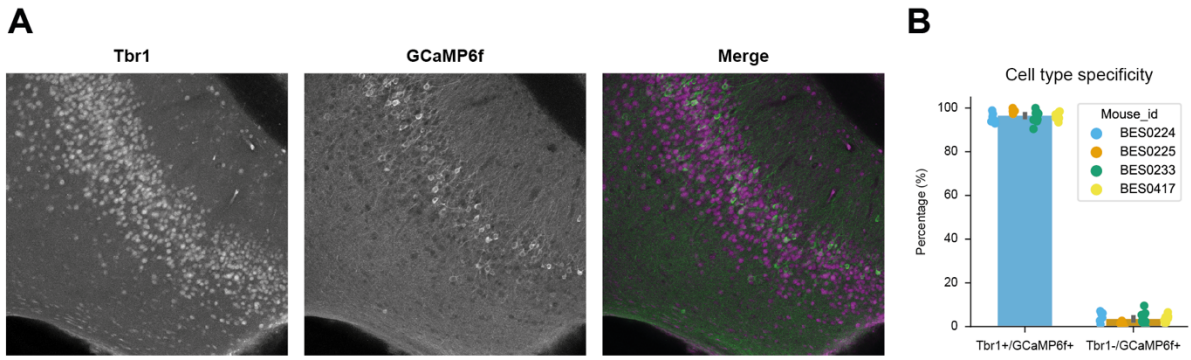

Figure 16. ***Cell type verification.*** *(**A**) Post-hoc immunostaining of GcaMP6f (GFP) and Tbr1+ in the aPC. (**B**) Quantification of cell types of aPC neurons across 4 different experimental mice. For (**B**) data are shown as mean ± s.e.m.*

I also presented two flavors of Ensure to the mice and could successfully identify different neuronal populations activated during slow feeding; ~10% of aPC excitatory neurons were activated by strawberry-flavored Ensure and another ~10% were activated by chocolate-flavored Ensure, with ~2% of aPC neurons non-selectively activated by either flavor of Ensure (Figure 17). The flavor-activated aPC neuron population matches with the reported numbers from other research groups studying odor-evoked aPC responses (Bolding and Franks, 2017; Miura et al., 2012; Poo and Isaacson, 2009; Poo and Isaacson, 2011; Rennaker et al., 2007; Roland et al., 2017; Stettler and Axel, 2009; Tantirigama et al., 2017; Zhan and Luo, 2010). Similar results are found when comparing Ensure to sucrose solution (Figure 18). Interestingly, water consumption also elicited ~10% of distinct aPC excitatory neurons' activation (Figure 20E), suggesting that aPC neurons may also respond to other sensory and motor components (e.g. somatosensory and motor responses, etc.).

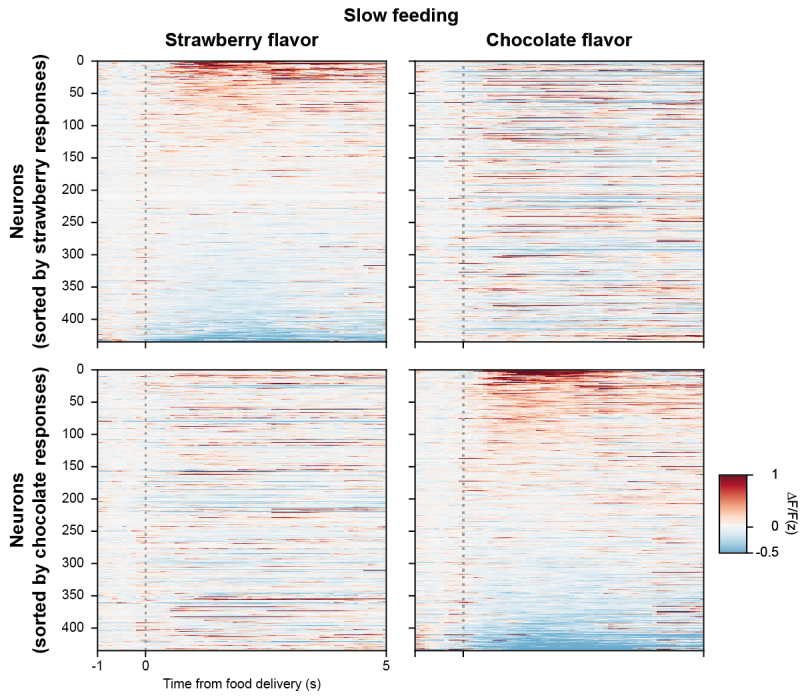

Figure 17. ***aPC neurons show distinct neuronal responses to different flavors of food.*** *Two flavors of Ensure were tested here in the same experimental session. The upper row is sorted by responses to strawberry-flavored Ensure, while the lower row is sorted by responses to chocolate-flavored Ensure (n = 440 neurons from 3 mice).*

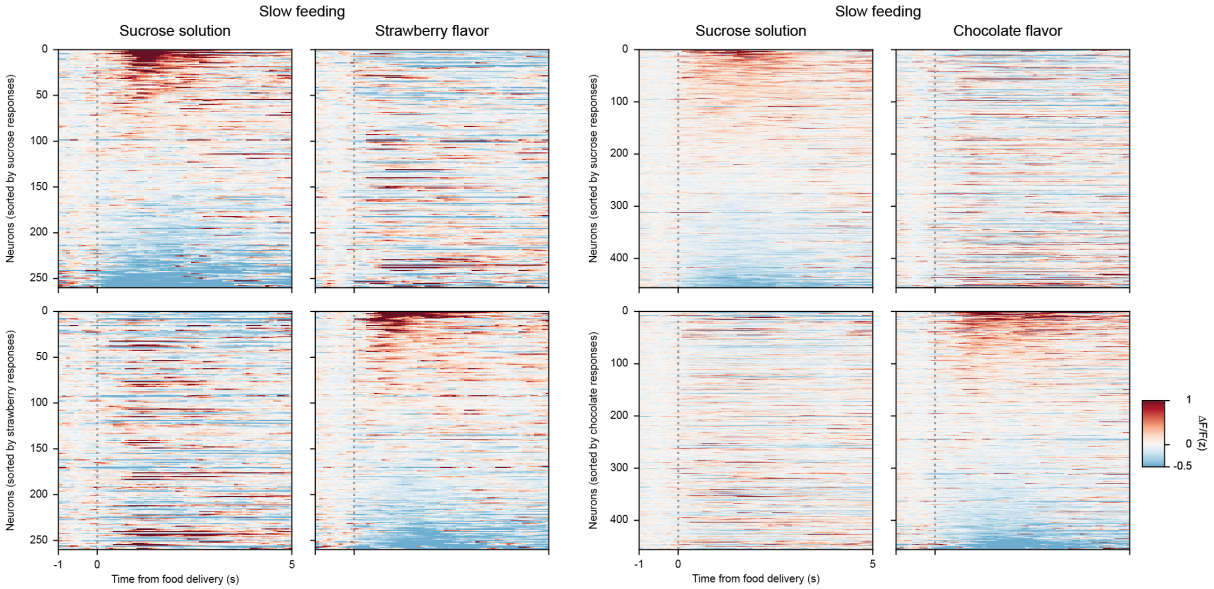

Figure 18. ***Distinct aPC neuronal responses to Ensure and sucrose solution.*** *Left, aPC neuronal responses to sucrose and to strawberry-flavored Ensure. Right, aPC neuronal responses to sucrose and to chocolate-flavored Ensure. The upper row is sorted by responses to sucrose solution, while the lower row is sorted by responses to Ensure. (n = 260 and 435 neurons from 3 mice).*

3.3. The feeding rate modulates flavor representation in the aPC

My Ca^{2+} imaging results showed distinct activity patterns upon slow feeding and binge feeding, whereby clear excitatory responses can be observed during slow feeding but there was a robust suppression of the aPC excitatory neurons upon binge feeding (Figure 19, A-C). Since slow feeding mode provides a larger number of clearly separated individual trials and I observed a lack of neuronal activity during binge feeding, I classified aPC neurons based on their responses during slow feeding. To distinguish neuronal responses to food flavors and non-specific neuronal responses generated by the feeding behavior, I interspersed brief water deliveries in the slow feeding mode. This setting allowed me to classify aPC excitatory neurons into four categories: food-activated neurons (10.5%), water-activated neurons (13.8%), non-selective feeding neurons (2.0%, responding to both food and water deliveries), and other neurons (73.7%, including non-responding and suppressed responding neurons to food or water deliveries) based on auROC analysis of individual neuronal responses (Figure 20A, see **Methods 2.10.3** for auROC calculation). Based on this classification, I showed that binge feeding-induced suppression is presented in not only the food-activated neurons but also in water-activated and non-responding neurons, except for the non-selective feeding neurons (Figure 20F, G), indicating that the majority of aPC excitatory neurons are suppressed during binge feeding. This result suggests that the odor representation of food is suppressed when binge feeding, with only feeding-related neuronal activity remaining intact.

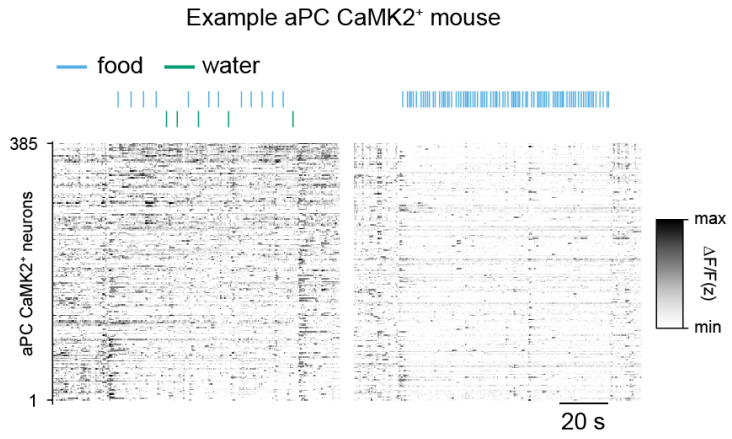

Figure 19. ***Distinct aPC neuronal responses to different feeding rates.*** *Example Ca^{2+} traces of recorded excitatory aPC neurons from one mouse in one experimental session. Left, neuronal activities during slow feeding. Right, neuronal activities during binge feeding from the same neurons.*

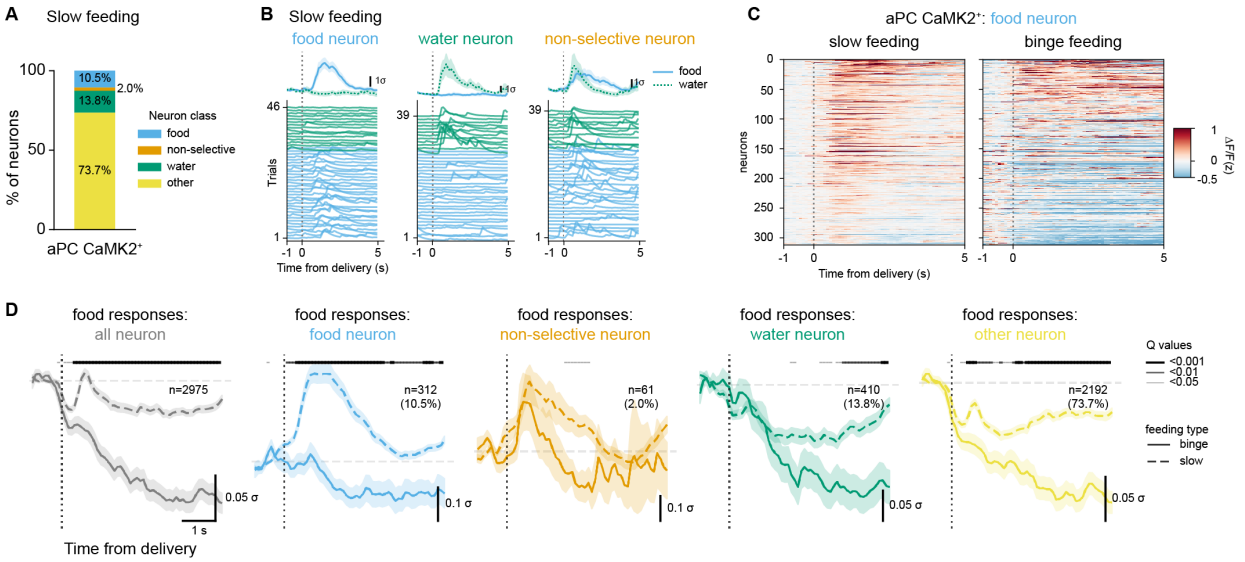

Figure 20. ***Effects of feeding rate on flavor representations in the aPC.*** *(**A**) Four responding classes of aPC neurons; aPC neurons are activated during slow feeding by food, water, or non-selective consumption and non-responding neurons. (n=2975 cells, 481 slow feeding trials, and 241 binge feeding trials in 8 mice). (**B**) Single-trial and trial-average responses of example aPC neurons. Left to right columns; food-activated, water-activated, and non-selective aPC neurons upon slow feeding. (**C**) Trial-averaged responses to food deliveries during slow feeding and binge feeding of individual aPC CaMK2$^+$ food-activated neurons (n=312 cells in 8 mice). (**D**) Trial-average responses to slow feeding and binge feeding of population and subclasses of aPC CaMK2$^+$ neurons (n is the same as in **A**). The dotted vertical line represents the onset of food deliveries. The shaded line on top of the average traces indicates the Q-values (adjusted P values) of individual time points. The different line widths represent different Q-values (from thin width to thick width: Q <0.05, <0.01, <0.001).*

Odor responses in the PC are through a distributed population code for both odor identity and concentration (Bolding and Franks, 2017; Miura et al., 2012; Rennaker et al., 2007; Stettler and Axel, 2009; Wilson and Sullivan, 2011). Odor information is then further transmitted to the downstream targets, e.g. ENT, HPC, AMY, OFC, etc. Slow feeding-activated aPC excitatory neurons are at a similar percentage as odor-evoked aPC neuron activation (Bolding and Franks, 2017; Miura et al., 2012; Poo and Isaacson, 2009; Poo and Isaacson, 2011; Rennaker et al., 2007; Roland et al., 2017; Stettler and Axel, 2009; Tantirigama et al., 2017; Zhan and Luo, 2010). aPC represents odors in a concentration-invariant manner (Bolding and Franks, 2018), meaning that when odors are presented at different concentrations, the distributed population code and neuronal firing rates remain stable. Based on these findings, despite the higher volume of food consumed during the binge feeding bouts causing a higher intensity/concentration of food flavor, we did not expect changes in the percentage of flavor-activated aPC neurons. Therefore, my data

point to a novel feeding rate-dependent modulation of flavor representation in the aPC excitatory neurons that radically alters the flavor-specific population code.

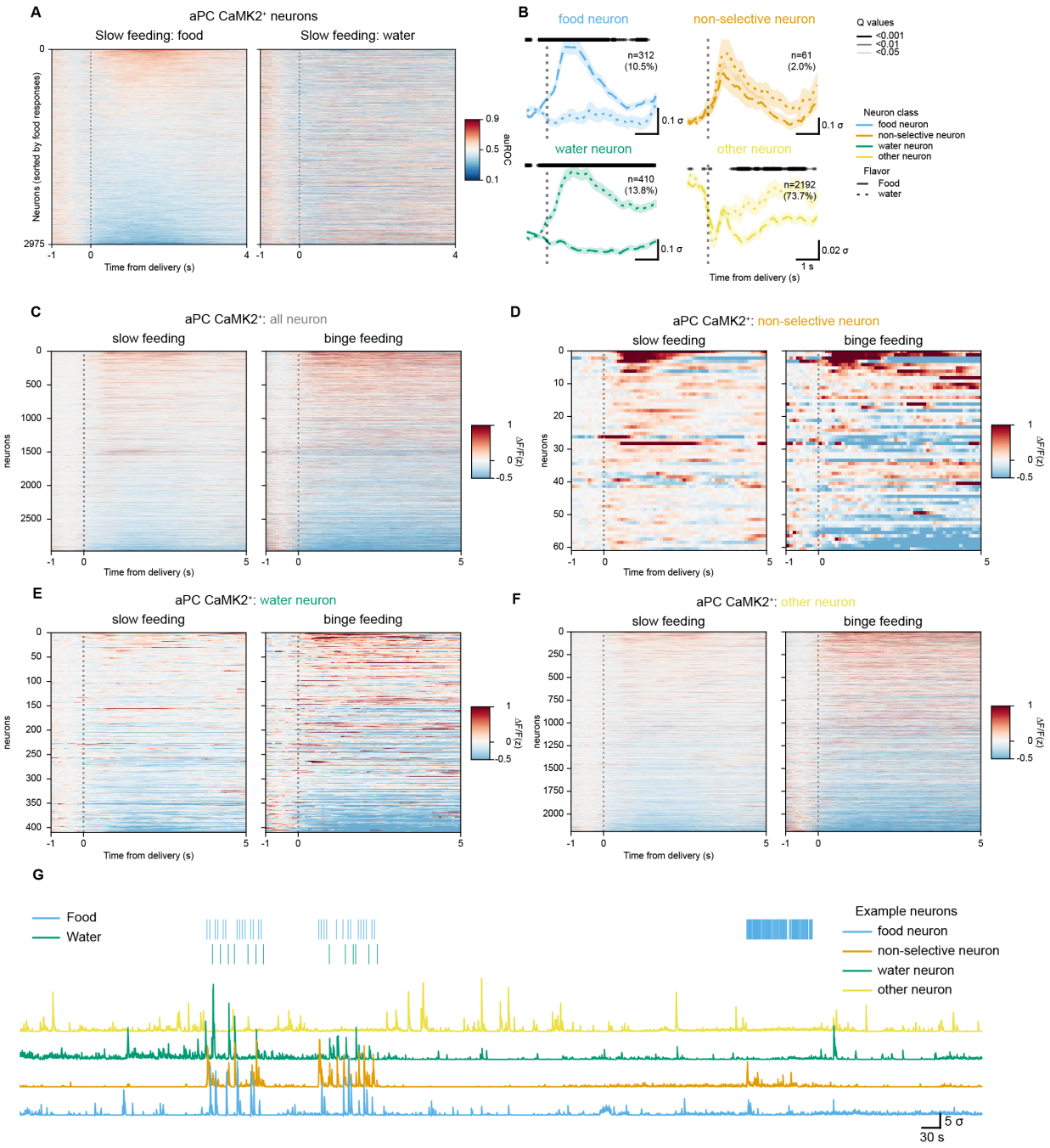

Figure 21. ***aPC CaMK2⁺ neuronal responses during.*** *(**A**) Slow feeding responses of aPC CaMK2⁺ neurons using the Area Under the Receiver Operating Characteristics (auROC) curve (see* ***Methods 2.10.3****, n is 2975 cells from 8 mice). (**B**) Average traces of four responding classes of aPC CaMK2⁺ neurons for food and water deliveries (n=312 food neurons, 61 non-selective neurons, 410 water neurons, 2192 other neurons from 8 mice). The shaded line on top of the average traces indicates the Q-values (adjusted P values) of individual time points. The different line widths represent different Q-values (from thin width to thick width: Q <0.05, <0.01, <0.001). (**C-F**) Responses of individual aPC CaMK2⁺ neurons in different subclasses during slow feeding and binge feeding. (**G**) Neuronal traces of example aPC CaMK2⁺ neurons from a recording session from one mouse.*

3.4. Flavor representation in the GC is stable across feeding rates

Behaviors have profound effects on brain activities, and the sensory cortices are no exception (Musall et al., 2019; Steinmetz et al., 2019; Stringer et al., 2019). To verify whether the binge feeding-induced aPC suppression is an area-specific phenotype or is a general cortical phenomenon and to directly compare the cortical olfactory flavor representation with another cortical flavor center, I recorded the neuronal activity in the gustatory cortex (GC, the dysgranular insular cortex, and the granular insular cortex) during feeding, since smell and taste are the two main sensory modalities that contribute to the perception of food flavors. Due to the lack of expression of GCaMP6f in the GC of CaMK2-Cre; Rosa-tTA; Ai93D triple transgenic mice (Figure 11), I switched to a different viral construct and transgenic mice line; I injected the hSyn-Cre virus in the GC in the Ai148 mice to express GCaMP6f in the GC and implanted prism-GRIN lenses in the GC for Ca^{2+} imaging with a miniscope to track taste representation during slow and binge feeding (Figure 22A, B).

I found that the gustatory flavor representation in the GC is robust in both feeding types, and the population means are similar during slow feeding and binge feeding (Figure 22C). Classification of GC neurons based on their response types during slow feeding resulted in similar activation percentages of the 4 classes as I observed in the aPC excitatory neurons: food-activated neurons (11.4%), water-activated neurons (13.0%), non-selective feeding neurons (4.2%) and other non-responding or suppressed neurons (71.4%) (Figure 22D, Figure 23). Stratifying neurons based on this classification, I found no difference between the area-under-curve (AUC) of neuronal responses upon slow feeding and binge feeding in the GC neurons, regardless of their individual responding types. This finding is opposite to the aPC results, where I observed a robust non-specific general suppression during binge feeding bouts, indicating that the binge feeding-induced suppression is mostly limited to the aPC and is not a general suppression mechanism in the flavor system caused by binge feeding (Figure 22E).

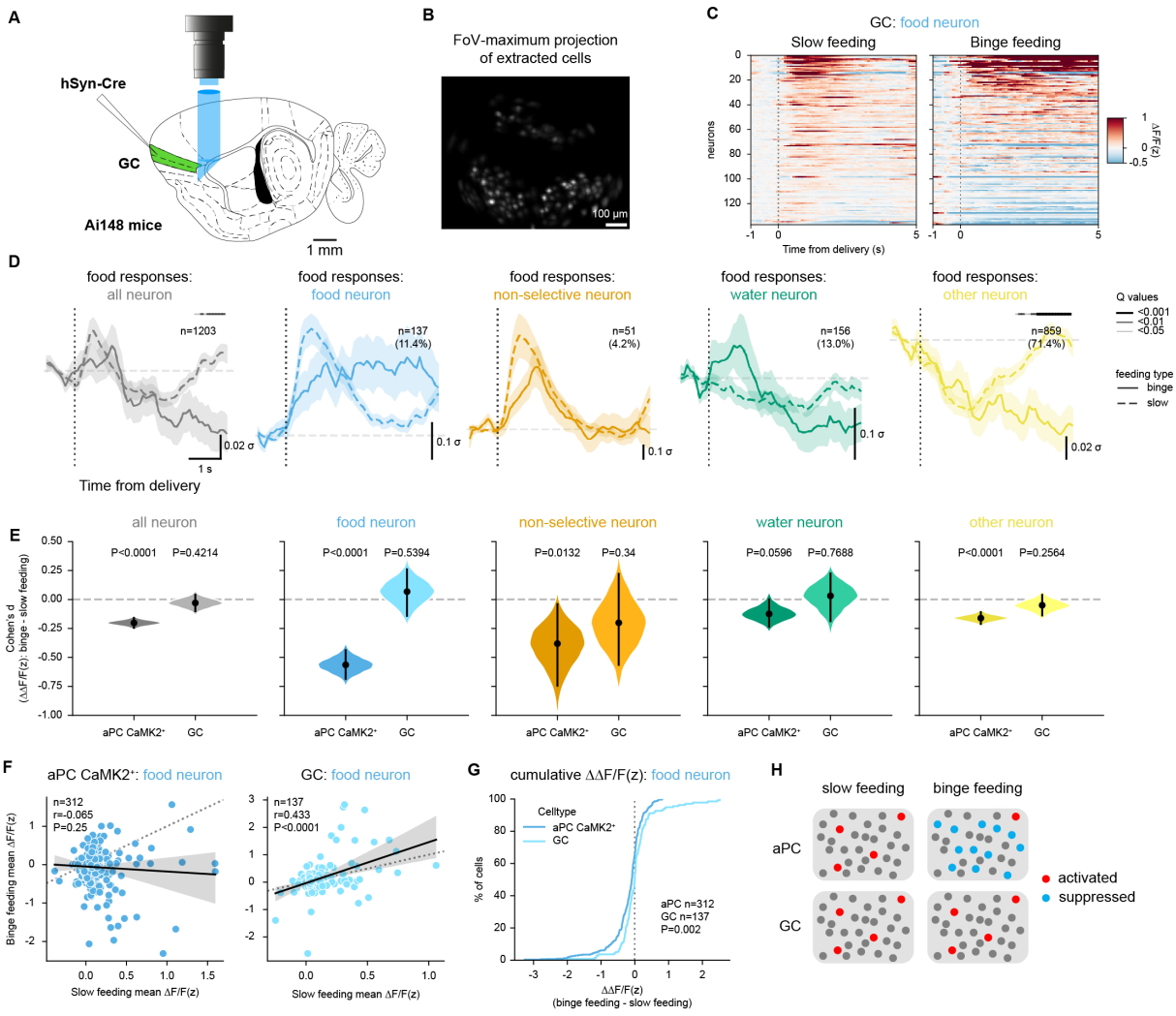

Figure 22. ***Flavor representation in the GC is independent of feeding rates.*** *(**A**) Schematics of miniscope implant in the GC. (**B**) Detected active neurons in the GC by CNMFe. (**C**) Trial-averaged responses of individual GC food-activated neurons upon slow feeding and binge feeding (n=137 from 3 mice). (**D**) Trial-averaged responses during slow feeding and binge feeding of all GC neurons and for subclasses of GC neurons (n=1203 cells from 3 mice). The shaded line on top of the average traces indicates the Q-values (adjusted P values) of individual time points. The different line widths represent different Q-values (from thin width to thick width: Q <0.05, <0.01, <0.001). (**E**) Cohen's d (estimated effect size) of binge feeding-induced modulation in individual subclasses. Left, aPC CaMK2$^+$ neurons. Right, GC neurons. P values are calculated with the permutation test with bootstrapping (resampled 5000 times) (n is the same as in **D**), and data are shown as means of bootstrapped effect sizes (Cohen's d) ± 95% confidence interval. (**F**) Comparison of individual neuron responses upon slow feeding and binge feeding in food-activated neurons. Left, aPC CaMK2$^+$ food-activated neurons. Right, GC food-activated neurons (n is the same as in Figure 20**F** and **C**), r (correlation coefficient), and P values are calculated with Pearson's r. (**G**) Cumulative distribution of the difference (binge feeding vs. slow feeding) of z-scored ΔF/F (ΔΔF/F(z)) in food-activated aPC CaMK2$^+$ and GC neurons (n is the same as in **F**, the P-value is calculated with the Kolmogorov-Smirnov test). (**H**) Illustration of neuronal responses in the aPC and the GC during slow feeding and binge feeding.*

To further analyze these two distinct behavioral modes of flavor representation across the two sensory cortices, I directly compared cell-wise correlations of neuronal activities in both slow feeding and binge feeding. In the food-activated neurons, a clear positive linear correlation of activity changes between slow feeding and binge feeding was found in the GC, suggesting that those food-activated neurons respond strongly to the food items during slow feeding and are still strongly responding to food upon binge feeding onsets (Figure 22F). In the aPC, however, I found no correlation between responses of food-activated neurons during slow feeding and binge feeding, which indicates that these food neurons lose their specificity for representing flavors during binge feeding (Figure 22F). When looking at the cumulative distribution of the difference in neuronal responses during slow feeding and binge feeding of food-activated neurons in both the aPC and GC, the net reduction is more prominent in the aPC food neurons with a much smaller proportion of positive net binge feeding-positive neurons compared to the GC food neurons (Figure 22G). Such differential distribution of the net reduction of neuronal responses was also observed in the non-responding other neurons (Figure 23G, Figure 24B). With this, I concluded that by switching from slow feeding to binge feeding, a non-specific cortical suppression occurs in the aPC but there is a stable flavor representation in the GC, implying that this behavior-induced modulation is not just a global flavor system event induced by an efference copy of binge feeding behavior (Figure 22H).

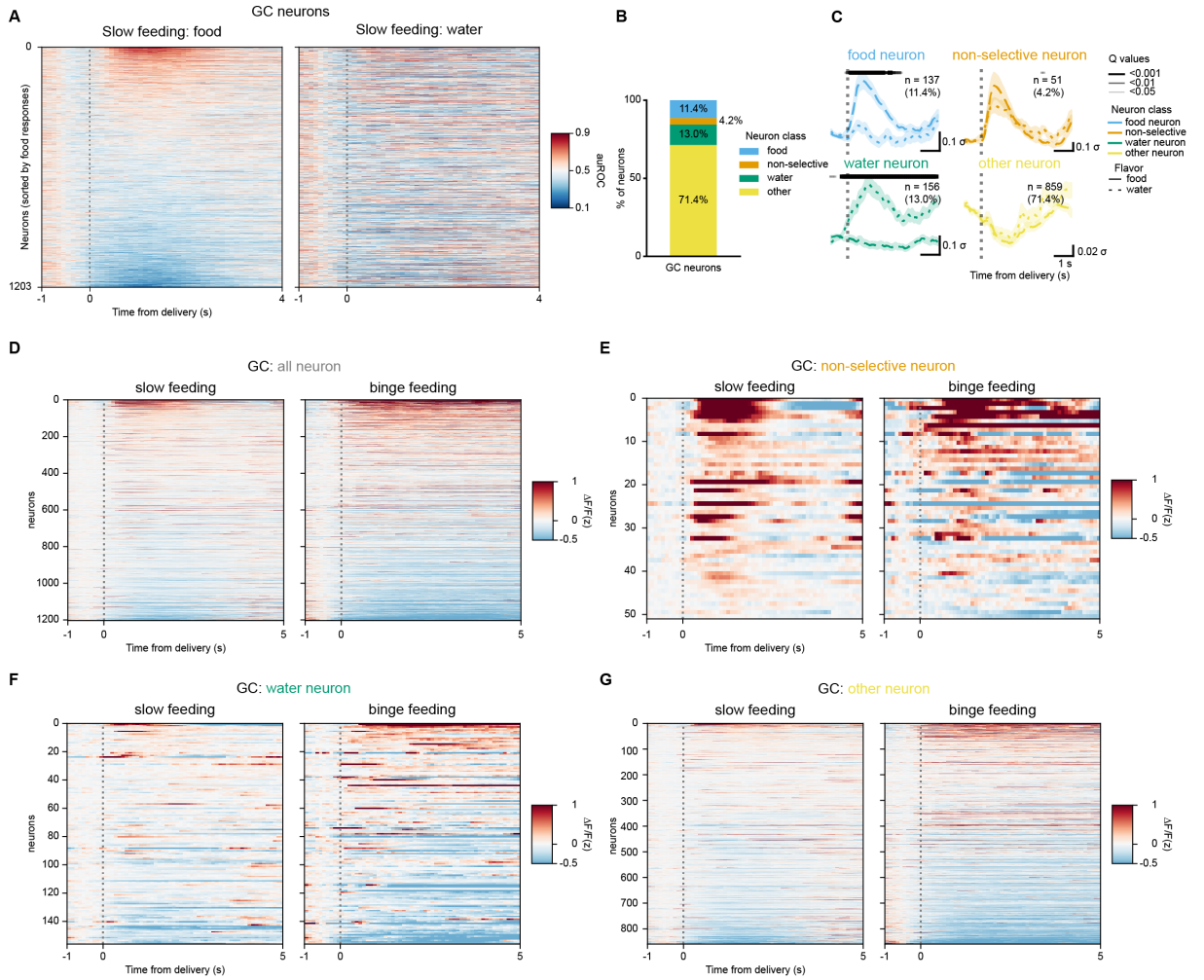

Figure 23. ***GC neuronal responses during feeding upon slow feeding and binge feeding.*** *(**A**) Slow feeding responses of GC neurons using the Area Under the Receiver Operating Characteristics (auROC) curve (see* ***Methods 2.10.3****). (**B**) Four responding classes of GC neurons; GC neurons are activated during slow feeding by food, water, or non-selective consumption and non-responding neurons. (n=1203 all neurons, 137 food-activated neurons, 51 non-selective neurons, 156 water-activated neurons, and 859 other neurons from 3 mice). (**C**) Neuronal responses of subclasses of GC neurons for food and water deliveries during slow feeding (n is the same as in **B**). The shaded line on top of the average traces indicates the Q-values (adjusted P values) of individual time points. The different line widths represent different Q-values (from thin width to thick width: Q <0.05, <0.01, <0.001). (**D-G**) Responses of individual GC neurons in different subclasses during slow feeding and binge feeding.*

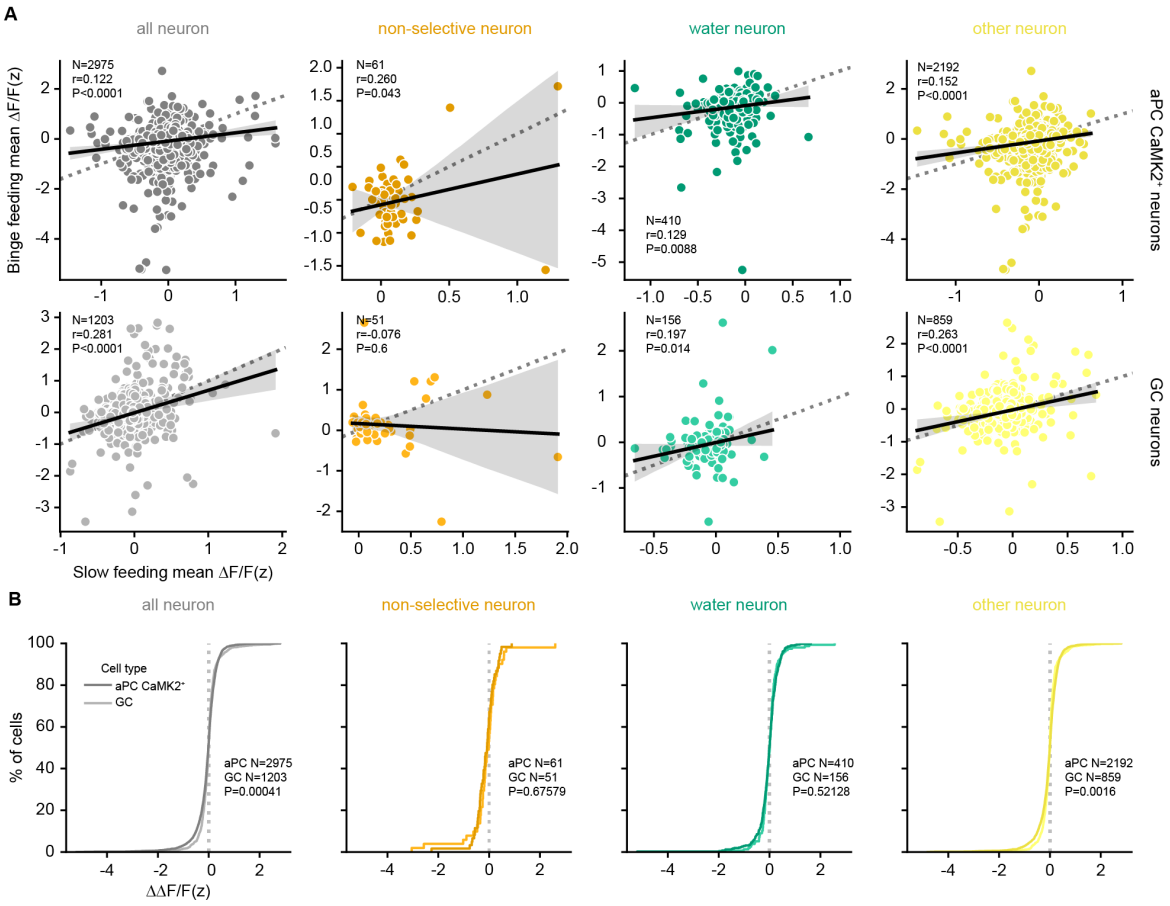

Figure 24. ***Comparison of binge feeding-induced modulation in individual aPC excitatory neurons and GC.*** *(**A**) Comparison of individual neuronal responses in aPC excitatory neurons and GC neurons upon slow feeding and binge feeding (For aPC CaMK2⁺ neurons, n=2975 for all neurons, 61 for non-selective neurons, 410 for water neurons, 2192 for other neurons from 8 mice. For GC neurons, n=1203 for all neurons, 51 for non-selective neurons, 156 for water neurons, and 859 for other neurons from 3 mice); correlation coefficient and P-value are calculated with Pearson's r. (**B**) The cumulative distribution of the binge feeding modulated activity for each cell (binge feeding - slow feeding, ΔΔ F/F(z), n is the same as in **A**.*

3.5. Alteration of respiration during binge feeding is limited

To examine the potential mechanism of binge feeding-induced aPC suppression, I tested the following four hypotheses: 1) alteration of respiration cycles by fast feeding, 2) degradation of odor inputs from the nostrils or the olfactory bulb (OB), 3) recruitment of local inhibitory (GABAergic) neurons in the aPC, and 4) neuromodulation. In the following sections, I will describe the experiments I designed to test each of these hypotheses.

Respiration is a strong modulator of brain oscillations (Karalis and Sirota, 2022), including the PC (Bolding and Franks, 2017). Odors can be detected by the olfactory sensory neurons (OSN) in the nasal cavity from the nostrils during inhalation (orthonasal route) and from the oral cavity during exhalation (retronasal route). Retronasal olfaction is usually combined with taste stimuli to form a synthetic orosensory flavor percept. Recent evidence also suggests that rodents perceive these 2 types of olfactory pathways differently (Blankenship et al., 2019), indicating the usage of these 2 modes of olfaction in different behavioral contexts. In my experimental setting, while orthonasal olfaction is limited by the airflow generated around the lick spout, the exact olfactory pathways are not distinguishable due to the lack of respiration monitoring as well as the limitations of the Ca^{2+} indicator kinetics and imaging setting for the fast oscillatory nature of respiration (~4 Hz for general breathing and up to 12 Hz for sniffing). I therefore tested the effect of binge feeding on respiration independent of the neuronal recordings by directly monitoring respiration with a head-fixed setup.

If respiration is disrupted during binge feeding, orthonasal, and retronasal olfaction will be equally affected, influencing olfactory coding in downstream brain regions. Usually, nasal airflow is measured using heat-sensitive thermistor probes. While the commonly used heat sensors for airflow measurements can provide a highly precise measure of respiration, these probes do not fit the geometry of my food delivery system. The main obstacle is the position of the lick spout. With support from a colleague, I decided to use a mechanical piezo sensor and visual camera monitoring instead to provide unrestricted access to the lick spout. In this setting, mice can drink from the lick spout with both a piezo sensor attached to the lateral part of their abdomen and a frontal camera on their chest. I found that a clear 4 Hz signal can be found during binge feeding bouts (Figure

25), suggesting that respiration is not disrupted during binge feeding, thus the altered respiratory pattern is not likely to be the key factor in binge feeding-induced modulation.

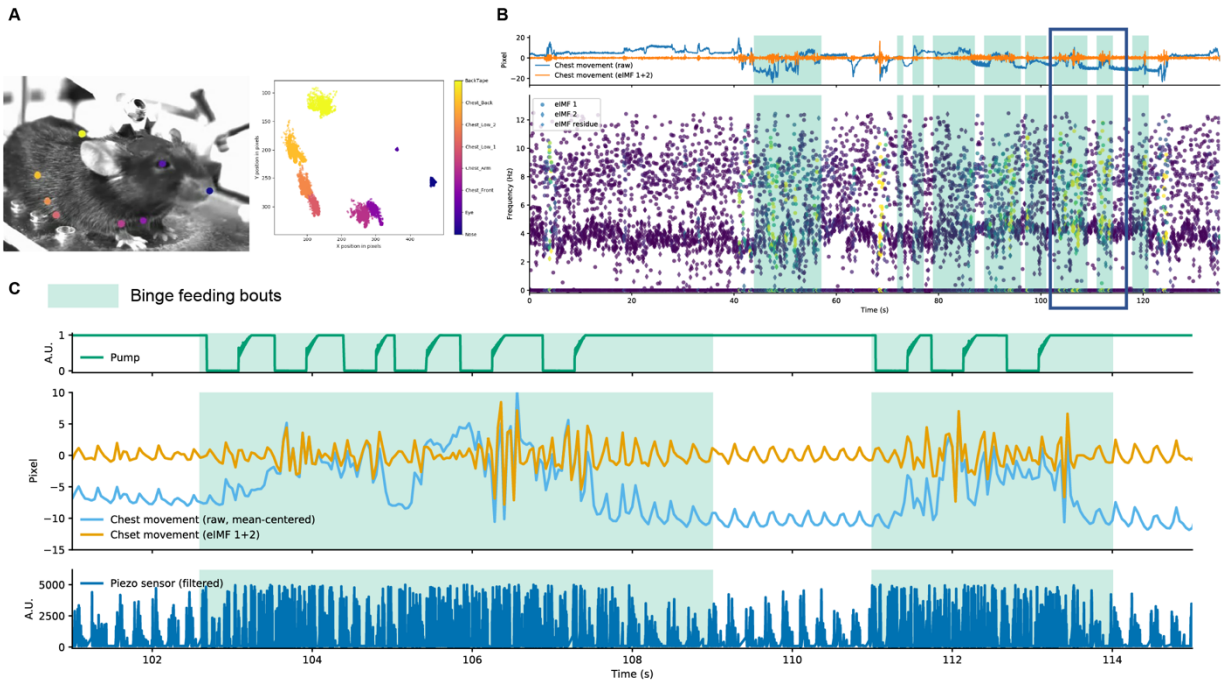

Figure 25. ***Respiration cycle during binge feeding.*** *(**A**) Left: Example image of DeepLabCut tracing of body parts of the mouse. Right: Extracted body parts over the time course. (**B**) Movement of the chest as a proxy for respiration. Upper panel: pixel values of the chest (raw and filtered traces). Bottom: Frequency time series of pixel movement using the Hilbert-Huang transform, the 4 Hz band is the respiration frequency. (**C**) Zoomed in on (**B**) to focus on two binge feeding bouts. The bottom panel represents the mechanical piezo sensor traces which are attached to the other side of the chest. (n = 2 mice).*

3.6. Binge feeding-induced aPC suppression is not inherited from the OB

Though that the respiration is intact during binge feeding, the exact olfactory sensation can still be altered in the OSNs or the OB. While aPC is capable of inferring odor identity by degraded odor inputs via pattern completion by recurrent networks (Bolding et al., 2019), binge feeding may already affect the odor transmission from the OSNs to the OB glomeruli. I therefore tested if the olfactory flavor representation can still be observed in the OB mitral cells during binge feeding. Mitral cells are the main output neuron type in the OB projecting to the aPC. Due to the anatomical location of the OB, an endomicroscopic implant combined with a miniscope is not a feasible option. I therefore decided to switch to a head-fixed setup with a 3-Photon (3P) microscope (Figure 26A). With support from colleagues, I measured the neuronal activities in the OB mitral cells by imaging the Ca^{2+} indicator GCaMP7s in the OB (Figure 27A). A preceding surgical procedure of viral injection of hSyn-GCaMP7s in the OB and a cranial window surgery was performed 3 weeks before the imaging session. The identification of OB mitral cells is based on the imaging panel at a depth (~200-300 μm) to reach the mitral cell layer underneath the OB glomeruli layer and the morphology of the mitral cells (large cell body size with a distinct shape of neurites, being generally larger than other cell types in the neighboring area) (Figure 26B). The Ca^{2+} imaging results show that OB mitral cell activity remains at a similar level of activity in both slow feeding and binge feeding behaviors, with no distinguishable population activity and single neuron level (Figure 26C, D, Figure 27). This net excitatory OB output to the aPC during both feeding types suggests a clear olfactory input signal to the aPC, despite an absence of activity in the aPC during binge feeding. I thus ruled out the hypothesis that degradation of upstream sensory input explains the suppression of aPC activity during binge feeding.

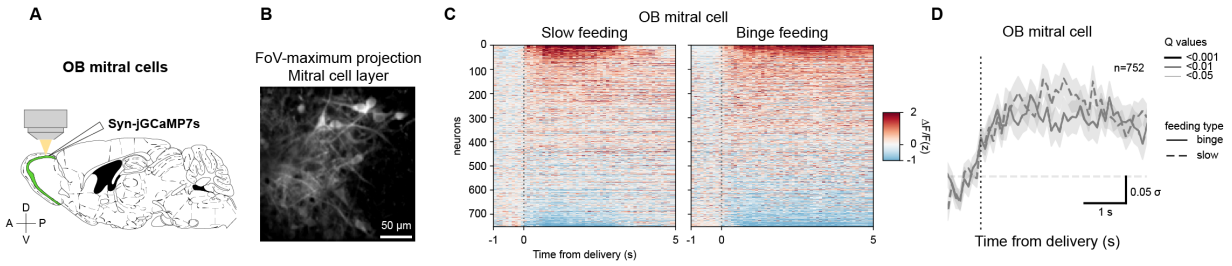

Figure 26. ***OB neuronal responses during feeding.*** *(**A**) Schematics of head-fixed 3P-Ca^{2+} imaging in OB mitral cells. (**B**) Example image of OB mitral cells in the OB. (**C**) Trial-average of individual OB mitral cells during feeding. Left, slow feeding. Right, binge feeding. (n=752 cells from 4 mice). (**D**) Trial-average of all OB mitral cells responses during slow and binge feeding (n is the same as in **C**). The shaded line on top of the average traces indicates the Q-values (adjusted P values) of individual time points. The different line widths represent different Q-values (from thin width to thick width: Q <0.05, <0.01, <0.001).*

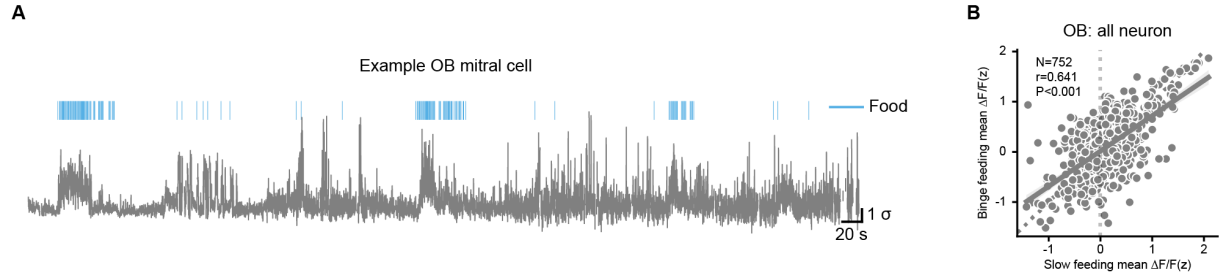

Figure 27. ***Example OB mitral cell trace and comparison of individual OB neurons.*** *(**A**) Ca^{2+} trace from an example OB mitral cell during slow feeding and binge feeding. (**B**) Comparison of individual OB mitral neuronal responses during slow feeding and binge feeding (n=752 cells from 4 mice). The correlation coefficient and P-value are calculated from Pearson's r.*

3.7. Binge feeding-induced aPC suppression extends to the major classes of local GABAergic neurons

From the abovementioned experimental results, I concluded that the excitatory sensory drive onto the aPC is unaffected by feeding rates, excluding upstream olfactory input alterations as the main cause of binge feeding-induced aPC suppression. This leaves me with two remaining hypotheses to examine. One of them is the straightforward hypothesis that the binge feeding behavior recruits local GABAergic neurons, which inhibit aPC neurons. Local inhibitory neurons in the aPC can be classified into two classes; feedforward inhibitory neurons that are activated by the OB mitral cell inputs and feedback inhibitory neurons that are activated by the recurrent excitatory aPC activity. A recent study has shown that the inhibitory effect from the feedforward neurons in the aPC scales with LOT stimulation strengths and these neurons do not perform supralinear sensory integration (Large et al., 2016a), meaning it is unlikely to constitute the global shutdown in the aPC. A different *in vivo* study also suggested that under *in vivo* awake recording in aPC, the inhibitory modulation is mostly contributed by the feedback inhibitory neurons instead of the feedforward inhibitory neurons (Bolding and Franks, 2018). Therefore, I focussed on the feedback inhibitory neurons in the aPC. Of the common three types of feedback-inhibitory GABAergic neurons in the aPC, I centered the study on PV^+ and SST^+ neurons in the aPC since they constitute most network suppression in the aPC. In contrast, the VIP^+ neurons usually suppress PV and SST neurons and trigger a disinhibitory effect on the aPC network. By injecting Cre-dependent GCaMP6f viruses in the aPC of PV-Cre or SST-Cre mouse lines, I could image Ca^{2+} dynamics in the desired aPC population with a miniscope (Figure 28A, B, E, F). Surprisingly, I found both PV^+ and SST^+ neurons showed strong suppression during binge feeding, while clear excitatory responses of both cell types are presented during slow feeding (Figure 28C, D, G, H, Figure 30, Figure 31). These results suggest that changes in the excitation-to-inhibition ratio of sensory afferent and local recurrent aPC circuits do not seem to mediate the binge feeding-induced non-specific global suppression of aPC activity. On the contrary, excitatory and inhibitory neurons in the aPC are suppressed during binge feeding, suggesting that binge feeding globally affects aPC circuits via a long-range modulatory mechanism (Figure 29).

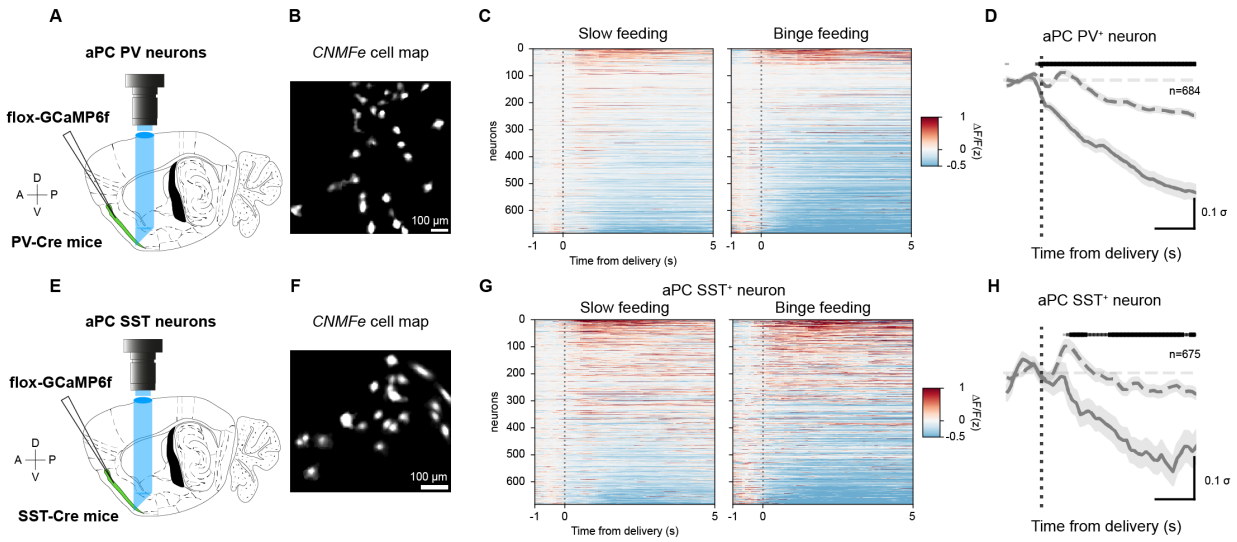

Figure 28. ***Effects of feeding rate in GABAergic aPC neurons.*** *(**A**) Schematics of miniscope Ca^{2+} imaging in aPC PV^{+} neurons. (**B**) Detected active PV^{+} neurons in the aPC, extracted by CNMFe. (**C**) Trial-average of neuronal responses during feeding of individual aPC PV^{+} neurons. Left, slow feeding. Right, binge feeding. (n=684 cells from 3 mice). (**D**) Trial-average of all aPC PV^{+} neurons during feeding (n is the same as in **C**). (**E**) Schematics of miniscope Ca^{2+} imaging in aPC SST^{+} neurons. (**F**) Detected active SST^{+} neurons in the aPC, extracted by CNMFe. (**G**) Trial-average of neuronal responses during feeding of individual aPC SST^{+} neurons. Left, slow feeding. Right, binge feeding (n=675 cells from 3 mice). (**H**) Trial-average of all aPC SST^{+} neurons during feeding (n is the same as in **G**). The shaded line on top of the average traces indicates the Q-values (adjusted P values) of individual time points. The different line widths represent different Q-values (from thin width to thick width: Q <0.05, <0.01, <0.001).*

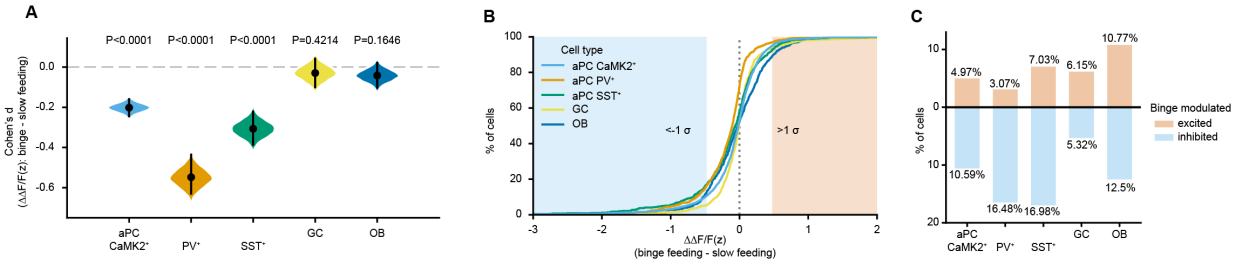

Figure 29. ***Binge feeding-induced modulation in aPC, GC, and OB.*** *(**A**) Binge-induced modulation in aPC $CaMK2^{+}$, aPC PV^{+}, aPC SST^{+}, GC, and OB mitral cells, units in Cohen's d (estimated effect sizes). (**B**) Cumulative distribution of binge-induced modulation. Units in difference in $\Delta F/F(z)$ ($\Delta\Delta F/F(z)$) in aPC $CaMK2^{+}$, aPC PV^{+}, aPC SST^{+}, GC, and OB mitral cells. (**C**) The proportion of excited and inhibited modulation induced by binge feeding in aPC $CaMK2^{+}$, aPC PV^{+}, aPC SST^{+}, GC, and OB mitral cells.*

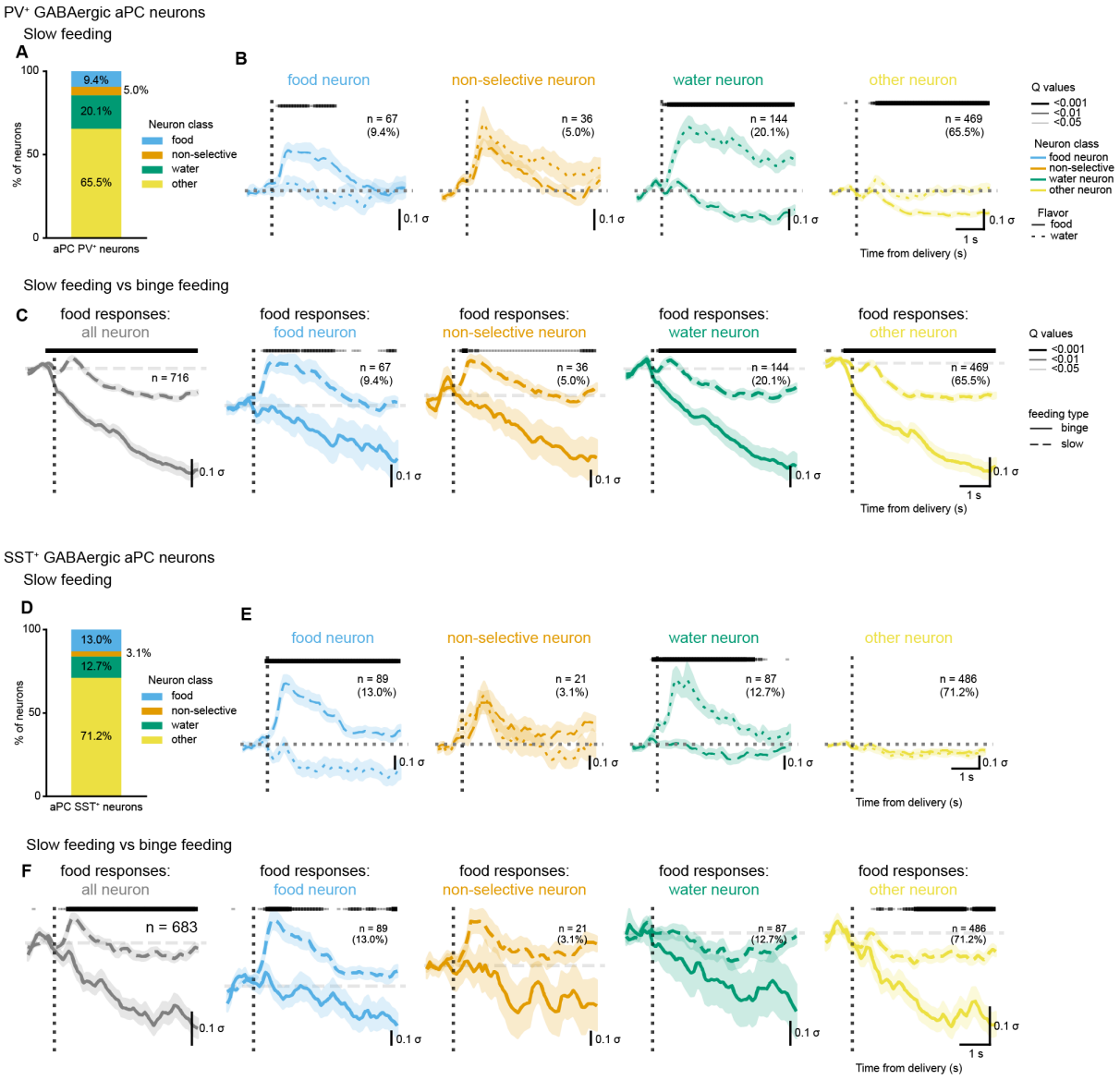

Figure 30. ***GABAergic aPC neuronal responses during feeding.*** *(**A**) Four subclasses of aPC PV⁺ neurons (n=67 cells for food neurons, 36 cells for non-selective neurons, 144 cells for water neurons, and 469 cells for other neurons from 3 mice). (**B**) Subclasses' responses during slow feeding for food and water deliveries (n is the same as in **A**, except n=716 cells for all neurons). (**C**) Neuronal responses for aPC PV⁺ neurons and each subclass during feeding (n is the same as in **B**). (**D**) Same as in (**A**) but for aPC SST⁺ neurons (n=89 cells for food neurons, 21 cells for non-selective neurons, 87 cells for water neurons, and 486 cells for other neurons from 3 mice). (**E**) Same as in (**B**) but for aPC SST⁺ neurons (n is the same as in **D**). (**F**) Same as in (**C**) but for aPC SST⁺ neurons (n is the same as in (**E**) except n=683 cells in all neurons). The shaded line on top of the average traces indicates the Q-values (adjusted P values) of individual time points. The different line widths represent different Q-values (from thin width to thick width: Q <0.05, <0.01, <0.001).*

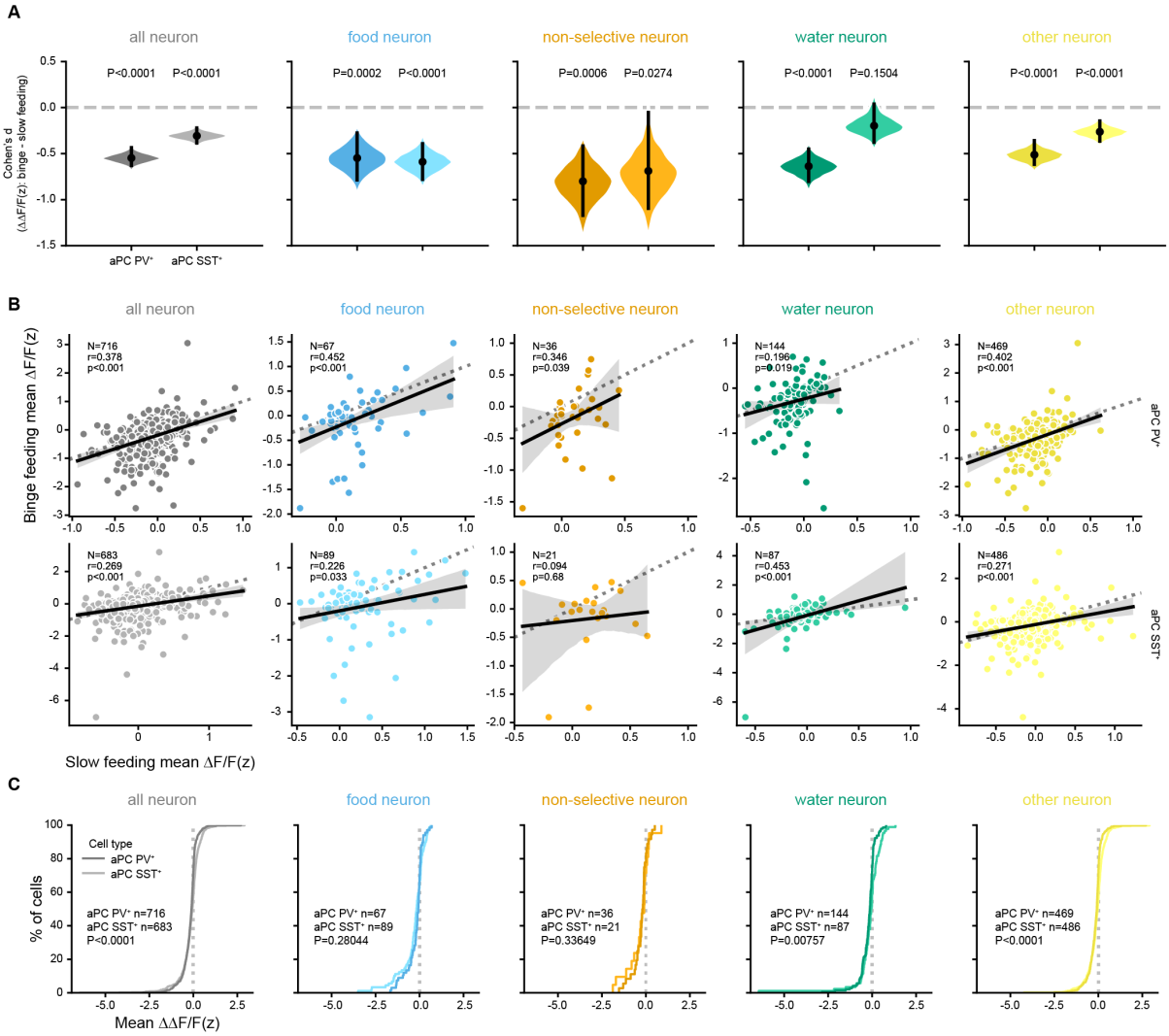

Figure 31. ***Additional analysis on GABAergic aPC neurons during feeding.*** *(**A**) Binge feeding-induced suppression in aPC PV⁺ and aPC SST⁺ subclasses, units in Cohen's d (estimated effect size) (For aPC PV⁺ neurons, n=716 cells for all neurons, 67 cells for food neurons, 36 cells for non-selective neurons, 144 cells for water neurons, 469 cells for other neurons from 3 mice. For aPC SST⁺ neurons, n=683 cells for all neurons, n=89 cells for food neurons, 21 cells for non-selective neurons, 87 cells for water neurons, and 486 cells for other neurons from 3 mice). (**B**) Comparison of individual GABAergic neurons during slow feeding and binge feeding in individual subclasses (n is the same as in **A**). (**C**) Cumulative distribution of the modulation induced by binge feeding (binge feeding - slow feeding, ΔΔ F/F(z)) in aPC PV⁺ and aPC SST⁺ subclasses (n is the same as in **A**).*

3.8. Serotonergic and dopaminergic neuromodulations are not coupled with the binge feeding-induced anterior piriform cortex suppression

Besides input degradation and local GABAergic modulations, neuromodulation could be another reason for binge feeding-induced aPC suppression. Two neuromodulators, serotonin (5HT) and dopamine (DA) are most likely to contribute to this suppression based on the projection, the receptor types, and their neurophysiological dynamics upon feeding.

One neuromodulatory mechanism that can suppress aPC activity is serotonergic modulation. Serotonergic neurons from the dorsal raphe nucleus produce and release serotonin to downstream areas, including the aPC. Serotonin binds to serotonergic receptors (5-HT receptors), including six families of GPCR receptors that activate an intracellular second messenger cascade to produce an excitatory or inhibitory response based on different G-protein subunits and one family (5-HT_3 receptor) of ligand-gated ion channels, which depolarizes cells via Na^+ and/or K^+ ions. In the aPC excitatory neurons, the expressing 5-HT receptors are 5-HT_1A (Piszár and Lőrincz, 2022) and 5-HT_2C (Sheldon and Aghajanian, 1991; Wang et al., 2020a), which have inhibitory effects via G_q protein pathways that ultimately increase the phospholipase C and calcium-activated potassium (BK) channel activity (Wang et al., 2020a). Conversely, the 5-HT_2A receptor is most expressed in the inhibitory neurons in the aPC (Marek and Aghajanian, 1994; Sheldon and Aghajanian, 1991), which activates neurons in the presence of 5-HT. These expression patterns of 5-HT receptors provide a general inhibitory effect in the aPC in the presence of 5-HT release. This is supported by the reduced aPC neuronal activity upon optogenetically stimulating 5HT neurons (Lottem et al., 2016). Serotonergic neurons in the dorsal raphe nucleus also actively respond to reward presentation and reward prediction errors, suggesting that serotonin is released upon positive valence experiences, including ingestion of hedonic food (Li et al., 2016; Paquelet et al., 2022; Ren et al., 2018).

To examine whether net inhibitory serotonin release can be the potential suppression mechanism of binge feeding-induced aPC suppression, I used a serotonin sensor (iSeroSnFR (Unger et al., 2020)), to track the dynamics of serotonin concentration in the aPC upon feeding behaviors. With support from Friedrich Johenning, I validated the sensor via

imaging the green fluorescence under the spinning disc confocal microscope with electrical stimulation of potential serotonergic fibers or bath wash-in of serotonin *in vitro* (Figure 32).

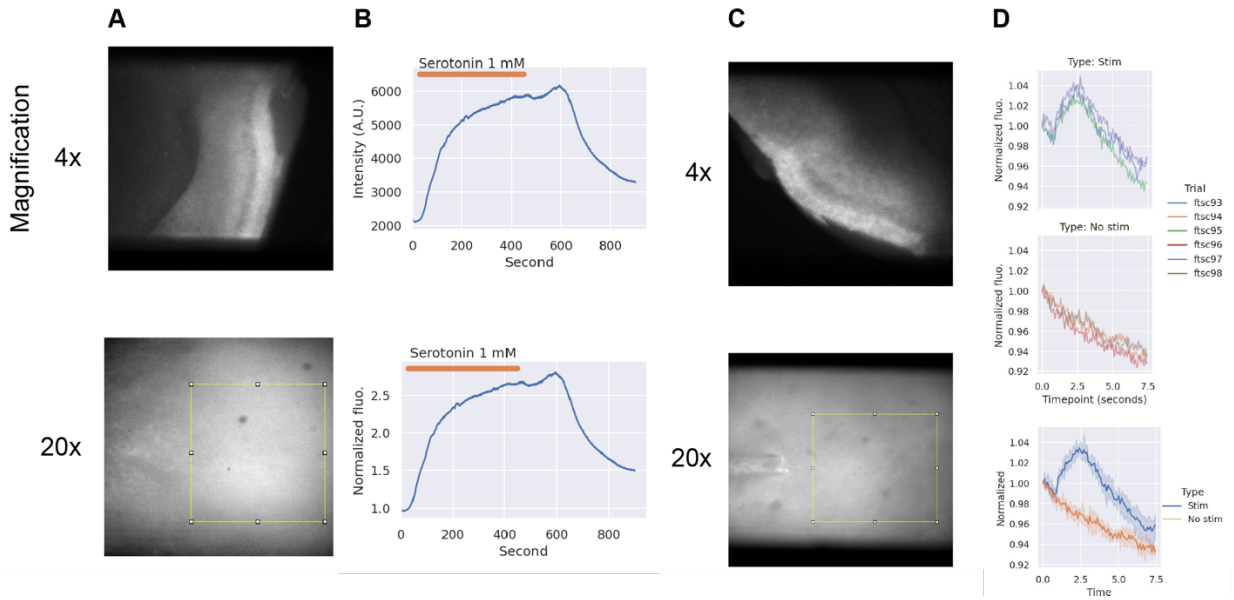

Figure 32. ***In vitro verification of a serotonin sensor, iSeroSnFR, in acute brain slices.*** *(**A**) iSeroSnFR expression in the acute aPC brain slice with bath-application of serotonin wash-in. Top row, 4x magnification image. Bottom row, 20x magnification image. (**B**) Top row, raw trace of fluorescence intensity from the FoV (highlighted in the bottom row image). Bottom row, normalized fluorescence trace from the top row. (**C**) iSeroSnFR expression in the acute aPC brain slice with electrical stimulation of putative serotonergic fibers in the aPC. Top row, 4x magnification image. Bottom row, 20x magnification image. (**D**) Fluorescence intensity traces from the FoV (highlighted in the (**C**) bottom row image) with and without electrical stimulations. The shaded area represents the s.e.m. of the data.*

Using a similar imaging technique for *in vivo* Ca^{2+} recording with a miniscope, I imaged the fluorescence of iSeroSnFR in the aPC to measure 5-HT concentrations during feeding. Surprisingly, I found that the serotonin concentration drops upon feeding, regardless of slow or binge feeding (Figure 33). This result, showing decreased serotonin release in the aPC, contradicted my expected outcome and the potential inhibitory mechanism via serotonergic modulation. This phenomenon can be explained by the heterogeneous projections and response patterns of serotonergic neurons (Paquelet et al., 2022; Ren et al., 2018; Seo et al., 2019), or by the decoupling of serotonergic neuron somata activity and the serotonergic fibers via presynaptic GABAergic disinhibition circuits (Yu et al., 2022). However, this does not support the hypothesis of binge feeding-induced aPC suppression via serotonergic modulation.

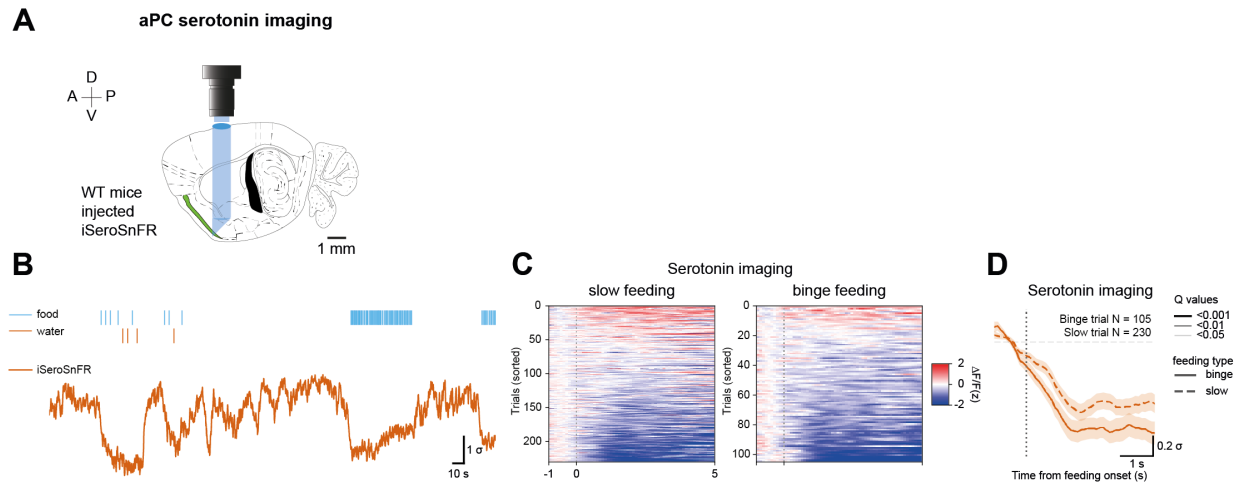

Figure 33. ***Serotonin release is decreased during feeding regardless of feeding rates.*** *(**A**) Schematics of serotonin imaging in the aPC. (**B**) Example trace of iSeroSnFR imaging during feeding bouts. (**C**) Heatmaps of individual feeding trials of different feeding types. Left, slow feeding. Right, binge feeding (n=230 trials for slow feeding, n=105 trials for binge feeding, from 3 mice). (**D**) Trial-average of serotonin traces during different feeding types The shaded line on top of the average traces indicates the Q-values (adjusted P values) of individual time points. The different line widths represent different Q-values (from thin width to thick width: Q <0.05, <0.01, <0.001)*

The other neuromodulatory mechanism in the aPC under investigation here is Dopamine. Dopamine (DA) is known to be tightly coupled with positive valences such as rewards and associated computations like reward prediction errors (Schultz, 2016; Schultz et al., 1997). A recent study has also suggested that dopaminergic neurons respond to the ingestion of water and osmolarity changes after ingesting water, providing a parallel circuit mechanism of homeostasis in regulating water consumption (Grove et al., 2022). While there are direct projections from VTA to aPC (Aransay et al., 2015), the projections are not as strong as VTA to NAcc or VTA to olfactory tubercle. Dopaminergic receptors in the aPC are also non-canonical. While most dopaminergic receptors expressed in the striatum regions are the mutually exclusive Drd1 and Drd2 (Cox and Witten, 2019; Fang and Creed, 2024), there are solely Drd3 receptors in the aPC (Zhang et al., 2021b). Drd3 receptors are GPCRs that activate the $G_{i/o}$ pathway and suppress the adenylyl cyclase when binding with DA (Ahlgren-Beckendorf and Levant, 2004; Robinson and Caron, 1997), but their function in the aPC has yet to be reported. I tested this by with bath applying DA on the acute aPC slices. I found reduced excitability in 60% of patched neurons (n=9/15 inhibited, n=4/15 [26.7%] not modulated, n=2/15 [13.3%] excited, Figure 34), suggesting that DA/Drd3 has an inhibitory effect in the aPC.

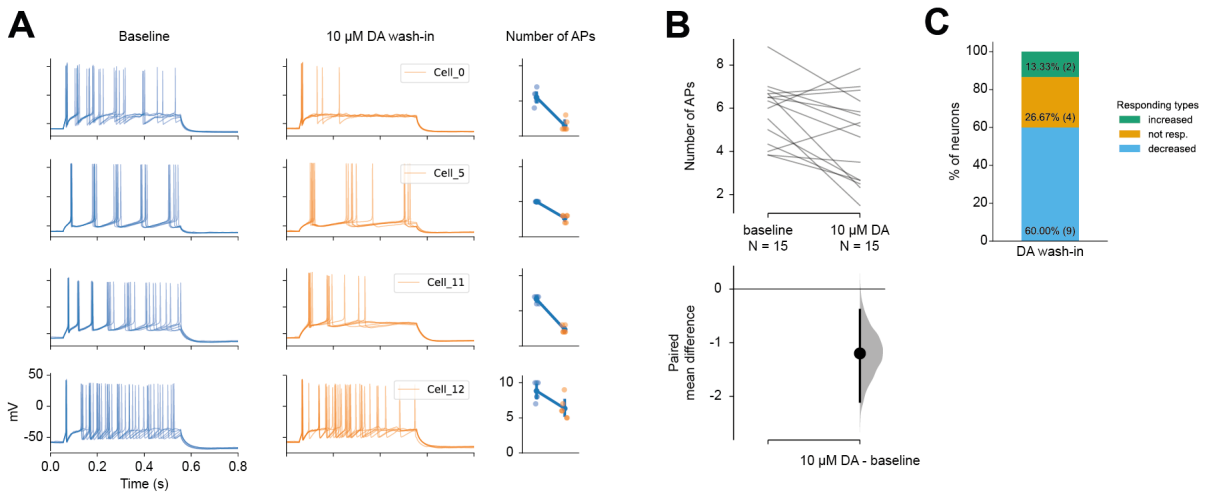

Figure 34. ***DA reduces the excitability of aPC neurons.*** *(**A**) Example aPC neurons with current injection in baseline or with DA wash-in. The number of action potentials (AP) is quantified on the right. (**B**) Effects of DA wash-in for individual aPC neurons (n=15 neurons from 3 mice). (**C**) The proportion of aPC neurons is modulated by DA.*

To track DA dynamics in the aPC during feeding, I injected the DA sensor dLight$_{1.3b}$ in the aPC and imaged it with a miniscope. The dLight$_{1.3b}$ trace revealed that, regardless of feeding rates, DA concentration had dropped during feeding, similarly to my results on 5-HT imaging. This finding was again unexpected and contrary to DA's general dynamic pattern upon reward presentations. Somata-axon decoupling via local ACh modulation is unlikely to explain the drop in DA concentration since the ACh-modulated DA concentration only releases more DA, rather than blocking the release of the DA (Liu et al., 2022).

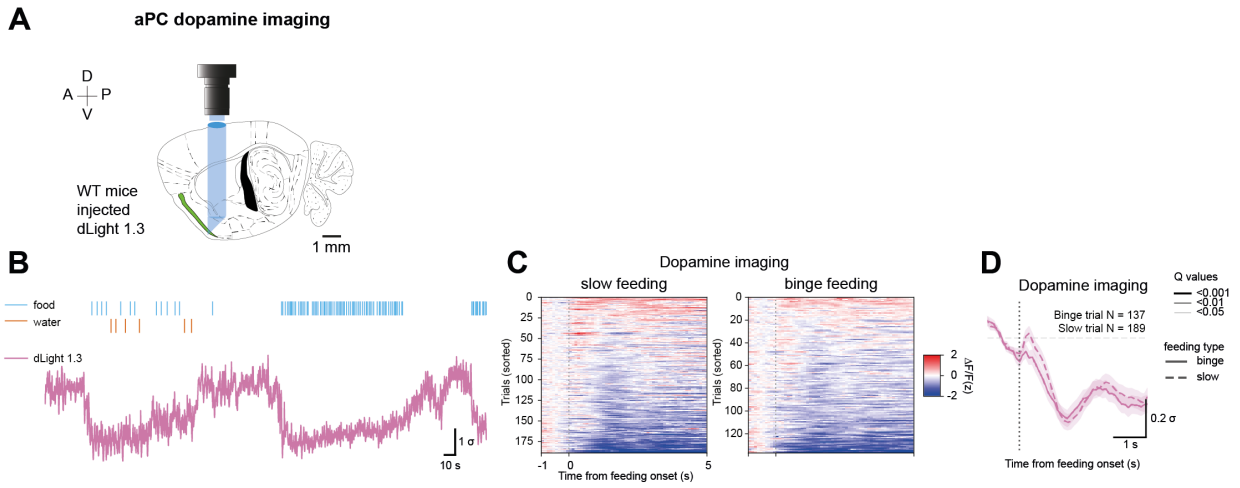

Figure 35. ***Dopamine release is decreased during feeding regardless of feeding rates.*** *(**A**) Schematics of dopamine imaging in the aPC. (**B**) Example trace of dLight$_{1.3b}$ imaging during feeding bouts. (**C**) Heatmaps of individual feeding trials of different feeding types. Left, slow feeding. Right, binge feeding. (n=189 trials for slow feeding, n=137 for binge feeding, from 3 mice). (**D**) Trial-average of dopamine traces during different feeding types. The shaded line on top of the average traces indicates the Q-values (adjusted P values) of individual time points. The different line widths represent different Q-values (from thin width to thick width: Q <0.05, <0.01, <0.001)*

I therefore concluded that neither long-range serotonergic nor dopaminergic modulations are likely to be the circuit mechanism of binge feeding-induced aPC suppression. These results may indirectly suggest a different long-range GABAergic modulation onto the projecting fibers in the aPC (see **Discussion 4.3.1** for long-range GABAergic modulation) via $GABA_A$ receptors on the projecting fibers (Yu et al., 2022).

3.9. The magnitude of binge feeding-induced aPC suppression correlates with appetite

Bypassing flavor perception through an intragastric catheter reduces satiation. This causes the acceleration of gastric emptying of identical food items, showing that experiencing the flavor of food items in the oral cavity (orosensory) contributes to satiation (Cecil et al., 1999). The binge feeding-induced aPC suppression may reduce the sensory representation of food items. Does the aPC suppression during binge feeding constitute a mechanistic link between a sensory neuronal representation in the flavor system and decreased satiation? I further hypothesized that the degrees of aPC suppression may reflect individual internal needs or the satiation level. Under ad libitum feeding conditions, mice consumed varied amounts of food on different experimental days, which can be used as a proxy for their level of appetite/satiation on each day. Despite the correlation being weak, mice consumed more food in the later behavioral sessions, suggesting that binge feeding gradually escalates over five weeks (Figure 36). I then analyzed the level of feeding-induced neuronal activity against the corresponding amount of food intake on each recording day. Using a linear mixed model, I found a robust time-independent correlation between the magnitude of feeding-related aPC neuronal activity reduction and subsequent food consumption, whereby stronger reduction correlates with enhanced consumption (Figure 37). This consumption-correlated neuronal modulation is only observed in binge feeding, thus not in slow feeding. My model contains only the neuronal responses upon the onset of the feeding bout as predictors and does not contain information about the length of the feeding bout. Therefore, the model quantifies the correlation independent of feeding duration. Among other cell types I have recorded, only aPC PV+ neurons exhibit similar consumption-correlated neuronal modulation. Other cell types like aPC SST+ and GC neurons do not show such correlations between neuronal modulation and food intake. These results indicate that the consumption-correlated neuronal modulation is mostly restricted to the olfactory domain of flavor perception. Since such a correlation is only observed during binge feeding, it may suggest a special role of binge feeding in satiation signaling.

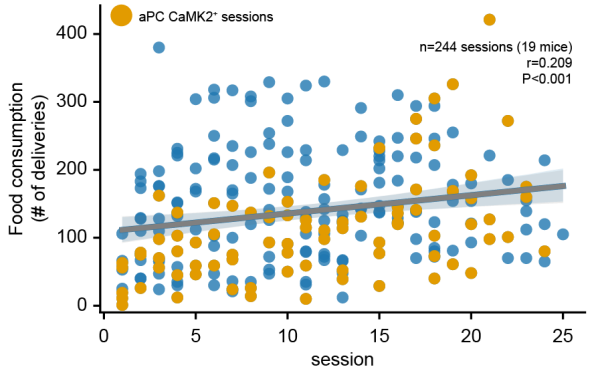

Figure 36. ***Food consumption across experimental sessions.*** *Amount of food consumed on different recording sessions (n=244 sessions from 19 mice). Orange dots represent recording sessions from aPC CaMK2⁺ mice (n=84 sessions from 8 mice). Blue dots represent all other recorded mice (aPC GABAergic and GC mice).*

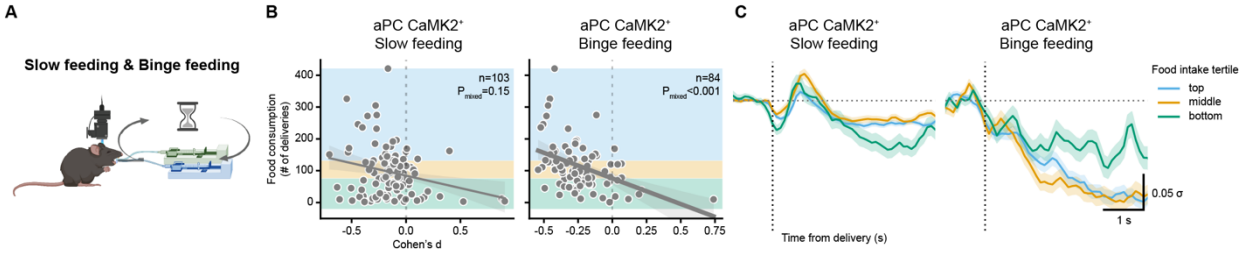

Figure 37. ***Correlation between food consumption and binge feeding-induced aPC modulation.*** *(**A**) Schematics of in vivo miniscope Ca^{2+} imaging and the feeding paradigm is the same as in* ***Results 3.2****. (**B**) Correlations between the total amount of food consumed in one recording session and the feeding-induced modulation in aPC CaMK2⁺ neurons. Left, slow feeding. Right, binge feeding. (n=103 slow feeding sessions and 84 binge feeding sessions from 8 mice). A linear mixed model was used for calculating the significance level of neuronal responses to food consumption. (**C**) Neuronal responses from aPC CaMK2⁺ neurons with tertile clustering, based on food consumption, with each tertile represented in one color (corresponding to **B**). (n=34, 35, 34 sessions for top, middle, and bottom clusters in slow feeding from 8 mice, respectively; n=28, 28, 28 sessions for top, middle, and bottom clusters in binge feeding from 8 mice, respectively).*

Table 7. Effects of aPC CaMK2^{+} neuronal activity during slow feeding on food consumption.

Fixed effects:	*Estimate*	*Std. Error*	*df*	*t value*	*Pr(>|t|)*
(Intercept)	28.423	16.154	22.387	1.76	0.0922 .
session	4.936	1.037	99.704	4.761	6.55e-06 ***
cohens_d	-36.306	25.239	102.971	-1.438	0.1533
---					

*Signif. codes: 0 '***' 0.001 '**' 0.01'*' 0.05'.' 0.1 ' ' 1*

Table 8. Effects of aPC CaMK2^{+} neuronal activity during binge feeding on food consumption.

Fixed effects:	*Estimate*	*Std. Error*	*df*	*t value*	*Pr(>|t|)*
(Intercept)	25.727	15.402	34.77	1.67	0.103833
session	4.764	1.016	79.382	4.691	1.12e-05 ***
cohens_d	-116.462	32.73	82.869	-3.558	0.000621 ***
---					

*Signif. codes: 0 '***' 0.001 '**' 0.01'*' 0.05'.' 0.1 ' ' 1*

3.10. Olfactory perception is necessary for the neuronal suppression-appetite correlation but not necessary for binge feeding-induced aPC suppression

Next, I further examined the necessary factors for the consumption-correlated neuronal suppression in the aPC during binge feeding. To check whether the olfactory perception of food items is necessary for the consumption-correlated suppression of neuronal activity, I reduced olfactory sensory inputs. With support from colleagues, I performed nasal lavage with 0.5% Triton X-100 solution to induce short-term anosmia in mice (Cummings et al., 2000). This treatment was verified with the buried food test, where overnight fasted mice must find a hidden food pellet buried in the beddings. Control mice with nasal lavage of phosphate-buffered saline (PBS) can successfully find food pellets in tens of seconds. In contrast, the Triton X-100 treated mice barely found the food pellets despite being highly motivated for food-seeking by fasting. At first, I found less detectable neurons after the Triton X-100 treatment. About 30% of the aPC excitatory neurons did not show olfaction-related activity after the Triton X-100 treatment (Figure 38), confirming a loss of olfactory sensory inputs. The Ca^{2+} imaging results from the anosmic mice showed that binge feeding-induced aPC suppression was still present, with no difference in the suppression magnitudes (Figure 39C, D), which may suggest that the binge feeding-induced suppression originates from outside the olfactory system. Anosmic mice ate more than their food intake amount preceding the Triton X-100 treatment, and the level of neuronal modulation no longer correlated with the amount of food intake (Figure 39B). The loss of neuronal correlates with appetite may come from the general increase in food consumption after treatment, so fewer data points are located in the lower range of food consumption. Alternatively, due to the loss of odor-responding neurons (presumably the 30% reduction of detected aPC neurons under anosmia), the neuronal representation I observed in the aPC during feeding under anosmia is only a subpopulation rather than the original population. This subpopulation may not reflect the general appetite levels, hences the loss of neuronal correlates with appetite. Here, I showed that the loss or decrease of olfactory perception of food items promotes feeding. Interestingly, olfactory perception is not a necessary factor of binge feeding-induced aPC suppression, suggesting the suppression mechanism is olfactory independent.

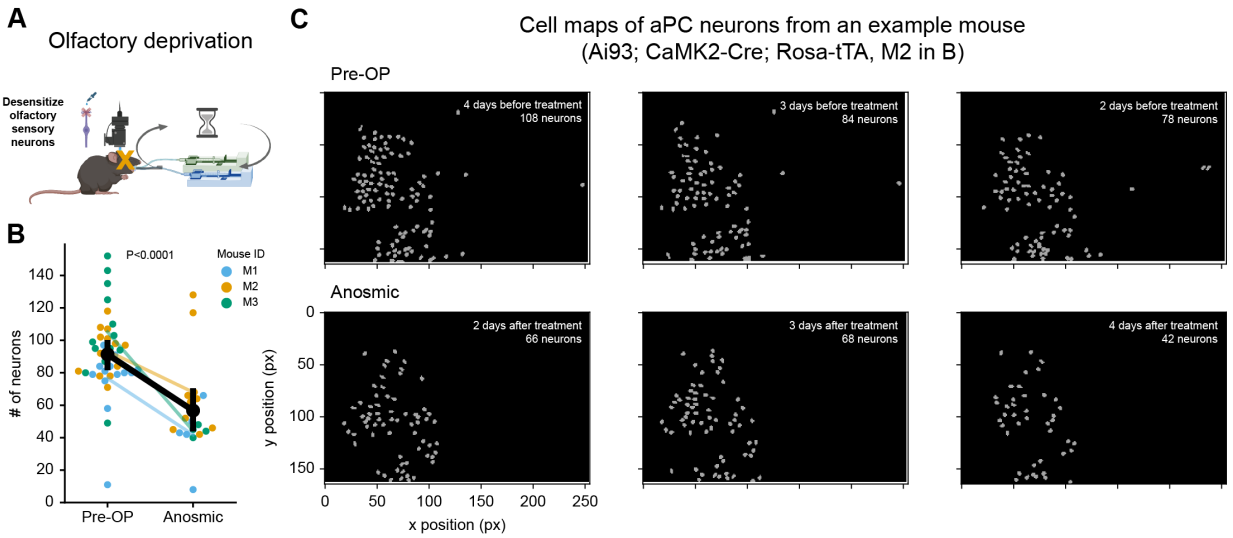

Figure 38. ***Effects of olfactory deprivation on detected cells in the aPC.*** *(**A**) Schematics of anosmic paradigm. (**B**) Detected active neuron number of aPC CaMK2⁺ mice before and after anosmia induction (n=21 before sessions and 15 anosmic sessions from the same 3 mice). (**C**) Cell maps of extracted aPC neurons by CNMFe before and after anosmia induction.*

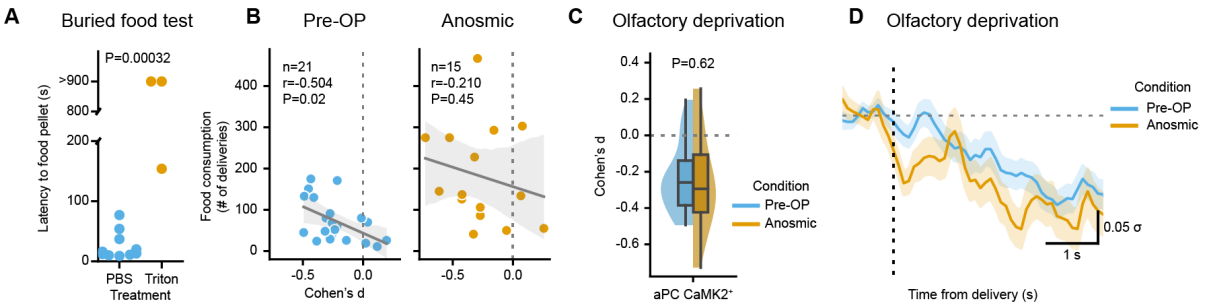

Figure 39. ***Effects of olfactory perception on feeding-induced aPC modulation.*** *(**A**) Amount of time for mice to find a buried food pellet. The buried food test is conducted 48 hrs after treatment (n=10 mice for PBS treated group, n=3 for the anosmic group). (**B**) Correlations of the amount of food consumed in each session and feeding-induced aPC CaMK2⁺ neuron modulation during binge feeding. Left, sessions before anosmia induction. Right, sessions after anosmia induction. (n=21 Pre-OP sessions and n=15 Anosmic sessions from the same 3 mice). (**C**) Binge feeding-induced neuronal modulation with intact olfaction and under anosmia (n is the same as in **B**). (**D**) Neuronal activity of aPC CaMK2⁺ neurons upon binge feeding. The blue line represents intact olfaction and the orange line represents anosmic (n is the same as in **B**).*

3.11. Effects of metabolic state on binge feeding-induced aPC modulation

Metabolic states like hunger often drastically affect neuronal dynamics to match the metabolic needs, especially enhancing the foraging-related sensory systems including olfaction (Aimé et al., 2007; Albrecht et al., 2009; Allen et al., 2019; Freeman, 1960; Prud'homme et al., 2009; Richman et al., 2023; Soria-Gómez et al., 2014). I have shown that the magnitude of binge feeding-induced aPC suppression correlates with general appetite in individual sessions. Whether the homeostatic needs modulate this consumption-related neuronal suppression is yet to be demonstrated. To test this, implanted mice were food-deprived overnight (~20-22 hours) before the recording session to ensure the hunger state. Fasted mice consumed more food, confirming the hunger state and an enhanced binge feeding-induced aPC suppression compared to *ad libitum*-fed conditions. Under the hunger state, the abovementioned correlation between food consumption and aPC neuronal activity suppression no longer exists. In the GC neurons, an enhanced suppression was also observed compared to *ad libitum*-fed conditions, despite no correlations between food consumption and binge feeding-induced neuronal modulation in either *ad libitum* or fasted conditions. This may suggest that the neuronal correlates of appetite in the aPC are mostly utilized for modulating hedonic feeding (feeding for pleasantness). When switching from hedonic feeding to homeostatic feeding (feeding for metabolic needs and pleasantness), the olfactory flavor feedback is not used as a fine-tuned feedback to control feeding (Avena, 2015). In the GC, the neuronal correlates of appetite only reflect larger homeostatic needs (e.g. overnight fasting) instead of a general appetite for food during hedonic feeding. Here, I concluded that hunger enhances binge feeding-induced suppression in both the aPC and GC, with differential influences of the consumption-related neuronal modulation in these two brain regions.

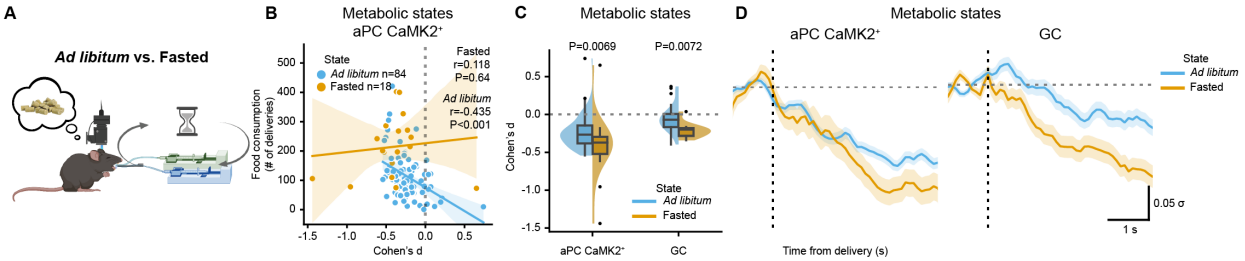

Figure 40. ***Effects of hunger on feeding-induced modulation****. (**A**) Schematics of different metabolic states. (**B**) Correlations between the amount of food consumed on each session and feeding-induced aPC CaMK2⁺ neurons modulation during binge feeding. Colors represent two different metabolic states. Blue, ad libitum. Orange, overnight fasted. (n=18 fasted sessions from 5 mice, n for ad libitum conditions is the same as in Figure 37**B**). (**C**) Binge feeding-induced neuronal modulation. Left, neuronal modulation in aPC CaMK2⁺ neurons. Right, neuronal modulation in GC neurons. Colors represent two different metabolic states. Blue, ad libitum. Orange, overnight fasted. (n is the same as in **B**). (**D**) Neuronal responses during feeding. Left, aPC CaMK2⁺ neurons. Right, GC neurons. Colors represent two different metabolic states. Blue, ad libitum. Orange, overnight fasted. (n is the same as in **B**).*

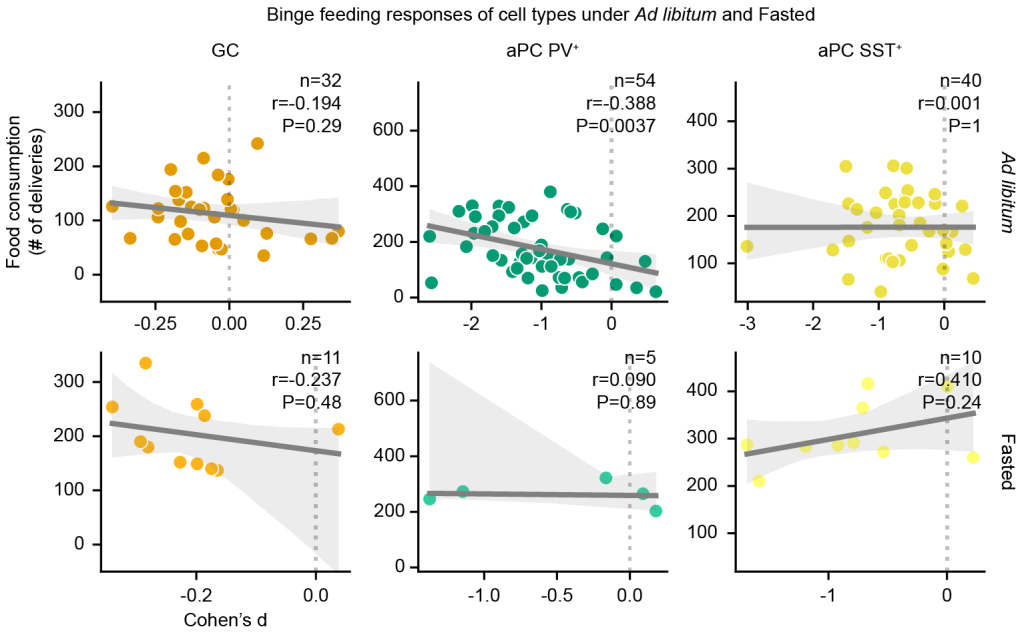

Figure 41. ***Effects of fasting on GC and GABAergic aPC neurons.*** *Binge feeding responses in different cell types under ad libitum and overnight fasted. Correlations between neuronal responses and the amount of food consumption are shown for each cell type. Upper row, ad libitum condition. Lower row, overnight fasted condition. (For GC, n=32 ad libitum sessions and 11 fasted sessions from 3 mice. For aPC PV⁺, n=54 ad libitum sessions and 11 fasted sessions from 3 mice. For aPC SST⁺, n=40 ad libitum sessions and 10 fasted sessions from 3 mice).*

3.12. Optogenetically suppressing aPC neurons promotes feeding

So far, I have demonstrated the relationship between feeding rate, olfactory flavor representation, and metabolic state. While binge feeding and appetite covary with the non-specific global suppression in the aPC, this correlation may reflect the desire for hedonic eating on different days or it may have an active role in promoting feeding. I hypothesized that either the observed sensory effect is an epiphenomenon (*H0*), or it reciprocally interacts with feeding behavior in a feedback loop (*H1*) (Figure 42). To decipher whether there is a causal relationship between aPC suppression and food intake, I employed the optogenetics technique to manipulate aPC activity during feeding. To prevent the alternative explanation of sensory hallucination caused by activating sensory cortex neurons, which may interrupt feeding behaviors as a neophobic response but not due to the increased level of satiation, I decided to pursue the opposite direction, by suppressing aPC neurons during feeding and measuring if this can decrease the satiation level and promote feeding. To manipulate neuronal activity at the behavioral timescale (tens of seconds) of binge feeding bouts while minimizing the illumination period, I chose the highly light-sensitive mosquito opsin eOPN3 to provide long-lasting suppression of recurrent excitatory fibers in the aPC (Mahn et al., 2021). With support from colleagues (Dr. Laura Moreno-Velasquez, Lukas Faiss and Dr. Benjamine Rost), I validated that the excitatory post-synaptic current (EPSC) of the recurrent circuits in the aPC was reduced by ~25% when a brief green light illumination (500 ms, 550-580 nm) was applied to the acute eOPN3-expressing aPC brain slices, and that this suppression could last for around 5-10 minutes before the EPSC returned to the original amplitude (Figure 43).

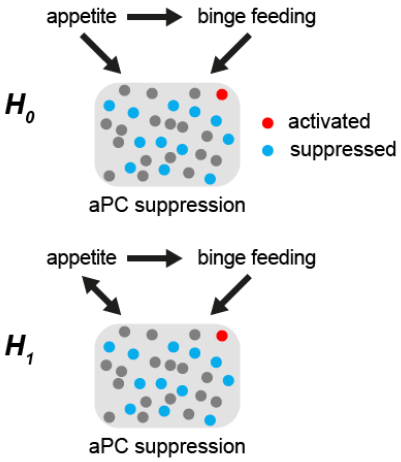

Figure 42. ***Illustration of different hypotheses.*** *H0, aPC suppression is modulated by appetite level and binge feeding behavior, and the modulation in the aPC does not feedback to these two factors. H1, aPC suppression is modulated by appetite level and binge feeding behavior, and the modulation in the aPC also regulates appetite level (reducing sensory satiety).*

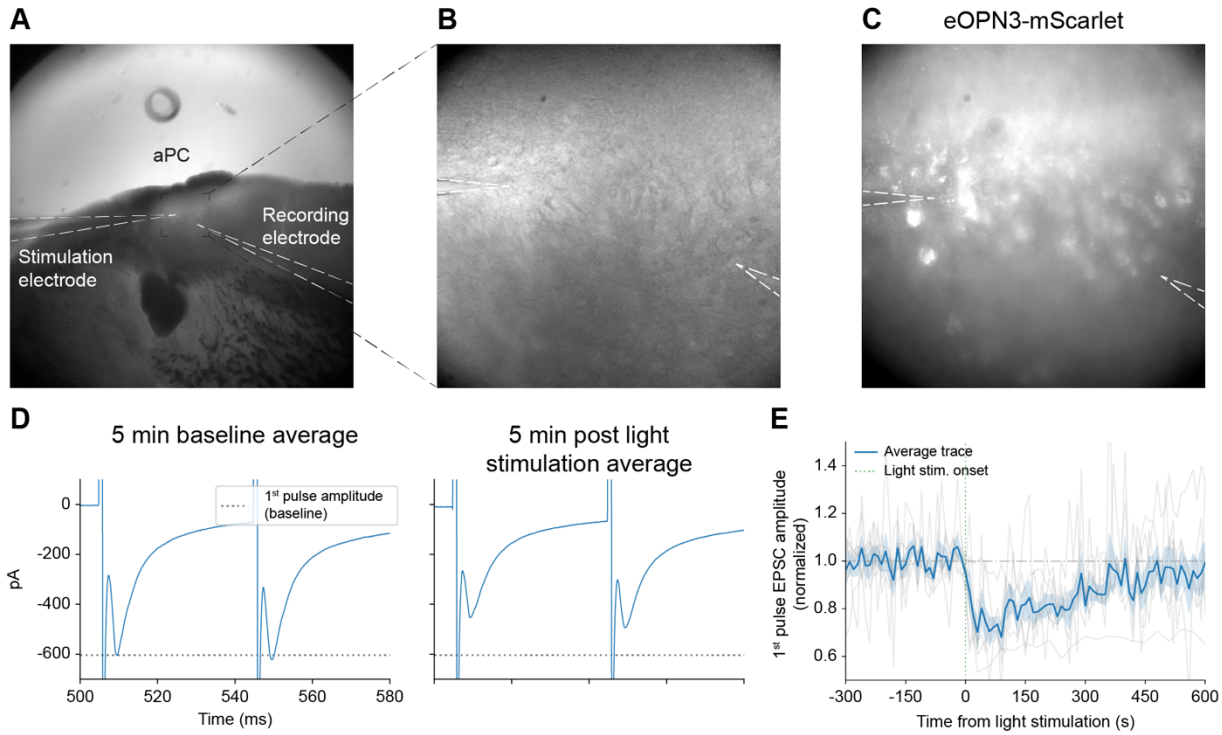

Figure 43. ***In vitro validation of eOPN3 in acute aPC brain slices.*** *(**A**) 4x magnification of aPC slice and electrode placement. (**B**) Zoomed-in image of the patching electrode and stimulation electrode. (**C**) Same as (**B**) but with a red channel showing the expression of eOPN3-mScarlet. (**D**) Left column, an example average trace of EPSC of patched aPC neurons with electrical stimulation of 1b recurrent fibers during baseline (averaged across 5 minutes to right before the light stimulation). Right column, an example average trace of EPSC of patched aPC neurons with electrical stimulation of 1b recurrent fibers after light stimulation (averaged across from right after light stimulation to 5 minutes after stimulation). (**E**) Individual trace (grey lines) and average trace (blue line) of the amplitude of the 1st EPSC pulse. (n=7 cells, 7 slices, from 2 mice).*

I virally injected the flox-eOPN3-mScarlet or flox-tdTomato (for control) in the aPC of CaMK2-Cre mice, and after 2-3 weeks of recovery, I implanted the optical fiber cannula in the aPC bilaterally (Figure 44, Figure 45). The implanted mice recovered for two weeks before starting the liquid food delivery system habituation and optical fiber patchcords were mounted. A closed-loop system was built to precisely activate the LED system when mice start binge feeding (criterion of 3-pump activations with an inter-activation interval of less than 1.5 seconds for verifying it is binge feeding). Under light stimulation to suppress aPC during feeding, I found the eOPN3-expressing mice consumed more food, and the total feeding duration was longer compared to no illumination days (Figure 46A-D). In contrast, the control mice consumed very similar amounts of food across illumination and no illumination days (Figure 46A-D). Performing a microanalysis of the feeding bouts, the total amount of bouts did not change between LED states (Figure 46F), but the eOPN3-expressing mice spent more time on individual feeding bouts (Figure 46E). My data supports the alternative hypothesis *H1* that binge feeding-induced aPC suppression reciprocally modulates appetite, implying that binge feeding-induced aPC suppression is causally linked to feeding behaviors and internal states (Figure 42).

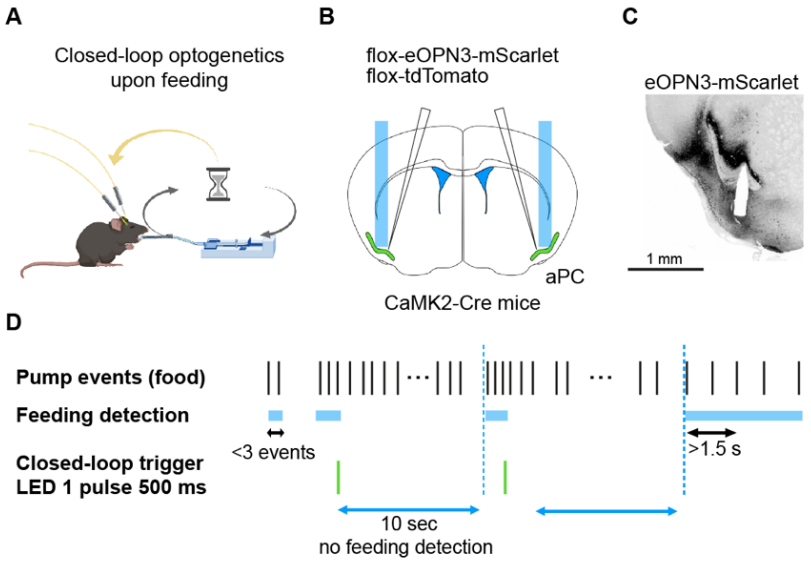

Figure 44. ***Closed-loop optogenetics paradigm.*** *(**A**) Schematics of closed-loop inhibitory optogenetics upon feeding onset. (**B**) Illustration of optogenetic viral injection and bilateral optical fiber implants. (**C**) Optical fiber implant path on an implanted brain slice. (**D**) Illustration of binge feeding bout detection, LED light triggers, and food deliveries.*

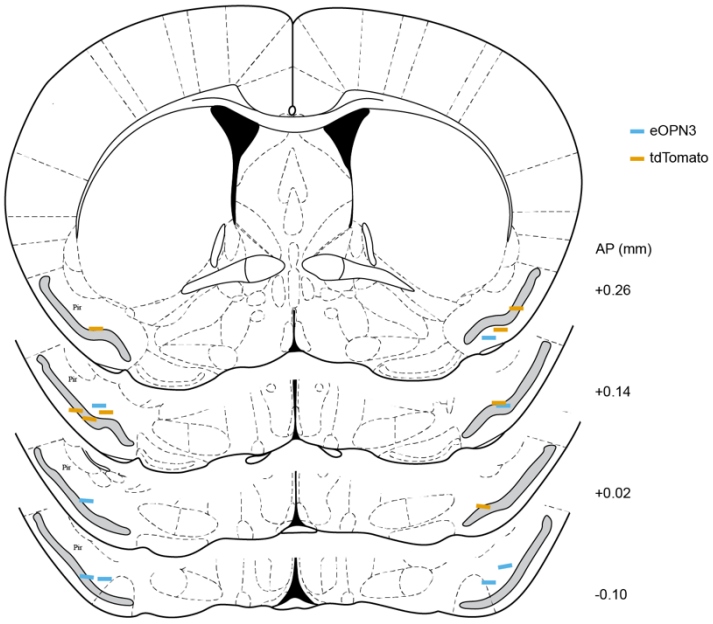

Figure 45. ***Optical fiber implant coordinates.*** *Implant coordinates of optical fiber cannulas. Blue lines denote the tips of optical fibers for eOPN3-expressing mice and orange lines denote the tips of optical fibers for tdTomato-expressing mice.*

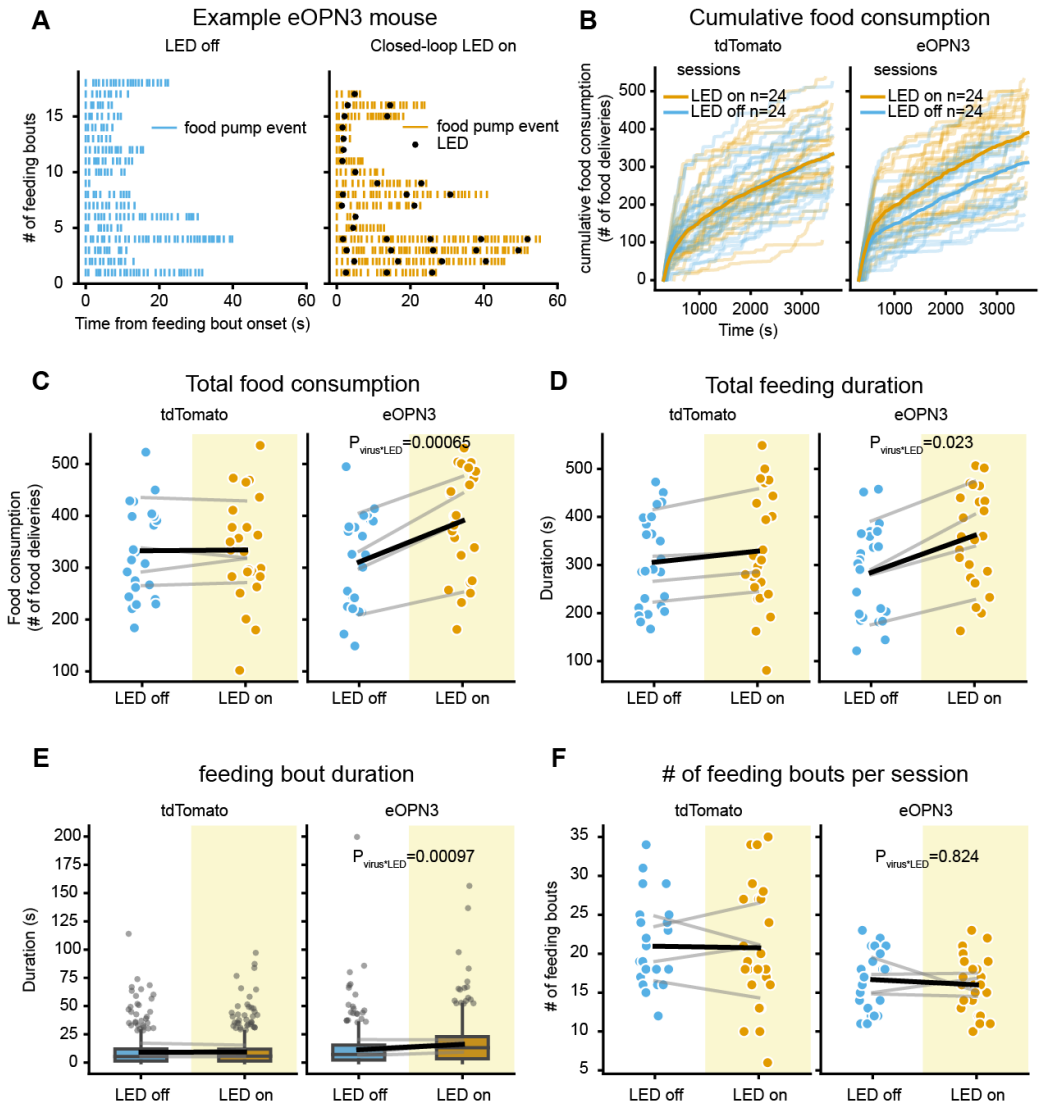

Figure 46. ***Effects of optogenetically suppressing aPC neurons.*** *(**A**) Feeding bout examples from mice expressing eOPN3 in the aPC. Left, no light stimulation (LED off) during feeding. Right, light stimulation (LED on) during feeding. (**B**) Time series of feeding events across experimental sessions. Left, feeding events from control mice (tdTomato expressed in the aPC, sessions=12 LED off, 12 LED on from 4 mice) with and without light stimulations. Right, feeding events from optogenetic suppression mice (eONP3 expressed in the aPC, sessions=12 LED off, 12 LED on from 4 mice). (**C**) Total food intake in one hour with or without light stimulation during feeding in control and optogenetic suppression mice. (**D**) Total feeding duration in one hour with or without light stimulation during feeding in control and optogenetic suppression mice. (**E**) Duration of individual feeding bout in one hour with or without light stimulation during feeding in control and optogenetic suppression mice. (**F**) Number of feeding bouts in one hour with or without light stimulation during feeding in control and optogenetic suppression mice. For (**C-F**), grey lines represent data obtained from the same mice and thick black lines indicate the mean value from all data. P values are measured with linear mixed models by calculating the contribution of the interaction term (virus type * LED states) between full and reduced models (see **Methods 2.10.6**).*

Table 9. Model comparison: effects of interactions of viral types and light stimulation on food consumption, related to Figure 46C.

Model comparison	npar	AIC	BIC	logLik	deviance	Chisq	Df	Pr(>Chisq)
Reduced model	9	1073.2	1096.3	-527.6	1055.2			
Full model	10	1063.6	1089.2	-521.78	1043.6	11.631	1	0.0006488 ***

Signif. codes: 0 '***' 0.001 '**' 0.01 '*' 0.05 '.' 0.1 ' ' 1								

Table 10. Contrast analysis: the difference between groups on food consumption, related to Figure 46C.

contrast	estimate	SE	df	t.ratio	p.value
LED off 0_tdTomato - LED off 1_eOPN3	39.4	61.9	16.4	0.637	0.8341
LED on 0_tdTomato - LED off 1_eOPN3	34.7	61.3	16.1	0.565	0.8687
LED on 1_eOPN3 - LED off 1_eOPN3	66	14.7	93.1	4.492	0.0001
Results are averaged over the levels of: sex					
Degrees-of-freedom method: kenward-roger					
P value adjustment: dunnettx method for 3 tests					

Table 11. Model comparison: effects of interactions of viral types and light stimulation on feeding duration, related to Figure 46D.

Model comparison	npar	AIC	BIC	logLik	deviance	Chisq	Df	Pr(>Chisq)
Reduced model	9	1071.1	1094.2	-526.54	1053.1			
Full model	10	1067.9	1093.5	-523.94	1047.9	5.1898	1	0.02272 *

Signif. codes: 0 '***' 0.001 '**' 0.01 '*' 0.05 '.' 0.1 ' ' 1								

Table 12. Contrast analysis: the difference between groups on feeding duration, related to Figure 46D.

Contrast	estimate	SE	df	t.ratio	p.value
LED off 0_tdTomato - LED off 1_eOPN3	48.1	66.2	16	0.727	0.7868
LED on 0_tdTomato - LED off 1_eOPN3	64.9	65.6	15.7	0.989	0.6325
LED on 1_eOPN3 - LED off 1_eOPN3	64	15	93.2	4.279	0.0001
Results are averaged over the levels of: sex					
Degrees-of-freedom method: kenward-roger					
P value adjustment: dunnettx method for 3 tests					

Table 13. Model comparison: effects of interactions of viral types and light stimulation on lick events, related to Figure 46.

Model comparison	npar	AIC	BIC	logLik	deviance	Chisq	Df	Pr(>Chisq)
Reduced model	9	1410.8	1433.8	-696.38	1392.8			
Full model	10	1403.9	1429.5	-691.95	1383.9	8.8472	1	0.002935 **

Signif. codes: 0 '***' 0.001 '**' 0.01 '*' 0.05 '.' 0.1 ' ' 1

Table 14. Contrast analysis: the difference between groups on lick events, related to Figure 46.

Contrast	estimate	SE	df	t.ratio	p.value
LED off 0_tdTomato - LED off 1_eOPN3	382	289.4	17.8	1.319	0.4339
LED on 0_tdTomato - LED off 1_eOPN3	261	285.6	17.6	0.915	0.6763
LED on 1_eOPN3 - LED off 1_eOPN3	249	88.6	92.8	2.816	0.0167

Results are averaged over the levels of: sex

Degrees-of-freedom method: kenward-roger

P value adjustment: dunnettx method for 3 tests

Table 15. Model comparison: effects of interactions of viral types and light stimulation on feeding bout duration, related to Figure 46E.

Model comparison	npar	AIC	BIC	logLik	deviance	Chisq	Df	Pr(>Chisq)
Reduced model	8	16006	16051	-7995	15990			
Full model	9	15997	16047	-7989.6	15979	10.882	1	0.0009711 ***

Signif. codes: 0 '***' 0.001 '**' 0.01 '*' 0.05 '.' 0.1 ' ' 1

Table 16. Contrast analysis: the difference between groups on feeding bout duration, related to Figure 46E.

Contrast	estimate	SE	df	t.ratio	p.value
LED off 0_tdTomato - LED off 1_eOPN3	-2.03	4.104	17.4	-0.495	0.8989
LED on 0_tdTomato - LED off 1_eOPN3	-1.92	4.069	16.9	-0.472	0.9083
LED on 1_eOPN3 - LED off 1_eOPN3	4.22	0.947	1983.4	4.46	<.0001

Results are averaged over the levels of: sex

Degrees-of-freedom method: kenward-roger

P value adjustment: dunnettx method for 3 tests

Table 17. Model comparison: effects of interactions of viral types and light stimulation on number of feeding bouts, related to Figure 46F.

Model comparison	npar	AIC	BIC	logLik	deviance	Chisq	Df	Pr(>Chisq)
Reduced model	8	598.58	619.1	-291.29	582.58			
Full model	9	600.53	623.61	-291.27	582.53	0.0495	1	0.824
---								

*Signif. codes: 0 '***' 0.001 '**' 0.01 '*' 0.05 '.' 0.1 ' ' 1*

Table 18. Contrast analysis: the difference between groups on the number of feeding bouts, related to Figure 46F.

Contrast	Estimate	SE	df	t.ratio	p.value
LED off 0_tdTomato - LED off 1_eOPN3	4.72	2.97	24.7	1.588	0.2899
LED on 0_tdTomato - LED off 1_eOPN3	4.1	2.92	24.9	1.404	0.3805
LED on 1_eOPN3 - LED off 1_eOPN3	-1.05	1.41	91	-0.746	0.7714

Results are averaged over the levels of: sex

Degrees-of-freedom method: kenward-roger

P value adjustment: dunnettx method for 3 tests

4. Discussion

While olfaction is known to be an essential sensory system for flavor representation, the role of olfactory flavor representation during feeding behaviors is poorly understood (Maier et al., 2015; Shepherd, 2006). Utilizing cell-type specific *in vivo* Ca^{2+} imaging and closed-loop optogenetics in freely behaving mice, I am providing circuit-level evidence that aPC flavor representation is strongly suppressed during binge feeding, and such suppression actively promotes food intake. Despite chronically manipulated olfactory functions being well established as impacting homeostatic eating and metabolism (Riera et al., 2017; Tucker et al., 2012), I am introducing a novel acute function of olfactory flavor representation during feeding at the timescale of individual feeding bouts (tens of seconds). This study illustrates a new concept of olfactory flavor representation of food items. Olfactory flavor representation during feeding serves as a negative feedback signal for satiation, and such satiation signals are blocked by an elevated feeding rate (binge feeding).

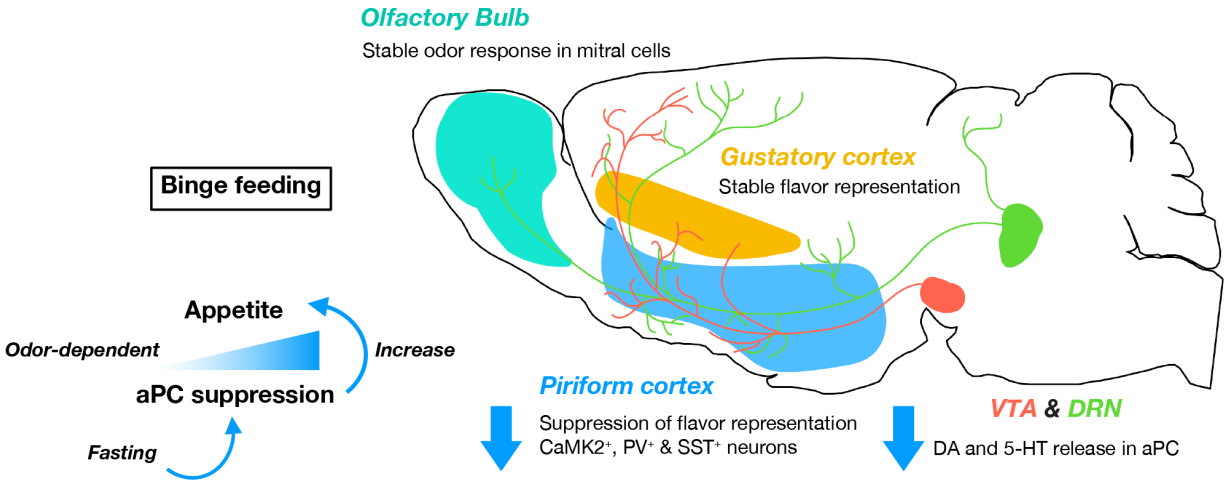

Figure 47. ***Graphic summary of the thesis.*** *In this thesis, I found that flavor representation in the olfactory cortex is dependent on feeding rates. When mice are binge feeding, the olfactory flavor representation in the aPC is suppressed (aPC excitatory neurons (**Results 3.3**) and aPC GABAergic neurons (**Results 3.7**)). In contrast, different feeding rates do not affect the gustatory flavor representation in the GC (**Results 3.4**). Different feeding rates do not affect olfactory inputs from the olfactory bulb, therefore the suppression in the aPC is not inherited from the olfactory bulb (**Results 3.6**). Two long-range neuromodulators, serotonin and dopamine, do not explain the binge feeding-induced aPC suppression (**Results 3.8**). Additionally, I discovered that the appetite level (measured by food consumption) is predicted by the strength of aPC suppression during binge feeding. This correlation also depends on the olfactory perception and the metabolic state (**Results 3.9, 3.10, 3.11**). I further demonstrated that artificially sup-*

*pressesing aPC during binge feeding can promote feeding, suggesting a mechanistic link between aPC flavor representation and feeding behavior (**Results 3.12**). In summary, I discovered a novel behavior-dependent flavor modulation in the olfactory cortex during feeding, which contributes to appetite control of hedonic feeding.*

In the following paragraphs, I will discuss how this study is embedded in the current knowledge of sensory and metabolism neuroscience, regarding its coherence with other findings, and what is unexpected. I will provide some additional ideas on the potential mechanisms of binge feeding-induced aPC suppression, what I have tested, and the future plans for testing new hypothese of mechanisms. I will also discuss the implications in the medical field and the future directions inspired by this work.

4.1. Role of the anterior piriform cortex in feeding behaviors

Despite its relevance, real-time assessment of olfactory flavor representation during active feeding has not been reported. In part due to the inconvenient anatomy involved, recording from the olfactory system, especially the PC, has been a challenging task for sensory neuroscientists studying olfaction. When recording from PC neurons *in vivo*, electrophysiological approaches like patch-clamp-, tetrodes-, or silicone probe recordings commonly face limited yields of recorded units (Bolding et al., 2019; Bolding and Franks, 2017; Bolding and Franks, 2018; Poo et al., 2021; Poo and Isaacson, 2009; Poo and Isaacson, 2011; Rennaker et al., 2007). Optical methods such as a 2P microscopy for population Ca^{2+} imaging of PC neurons often encounter accessibility issues, in that reaching the PC from the bottom of the skull can only be achieved under anesthesia, and this procedure is a terminal experiment with no possibility of recovering the recorded mice (Pashkovski et al., 2020; Stettler and Axel, 2009; Tantirigama et al., 2017). Technological limitations have made the investigation of the PC challenging, leaving the olfactory flavor representation question unanswered.

In this study, my colleagues and I successfully established a stable optical recording method (an implanted endomicroscopic GRIN lens with a prism combined with a miniscope) that allows awake, freely moving, and repeated measurement for up to 2 months, and is therefore suitable for examining the current flavor representation in the aPC and its development over time. For the first time, I showed that flavor-responding neurons in the aPC are strongly modulated by feeding rates, regardless of excitatory or inhibitory neurons. I further tested the flavor representation in the GC and found no difference between feeding rates, demostrating that distinct behavior-dependent neuronal dynamics were exhibited in these two main cortical sensory areas in flavor representation.

By showing differential neuronal activity patterns of the same identity of olfactory components under different feeding rates, I am proposing a new function of the olfactory sensation of food used as an early feedback of the satiation signal in parallel to the visceral feedback (De Araujo et al., 2020). While the PC has been known for odor discrimination (Bolding and Franks, 2017; Miura et al., 2012; Poo and Isaacson, 2009; Poo and Isaacson, 2011; Rennaker et al., 2007; Stettler and Axel, 2009; Tantirigama et

al., 2017), associative learning of pairing odors with reward outcomes and flexible representation of reward-associated odor mixtures (Chapuis and Wilson, 2012), it has not been studied in the context of feeding, a naturalistic behavior. If we treat food as a reward signal, then the flavor experience of eating the food item is the conditional cue for Pavlovian conditioning. This suggests that during each meal, a positive-reinforcement conditioning task takes place and it enhances flavor-value association, strengthening what flavors benefit the individual (most likely maximizing the flavors associated with the enrichment of fat and sugar contents). The conditioning also goes in the opposite direction, whereby food poisoning (experiencing malaise including symptoms like diarrhea or vomiting) is a strong negative valence feedback that triggers a robust one-shot learning conditioning to avoid the experienced flavor in the future (Zimmerman et al., 2023). A recent study focusing on the neural mechanism for learning from delayed post-ingestive feedback showed that novel flavors are strongly encoded in the PC, while the amygdala mostly contributes to the learning of a 30-minute late malaise. This result complements our study on the temporal dynamics of the flavor responses in the sensory systems, whereby immediate sensory representations are presented in the primary sensory cortices like PC and GC, and the delayed visceral signals are presented in the amygdala area.

In summary, my study provides new insights into flavor representation in the primary olfactory and gustatory cortices, and its relationship with feeding rates and appetite, which is valuable for future works on the intersection of the fields of sensory neuroscience and metabolism.

4.2. Sensory experience of food items contributes to satiation

Bypassing sensory experiences of food within the oral cavity by direct gastric infusion reduces satiety and accelerates gastric emptying compared to regular feeding in humans and rodents (Berkun et al., 1952; Cecil et al., 1999; Stratton and Elia, 1999). Several human behavioral studies have demonstrated that slowing down feeding rates by decreasing bite or sip sizes (Bolhuis et al., 2014b), harder food textures (Bolhuis et al., 2014a), or spoon-feeding the food (Mattes, 2005) can decrease food intake and increase satiety, suggesting oral sensory feedback has profound effects on satiation. These studies demonstrated that the orosensory aspect of food items is important for satiety, despite lacking the exact physiological mechanistic evidence.

Two recent studies published at the writing stage of this thesis have reported additional insights about how the gustatory sensory feedback of food contributes to satiation with neurophysiological measures (Aitken et al., 2023; Ly et al., 2023). One study in mice brainstem circuits has reported sequential appetite signals by oral sensory and visceral sensory feedback control satiation (Ly et al., 2023). The prolactin-releasing hormone (PRLH)-expressing neurons in the caudal nucleus of the solitary tract (cNTS) respond actively when mice start ingesting food, and the preproglucagon (GCG)-expressing (the main source of glucagon release in the brain) cNTS neurons only respond to sensory feedback from the GI tract. Both neuronal types trigger satiation, but at very different timescales; the “sensory responsive” PRLH cNTS neurons rapidly modulate feeding bout size in seconds, whereas the “visceral feedback responsive” GCG cNTS neurons modulate long-lasting satiety at a tens of minutes scale by reducing the feeding bout number.

A further study looked at the leptin receptor-expressing neurons in the dorsomedial hypothalamus (DMH^{LepR}), which respond to sweet or fatty tastes upon feeding (Aitken et al., 2023). DMH^{LepR} neurons’ activity pattern mirrors the downstream neuronal activity patterns in the AgRP neurons in the hypothalamus, which are rapidly suppressed upon initiation of feeding, for which the circuit was previously identified (Berrios et al., 2021; Garfield et al., 2016). The authors further reported that blocking the satiation signal from DMH^{LepR} neurons by a closed-loop optogenetics stimulation of AgRP neurons further

enhanced food intake, indicating a rapid dynamic function of AgRP neurons in appetite and satiation.

In this study, I have demonstrated that olfactory sensory representation is modulated by feeding rate and reciprocally contributes to satiation using real-time neurophysiological data by miniscope recording and closed-loop optogenetics. My study is complementary to the abovementioned two studies on the gustatory senses of food, with more insights into olfaction, feeding rate, and a novel cortical mechanism of feeding control.

4.3. Potential mechanisms of aPC suppression during binge feeding

In this study, I have tested four hypotheses regarding binge feeding-induced aPC suppression, which are: 1) disrupted respiration cycles, 2) degradation of odor inputs from the nostrils or the OB, 3) recruitment of local inhibitory neurons in the aPC, and 4) neuromodulations. Despite extensive efforts, all of the results above did not support these hypotheses, leaving the circuit mechanism of this behavior-driven neuronal modulation unclear. In the following paragraphs, I will discuss other potential explanations and some limitations on testing them with the current technologies.

4.3.1. Long-range GABAergic inputs

While the local GABAergic interneurons in the aPC do not drive the binge feeding-induced suppression, this does not rule out the possibility of long-range GABAergic projections. A few brain regions contain long-projecting GABAergic neurons and are involved in feeding-related behaviors, including the 1) basal forebrain, 2) zona incerta, and 3) mediodorsal hypothalamus. Based on the anatomical projections and their neuronal dynamic during feeding, I will discuss the probability of their contributions to aPC suppression during binge feeding.

Basal forebrain

The basal forebrain consists of glutamatergic, cholinergic, and GABAergic neurons, and can be subdivided into different subregions. For example, the medial septum glutamatergic (Fuhrmann et al., 2015), cholinergic (Dannenberg et al., 2015; Vandecasteele et al., 2014), and GABAergic (Zutshi et al., 2018) neurons have robust projections to the hippocampus and strongly modulate the theta rhythm. The horizontal limb of the diagonal band (HDB) and magnocellular preoptic nucleus (MCPO) of the basal forebrain project to the PC, with a mixture of cholinergic and GABAergic projections. A functional inhibitory projection from the GABAergic neurons in MCPO to the PC has demonstrated that the inhibitory inputs to the PC are broadly connected to most cell types in the PC, including layer 1 interneurons and layer 2/3 pyramidal neurons (personal communication, Dr. Ricardo. C. Araneda, Maryland University, 2021 Nov, SfN, online conference).

The ventral portion of the basal forebrain (including HDB, MCPO, and substantia innominata (SI)) is involved in feeding behaviors, including licking and swallowing (Harrison et al., 2016), making these brain structures plausible for feeding-induced aPC suppression. The dorsal part of the basal forebrain (ventral pallidum, VP) also consists of GABAergic neurons. It represents the hedonic values of food items (Tindell et al., 2006), suggesting its function in hedonic feeding. In the following paragraphs, I will focus on GABAergic modulation; there is further discussion of cholinergic modulation in the section below on the potential mechanism by neuromodulations.

Fiber photometry of Ca^{2+} indicators showed that SST^{+} (but not PV^{+}), GABAergic neurons in the HDB/MCPO activate upon receiving odors or rewards in Pavlovian conditioning tasks (Moss et al., 2022), proposing a possible temporal-matched GABAergic input to the aPC. GABAergic neurons in the basal forebrain can also actively drive feeding behaviors; Activating SST^{+} GABAergic neurons in the ventral basal forebrain (HDB, MCPO, and SI) promotes hedonic feeding, but not regular feeding with standard chow (Zhu et al., 2017). Activating the GABAergic neurons in the dorsal part of the basal forebrain VP triggers feeding behaviors for both hedonic feeding and also regular feeding. Optogenetic activation of the GABAergic ventral basal forebrain fibers in the LH can replicate the same effects of promoting hedonic feeding but not for regular feeding. A different study also showed similar results, i.e., activating basal forebrain GABAergic neurons can promote feeding, reward, and predatory (hunting) behaviors (Roman-Ortiz et al., 2021). Local activation of GABAergic basal forebrain neurons' fibers projecting in the PAG can recapitulate the same behavioral alterations as by activation of their somata. Conversely, recent research demonstrated that the HDB GABAergic neurons are suppressed during feeding bouts mediated by GABAergic inputs from the LH (Cassidy et al., 2019). These studies, except for the last one, support the hypothesis that GABAergic neurons in the basal forebrain promote feeding behaviors and cause the suppression in the aPC during feeding.

To verify these results, I tested several retrograde labeling methods with the aim of labeling the aPC-projecting GABAergic neurons in the HDB/MCPO/SI with GCaMP and performing Ca^{2+} imaging in the region during feeding. I mainly utilized retrograde labeling viruses to obtain circuit-specific basal forebrain neurons that project to the aPC.

Unfortunately, after testing many combinations of viral constructs and transgenic mouse lines, the efficacy of the retrograde labeling remained suboptimal, and only 1 out of all tested mice showed promising labeling (see Table 19 and Figure 48 to Figure 68 for examples), putting the imaging experiment on hold. After a few exchanges with the Araneda lab, I now have sufficient technical details (different Cre lines and viruses) for further testing.

Table 19. Viral and transgenic mice combinations for retrograde labeling pre-synaptic regions of aPC.

Virus	*Mouse line*	*Expression in basal forebrain*	*Expression in injection site (aPC)*	*Expression in other brain regions*	*Example figure*
AAVrg:: syn-flex-GCaMP6f	SST-Cre	No expression	Yes	No expression	Figure 48
AAVrg:: syn-flex-jGCaMP7f	SST-Cre	1 out of 4 mice shows labeling (Figure 49, Figure 50)	Yes, but only for 44, 45 days, not for 57 days	1 out of 4 mice shows expression in anterior and cortical amygdala. Others show no expression	Figure 49, Figure 50, Figure 51, Figure 52, Figure 53
HSV:: hEF1α - LSL-GCaMP6f	SST-Cre	No expression	Yes, but only for 44 days (and is very sparse), not for 80 days	No expression	Figure 54, Figure 55, Figure 56
AAVrg:: syn-iCre-RFP	Ai148D (flox-GCaMP6f)	Yes, but very sparse	Good	Good expression in neocortex (insular cortex, S1/2)	Figure 57, Figure 58, Figure 59
AAVrg:: syn-flox-ChR2-EYFP	SST-Cre	No expression	Barely	No expression	Figure 60, Figure 61
Rabies:: Switch-Cre	Ai148D (flox-GCaMP6f)	No expression	Yes	Good expression in OB	Figure 62, Figure 63
Rabies:: Switch-Flpo	Ai210D (flox-flp-	No expression	No expression	No expression	Figure 64, Figure 65, Figure 66

Virus	*Mouse line*	*Expression in basal forebrain*	*Expression in injection site (aPC)*	*Expression in other brain regions*	*Example figure*
	GCaMP7f); SST-Cre				
(local injection in aPC and BF for testing) AAV:: hSyn-flpo	Ai210D (flox-flp-GCaMP7f); SST-Cre	No expression (meaning Ai210D; SST-Cre combination is not a good strategy to capture GABAergic neurons in BF)	Yes	N/A	Figure 67, Figure 68

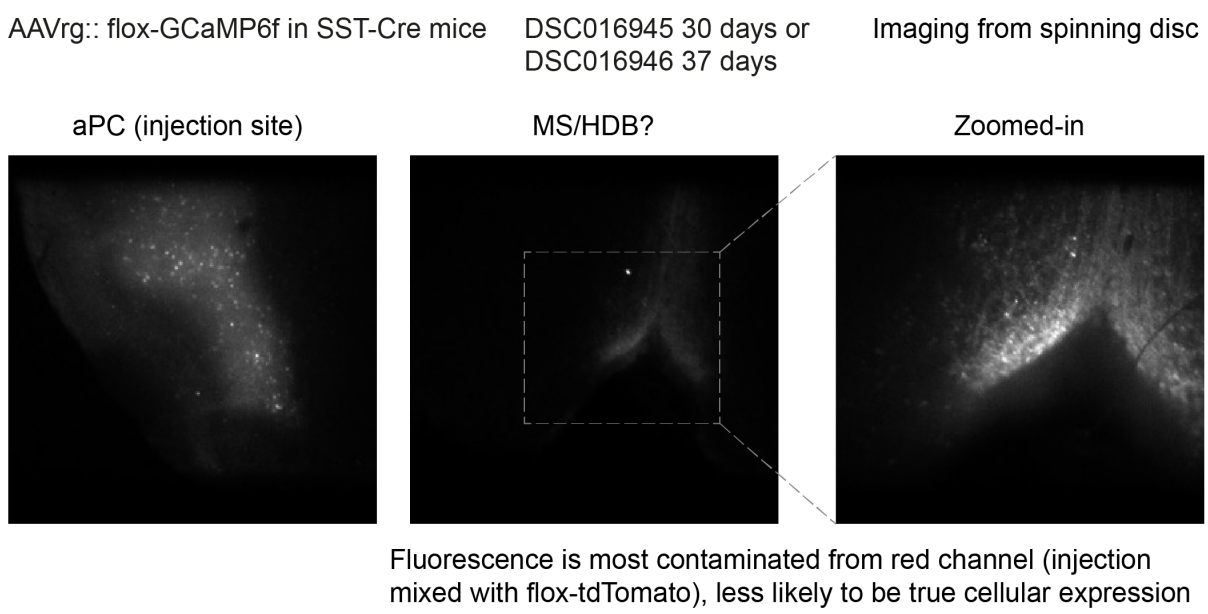

Figure 48. ***AAVrg::flox-GCaMP6f injected in SST-Cre mice.***

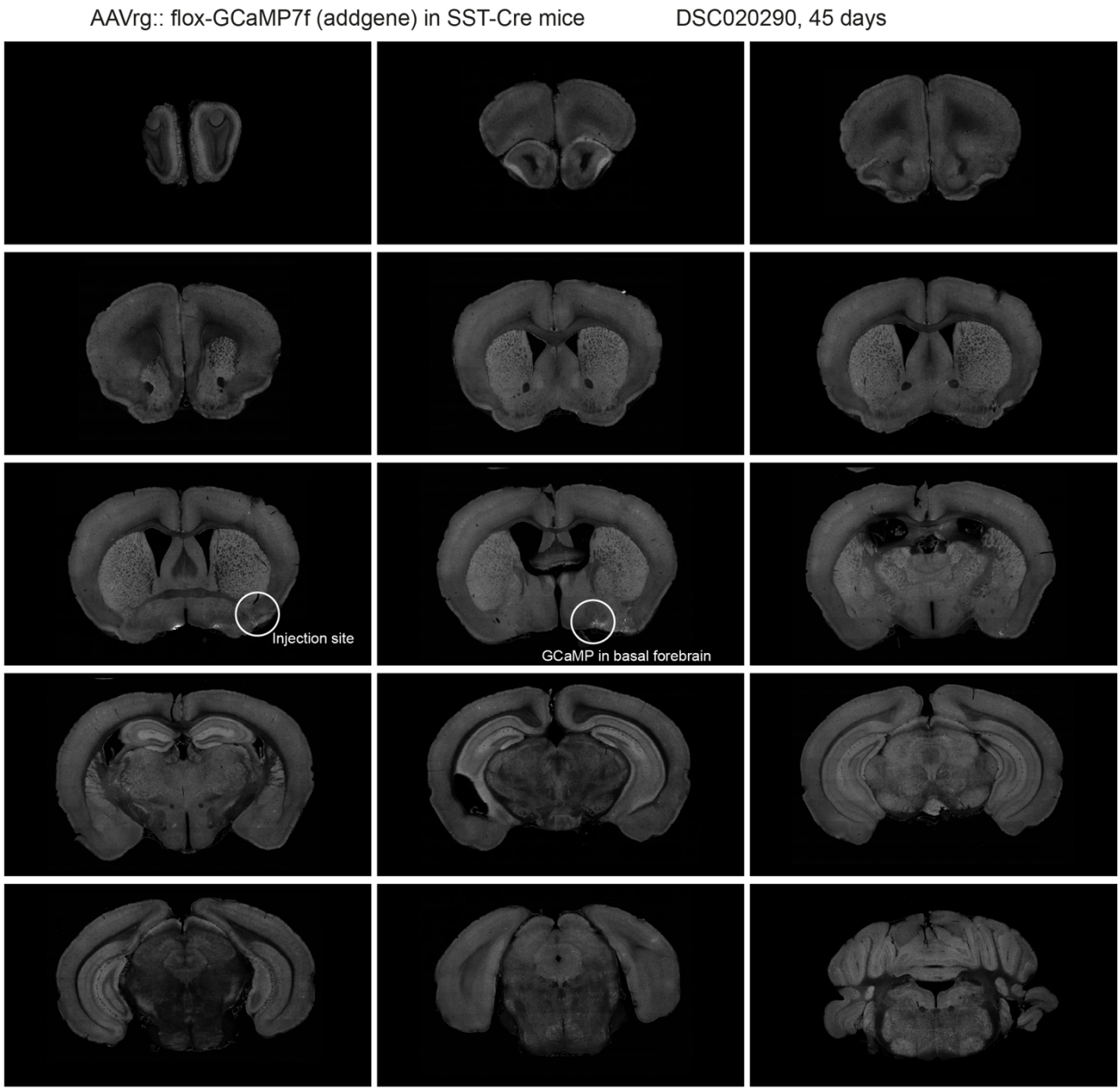

Figure 49. ***AAVrg::flox-jGCaMP7f injected in SST-Cre mice, example 1.*** *One out of four injected mice showed successful retrograde labeling of basal forebrain SST⁺ neurons.*

AAVrg:: flox-GCaMP7f (addgene) in SST-Cre mice

DSC020290, 45 days
Zoomed-in

Registered with Allen brain atlas

Labeled with cellfinder

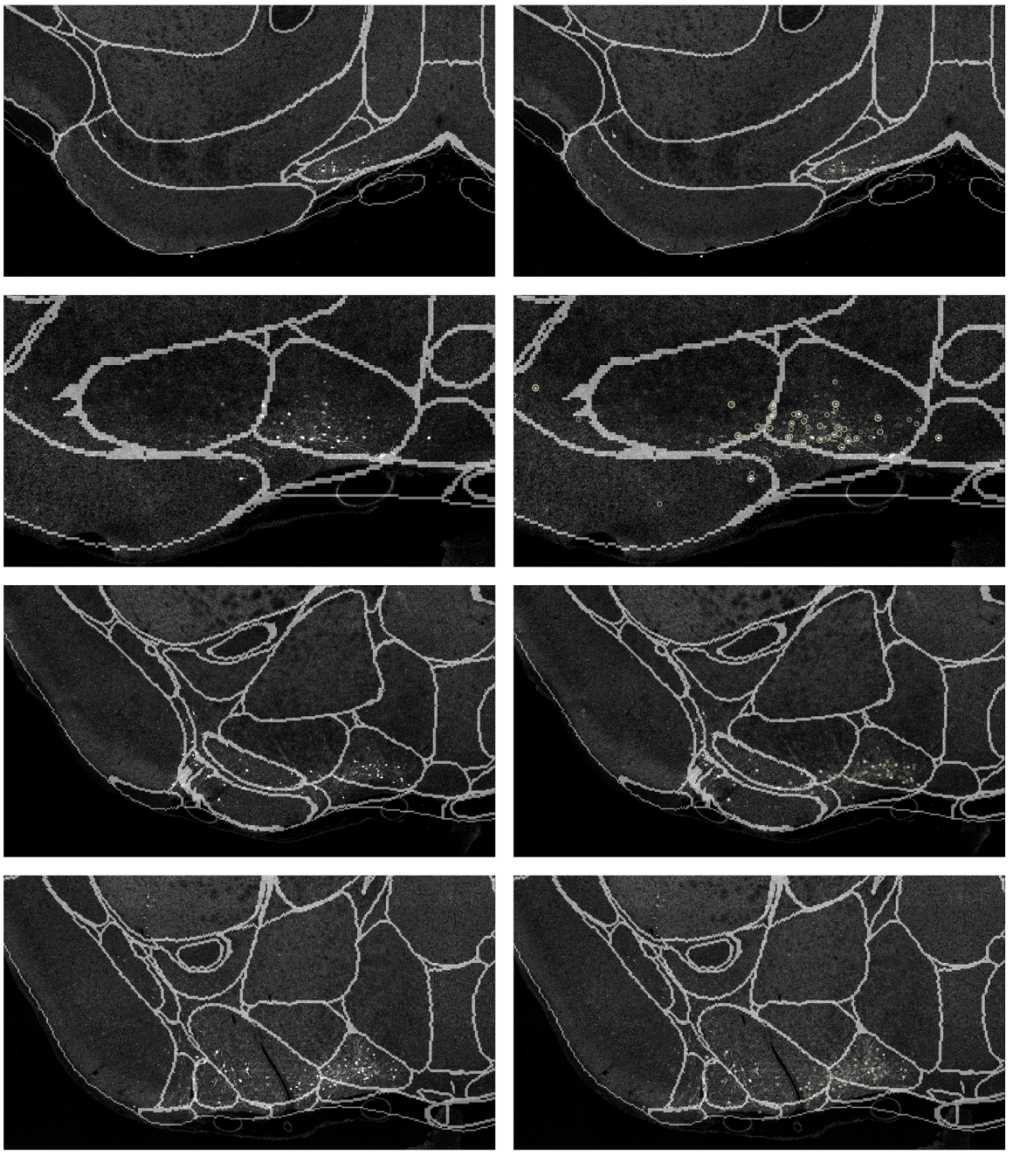

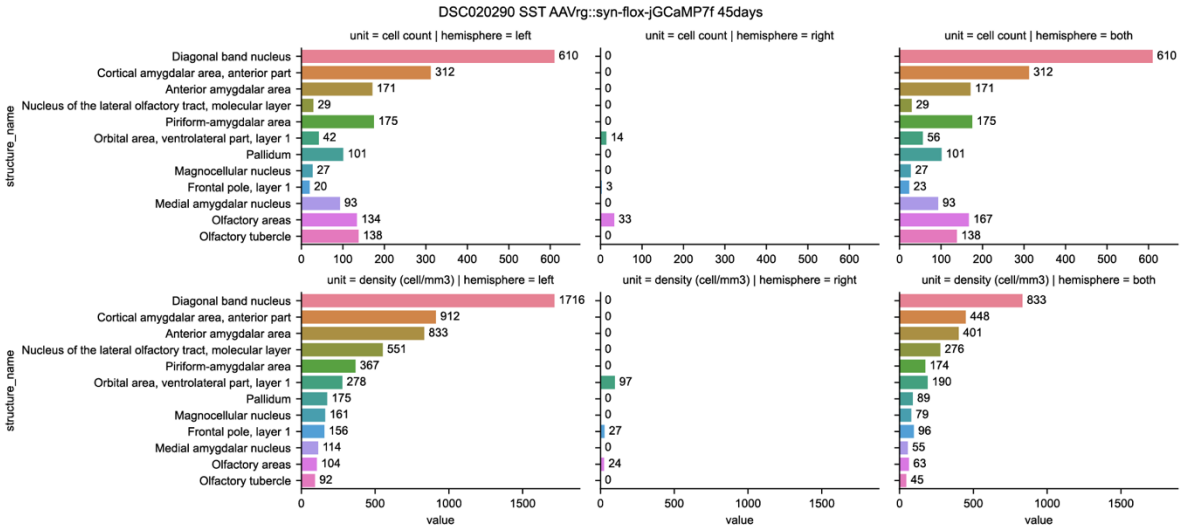

Figure 50. ***AAVrg::flox-jGCaMP7f injected in SST-Cre mice, example 1, continued.*** *Left, zoom-in images of retrogradely labeled SST$^+$ neurons in the basal forebrain (mostly in diagonal band nucleus) and the anterior/cortical amygdalar areas. Right, same images with cell detection using Cellfinder. Bottom, the quantification of these retrogradely labeled neurons in the whole brain, the upper row is the exact cell count, the bottom row is the normalization of the brain region volumes (counts/mm^3). Each column represents the left hemisphere (injected hemisphere), right hemisphere, and both hemispheres.*

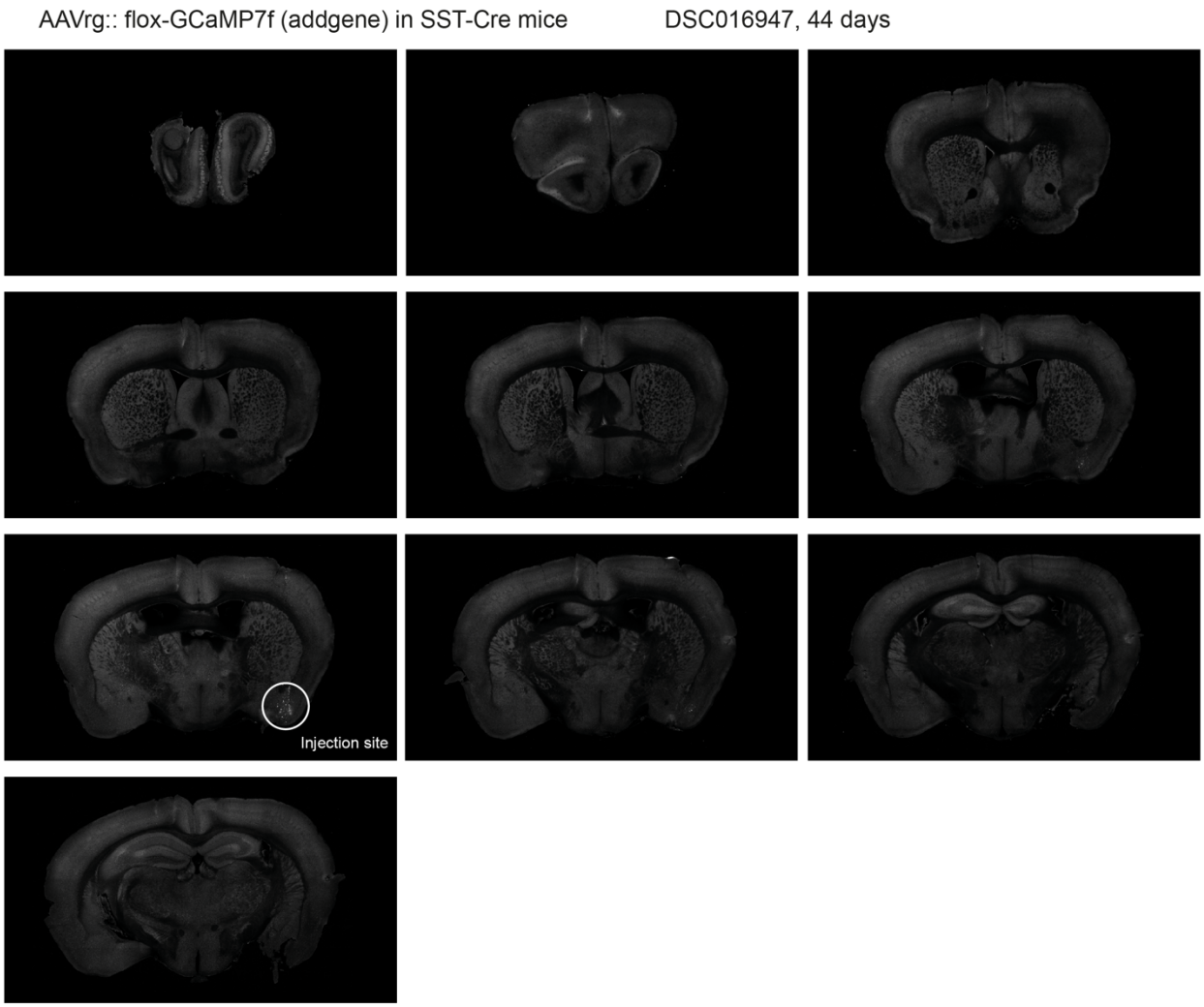

Figure 51. ***AAVrg::flox-jGCaMP7f injected in SST-Cre mice, example 2.*** *No expression in presynaptic neurons, only expression in aPC neurons.*

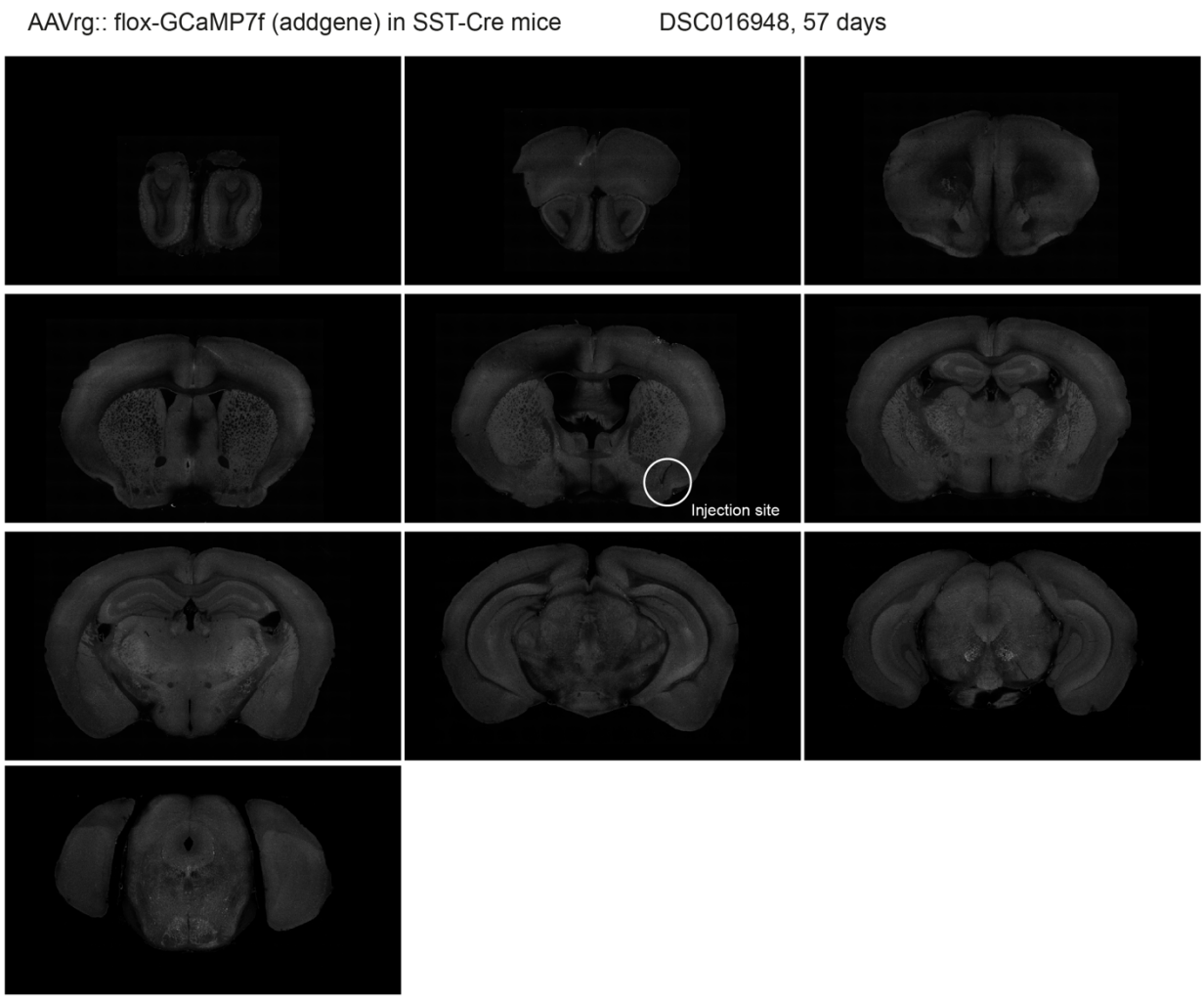

Figure 52. ***AAVrg::flox-jGCaMP7f injected in SST-Cre mice, example 3.*** *No expression of GCaMP7f in all brain regions.*

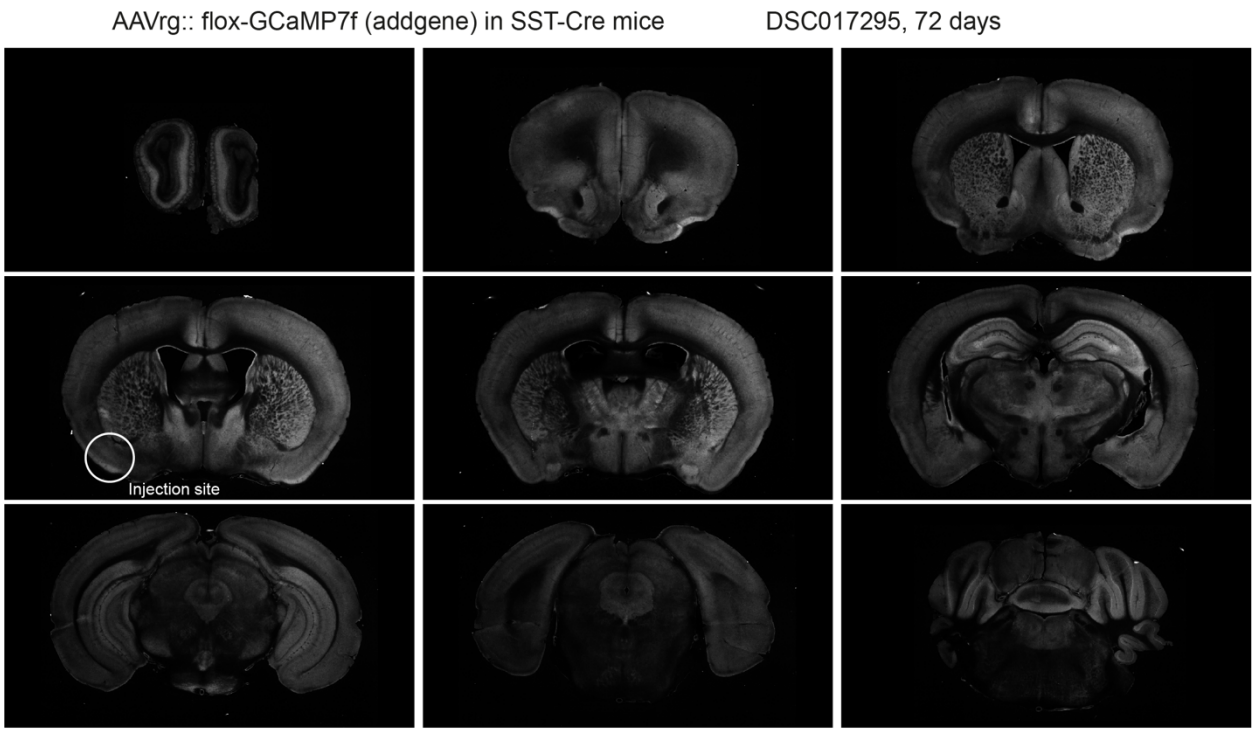

Figure 53. ***AAVrg::flox-jGCaMP7f injected in SST-Cre mice, example 4.*** *No expression of GCaMP7f in all brain regions.*

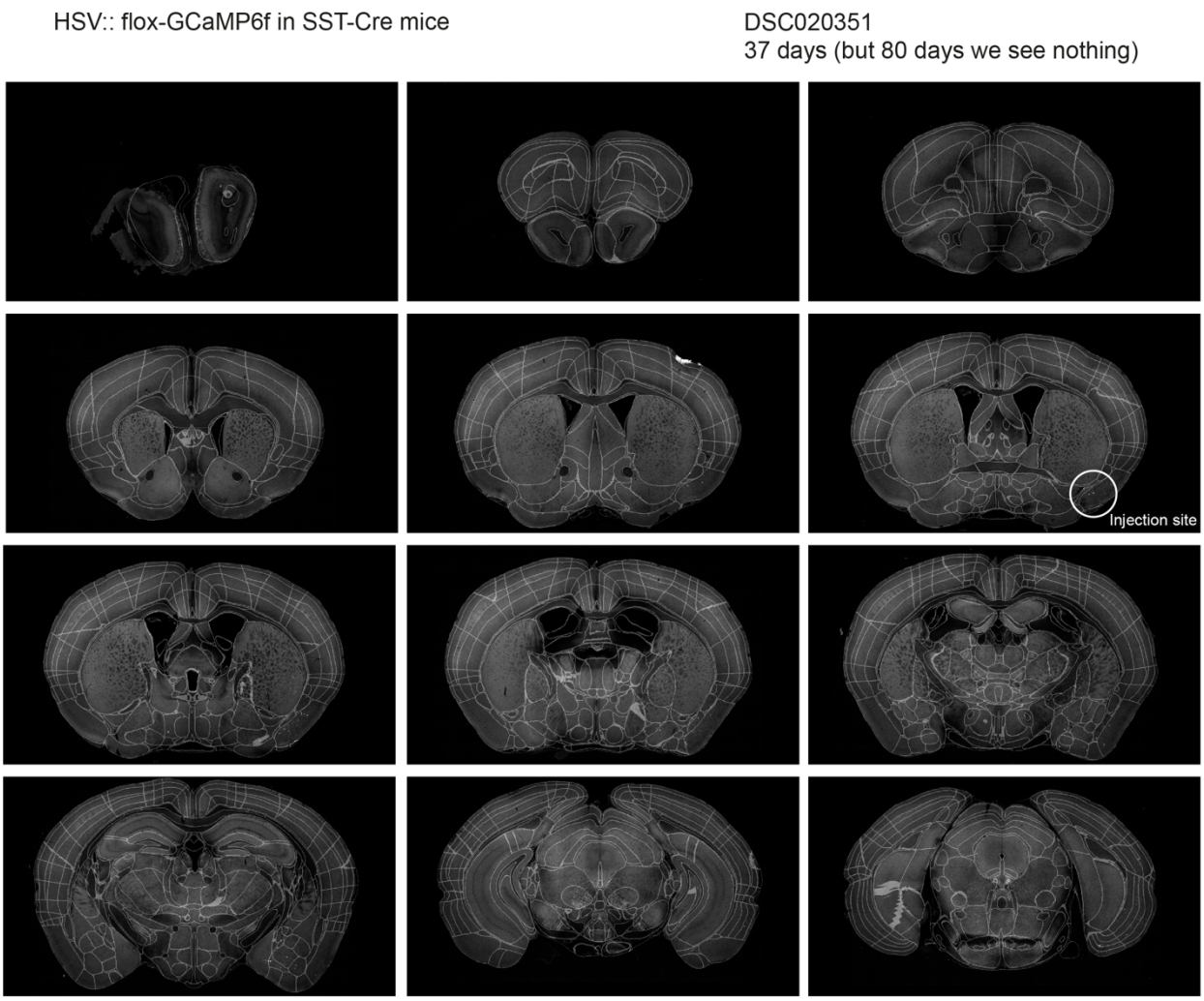

Figure 54. ***HSV::flox-GCaMP6f injected in SST-Cre mice.***

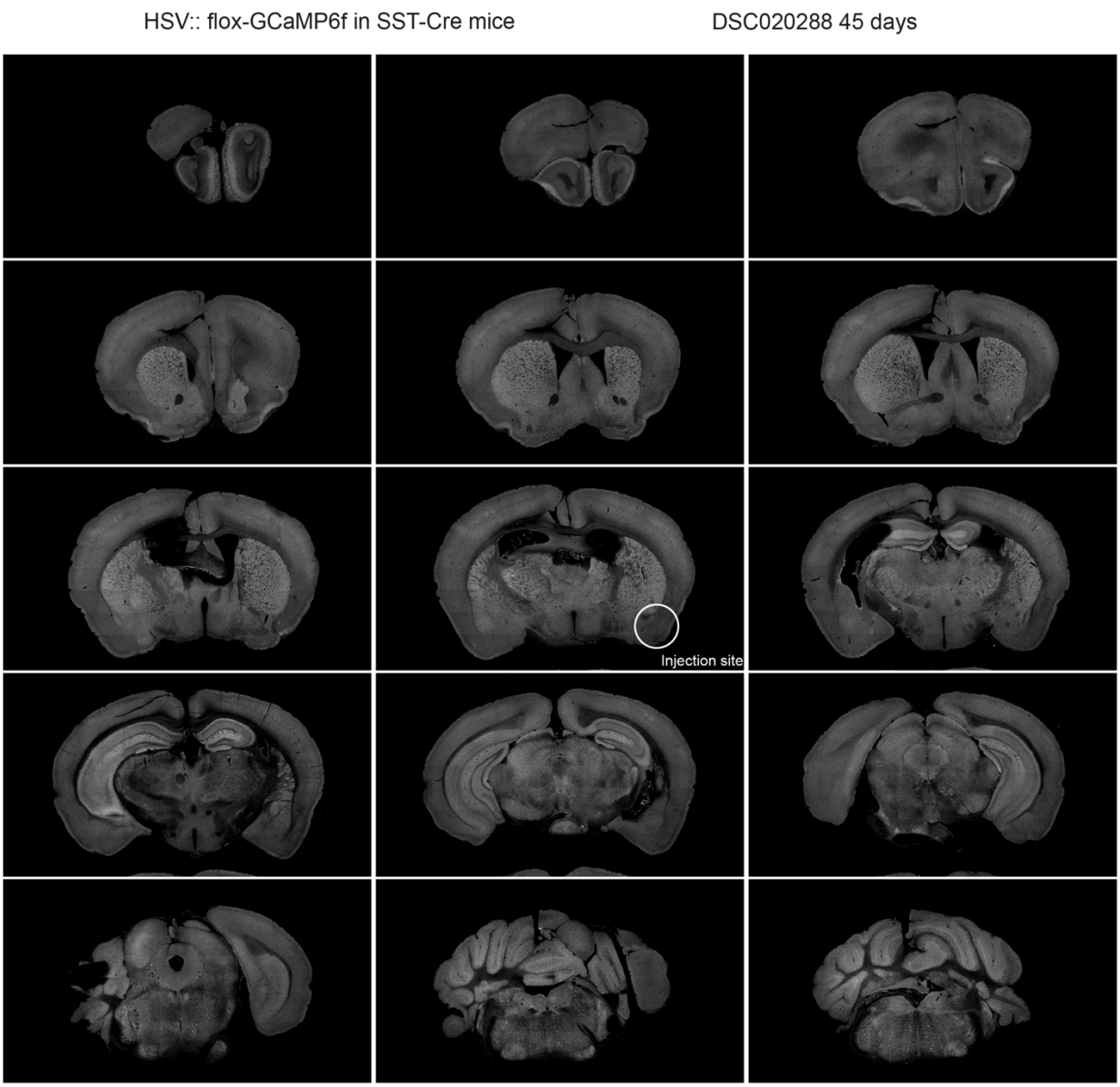

Figure 55. ***HSV::flox-GCaMP6f injected in SST-Cre mice, example 2.***

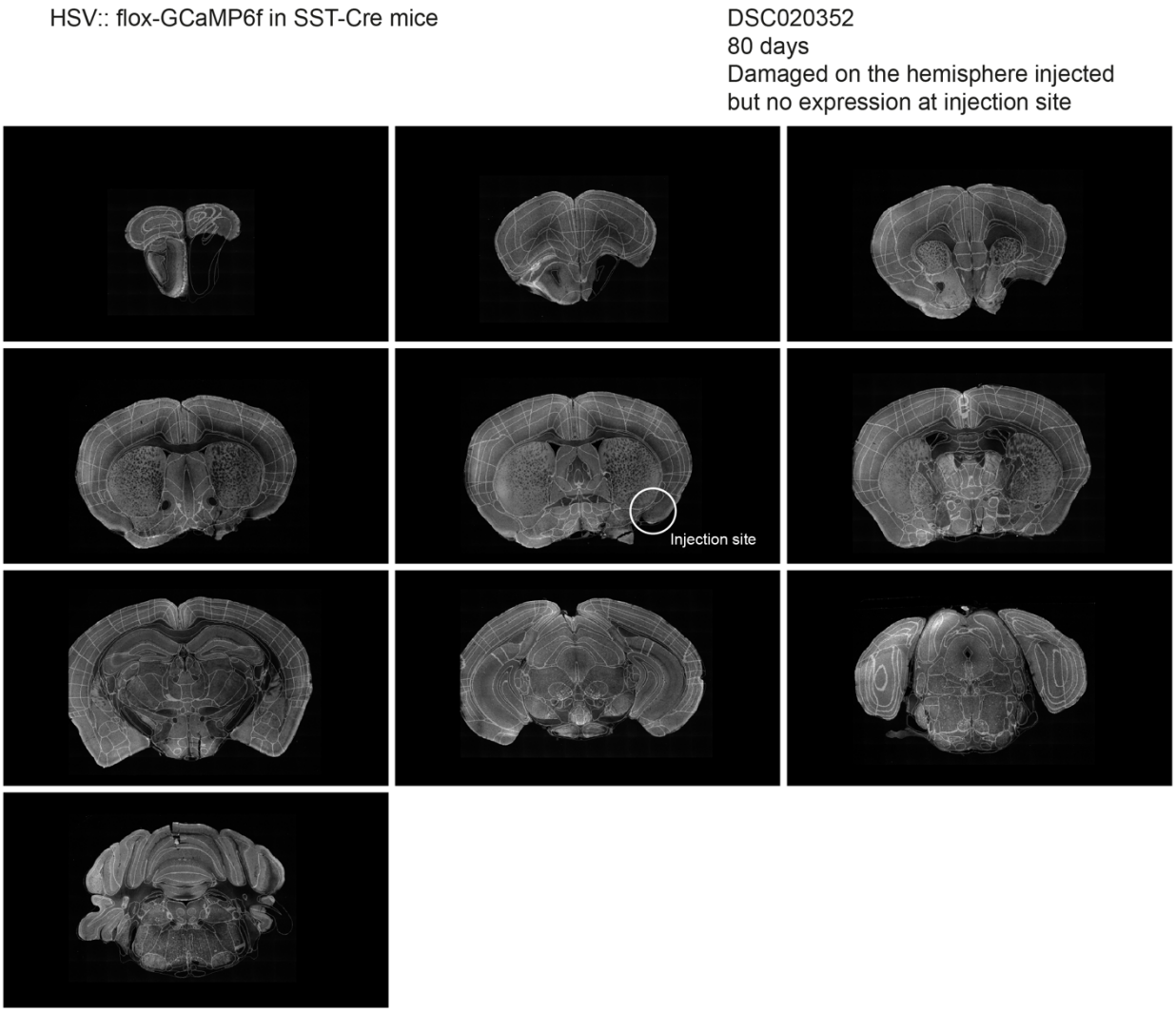

Figure 56. ***HSV::flox-GCaMP6f injected in SST-Cre mice, example 3.***

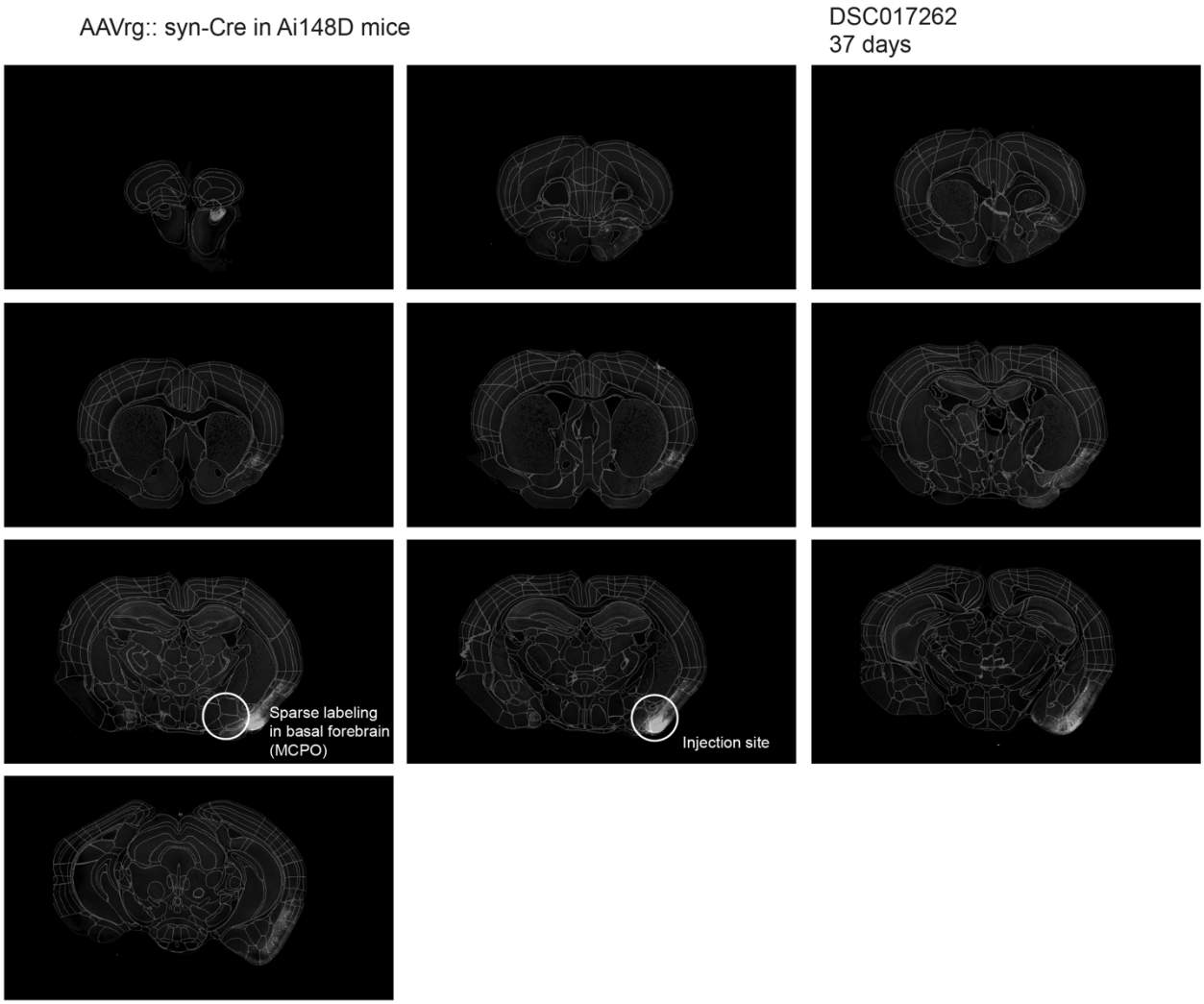

Figure 57. ***AAVrg::hSyn-Cre injected in Ai148 mice.***

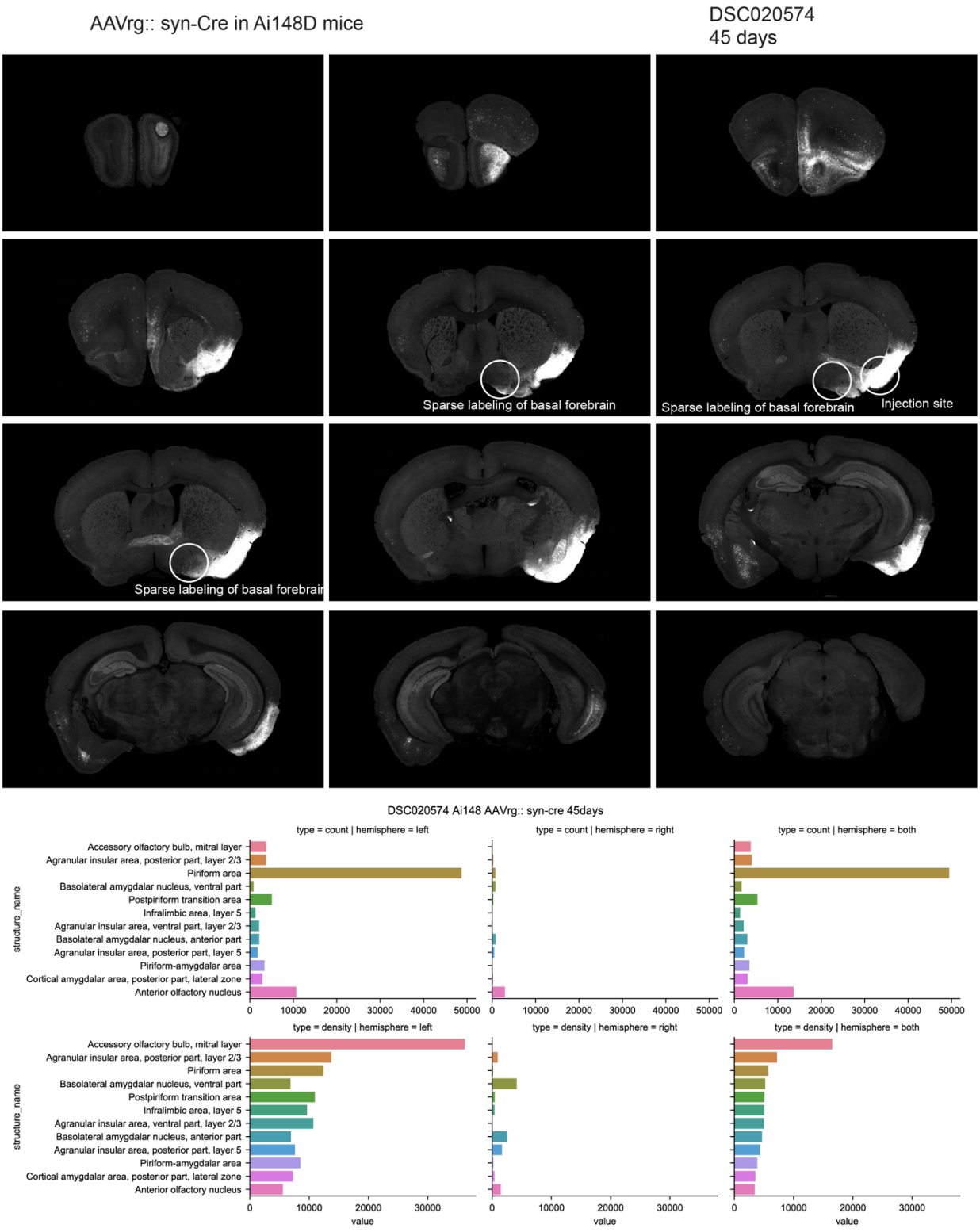

Figure 58. ***AAVrg::hSyn-Cre injected in Ai148 mice, example 2.*** *Upper, images of brain sections with retrograde labeled neurons. Bottom, quantification of labeled neurons in different brain regions with Cellfinder.*

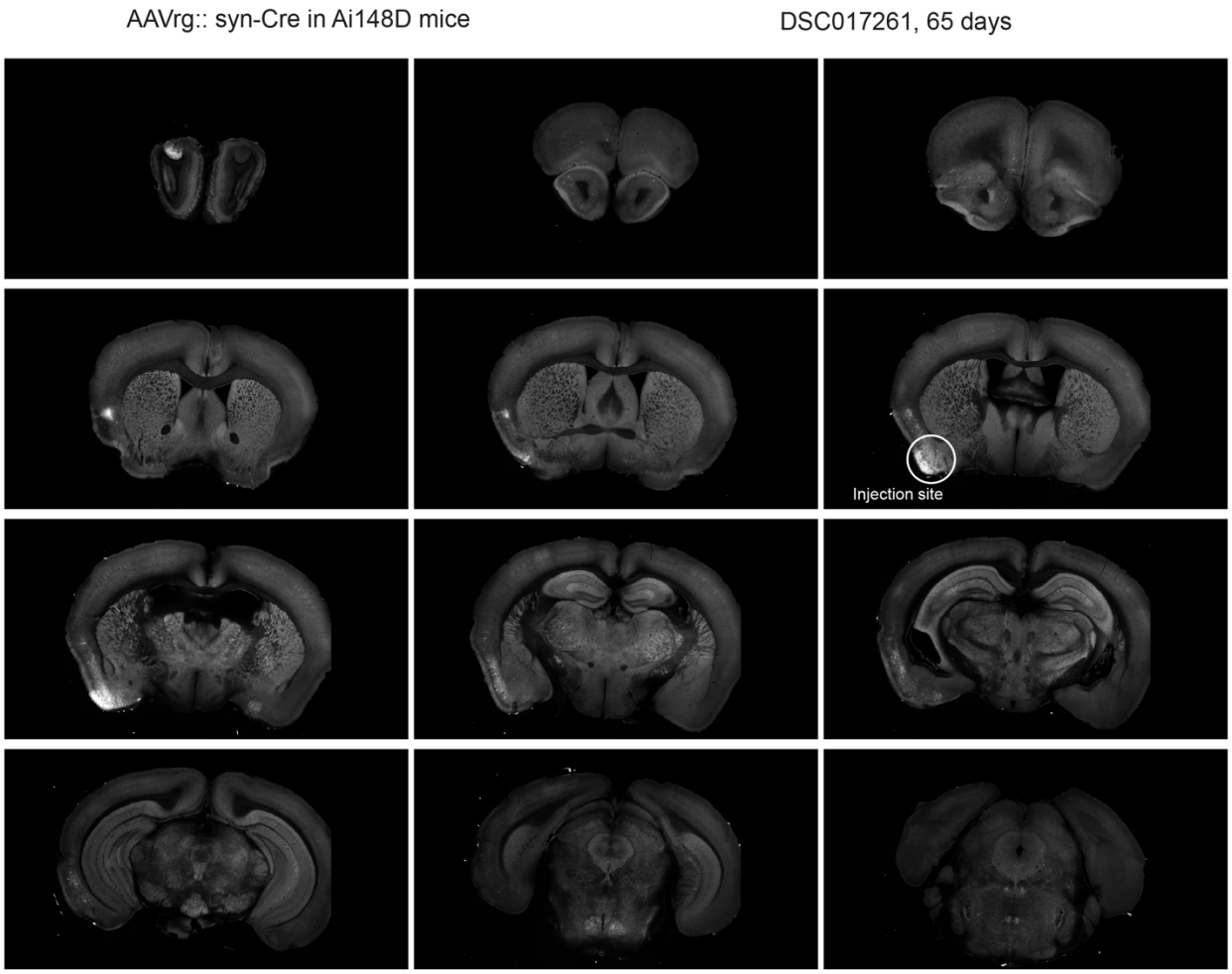

Figure 59. ***AAVrg::hSyn-Cre injected in Ai148 mice, example 3.***

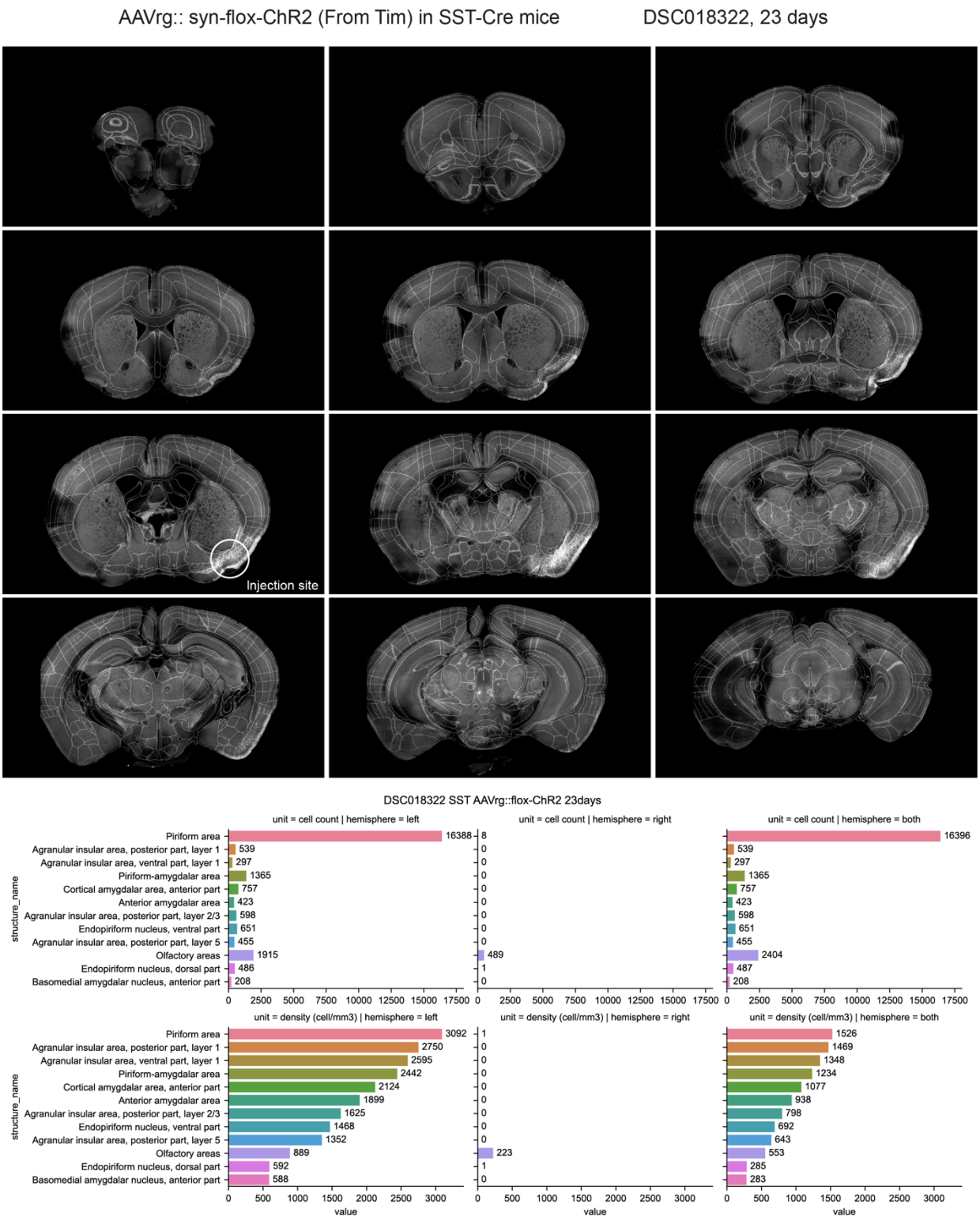

Figure 60. ***AAVrg::flox-ChR2 injected in SST-Cre mice.*** *Upper, images of brain sections with retrograde labeled neurons. Bottom, quantification of labeled neurons in different brain regions with Cellfinder.*

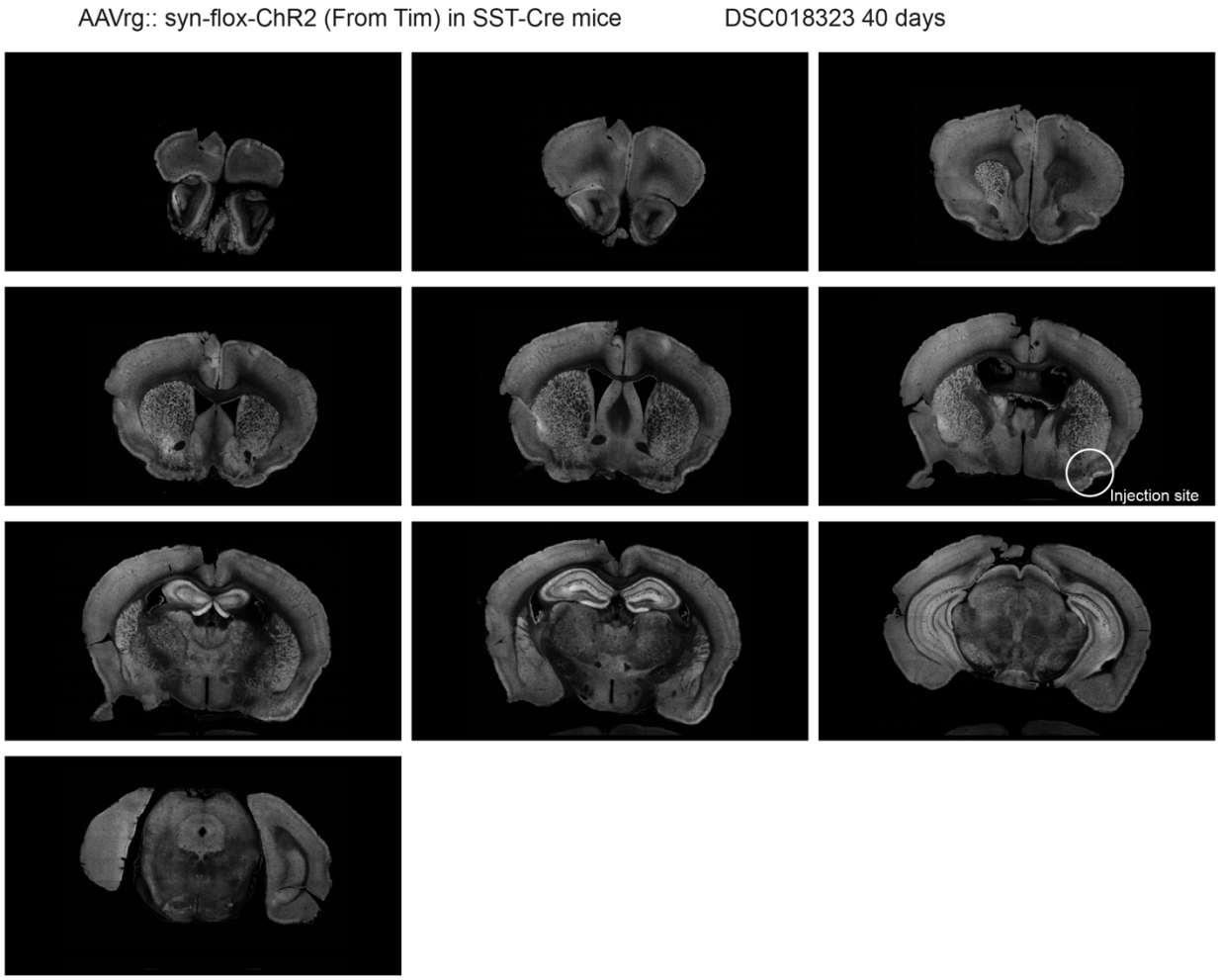

Figure 61. ***AAVrg::flox-ChR2 injected in SST-Cre mice, example 2.***

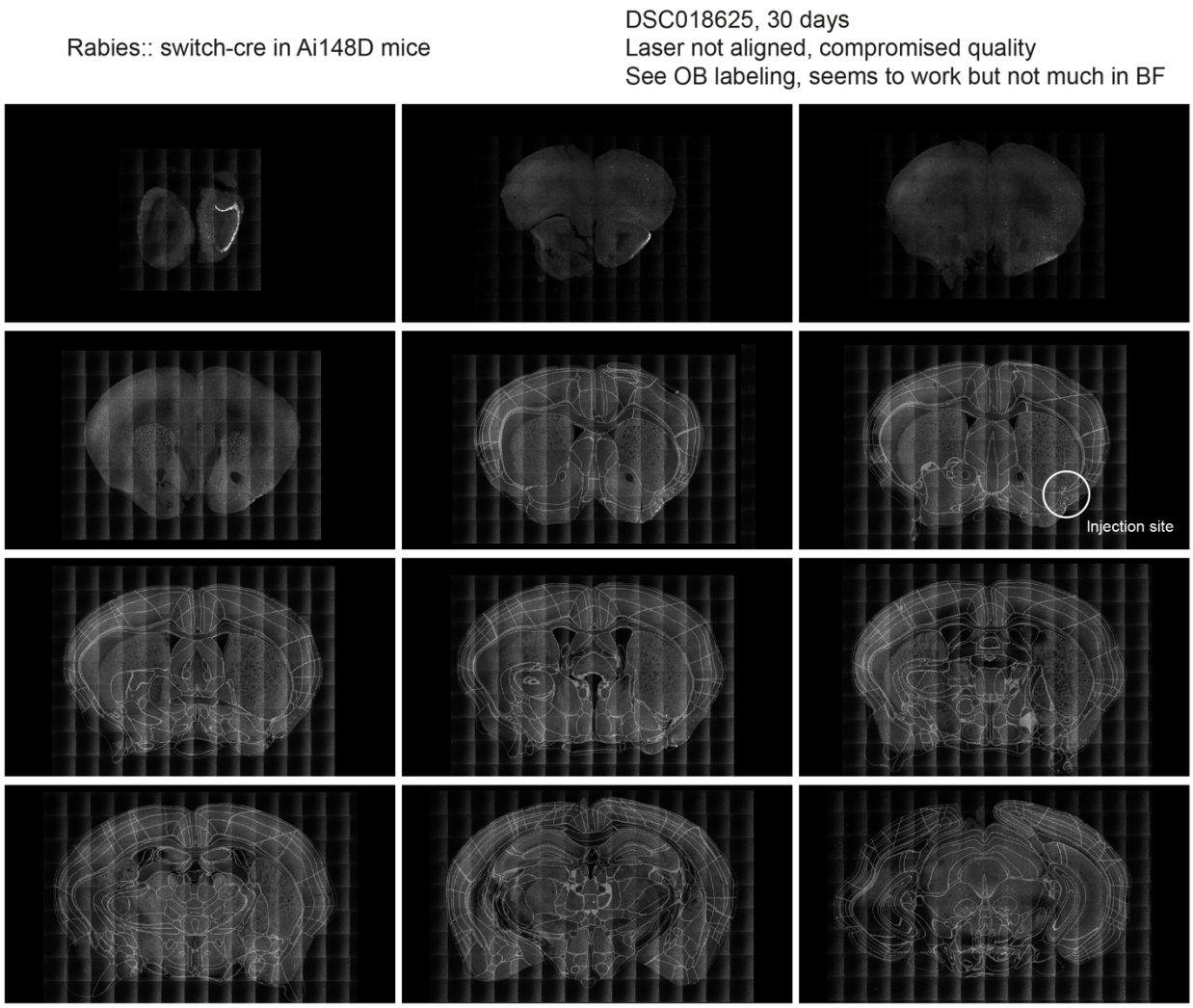

Figure 62. ***Rabies virus::switch-Cre injected in Ai148 mice.***

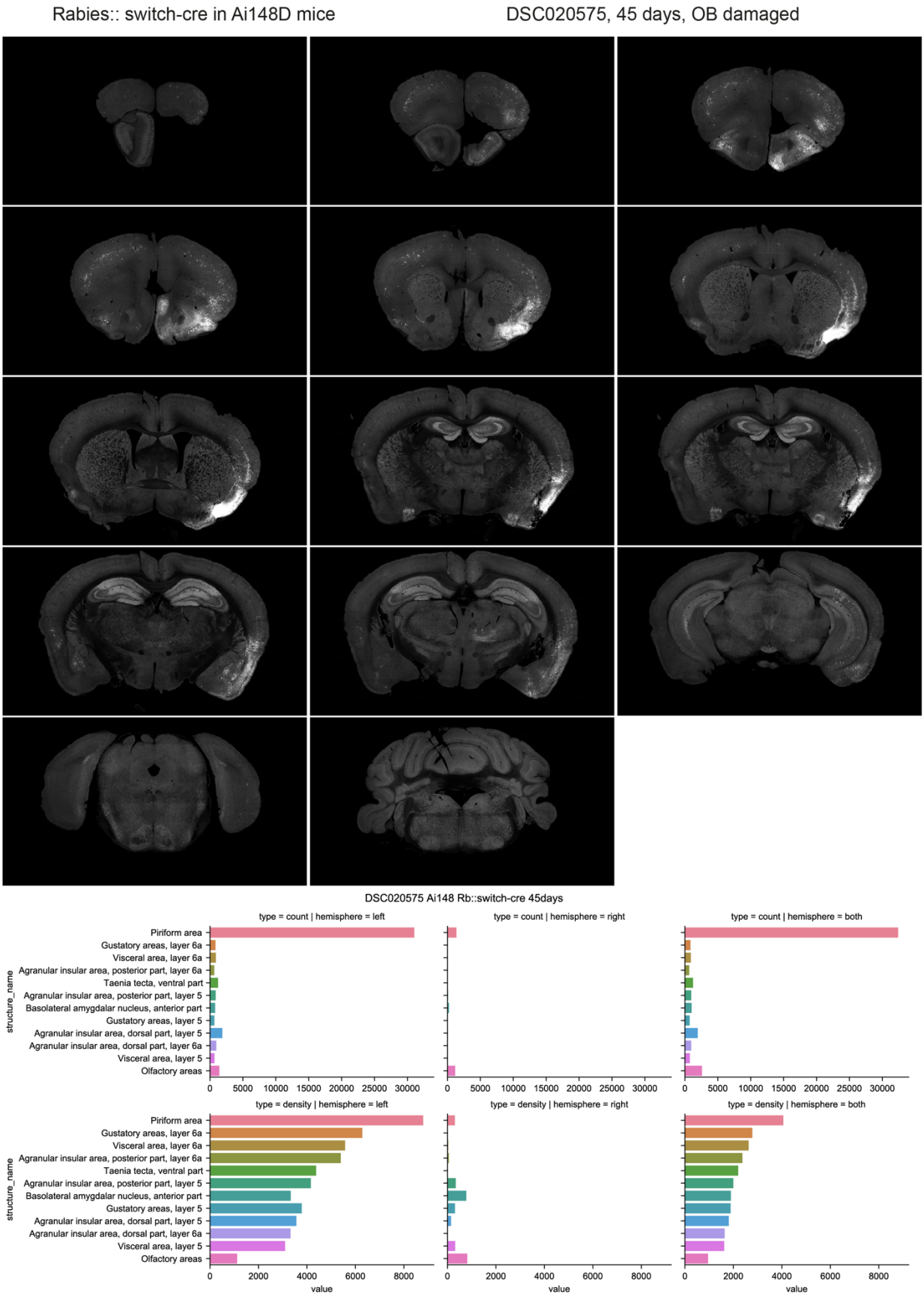

Figure 63. ***Rabies virus::switch-Cre injected in Ai148 mice, example 2.*** *Upper, images of brain sections with retrograde labeled neurons. Bottom, quantification of labeled neurons in different brain regions with Cellfinder.*

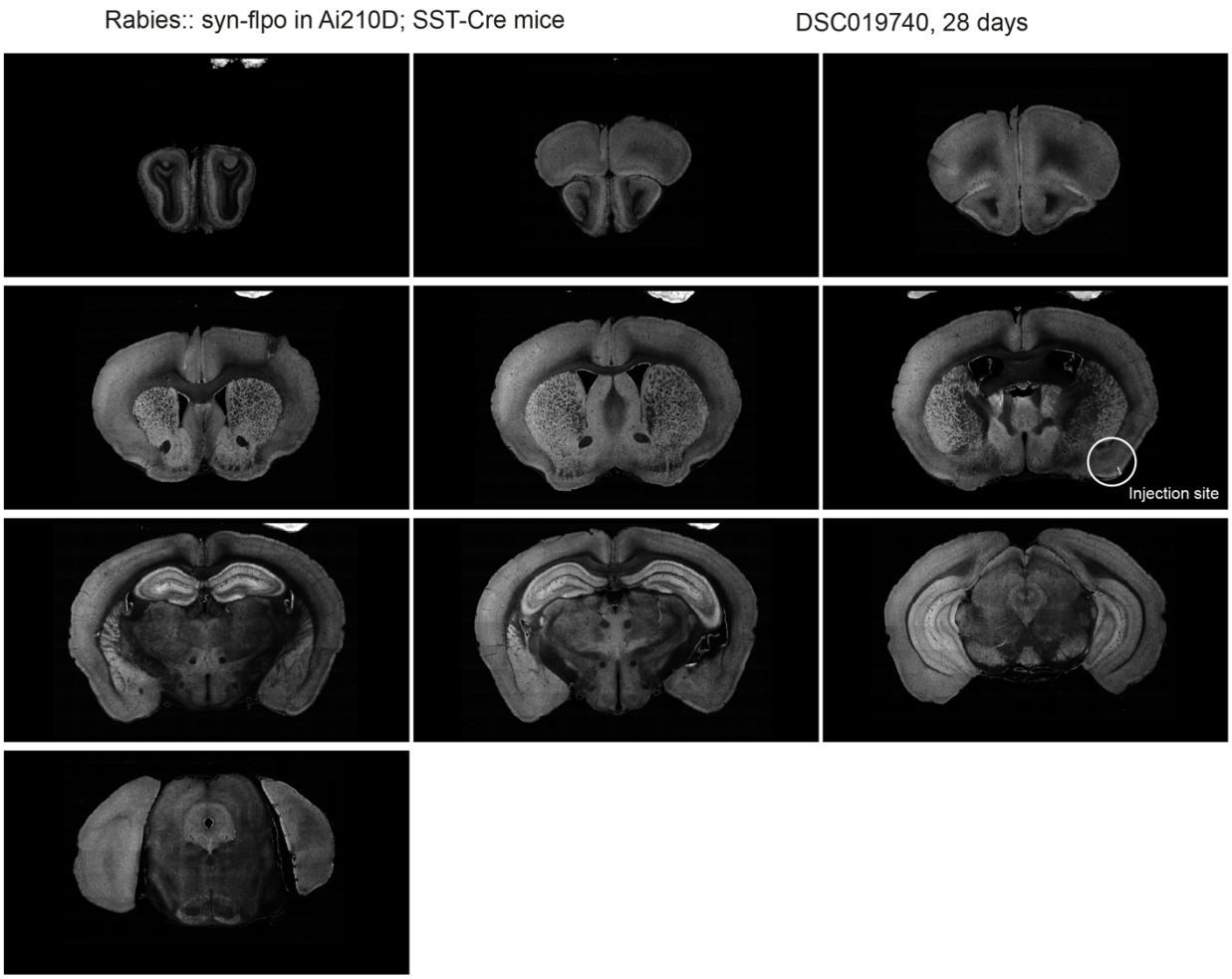

Figure 64. ***Rabies virus::switch-flpo injected in Ai210; SST-Cre mice.***

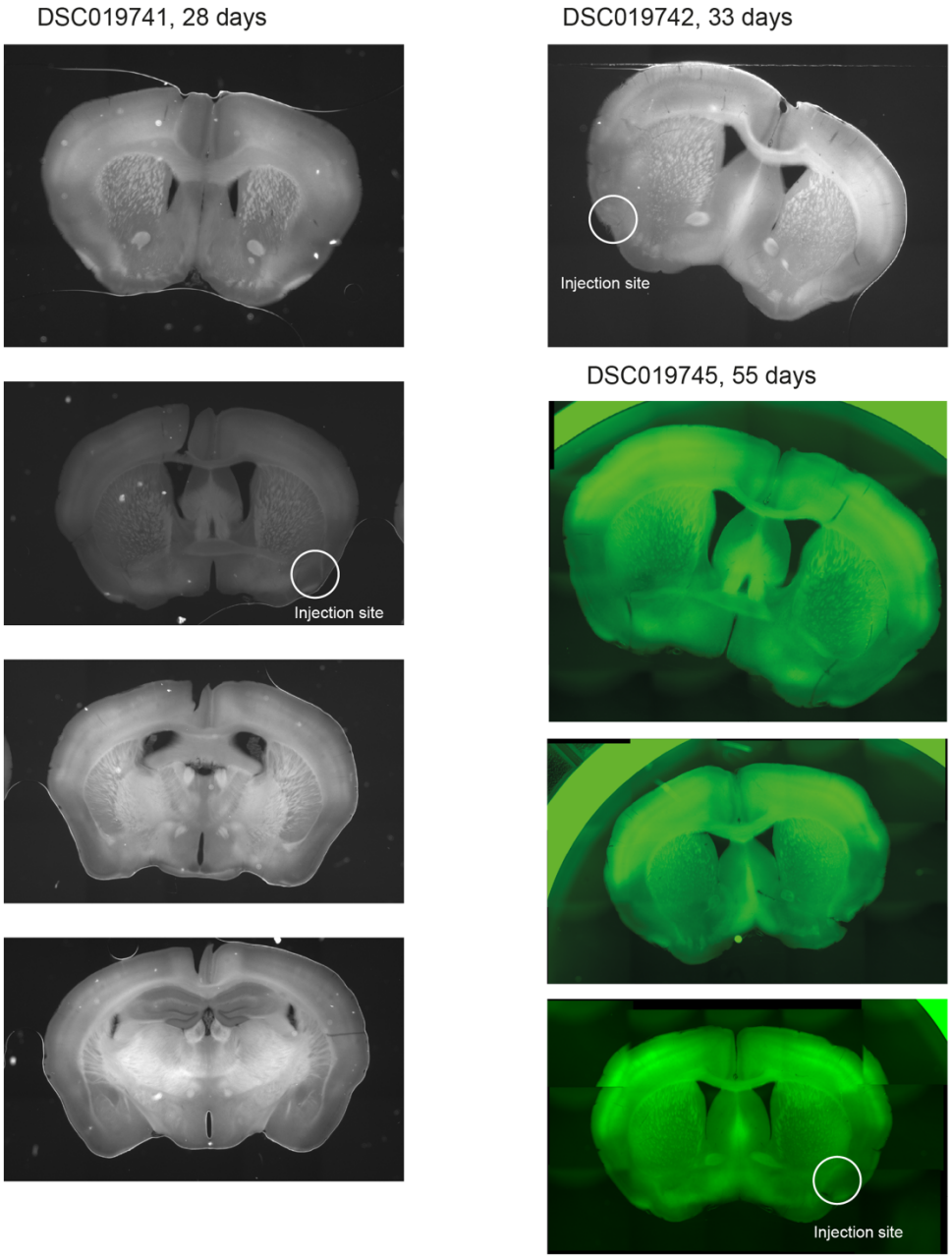

Figure 65. ***Rabies virus::switch-flpo injected in Ai210; SST-Cre mice, example 2.***

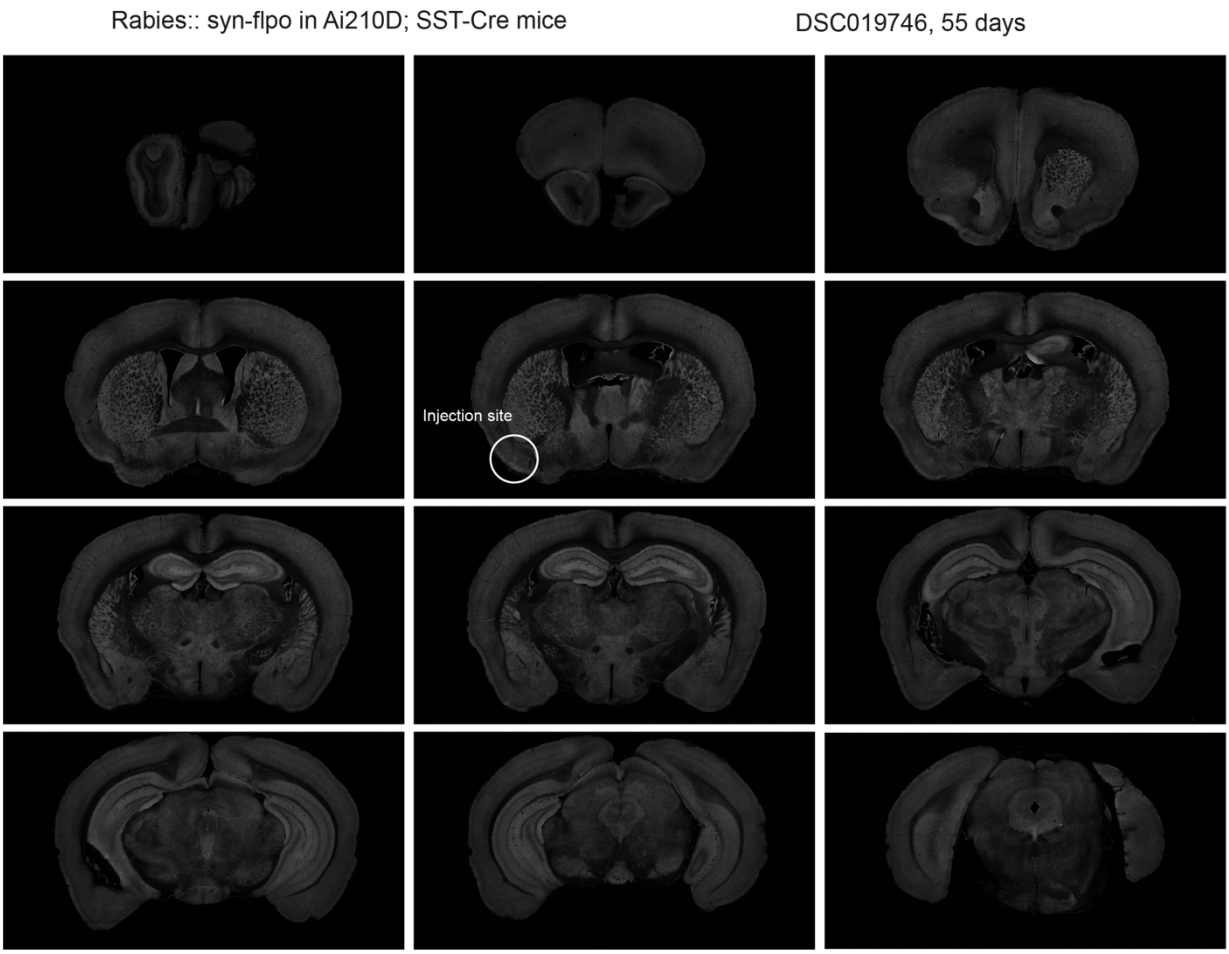

Figure 66. ***Rabies virus::switch-flpo injected in Ai210; SST-Cre mice, example 3.***

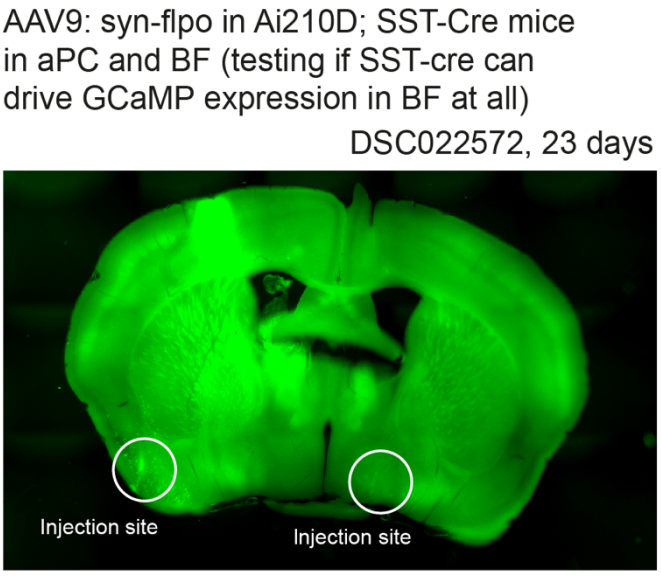

Figure 67. ***Local injection of AAV9::Syn-flpo virus in Ai210D; SST-Cre mice.***

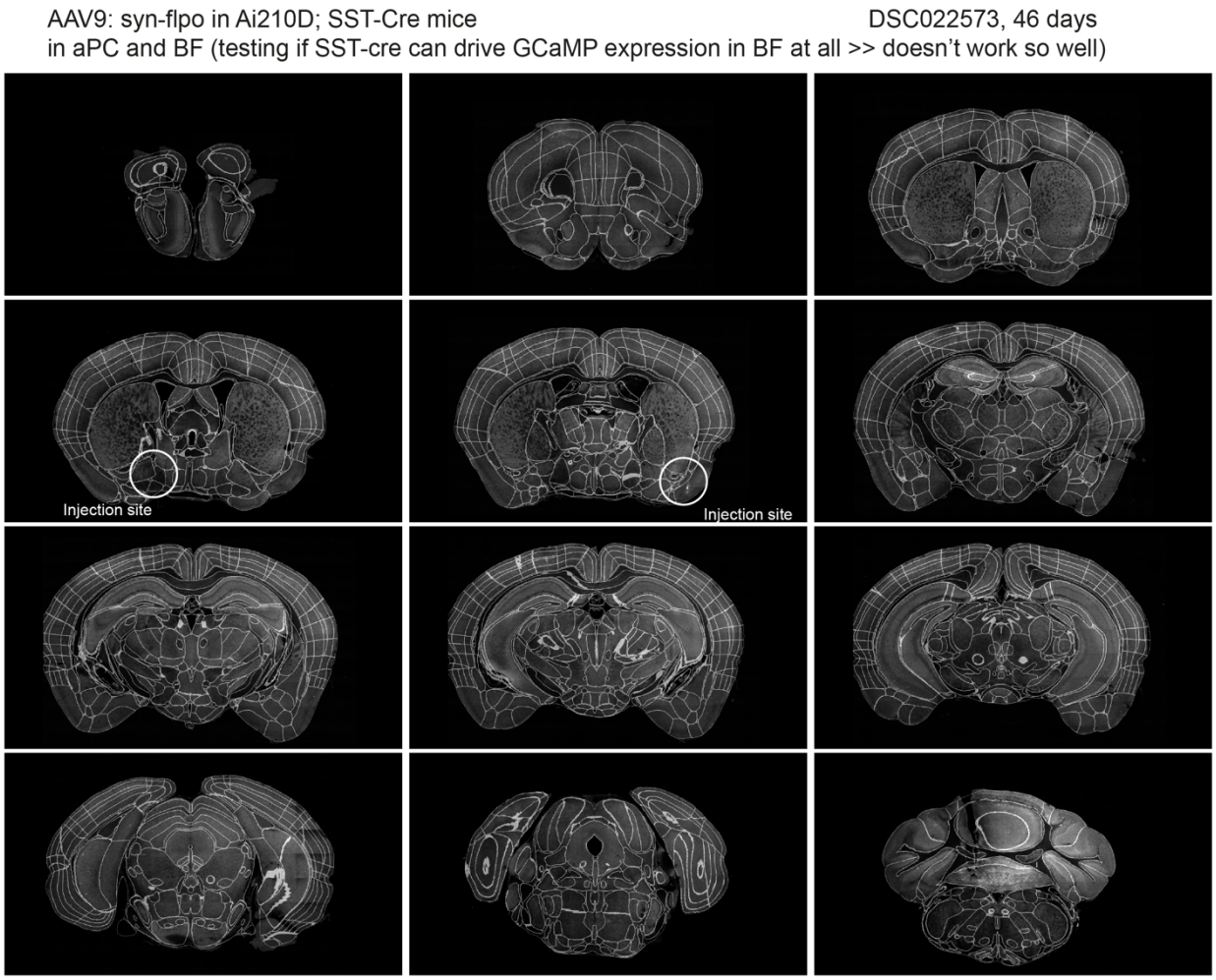

Figure 68. ***Local injection of AAV9::Syn-flpo virus in Ai210D; SST-Cre mice, example 2.***

The central nucleus of the amygdala

The central nucleus of the amygdala (CeA) consists of mostly GABAergic neurons and most subtypes of these GABAergic neurons have been reported to be involved in promoting appetitive behaviors (Kim et al., 2017) or predatory behaviors (Han et al., 2017). One exception is the protein kinase Cδ-expressing CeA ($CeA^{PKC\delta+}$) neurons, which inhibit most other GABAergic CeA neurons. The $CeA^{PKC\delta+}$ neurons are activated by various anorexigenic signals (Cai et al., 2014); these neurons show strong cFos expressions, an immediate early gene which was used as a proxy of neuronal activities when mice were re-fed after 24 hours fasting, injected with satiation hormones cholecystokinin (CCK), or injected with lithium chloride (LiCl) which induces nausea and visceral malaise, or with lipopolysaccharide (LPS), which triggers a wide range of inflammatory and sickness responses. By manipulating the $CeA^{PKC\delta+}$ neurons, the authors showed that optogenetically activating these neurons leads to suppression of feeding regardless of whether activating the neurons in closed-loop or open-loop manners, and optogenetically or chemogenetically silencing these neurons promotes feeding. Importantly, activating the $CeA^{PKC\delta+}$ neurons does not increase anxious behaviors in the mice. $CeA^{PKC\delta+}$ neurons mostly form monosynaptic inhibition to the $CeA^{PKC\delta-}$ neurons, and photostimulation-induced feeding suppression by activation of $CeA^{PKC\delta+}$ neurons is blocked by local infusion of bicuculline (a GABA receptor blocker), suggesting that the local GABAergic signaling in the CEA is required for feeding suppression. Additionally, optogenetically suppressing the $CeA^{PKC\delta-}$ neurons can reduce the food intake, suggesting that this downstream subpopulation of CeA neurons contributes to the feeding suppression. While opto-activating these $CeA^{PKC\delta-}$ neurons does not necessarily increase food intake, this may be explained by the heterogeneity of the $CeA^{PKC\delta-}$ neurons.

A different subpopulation of $CeA^{PKC\delta-}$ neurons, the serotonin receptor 2a (Htr2a)-expressing CeA GABAergic (CeA^{Htr2a}) neurons were identified a few years later, and *in vivo* Ca^{2+} imaging of this subpopulation showed prominent activation during feeding (Douglass et al., 2017) and that the responses gradually increase throughout the meal, indicating these neurons also track satiation levels. Optogenetically and chemogenetically activating these neurons promotes feeding under *ad libitum*-fed conditions and other anorexigenic conditions such as following LiCl or LPS injections, suggesting that the CeA^{Htr2a} neurons are the downstream targets of the $CeA^{PKC\delta+}$ neurons

and can overwrite the sickness-induced anorexia. Ablation of the CeA^{Htr2a} neurons by diphtheria toxin-expressing AAV does not affect daily food intake or body weights, but decreases food consumption after fasting, suggesting that they are involved in high-motivation feeding, but not in long-term energy homeostasis. Optogenetically silencing the CeA^{Htr2a} neurons leads to less food consumption, mostly reducing feeding bout size but not the number of feeding bouts. A different study also suggests that CeA^{Htr2a} neurons inhibit the PBN and promote feeding (Peters et al., 2023). This subpopulation of GABAergic CeA neurons may have projections to the aPC (Allen Institute, mouse brain connectivity experiment id: 299245589) and suppress the aPC during feeding. Connectivity studies are required to decipher the CeA to aPC circuit and whether this is the main source of binge feeding-induced aPC suppression.

Another subpopulation of CeA GABAergic neurons, the CeA prepronociceptin-expressing neurons (CeA^{Pnoc}), also activate during feeding (Hardaway et al., 2019). CeA^{Pnoc} neurons share few overlaps of gene expression with the CeA^{PKCδ} and CeA^{Htr2a} neurons, with slightly more co-expression of SST, indicating that this subpopulation is genetically different from other CeA GABAergic neurons. CeA^{Pnoc} neurons respond to feeding with a higher proportion of activating neurons compared to other CeA^{Pnoc-} neurons. Ablation of these neurons leads to less HFD consumption and less body weight increases throughout one week, while consumption of regular chow is not affected. Ablation of CeA^{Pnoc} neurons also decreases palatable food (water sweetened by saccharin or sucrose) preference, thus inducing this subpopulation signals the palatability of food items. Similarly to the ablation experiment, chemogenetically suppressing the CeA^{Pnoc} neurons also results in increased HFD consumption but not normal chow. Activating CeA^{Pnoc} neurons is reinforcing motivation (more nose pokes), however activating CeA^{Pnoc} neurons or their downstream targets does not promote feeding, suggesting that CeA^{Pnoc} neurons may function on a longer time scale (related to neuronal ablation and chemogenetics experiments) instead of only for the short, brief activation with light stimulations.

Taken together, GABAergic CeA neurons may contribute to the binge feeding-induced aPC suppression, especially the CeA^{Htr2a} neurons, based on their neuronal dynamics during feeding and their anatomical projections.

Zona incerta

The zona incerta (ZI) is an elongated brain region within the posterior subthalamus consisting of GABAergic (Zhang and van den Pol, 2017) and dopaminergic (Ye et al., 2023) neurons, and both types of neurons are involved in feeding behaviors by inhibiting the downstream projection to the paraventricular nucleus of the thalamus (PVT). Both neuron types are activated upon retrieving food pellets and then decrease their activities for around 10 seconds. ZI-DA neurons exhibit a stronger activation upon pellet retrieval and ZI-GABA neurons show a stronger and longer suppression when consuming the food pellets. Neuron ablation in the ZI reduces meal size and chemogenetically activating ZI neurons promotes feeding (de Git et al., 2021).

While the neuronal dynamics of ZI neurons fit with the temporal profile of binge feeding-induced aPC suppression, there is minimal projection from the ZI to the aPC (Allen Institute, mouse brain connectivity experiment id: 175018829), despite robust ZI projections in the layer 1 neocortex. The anatomical separation prohibits the ZI circuits, making it an unlikely mechanism for binge feeding-induced aPC suppression.

Dorsomedial hypothalamus

The dorsomedial hypothalamus (DMH) consists of GABAergic neurons that respond to food taste and serve as a negative feedback signal for satiation (Aitken et al., 2023) (see **Discussion 4.2** above on how the sensory experience of food contributes to satiation). The DMH neurons inhibit appetite by inhibiting the AgRP neurons, resulting in an enhanced satiation level. Anatomically, DMH neurons project to the frontal cortices, especially to the insular cortex (including the gustatory cortex), with limited projection to the aPC. While it is possible to have differential projecting population neuronal dynamics in the subgroup of DMH neurons, this projection would suggest a stronger inhibition in the GC over the aPC based on the DMH fiber densities in these two areas, making this circuit unlikely to contribute to the binge feeding-induced suppression in the aPC.

General GABAergic modulation

Current efforts to search for the inhibitory modulation by binge feeding have not revealed the true inhibitory modulation. Including the abovementioned long-range GABAergic inputs, local GABAergic neurons in layer 1 of the aPC involved in the feedforward inhibition (Suzuki and Bekkers, 2010; Suzuki and Bekkers, 2012; Suzuki et al., 2022), despite it being unlikely (Bolding and Franks, 2018), may still overtake the excitation-inhibition-ratio, resulting in a net inhibitory effect in the aPC excitatory neurons and PV^+ and SST^+ neurons. Imaging Ca^{2+} responses in the aPC layer 1 is challenging due to the geometry of the location; only a small portion of the prism tip is in contact with layer 1, and based on the excitatory aPC neuron cell map, it is unlikely that I have covered a sufficient field of view of layer 1 in the aPC. Regardless of circuit- and cell type-specific modulation, another way to examine whether such suppression is GABA-mediated is by testing the general GABA concentration in the aPC, which can be achieved by using a GABA sensor (e.g. iGABASnFR (Marvin et al., 2019)). With this approach, I can test if the GABA neurotransmitter mediates the suppression. However, this approach may still be obstrcted by the reduction of GABA release from the aPC PV^+ and SST^+ neurons, resulting in suboptimal validation of this hypothesis.

4.3.2. Neuromodulations beyond DA and 5HT

Acetylcholine

Cholinergic (ChAT) neurons are mostly located in the basal forebrain and in the striatum/nucleus accumbens, and the former mostly projects widely and diffusely throughout the brain, while the latter one projects within the structure.

Jackie Schiller's lab (Technion - Israel Institute of Technology, Israel), during my personal communication with them regarding their unpublished work on cholinergic modulation in the aPC, reported that by optogenetically activating basal forebrain ChAT fibers in the aPC, aPC pyramidal neurons became more excitable (lower rheobase, increased resting membrane potentials), but weakened synaptic transmission (lower amplitude for EPSP/EPSC) of the recurrent fibers. This modulation may correspond with the binge feeding-induced aPC suppression by reducing recurrent inputs, though may not fit for the

cholinergic modulated increased signal-to-noise ratio, since the food-activated aPC neurons mostly do not respond to food items during binge feeding.

Cholinergic projection from the basal forebrain to the aPC may contribute to binge feeding-induced aPC suppression since this population is also activated during feeding (Harrison et al., 2016). However, a separate research paper suggested that basal forebrain cholinergic neurons suppress feeding (Herman et al., 2016); optogenetic suppression of cholinergic neurons in the basal forebrain decreases food intake by 10-20%, in both chronic and acute conditions. This suppression is likely to be due to direction projection from the basal forebrain to the ARC since light stimulation of cholinergic fibers in the ARC can also induce 10-20% food intake. Ablation of $ChAT^{+}$ neurons or conditional knockout of the ChAT gene in the diagonal band of Broca (DBB) both induce overeating and obesity, suggesting a general function of cholinergic modulation in appetite suppression.

While the neuronal dynamic of cholinergic neurons in the basal forebrain correlates nicely with the feeding behavior, with a promising projection to the aPC, its function is likely to trigger the onset of satiation to decrease food consumption, making it an unlikely potential neuromodulation mechanism.

Noradrenaline / Norepinephrine

Noradrenergic (NE) neurons in the locus coeruleus (LC) widely project to the neocortex. NE modulation is commonly linked to arousal, attention, and anxiety and it promotes learning and memory. LC-NE (dopamine-beta-hydroxylase positive neurons, Dbh^{+}) neurons in the LC are activated upon approaching food items but are suppressed on feeding onset. Their amplitude scales negatively with the feeding progression (Sciolino et al., 2022). Optogenetic and chemogenetic activation of NE neurons reduces food intake, and this is through LC to lateral hypothalamus (LH) projections, whereby activating the LC fibers in LH can reproduce the same feeding inhibition. Inhibiting the LC noradrenergic neurons or noradrenergic fibers in LH does not affect feeding. LC NE neurons project broadly to the dorsal neocortex and strongly influence arousal and predictive coding. LC-NE neurons also project to the aPC, and under the Alzheimer's disease model in mice, the LC-NE fibers are lost in the aPC, and mice showed a decreased odor discrimination

performance (Ghosh et al., 2019; Omoluabi et al., 2021). NE modulates aPC synapses by reducing EPSP in stimulating recurrent fibers at layer 1b and weakly reduces the EPSP of layer 1a fiber stimulation (Hasselmo et al., 1997). The phasic activation of LC-NE neurons upon approaching food may introduce a reduction of network activity in the aPC, although the sustained suppression in the aPC may be recruited by a different circuit. On the contrary, a different study shows that NE concentration in the LH is not modulated during feeding (Feng et al., 2019), which may suggest that NE is generally not involved in feeding control in the hypothalamic regions. Whether there are direct noradrenergic projections from the LC to the aPC is still unclear. A connectivity verification would be necessary before continuing the validation of noradrenergic modulation in feeding. A NE sensor, e.g. $GRAB_{NE}$ (Feng et al., 2019), could be utilized to test this hypothesis by measuring the dynamics of NE concentrations within the aPC.

4.3.3. Summary of potential mechanisms of aPC suppression during binge feeding

In this thesis, despite extensive explorations, I could not easily identify the circuit mechanisms of binge feeding-induced aPC suppression. The abovementioned brain circuits and neuromodulatory systems may contribute to the phenomenon, with the basal forebrain GABAergic neurons and CeA^{htr2a} neurons as the best candidates based on their functional role in feeding regulation and connectivity with the aPC. Notably, the list of potential aPC modulations is not exhaustive. Many other potential modulations can also be involved in the process, e.g. homeostasis hormones (Ghrelin, Insulin, Leptin, and GLP-1 signalings, etc). These hormones are currently excluded from the discussion, mainly due to their slow kinetics (tens of minutes during meals), which are unlikely to be time-locked with the feeding rate-dependent dynamics (seconds) I observed in the thesis. For clarity, I have summarized all the potential mechanisms of binge feeding-induced aPC suppression, both tested and hypothesized, in Table 20.

Table 20. Potential mechanisms for binge feeding-induced aPC suppression.

Potential mechanisms	*Brain regions involved*	*Neuronal dynamics*	*Anatomical connectivity and receptors*	*Probability of true*	*Confirmation*
Input reduction	OB	Unknown before this study	Direct projection	High	Rejected. No reduction in OB mitral cells during binge feeding (Figure 26).
GABAergic	aPC	Unknown	Direct projection (Large et al., 2016a; Large et al., 2018; Large et al., 2016b; Bolding and Franks, 2018)	High	Rejected. Strong suppression is observed in PV^+ and SST^+ aPC neurons during binge feeding (Figure 28).
GABAergic	Basal forebrain	Matched (Harrison et al., 2016); but see (Cassidy et al., 2019) for opposite finding.	Direct projection. (Allen institute mouse brain connectivity experiment id: 299245589) (Do et al., 2016)	High	Yet to be tested, see Discussion 4.3.1.1
GABAergic	CeA	Matched (for CeA^{Htr2a} neurons) (Douglass et al., 2017; Peters et al., 2023)	Semi-direct projection. (Allen institute mouse brain connectivity experiment id: 127761449, note this is without cell-type-specificity)	Medium	Yet to be tested.

Potential mechanisms	*Brain regions involved*	*Neuronal dynamics*	*Anatomical connectivity and receptors*	*Probability of true*	*Confirmation*
GABAergic	ZI	Matched (Zhang and van den Pol, 2017)	Sparse projection. (Allen institute mouse brain connectivity experiment id: 175018829)	Low	Yet to be tested.
GABAergic	DMH	Matched (Aitken et al., 2023)	Unclear. There are direct excitatory projection to aPC, but more densely project to other brain regions including insular cortex. (Allen institute mouse brain connectivity experiment id: 304617742, note this experiment is done in excitatory Cre line)	Low	Yet to be tested.
Serotonergic	DRN	Matched (Ren et al., 2018; Li et al., 2016; Zhong et al., 2017; Paquelet et al., 2022)	Direct projection (Lottem et al., 2016) Matched receptor types: (Piszár and Lőrincz, 2022; Sheldon and Aghajanian,	High	Rejected. I found decreased serotonin release during both slow and binge feeding.

Potential mechanisms	*Brain regions involved*	*Neuronal dynamics*	*Anatomical connectivity and receptors*	*Probability of true*	*Confirmation*
			1991; Wang et al., 2020a)		
Dopaminergic	VTA/SNc	Matched (Schultz, 2016; Schultz et al., 1997)	Direct but sparse (Aransay et al., 2015) Matched receptor types: (Zhang et al., 2021b; Ahlgren-Beckendorf and Levant, 2004; Robinson and Caron, 1997)	Medium	Rejected. I found decreased dopamine release during both slow and binge feeding.
Cholinergic	Basal forebrain	Matched (Harrison et al., 2016)	Direct projection. (Do et al., 2016)	Medium-low Cholinergic modulation seems to have suppressing effect on feeding (Herman et al., 2016), does not match with the aPC suppression promotes feeding results I presented in this thesis.	Yet to be tested.
Noradrenergic	LC	Mismatched (Sciolino et al., 2022)	Direct projection. (Ghosh et al., 2019; Omoluabi et al., 2021; Hasselmo et al., 1997)	Medium-low	Yet to be tested.

Potential mechanisms	*Brain regions involved*	*Neuronal dynamics*	*Anatomical connectivity and receptors*	*Probability of true*	*Confirmation*
Global suppression during binge feeding	Unclear	Unclear	Unclear	Medium-high	Rejected. I tested with recording in the GC but no binge feeding-induced suppression is observed.

4.4. The potential downstream target of aPC regulates feeding

In this study, I have shown that aPC suppression regulates feeding, even though it has not been identified how the olfactory cortex suppression leads to the feeding/appetite. Here, I will discuss a few potential downstream target areas that might be involved in feeding regulation.

4.4.1. aPC projection to the hypothalamus

Arcuate nucleus of the hypothalamus

A recent preprint has tried to link the connection between the olfactory areas to the neurons in the arcuate nucleus (ARC) of the hypothalamus, the AgRP, and POMC neurons, respectively (Kuang et al., 2023). They found that higher olfactory areas, including the posterior piriform cortex (pPC), the olfactory tubercle, and the posterior lateral cortical amygdala, indirectly project to both AgRP and POMC neurons. The direct projection from the olfactory area to the ARC is the medial amygdala. In this study, the aPC was not included in the analysis, thus it was not determined aPC has an indirect projection to the ARC.

These direct and indirect links may explain odor-driven rapid neuronal modulation in the AgRP/POMC neurons. AgRP and POMC neurons are differentially modulated by feeding,

whereby AgRP neurons are suppressed by feeding and POMC neurons are activated, respectively. Although the AgRP and POMC neurons are already modulated slightly before the feeding onset (~2 to tens of seconds), this rapid modulation of ARC neurons is more likely to be driven by the sensory detection of food instead of the food flavor itself (Betley et al., 2015; Chen et al., 2015), which is different from my observation here that the aPC modulation only takes place after feeding onset. In my histology results (Figure 69), no clear projection from the aPC excitatory neurons to the ARC can be observed, suggesting very little direct projection. This result coincides with the abovementioned retrograde tracing results (Kuang et al., 2023), in that the PC does not directly project to the ARC.

Ventromedial hypothalamus

In my aPC excitatory fiber projection data, I noticed a semi-dense projection to the ventromedial hypothalamus (VMH), which has been reported to have a satiation function (Zhang et al., 2020) and is also known for other functions in aggressive and maternal behaviors (Lin et al., 2011; Mei et al., 2023). Early studies showed that lesioning VMH leads to overeating (Balagura and Devenport, 1970; Becker and Kissileff, 1974; Berthoud and Jeanrenaud, 1979; Brooks et al., 1946; Epstein, 1960; Larkin, 1975; Maes, 1980), and chemogenetically (Coutinho et al., 2017; Viskaitis et al., 2017) or optogenetically activating of VMH neurons triggers satiation (Zhang et al., 2020). The satiation effect from activating VMH neurons is mediated by the downstream excitatory projections to the paraventricular thalamus (PVT), a thalamic gate between hypothalamic and brainstem regions. Suppression of PVT neurons via ZI GABAergic (Zhang and van den Pol, 2017) inputs or AgRP GABAergic (Horio and Liberles, 2021) inputs can robustly promote feeding behaviors. In this working hypothesis, reduced odor input from the aPC to the VMH can decrease VMH network excitation levels, therefore decreasing the satiation signal to the PVT. To verify this idea, I should be able to repeat my optogenetic suppression experiment and suppress aPC fibers in the VMH.

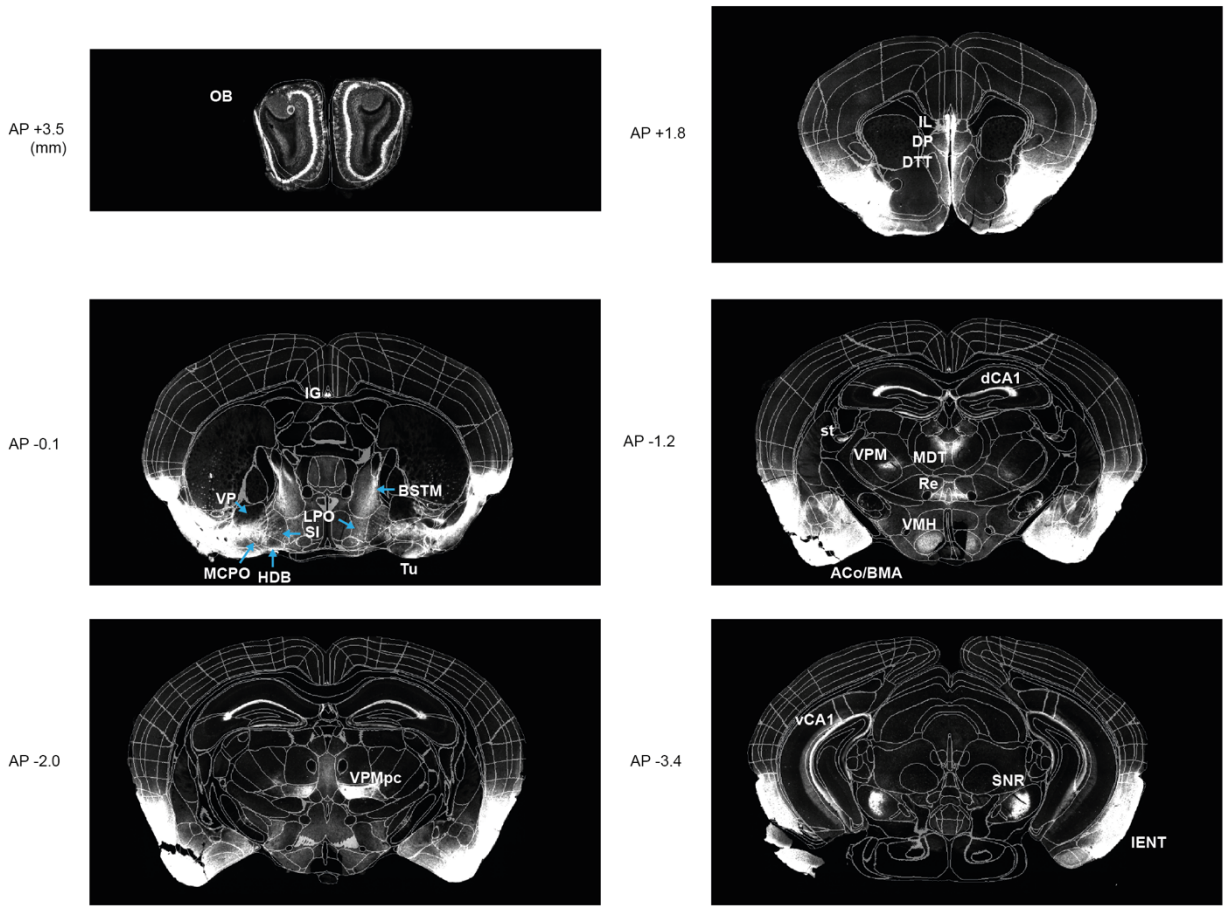

Figure 69. ***Projection of excitatory aPC neurons.*** *Abbreviations: OB, olfactory bulb, IL, infralimbic cortex, DP, dorsal peduncular cortex, DTT, dorsal tenia tecta, IG, indusium griseum, VP, ventral pallidum, LPO, lateral preoptic area, BSTM, bed nucleus of the stria terminals, medial division, SI, substantia innominata, MCPO, magnocellular preoptic nucleus, HDB, nucleus of the horizontal limb of the diagonal band, Tu, olfactory tubercle, dCA1, dorsal hippocampal CA1, st, stria terminalis, VPMpc, ventroposteromedial nucleus of the thalamus, vCA1, ventral hippocampal CA1, SNR, substantia nigra, reticular, lENT, lateral entorhinal cortex.*

Lateral hypothalamus

The lateral hypothalamus (LH) is another important feeding-related brain region, where activating LH^{VGAT} and inhibiting LH^{VGLUT2} neurons increases food intake through direct projections to the ventral tegmental area (VTA), the reward center hosting dopaminergic neurons. ARC AgRP neurons inhibit LH, and this suppression drives foraging and feeding behaviors. Upon feeding, different subpopulations of LH GABAergic neurons are activated by appetitive behavior (nose poke) or consummatory behavior, with a few shared neurons responding to both behaviors (Jennings et al., 2015). A reduced inhibition

from other inhibitory neurons (D1 MSN) to LH GABAergic neurons is also required to sustain feeding bouts as a filter for distractions (O'Connor et al., 2015).

While it is unclear if aPC neurons directly project to the LH, a related study on the GABAergic neurons in the ventral olfactory nucleus (VON) found projections to the LH (Murata et al., 2019). In the same study, several LH-projecting aPC neurons were also observed in the images, despite the numbers of projecting neurons being much lower and the cell type not being specified. In my excitatory aPC fiber projection results, there do not seem to be fibers projecting to the LH, while an alternative explanation could be that this aPC to LH circuit is GABAergic and thus is not captured by the excitatory projection result.

4.4.2. aPC projection to the gustatory cortex/insular cortex

The gustatory cortex (GC), located right above the aPC, is the first cortical area for gustatory processing in the dorsal part of the insular cortex. The GC has extensive reciprocal functional connections with the aPC (Blankenship et al., 2019; Maier et al., 2015; Maier et al., 2012; Samuelsen and Fontanini, 2017; Vincis and Fontanini, 2016). This interconnection indicates a direct interaction of olfactory and gustatory signals in both cortical areas, whereby scientists have discovered taste responses in the PC (Maier et al., 2012) and smell responses in the GC (Samuelsen and Fontanini, 2017; Vincis and Fontanini, 2016). Several studies have suggested the functional role of GC in olfactory learning (STFP) (Fortis-Santiago et al., 2010) and olfactory processing (Blankenship et al., 2019; Maier et al., 2015).

The insular cortex (IC) has active roles in integrating emotional processing, interoception, and feeding control. A study on the unilateral IC circuit of feeding control has revealed that in the right hemisphere, but not the left hemisphere, anterior IC (aIC), is activated upon LiCl-, LPS-, and Cisplatin-injection-induced discomfort, representing the unpleasant physiological states (Wu et al., 2020). Optogenetically activating the excitatory neurons in the right aIC suppresses feeding, while suppressing these excitatory neurons promotes feeding, suggesting that the right aIC directly inhibits feeding behavior upon artificial activation of discomfort representation. The right aIC directly projects to the LH, and

activating or suppressing aIC excitatory fibers in the LH can replicate the feeding suppression or promotion. The recording site of this research is likely to include the GC, despite the authors not specifying the optical fiber cannula implantation site in greater detail.

During binge feeding, the absence of odor signals from the aPC to the GC may also contribute to decreasing general activity in the insular cortex and promote feeding. However, I did not observe differences in GC responses across different feeding rates, suggesting that there is no general reduction of neuronal activities. Thus, the binge feeding-induced overeating is not likely to be contributed by the GC or IC. An important limitation here is that I only recorded the GC in the left hemisphere, so different neuronal dynamics can still be possible in the right GC/IC during binge feeding. Another limitation is that I performed the recording in the non-specific neuronal populations in the GC instead of only $CaMK2^{+}$/excitatory neurons (see **Methods 2.1**), thus exact neuronal responses may be masked by the mixture of cell types. To elucidate the contribution of GC/IC in feeding control caused by aPC suppression during binge feeding, recording from the right hemisphere excitatory GC neurons may demonstrate whether a general activity reduction is inherited from aPC and, therefore, promotes feeding.

4.4.3. aPC projection to the orbitofrontal cortex

The orbitofrontal cortex (OFC) is known to be involved in decision-making and reward processing. Both olfactory and gustatory signals converge in the OFC (Barreiros et al., 2021), where they represent flavor perception (Small, 2012) and encode flavor hedonics. One recent study reported that mice would increase licking behaviors during reward presentation by directly optogenetically activating the feeding-responsive OFC neurons (Jennings et al., 2019). Notably, stimulation of feeding-responsive OFC neurons does not increase licking if no rewards or non-caloric rewards are presented, indicating that the functional role of these feeding-responsive OFC neurons is relevant to caloric nutrients rather than to just reward or licking behaviors. aPC neurons extensively project to the prefrontal cortex including the OFC (Chen et al., 2014), suggesting that odor information is further transferred to the frontal cortex for decision-making and reward processing.

In the presence of binge feeding, the odor encoding in the aPC is mostly suppressed, indicating a much lower input transfer from the aPC to the OFC. Since both odor signals and taste signals converge at the OFC, the divergence of these two signals may cause a massive alteration in flavor perception, and such an alteration may contribute to the hedonic coding, which promotes more feeding-related behaviors like licking. My colleagues and I recently started miniscope recording in the OFC, and the preliminary results suggest that binge feeding induces a similar suppression to that I had observed in the aPC. Further examination of whether the feeding-responding OFC neurons remain active during binge feeding, which may support the hedonic encoding flavors, is currently under investigation.

4.4.4. aPC projection to the ventral hippocampal formation

The ventral hippocampal formation (vHPF) is involved in emotional memory consolidation through intense connectivity with the basolateral amygdala (BLA) and medial prefrontal cortex (mPFC) (Pronier et al., 2023). Interestingly, new studies have shown the potential roles of vHPF in regulating feeding behaviors (Mohammad et al., 2021; Wee et al., 2023). One is through ventral subiculum (vSub) projection to the somatostatin (TN^{SST}) neurons in the mouse hypothalamic tuberal nucleus, potentiating the contextual feeding conditions (Mohammad et al., 2021). Chemogenetic suppression of vSub neurons or the TN^{SST}-projecting vSub blocks conditioned feeding behaviors, however, while chemogenetic activation of vSub is not sufficient to promote more feeding behaviors, indicating that the temporal dynamics of this vSub-TN circuit are crucial for the circuit manipulation.

A different study showed that two different populations of the ventral CA1 and subiculum (vS) area of the ventral hippocampus project to two brain areas (Nucleus Accumbens (NAc) and LH, respectively), and only the NAc-projecting vS (vS-NAc) neurons are suppressed during the transition from food investigation to feeding onset (Wee et al., 2023). Activating the vS-NAc neurons, both optogenetically and chemogenetically, largely decreased the transition probability from food investigation to feeding, suggesting a functional role of vS in feeding controls.

In my aPC excitatory fiber projection data, I observed a known strong aPC-vHPC projection (Figure 69). While this projection was mostly assumed to be involved in odor memory formation, it may have additional roles in feeding behaviors. When the aPC is suppressed, the inputs from the aPC to the vHPC are also largely decreased, supporting the suppression in the vHPC during feeding transitions. The temporal dynamics may not necessarily match since the vHPC suppression seems to take place slightly earlier than the investigation-feeding transition. In contrast, binge feeding-induced aPC suppression happens upon feeding onsets, making this connection a less likely mechanism of aPC suppression driven by feeding promotion.

4.4.5. Other unknown aPC projections

A few additional aPC targets were discovered in my projection study, including the substantia nigra, the red nucleus, the reuniens nucleus, the perireuniens nucleus, and the ventroposterior medialis parvocellularis nucleus of the thalamus. While these areas are not necessarily known for being homeostasis controls, they may have unexplored roles in feeding controls. Further studies are needed to explore the potentialities of these downstream brain regions in feeding rate-dependent feeding controls.

4.4.6. Summary of potential downstream targets of aPC feeding regulation

In summary, several potential downstream brain areas are proposed here to be the functional targets of binge feeding-induced suppression in the aPC, of which, hypothalamic areas including the ARC, VMH, and LH, and cortical areas like the IC are the most prominent candidates. These areas have been reported to have crucial roles in regulating feeding behaviors and functionally manipulating aPC axons in these regions during feeding can be used to verify their exact contribution to binge feeding-induced overeating.

4.5. Evolutionary perspective on feeding-induced sensory modulation

In this thesis, I have revealed a new modulation of olfactory flavor representation by binge feeding that promotes overeating. One unsolved question in this research remains: what

is the binge feeding-induced aPC suppression good for? Is there a beneficial function of sensory suppression during binge feeding?

From an evolutionary perspective, where food accessibility is mostly limited, overeating would be pro-survival; securing more calories and nutrients than the individual needs at the given moment is beneficial since one would not know when the next meal will be available. Following the same line, binge feeding-induced sensory suppression may be an evolutionary conserved mechanism to reduce satiation and promote a better survival chance. Following the enrichment of food accessibility of the modern era that human beings are faced with nowadays, this preserved mechanism becomes problematic; an increased eating rate is commonly linked to overeating (Hall et al., 2019) and obesity (Ohkuma et al., 2015), while reducing the eating rate can effectively control food consumption (Bolhuis et al., 2014a; Bolhuis et al., 2014b; Hurst and Fukuda, 2018; Scisco et al., 2011; Bolhuis et al., 2013).

4.6. Implications for the clinical relevance

In modern societies with excessive accessibility to hedonic food items, loss of control during fast eating, commonly referred to as binge eating, is a usual phenomenon that individuals experience. A frequent loss of control over eating may lead to eating disorders, including binge eating disorders and bulimia nervosa. Among other treatments, the most effective ones are behavioral interventions, usually referred to as “mindful eating”. This means paying attention to one's experiences of eating, body-related sensations, and thoughts and feelings about food, with elevated awareness. One aspect of mindful eating focuses on slowing down the eating process, which increases the full experience of food flavors and the awareness of the satiation signals. Recent studies in human behavior fields have demonstrated that fast eating is associated with overeating and obesity, which is enhanced by high-processed food products that tend to require less chewing and contain higher sugar and fat content. Slowing down feeding rates has also been shown to be an effective intervention and largely beneficial for weight control. By changing food textures such as decreasing the bite or sip size (Bolhuis et al., 2013; Bolhuis et al., 2014b) and increasing the crunchiness (Bolhuis et al., 2014a), scientists have successfully

shown that, without decreasing the pleasantness of eating food, people eat much less than they would usually do.

Despite slowing down eating being an effective approach to treating eating disorders and weight control, the underlying neural mechanism of this feeding rate-related modulation has not been explored. To my knowledge, this is the first ever study that demonstrates that eating speed has a direct impact on satiety via modulating cortical flavor representation with real-time *in vivo* physiological recordings and optogenetic manipulation. With this thesis, I provided new insights into how flavor representation is modulated and also modulating feeding behaviors and complemented the long-lasting knowledge gaps between the clinical practices and the circuit-level mechanisms in the metabolic field and sensory neuroscience fields.

5. Conclusions

In the present study, I have demonstrated that the feeding rate has a strong impact on olfactory flavor representations, but not on gustatory representations. The binge feeding-induced modulation in the aPC extends to most cell types in the aPC, but the OB output neurons and the GC neurons are not affected. I have further illustrated that the strong neuronal suppression in the aPC during binge feeding functions as a reduction of satiation, which promotes food consumption by lengthening the feeding bouts, providing a surprising role of cortical olfaction during feeding. While the exact suppression mechanism remains to be discovered, the extensive efforts of exploring the possible circuits have excluded several crucial, but parallel, circuits that may contribute to the binge feeding-induced neuronal modulations. Given that this is the first study on feeding rate modulations on flavor perceptions, these results provide the basis for new ideas for future research in the sensory neuroscience and metabolic fields, which could lead to a better understanding of how the brain and body interact with the world, from the nose and the mouth to the gut between each bite.

6. Reference list

Ahlgren-Beckendorf, J. A. & Levant, B. 2004. Signaling Mechanisms of the D3 Dopamine Receptor. *Journal of Receptors and Signal Transduction,* 24**,** 117-130.

Aimé, P., Duchamp-Viret, P., Chaput, M. A., Savigner, A., Mahfouz, M. & Julliard, A. K. 2007. Fasting increases and satiation decreases olfactory detection for a neutral odor in rats. *Behav. Brain Res.,* 179**,** 258-264.

Aimé, P., Hegoburu, C., Jaillard, T., Degletagne, C., Garcia, S., Messaoudi, B., Thevenet, M., Lorsignol, A., Duchamp, C., Mouly, A.-M. & Julliard, A. K. 2012. A Physiological Increase of Insulin in the Olfactory Bulb Decreases Detection of a Learned Aversive Odor and Abolishes Food Odor-Induced Sniffing Behavior in Rats. *PLOS ONE,* 7**,** e51227.

Aitken, T. J., Ly, T., Shehata, S., Sivakumar, N., La Santa Medina, N., Gray, L. A., Dundar, N., Barnes, C. & Knight, Z. A. 2023. Negative feedback control of hunger circuits by the taste of food. Neuroscience.

Albrecht, J., Schreder, T., Kleemann, A. M., Schöpf, V., Kopietz, R., Anzinger, A., Demmel, M., Linn, J., Kettenmann, B. & Wiesmann, M. 2009. Olfactory detection thresholds and pleasantness of a food-related and a non-food odour in hunger and satiety. *Rhinology,* 47**,** 160-165.

Allen, W. E., Chen, M. Z., Pichamoorthy, N., Tien, R. H., Pachitariu, M., Luo, L. & Deisseroth, K. 2019. Thirst regulates motivated behavior through modulation of brainwide neural population dynamics. *Science,* 364**,** eaav3932.

Andermann, M. L. & Lowell, B. B. 2017. Toward a Wiring Diagram Understanding of Appetite Control. *Neuron,* 95**,** 757-778.

Andrade, A. M., Greene, G. W. & Melanson, K. J. 2008. Eating slowly led to decreases in energy intake within meals in healthy women. *J. Am. Diet. Assoc.,* 108**,** 1186-1191.

Aponte, Y., Atasoy, D. & Sternson, S. M. 2011. AGRP neurons are sufficient to orchestrate feeding behavior rapidly and without training. *Nature Neuroscience,* 14**,** 351-355.

Araneda, R. C., Kini, A. D. & Firestein, S. 2000. The molecular receptive range of an odorant receptor. *Nature Neuroscience,* 3**,** 1248-1255.

Aransay, A., Rodrã-Guez-Lã³pez, C., Garcã-a-Amado, M. A., Clascã¡, F. & Prensa, L. A. 2015. Long-range projection neurons of the mouse ventral tegmental area: a single-cell axon tracing analysis. *Frontiers in Neuroanatomy,* 9.

Arneodo, E. M., Penikis, K. B., Rabinowitz, N., Licata, A., Cichy, A., Zhang, J., Bozza, T. & Rinberg, D. 2018. Stimulus dependent diversity and stereotypy in the output of an olfactory functional unit. *Nature Communications,* 9**,** 1347.

Atasoy, D., Betley, J. N., Su, H. H. & Sternson, S. M. 2012. Deconstruction of a neural circuit for hunger. *Nature,* 488**,** 172-177.

Avena, N. 2015. *Hedonic Eating: How the Pleasure of Food Affects Our Brains and Behavior,* Oxford, New York, Oxford University Press.

Bai, L., Sivakumar, N., Yu, S., Mesgarzadeh, S., Ding, T., Ly, T., Corpuz, T. V., Grove, J. C. R., Jarvie, B. C. & Knight, Z. A. 2022. Enteroendocrine cell types that drive food reward and aversion. *eLife,* 11**,** e74964.

Balagura, S. & Devenport, L. D. 1970. Feeding patterns of normal and ventromedial hypothalamic lesioned male and female rats. *Journal of Comparative and Physiological Psychology,* 71**,** 357-364.

Barreiros, I. V., Panayi, M. C. & Walton, M. E. 2021. Organization of Afferents along the Anterior–posterior and Medial–lateral Axes of the Rat Orbitofrontal Cortex. *Neuroscience,* 460**,** 53-68.

Baskin, D. G., Porte, D., Guest, K. & Dorsa, D. M. 1983. Regional concentrations of insulin in the rat brain. *Endocrinology,* 112**,** 898-903.

Bates, D., Mächler, M., Bolker, B. & Walker, S. 2015. Fitting Linear Mixed-Effects Models Using lme4. *Journal of Statistical Software,* 67**,** 1-48.

Becker, E. E. & Kissileff, H. R. 1974. Inhibitory controls of feeding by the ventromedial hypothalamus. *The American Journal of Physiology,* 226**,** 383-396.

Berkun, M. M., Kessen, M. L. & Miller, N. E. 1952. Hunger-reducing effects of food by stomach fistula versus food by mouth measured by a consummatory response. *J. Comp. Physiol. Psychol.,* 45**,** 550-554.

Berners-Lee, A., Shtrahman, E., Grimaud, J. & Murthy, V. N. 2023. Experience-dependent evolution of odor mixture representations in piriform cortex. *PLOS Biology,* 21**,** e3002086.

Berrios, J., Li, C., Madara, J. C., Garfield, A. S., Steger, J. S., Krashes, M. J. & Lowell, B. B. 2021. Food cue regulation of AGRP hunger neurons guides learning. *Nature,* 595**,** 695-700.

Berthoud, H. R. & Jeanrenaud, B. 1979. Changes of insulinemia, glycemia and feeding behavior induced by VMH-procainization in the rat. *Brain Research,* 174**,** 184-187.

Best, A. R. & Wilson, D. A. 2004. Coordinate Synaptic Mechanisms Contributing to Olfactory Cortical Adaptation. *Journal of Neuroscience,* 24**,** 652-660.

Betley, J. N., Cao, Z. F. H., Ritola, K. D. & Sternson, S. M. 2013. Parallel, Redundant Circuit Organization for Homeostatic Control of Feeding Behavior. *Cell,* 155**,** 1337-1350.

Betley, J. N., Xu, S., Cao, Z. F. H., Gong, R., Magnus, C. J., Yu, Y. & Sternson, S. M. 2015. Neurons for hunger and thirst transmit a negative-valence teaching signal. *Nature,* 521**,** 180-185.

Beutler, L. R., Chen, Y., Ahn, J. S., Lin, Y.-C., Essner, R. A. & Knight, Z. A. 2017. Dynamics of Gut-Brain Communication Underlying Hunger. *Neuron,* 96**,** 461-475.e5.

Biglari, N., Gaziano, I., Schumacher, J., Radermacher, J., Paeger, L., Klemm, P., Chen, W., Corneliussen, S., Wunderlich, C. M., Sue, M., Vollmar, S., Klöckener, T., Sotelo-Hitschfeld, T., Abbasloo, A., Edenhofer, F., Reimann, F., Gribble, F. M., Fenselau, H., Kloppenburg, P., Wunderlich, F. T. & Brüning, J. C. 2021. Functionally distinct POMC-expressing neuron subpopulations in hypothalamus revealed by intersectional targeting. *Nature Neuroscience,* 24**,** 913-929.

Bitzenhofer, S. H., Westeinde, E. A., Zhang, H.-X. B. & Isaacson, J. S. 2022. Rapid odor processing by layer 2 subcircuits in lateral entorhinal cortex. *eLife,* 11**,** e75065.

Blankenship, M. L., Grigorova, M., Katz, D. B. & Maier, J. X. 2019. Retronasal Odor Perception Requires Taste Cortex, but Orthonasal Does Not. *Current Biology,* 29**,** 62-69.e3.

Blazing, R. M. & Franks, K. M. 2020. Odor coding in piriform cortex: mechanistic insights into distributed coding. *Current Opinion in Neurobiology,* 64**,** 96-102.

Bolding, K. A. & Franks, K. M. 2017. Complementary codes for odor identity and intensity in olfactory cortex. *eLife,* 6**,** e22630.

Bolding, K. A. & Franks, K. M. 2018. Recurrent cortical circuits implement concentration-invariant odor coding. *Science,* 361.

Bolding, K. A., Nagappan, S., Han, B.-X., Wang, F. & Franks, K. M. 2019. Robust odor coding across states in piriform cortex requires recurrent circuitry: evidence for pattern completion in an associative network. Neuroscience.

Bolhuis, D. P., Forde, C. G., Cheng, Y., Xu, H., Martin, N. & De Graaf, C. 2014a. Slow Food: Sustained Impact of Harder Foods on the Reduction in Energy Intake over the Course of the Day. *PLoS ONE,* 9**,** e93370.

Bolhuis, D. P., Lakemond, C. M. M., De Wijk, R. A., Luning, P. A. & De Graaf, C. 2013. Consumption with large sip sizes increases food intake and leads to underestimation of the amount consumed. *PLoS One,* 8**,** e53288.

Bolhuis, D. P., Lakemond, C. M. M., De Wijk, R. A., Luning, P. A. & De Graaf, C. 2014b. Both a higher number of sips and a longer oral transit time reduce ad libitum intake. *Food Quality and Preference,* 32**,** 234-240.

Boone, M. H., Liang-Guallpa, J. & Krashes, M. J. 2021. Examining the role of olfaction in dietary choice. *Cell Reports,* 34**,** 108755.

Boyd, A. M., Sturgill, J. F., Poo, C. & Isaacson, J. S. 2012. Cortical Feedback Control of Olfactory Bulb Circuits. *Neuron,* 76**,** 1161-1174.

Brooks, C. M., Lockwood, R. A. & Wiggins, M. L. 1946. A study of the effect of hypothalamic lesions on the eating habits of the albino rat. *The American Journal of Physiology,* 147**,** 735-741.

Brüning, J. C. & Fenselau, H. 2023. Integrative neurocircuits that control metabolism and food intake. *Science,* 381**,** eabl7398.

Buchanan, K. L., Rupprecht, L. E., Kaelberer, M. M., Sahasrabudhe, A., Klein, M. E., Villalobos, J. A., Liu, W. W., Yang, A., Gelman, J., Park, S., Anikeeva, P. & Bohórquez, D. V. 2022. The preference for sugar over sweetener depends on a gut sensor cell. *Nature Neuroscience,* 25**,** 191-200.

Buck, L. & Axel, R. 1991. A novel multigene family may encode odorant receptors: A molecular basis for odor recognition. *Cell,* 65**,** 175-187.

Burton, S. D., Brown, A., Eiting, T. P., Youngstrom, I. A., Rust, T. C., Schmuker, M. & Wachowiak, M. 2022. Mapping odorant sensitivities reveals a sparse but structured representation of olfactory chemical space by sensory input to the mouse olfactory bulb. *eLife,* 11**,** e80470.

Bushdid, C., Magnasco, M. O., Vosshall, L. B. & Keller, A. 2014. Humans Can Discriminate More than 1 Trillion Olfactory Stimuli. *Science,* 343**,** 1370-1372.

Buzsáki, G. 2019. *The Brain from Inside Out*, Oxford University Press.

Cai, H., Haubensak, W., Anthony, T. E. & Anderson, D. J. 2014. Central amygdala PKC-δ+ neurons mediate the influence of multiple anorexigenic signals. *Nature Neuroscience,* 17**,** 1240-1248.

Cai, J., Chen, J., Ortiz-Guzman, J., Huang, J., Arenkiel, B. R., Wang, Y., Zhang, Y., Shi, Y., Tong, Q. & Zhan, C. 2023. AgRP neurons are not indispensable for body weight maintenance in adult mice. *Cell Reports,* 42**,** 112789.

Calu, D. J., Roesch, M. R., Stalnaker, T. A. & Schoenbaum, G. 2007. Associative Encoding in Posterior Piriform Cortex during Odor Discrimination and Reversal Learning. *Cerebral Cortex,* 17**,** 1342-1349.

Cameron, J. D., Goldfield, G. S. & Doucet, É. 2012. Fasting for 24h improves nasal chemosensory performance and food palatability in a related manner. *Appetite,* 58**,** 978-981.

Carter, M. E., Han, S. & Palmiter, R. D. 2015. Parabrachial Calcitonin Gene-Related Peptide Neurons Mediate Conditioned Taste Aversion. *Journal of Neuroscience,* 35**,** 4582-4586.

Cassidy, R. M., Lu, Y., Jere, M., Tian, J.-B., Xu, Y., Mangieri, L. R., Felix-Okoroji, B., Selever, J., Xu, Y., Arenkiel, B. R. & Tong, Q. 2019. A lateral hypothalamus to basal forebrain neurocircuit promotes feeding by suppressing responses to anxiogenic environmental cues. *Science Advances,* 5**,** eaav1640.

Cecil, J. E., Francis, J. & Read, N. W. 1999. Comparison of the Effects of a High-Fat and High-Carbohydrate Soup Delivered Orally and Intragastrically on Gastric Emptying, Appetite, and Eating Behaviour. *Physiology & Behavior,* 67**,** 299-306.

Chapuis, J. & Wilson, D. A. 2012. Bidirectional plasticity of cortical pattern recognition and behavioral sensory acuity. *Nature Neuroscience,* 15**,** 155-161.

Chen, C.-F. F., Zou, D.-J., Altomare, C. G., Xu, L., Greer, C. A. & Firestein, S. J. 2014. Nonsensory target-dependent organization of piriform cortex. *Proceedings of the National Academy of Sciences,* 111**,** 16931-16936.

Chen, T.-W., Wardill, T. J., Sun, Y., Pulver, S. R., Renninger, S. L., Baohan, A., Schreiter, E. R., Kerr, R. A., Orger, M. B., Jayaraman, V., Looger, L. L., Svoboda, K. & Kim, D. S. 2013. Ultrasensitive fluorescent proteins for imaging neuronal activity. *Nature,* 499**,** 295-300.

Chen, Y., Chen, X., Baserdem, B., Zhan, H., Li, Y., Davis, M. B., Kebschull, J. M., Zador, A. M., Koulakov, A. A. & Albeanu, D. F. 2022. High-throughput sequencing of single neuron projections reveals spatial organization in the olfactory cortex. *Cell,* 185**,** 4117-4134.e28.

Chen, Y. & Knight, Z. A. 2016. Making sense of the sensory regulation of hunger neurons. *BioEssays,* 38**,** 316-324.

Chen, Y., Lin, Y.-C., Kuo, T.-W. & Knight, Zachary a. 2015. Sensory Detection of Food Rapidly Modulates Arcuate Feeding Circuits. *Cell,* 160**,** 829-841.

Cho, J. H., Prince, J. E. A. & Cloutier, J.-F. 2009. Axon Guidance Events in the Wiring of the Mammalian Olfactory System. *Molecular Neurobiology,* 39**,** 1-9.

Chong, E., Moroni, M., Wilson, C., Shoham, S., Panzeri, S. & Rinberg, D. 2020. Manipulating synthetic optogenetic odors reveals the coding logic of olfactory perception. *Science,* 368**,** eaba2357.

Clark, S. A., Allard, T., Jenkins, W. M. & Merzenich, M. M. 1988. Receptive fields in the body-surface map in adult cortex defined by temporally correlated inputs. *Nature,* 332**,** 444-445.

Cohen, J. Y., Haesler, S., Vong, L., Lowell, B. B. & Uchida, N. 2012. Neuron-type-specific signals for reward and punishment in the ventral tegmental area. *Nature,* 482**,** 85-88.

Cone, R. D. 2005. Anatomy and regulation of the central melanocortin system. *Nature Neuroscience,* 8**,** 571-578.

Conway, M., Oncul, M., Allen, K. & Johnston, J. 2023. Perceptual constancy for an odour is acquired through changes in primary sensory neurons. bioRxiv.

Coutinho, E. A., Okamoto, S., Ishikawa, A. W., Yokota, S., Wada, N., Hirabayashi, T., Saito, K., Sato, T., Takagi, K., Wang, C.-C., Kobayashi, K., Ogawa, Y., Shioda, S., Yoshimura, Y. & Minokoshi, Y. 2017. Activation of SF1 Neurons in the Ventromedial Hypothalamus by DREADD Technology Increases Insulin Sensitivity in Peripheral Tissues. *Diabetes,* 66**,** 2372-2386.

Cowley, M. A., Smart, J. L., Rubinstein, M., Cerdán, M. G., Diano, S., Horvath, T. L., Cone, R. D. & Low, M. J. 2001. Leptin activates anorexigenic POMC neurons through a neural network in the arcuate nucleus. *Nature,* 411**,** 480-484.

Cox, J. & Witten, I. B. 2019. Striatal circuits for reward learning and decision-making. *Nature Reviews Neuroscience,* 20**,** 482-494.

Cui, G., Jun, S. B., Jin, X., Pham, M. D., Vogel, S. S., Lovinger, D. M. & Costa, R. M. 2013. Concurrent activation of striatal direct and indirect pathways during action initiation. *Nature,* 494**,** 238-242.

Cummings, D. M., Emge, D. K., Small, S. L. & Margolis, F. L. 2000. Pattern of olfactory bulb innervation returns after recovery from reversible peripheral deafferentation. *The Journal of Comparative Neurology,* 421**,** 362-373.

Dannenberg, H., Pabst, M., Braganza, O., Schoch, S., Niediek, J., Bayraktar, M., Mormann, F. & Beck, H. 2015. Synergy of Direct and Indirect Cholinergic Septo-Hippocampal Pathways Coordinates Firing in Hippocampal Networks. *Journal of Neuroscience,* 35**,** 8394-8410.

Davis, B. J. & Macrides, F. 1981. The organization of centrifugal projections from the anterior olfactory nucleus, ventral hippocampal rudiment, and piriform cortex to the main olfactory bulb in the hamster: An autoradiographic study. *Journal of Comparative Neurology,* 203**,** 475-493.

De Araujo, I. E., Schatzker, M. & Small, D. M. 2020. Rethinking Food Reward. *Annual Review of Psychology,* 71**,** 139-164.

De Git, K. C. G., Hazelhoff, E. M., Nota, M. H. C., Schele, E., Luijendijk, M. C. M., Dickson, S. L., Van Der Plasse, G. & Adan, R. a. H. 2021. Zona incerta neurons projecting to the ventral tegmental area promote action initiation towards feeding. *The Journal of Physiology,* 599**,** 709-724.

Diodato, A., Ruinart De Brimont, M., Yim, Y. S., Derian, N., Perrin, S., Pouch, J., Klatzmann, D., Garel, S., Choi, G. B. & Fleischmann, A. 2016. Molecular signatures of neural connectivity in the olfactory cortex. *Nature Communications,* 7**,** 12238.

Do, J. P., Xu, M., Lee, S.-H., Chang, W.-C., Zhang, S., Chung, S., Yung, T. J., Fan, J. L., Miyamichi, K., Luo, L. & Dan, Y. 2016. Cell type-specific long-range connections of basal forebrain circuit. *eLife,* 5**,** e13214.

Douglass, A. M., Kucukdereli, H., Ponserre, M., Markovic, M., Gründemann, J., Strobel, C., Alcala Morales, P. L., Conzelmann, K.-K., Lüthi, A. & Klein, R. 2017. Central amygdala circuits modulate food consumption through a positive-valence mechanism. *Nature Neuroscience,* 20**,** 1384-1394.

Driscoll, L. N., Duncker, L. & Harvey, C. D. 2022. Representational drift: Emerging theories for continual learning and experimental future directions. *Current Opinion in Neurobiology,* 76**,** 102609.

Driscoll, L. N., Pettit, N. L., Minderer, M., Chettih, S. N. & Harvey, C. D. 2017. Dynamic Reorganization of Neuronal Activity Patterns in Parietal Cortex. *Cell,* 170**,** 986-999.e16.

Edwin Thanarajah, S., Hoffstall, V., Rigoux, L., Hanssen, R., Brüning, J. C. & Tittgemeyer, M. 2019. The role of insulin sensitivity and intranasally applied insulin on olfactory perception. *Scientific Reports,* 9**,** 7222.

Egnor, S. R. & Seagraves, K. M. 2016. The contribution of ultrasonic vocalizations to mouse courtship. *Current Opinion in Neurobiology,* 38**,** 1-5.

Elmquist, J. K., Bjørbæk, C., Ahima, R. S., Flier, J. S. & Saper, C. B. 1998. Distributions of leptin receptor mRNA isoforms in the rat brain. *Journal of Comparative Neurology,* 395**,** 535-547.

Epstein, A. N. 1960. Reciprocal changes in feeding behavior produced by intrahypothalamic chemical injections. *The American Journal of Physiology,* 199**,** 969-974.

Fadool, D. A., Tucker, K., Perkins, R., Fasciani, G., Thompson, R. N., Parsons, A. D., Overton, J. M., Koni, P. A., Flavell, R. A. & Kaczmarek, L. K. 2004. Kv1.3 Channel Gene-Targeted Deletion Produces “Super-Smeller Mice” with Altered Glomeruli, Interacting Scaffolding Proteins, and Biophysics. *Neuron,* 41**,** 389-404.

Fang, L. Z. & Creed, M. C. 2024. Updating the striatal–pallidal wiring diagram. *Nature Neuroscience,* 27**,** 15-27.

Feng, J., Zhang, C., Lischinsky, J. E., Jing, M., Zhou, J., Wang, H., Zhang, Y., Dong, A., Wu, Z., Wu, H., Chen, W., Zhang, P., Zou, J., Hires, S. A., Zhu, J. J., Cui, G., Lin, D., Du, J. & Li, Y. 2019. A Genetically Encoded Fluorescent Sensor for Rapid and Specific In Vivo Detection of Norepinephrine. *Neuron,* 102**,** 745-761.e8.

Fenselau, H., Campbell, J. N., Verstegen, A. M. J., Madara, J. C., Xu, J., Shah, B. P., Resch, J. M., Yang, Z., Mandelblat-Cerf, Y., Livneh, Y. & Lowell, B. B. 2017. A rapidly acting glutamatergic ARC→PVH satiety circuit postsynaptically regulated by α-MSH. *Nature Neuroscience,* 20**,** 42-51.

Fernández-Aranda, F., Agüera, Z., Fernández-García, J. C., Garrido-Sanchez, L., Alcaide-Torres, J., Tinahones, F. J., Giner-Bartolomé, C., Baños, R. M., Botella, C., Cebolla, A., De La Torre, R., Fernández-Real, J. M., Ortega, F. J., Frühbeck, G., Gómez-Ambrosi, J., Granero, R., Islam, M. A., Jiménez-Murcia, S., Tárrega, S., Menchón, J. M., Fagundo, A. B., Sancho, C., Estivill, X., Treasure, J. & Casanueva, F. F. 2016. Smell–taste dysfunctions in extreme weight/eating conditions: analysis of hormonal and psychological interactions. *Endocrine,* 51**,** 256-267.

Fernandez-Garcia, J. C., Alcaide, J., Santiago-Fernandez, C., Roca-Rodriguez, M., Aguera, Z., Baños, R., Botella, C., Torre, R. D. L., Fernandez-Real, J. M., Fruhbeck, G., Gomez-Ambrosi, J., Jimenez-Murcia, S., Menchon, J. M., Casanueva, F. F., Fernandez-Aranda, F., Tinahones, F. J. & Garrido-Sanchez, L. 2017. An increase in visceral fat is associated with a decrease in the taste and olfactory capacity. *PLOS ONE,* 12**,** e0171204.

Fortis-Santiago, Y., Rodwin, B. A., Neseliler, S., Piette, C. E. & Katz, D. B. 2010. State dependence of olfactory perception as a function of taste cortical inactivation. *Nature Neuroscience,* 13**,** 158-159.

Freeman, W. J. 1960. Correlation of electrical activity of prepyriform cortex and behavior in cat. *Journal of Neurophysiology,* 23**,** 111-131.

Fuhrmann, F., Justus, D., Sosulina, L., Kaneko, H., Beutel, T., Friedrichs, D., Schoch, S., Schwarz, M. K., Fuhrmann, M. & Remy, S. 2015. Locomotion, Theta Oscillations, and the Speed-Correlated Firing of Hippocampal Neurons Are Controlled by a Medial Septal Glutamatergic Circuit. *Neuron,* 86**,** 1253-1264.

Galef, B. G. & Wigmore, S. W. 1983. Transfer of information concerning distant foods: A laboratory investigation of the 'information-centre' hypothesis. *Animal Behaviour,* 31**,** 748-758.

Garb, J. L. & Stunkard, A. J. 1974. Taste aversions in man. *The American Journal of Psychiatry,* 131**,** 1204-1207.

Garcia, J., Kimeldorf, D. J. & Koelling, R. A. 1955. Conditioned Aversion to Saccharin Resulting from Exposure to Gamma Radiation. *Science,* 122**,** 157-158.

Garcia, J. & Koelling, R. A. 1966. Relation of cue to consequence in avoidance learning. *Psychonomic Science,* 4**,** 123-124.

Garfield, A. S., Li, C., Madara, J. C., Shah, B. P., Webber, E., Steger, J. S., Campbell, J. N., Gavrilova, O., Lee, C. E., Olson, D. P., Elmquist, J. K., Tannous, B. A., Krashes, M. J. & Lowell, B. B. 2015. A neural basis for melanocortin-4 receptor–regulated appetite. *Nature Neuroscience,* 18**,** 863-871.

Garfield, A. S., Shah, B. P., Burgess, C. R., Li, M. M., Li, C., Steger, J. S., Madara, J. C., Campbell, J. N., Kroeger, D., Scammell, T. E., Tannous, B. A., Myers, M. G., Andermann, M. L., Krashes, M. J. & Lowell, B. B. 2016. Dynamic GABAergic afferent modulation of AgRP neurons. *Nature Neuroscience,* 19**,** 1628-1635.

Genné-Bacon, E. A., Trinko, J. R. & Dileone, R. J. 2016. Innate Fear-Induced Weight Regulation in the C57BL/6J Mouse. *Frontiers in Behavioral Neuroscience,* 10.

Ghosh, A., Torraville, S. E., Mukherjee, B., Walling, S. G., Martin, G. M., Harley, C. W. & Yuan, Q. 2019. An experimental model of Braak's pretangle proposal for the origin of Alzheimer's disease: the role of locus coeruleus in early symptom development. *Alzheimer's Research & Therapy,* 11**,** 59.

Gilbert, C. D. & Wiesel, T. N. 1992. Receptive field dynamics in adult primary visual cortex. *Nature,* 356**,** 150-152.

Giovannucci, A., Friedrich, J., Gunn, P., Kalfon, J., Brown, B. L., Koay, S. A., Taxidis, J., Najafi, F., Gauthier, J. L., Zhou, P., Khakh, B. S., Tank, D. W., Chklovskii, D. B. & Pnevmatikakis, E. A. 2019. CaImAn an open source tool for scalable calcium imaging data analysis. *eLife,* 8**,** e38173.

Godfrey, P. A., Malnic, B. & Buck, L. B. 2004. The mouse olfactory receptor gene family. *Proceedings of the National Academy of Sciences,* 101**,** 2156-2161.

Grove, J. C. R., Gray, L. A., La Santa Medina, N., Sivakumar, N., Ahn, J. S., Corpuz, T. V., Berke, J. D., Kreitzer, A. C. & Knight, Z. A. 2022. Dopamine subsystems that track internal states. *Nature,* 608**,** 374-380.

Gunaydin, L. A., Grosenick, L., Finkelstein, J. C., Kauvar, I. V., Fenno, L. E., Adhikari, A., Lammel, S., Mirzabekov, J. J., Airan, R. D., Zalocusky, K. A., Tye, K. M., Anikeeva, P., Malenka, R. C. & Deisseroth, K. 2014. Natural Neural Projection Dynamics Underlying Social Behavior. *Cell,* 157**,** 1535-1551.

Gupta, G., Azam, M. & Baquer, N. Z. 1992. Modulation of rat brain insulin receptor kinase activity in diabetes. *Neurochemistry International,* 20**,** 487-492.

Hafting, T., Fyhn, M., Molden, S., Moser, M.-B. & Moser, E. I. 2005. Microstructure of a spatial map in the entorhinal cortex. *Nature,* 436**,** 801-806.

Hagiwara, A., Pal, S. K., Sato, T. F., Wienisch, M. & Murthy, V. N. 2012. Optophysiological analysis of associational circuits in the olfactory cortex. *Frontiers in Neural Circuits,* 6.

Hall, K. D., Ayuketah, A., Brychta, R., Cai, H., Cassimatis, T., Chen, K. Y., Chung, S. T., Costa, E., Courville, A., Darcey, V., Fletcher, L. A., Forde, C. G., Gharib, A. M., Guo, J., Howard, R., Joseph, P. V., Mcgehee, S., Ouwerkerk, R., Raisinger, K., Rozga, I., Stagliano, M., Walter, M., Walter, P. J., Yang, S. & Zhou, M. 2019. Ultra-Processed Diets Cause Excess Calorie Intake and Weight Gain: An Inpatient Randomized Controlled Trial of Ad Libitum Food Intake. *Cell Metabolism,* 30**,** 67-77.e3.

Hallem, E. A., Ho, M. G. & Carlson, J. R. 2004. The Molecular Basis of Odor Coding in the Drosophila Antenna. *Cell,* 117**,** 965-979.

Han, P., Roitzsch, C., Horstmann, A., Pössel, M. & Hummel, T. 2021. Increased Brain Reward Responsivity to Food-Related Odors in Obesity. *Obesity,* 29**,** 1138-1145.

Han, W., Tellez, L. A., Perkins, M. H., Perez, I. O., Qu, T., Ferreira, J., Ferreira, T. L., Quinn, D., Liu, Z.-W., Gao, X.-B., Kaelberer, M. M., Bohórquez, D. V., Shammah-Lagnado, S. J., De Lartigue, G. & De Araujo, I. E. 2018. A Neural Circuit for Gut-Induced Reward. *Cell,* 175**,** 665-678.e23.

Han, W., Tellez, L. A., Rangel, M. J., Motta, S. C., Zhang, X., Perez, I. O., Canteras, N. S., Shammah-Lagnado, S. J., Van Den Pol, A. N. & De Araujo, I. E. 2017. Integrated Control of Predatory Hunting by the Central Nucleus of the Amygdala. *Cell,* 168**,** 311-324.e18.

Hannum, M. E., Ramirez, V. A., Lipson, S. J., Herriman, R. D., Toskala, A. K., Lin, C., Joseph, P. V. & Reed, D. R. 2020. Objective Sensory Testing Methods Reveal a Higher Prevalence of Olfactory Loss in COVID-19-Positive Patients Compared to Subjective Methods: A Systematic Review and Meta-Analysis. *Chem Senses,* 45**,** 865-874.

Hardaway, J. A., Halladay, L. R., Mazzone, C. M., Pati, D., Bloodgood, D. W., Kim, M., Jensen, J., Diberto, J. F., Boyt, K. M., Shiddapur, A., Erfani, A., Hon, O. J., Neira, S., Stanhope, C. M., Sugam, J. A., Saddoris, M. P., Tipton, G., Mcelligott, Z., Jhou,

T. C., Stuber, G. D., Bruchas, M. R., Bulik, C. M., Holmes, A. & Kash, T. L. 2019. Central Amygdala Prepronociceptin-Expressing Neurons Mediate Palatable Food Consumption and Reward. *Neuron,* 102**,** 1037-1052.e7.

Harris, C. R., Millman, K. J., Van Der Walt, S. J., Gommers, R., Virtanen, P., Cournapeau, D., Wieser, E., Taylor, J., Berg, S., Smith, N. J., Kern, R., Picus, M., Hoyer, S., Van Kerkwijk, M. H., Brett, M., Haldane, A., Del Río, J. F., Wiebe, M., Peterson, P., Gérard-Marchant, P., Sheppard, K., Reddy, T., Weckesser, W., Abbasi, H., Gohlke, C. & Oliphant, T. E. 2020. Array programming with NumPy. *Nature,* 585**,** 357-362.

Harrison, T. C., Pinto, L., Brock, J. R. & Dan, Y. 2016. Calcium Imaging of Basal Forebrain Activity during Innate and Learned Behaviors. *Frontiers in Neural Circuits,* 10.

Hasselmo, M. E., Linster, C., Patil, M., Ma, D. & Cekic, M. 1997. Noradrenergic Suppression of Synaptic Transmission May Influence Cortical Signal-to-Noise Ratio. *Journal of Neurophysiology,* 77**,** 3326-3339.

Herman, A. M., Ortiz-Guzman, J., Kochukov, M., Herman, I., Quast, K. B., Patel, J. M., Tepe, B., Carlson, J. C., Ung, K., Selever, J., Tong, Q. & Arenkiel, B. R. 2016. A cholinergic basal forebrain feeding circuit modulates appetite suppression. *Nature,* 538**,** 253-256.

Hill, J. M., Lesniak, M. A., Pert, C. B. & Roth, J. 1986. Autoradiographic localization of insulin receptors in rat brain: prominence in olfactory and limbic areas. *Neuroscience,* 17**,** 1127-1138.

Ho, J., Tumkaya, T., Aryal, S., Choi, H. & Claridge-Chang, A. 2019. Moving beyond P values: data analysis with estimation graphics. *Nature Methods,* 16**,** 565-566.

Holman, E. W. 1975. Immediate and delayed reinforcers for flavor preferences in rats. *Learning and Motivation,* 6**,** 91-100.

Horio, N. & Liberles, S. D. 2021. Hunger enhances food-odour attraction through a neuropeptide Y spotlight. *Nature,* 592**,** 262-266.

Howard, J. D., Plailly, J., Grueschow, M., Haynes, J.-D. & Gottfried, J. A. 2009. Odor quality coding and categorization in human posterior piriform cortex. *Nature Neuroscience,* 12**,** 932-938.

Hubel, D. H. & Wiesel, T. N. 1962. Receptive fields, binocular interaction and functional architecture in the cat's visual cortex. *The Journal of Physiology,* 160**,** 106-154.

Hunter, J. D. 2007. Matplotlib: A 2D Graphics Environment. *Computing in Science & Engineering,* 9**,** 90-95.

Hurst, Y. & Fukuda, H. 2018. Effects of changes in eating speed on obesity in patients with diabetes: a secondary analysis of longitudinal health check-up data. *BMJ Open,* 8**,** e019589.

Ichihara, Y. G., Okabe, M., Iga, K., Tanaka, Y., Musha, K. & Ito, K. Color universal design: the selection of four easily distinguishable colors for all color vision types. *In:*

ESCHBACH, R., MARCU, G. G. & TOMINAGA, S., eds. Electronic Imaging 2008, 2008/01/27/ 2008. San Jose, CA, 68070O.

Illig, K. R. & Haberly, L. B. 2003. Odor-evoked activity is spatially distributed in piriform cortex. *Journal of Comparative Neurology,* 457**,** 361-373.

Iravani, B., Frasnelli, J., Arshamian, A. & Lundstrom, J. N. 2024. Metabolic state modulates neural processing of odors in the human olfactory bulb. *Biol Psychol***,** 108770.

Jennings, J. H., Kim, C. K., Marshel, J. H., Raffiee, M., Ye, L., Quirin, S., Pak, S., Ramakrishnan, C. & Deisseroth, K. 2019. Interacting neural ensembles in orbitofrontal cortex for social and feeding behaviour. *Nature,* 565**,** 645-649.

Jennings, J. H., Ung, R. L., Resendez, S. L., Stamatakis, A. M., Taylor, J. G., Huang, J., Veleta, K., Kantak, P. A., Aita, M., Shilling-Scrivo, K., Ramakrishnan, C., Deisseroth, K., Otte, S. & Stuber, G. D. 2015. Visualizing Hypothalamic Network Dynamics for Appetitive and Consummatory Behaviors. *Cell,* 160**,** 516-527.

Jovanovic, P. & Riera, C. E. 2022. Olfactory system and energy metabolism: a two-way street. *Trends in Endocrinology & Metabolism,* 33**,** 281-291.

Julliard, A. K., Chaput, M. A., Apelbaum, A., Aimé, P., Mahfouz, M. & Duchamp-Viret, P. 2007. Changes in rat olfactory detection performance induced by orexin and leptin mimicking fasting and satiation. *Behavioural Brain Research,* 183**,** 123-129.

Junek, S., Kludt, E., Wolf, F. & Schild, D. 2010. Olfactory Coding with Patterns of Response Latencies. *Neuron,* 67**,** 872-884.

Kandel, E. R. 2013. *Principles of neural science,* New York, McGraw-Hill New York.

Karalis, N. & Sirota, A. 2022. Breathing coordinates cortico-hippocampal dynamics in mice during offline states. *Nature Communications,* 13**,** 467.

Kato, H. K., Gillet, S. N. & Isaacson, J. S. 2015. Flexible Sensory Representations in Auditory Cortex Driven by Behavioral Relevance. *Neuron,* 88**,** 1027-1039.

Kay, L. M. & Sherman, S. M. 2007. An argument for an olfactory thalamus. *Trends Neurosci,* 30**,** 47-53.

Kentros, C. G., Agnihotri, N. T., Streater, S., Hawkins, R. D. & Kandel, E. R. 2004. Increased Attention to Spatial Context Increases Both Place Field Stability and Spatial Memory. *Neuron,* 42**,** 283-295.

Kim, J., Zhang, X., Muralidhar, S., Leblanc, S. A. & Tonegawa, S. 2017. Basolateral to Central Amygdala Neural Circuits for Appetitive Behaviors. *Neuron,* 93**,** 1464-1479.e5.

Koch, M., Varela, L., Kim, J. G., Kim, J. D., Hernández-Nuño, F., Simonds, S. E., Castorena, C. M., Vianna, C. R., Elmquist, J. K., Morozov, Y. M., Rakic, P., Bechmann, I., Cowley, M. A., Szigeti-Buck, K., Dietrich, M. O., Gao, X.-B., Diano,

S. & Horvath, T. L. 2015. Hypothalamic POMC neurons promote cannabinoid-induced feeding. *Nature,* 519**,** 45-50.

Kogan, J. H., Frankland, P. W., Blendy, J. A., Coblentz, J., Marowitz, Z., Schütz, G. & Silva, A. J. 1997. Spaced training induces normal long-term memory in CREB mutant mice. *Current Biology,* 7**,** 1-11.

Krashes, M. J., Koda, S., Ye, C., Rogan, S. C., Adams, A. C., Cusher, D. S., Maratos-Flier, E., Roth, B. L. & Lowell, B. B. 2011. Rapid, reversible activation of AgRP neurons drives feeding behavior in mice. *The Journal of Clinical Investigation,* 121**,** 1424-1428.

Krashes, M. J., Shah, B. P., Koda, S. & Lowell, B. B. 2013. Rapid versus Delayed Stimulation of Feeding by the Endogenously Released AgRP Neuron Mediators GABA, NPY, and AgRP. *Cell Metabolism,* 18**,** 588-595.

Krude, H., Biebermann, H., Luck, W., Horn, R., Brabant, G. & Grüters, A. 1998. Severe early-onset obesity, adrenal insufficiency and red hair pigmentation caused by POMC mutations in humans. *Nature Genetics,* 19**,** 155-157.

Kuang, D., Hanchate, N. K., Lee, C.-Y., Heck, A., Ye, X., Erdenebileg, M. & Buck, L. B. 2023. Olfactory and neuropeptide inputs to appetite neurons in the arcuate nucleus. bioRxiv.

Kumar, A., Barkai, E. & Schiller, J. 2021. Plasticity of olfactory bulb inputs mediated by dendritic NMDA-spikes in rodent piriform cortex. *eLife,* 10**,** e70383.

Kumar, A., Schiff, O., Barkai, E., Mel, B. W., Poleg-Polsky, A. & Schiller, J. 2018. NMDA spikes mediate amplification of inputs in the rat piriform cortex. *eLife,* 7**,** e38446.

Kurahashi, T. & Menini, A. 1997. Mechanism of odorant adaptation in the olfactory receptor cell. *Nature,* 385**,** 725-729.

Lange, R. D., Shivkumar, S., Chattoraj, A. & Haefner, R. M. 2023. Bayesian encoding and decoding as distinct perspectives on neural coding. *Nature Neuroscience,* 26**,** 2063-2072.

Large, A. M., Kunz, N. A., Mielo, S. L. & Oswald, A.-M. M. 2016a. Inhibition by Somatostatin Interneurons in Olfactory Cortex. *Frontiers in Neural Circuits,* 10.

Large, A. M., Vogler, N. W., Canto-Bustos, M., Friason, F. K., Schick, P. & Oswald, A.-M. M. 2018. Differential inhibition of pyramidal cells and inhibitory interneurons along the rostrocaudal axis of anterior piriform cortex. *Proceedings of the National Academy of Sciences,* 115**,** E8067-E8076.

Large, A. M., Vogler, N. W., Mielo, S. & Oswald, A.-M. M. 2016b. Balanced feedforward inhibition and dominant recurrent inhibition in olfactory cortex. *Proc. Natl. Acad. Sci. U. S. A.,* 113**,** 2276-2281.

Larkin, R. P. 1975. Effect of ventromedial hypothalamic procaine injections on feeding, lever pressing, and other behavior in rats. *Journal of Comparative and Physiological Psychology,* 89**,** 1100-1108.

Lechien, J. R., Chiesa-Estomba, C. M., De Siati, D. R., Horoi, M., Le Bon, S. D., Rodriguez, A., Dequanter, D., Blecic, S., El Afia, F., Distinguin, L., Chekkoury-Idrissi, Y., Hans, S., Delgado, I. L., Calvo-Henriquez, C., Lavigne, P., Falanga, C., Barillari, M. R., Cammaroto, G., Khalife, M., Leich, P., Souchay, C., Rossi, C., Journe, F., Hsieh, J., Edjlali, M., Carlier, R., Ris, L., Lovato, A., De Filippis, C., Coppee, F., Fakhry, N., Ayad, T. & Saussez, S. 2020. Olfactory and gustatory dysfunctions as a clinical presentation of mild-to-moderate forms of the coronavirus disease (COVID-19): a multicenter European study. *Eur Arch Otorhinolaryngol,* 277**,** 2251-2261.

Lee, B. K., Mayhew, E. J., Sanchez-Lengeling, B., Wei, J. N., Qian, W. W., Little, K. A., Andres, M., Nguyen, B. B., Moloy, T., Yasonik, J., Parker, J. K., Gerkin, R. C., Mainland, J. D. & Wiltschko, A. B. 2023. A principal odor map unifies diverse tasks in olfactory perception.

Lee, E. J., Hanchate, N. K., Kondoh, K., Tong, A. P. S., Kuang, D., Spray, A., Ye, X. & Buck, L. B. 2020a. A psychological stressor conveyed by appetite-linked neurons. *Science Advances,* 6**,** eaay5366.

Lee, E. J., Saraiva, L. R., Hanchate, N. K., Ye, X., Asher, G., Ho, J. & Buck, L. B. 2022. Odor blocking of stress hormone responses. *Scientific Reports,* 12**,** 8773.

Lee, J. S., Briguglio, J. J., Cohen, J. D., Romani, S. & Lee, A. K. 2020b. The Statistical Structure of the Hippocampal Code for Space as a Function of Time, Context, and Value. *Cell,* 183**,** 620-635.e22.

Legland, D., Arganda-Carreras, I. & Andrey, P. 2016. MorphoLibJ: integrated library and plugins for mathematical morphology with ImageJ. *Bioinformatics,* 32**,** 3532-3534.

Li, W., Howard, J. D., Parrish, T. B. & Gottfried, J. A. 2008. Aversive Learning Enhances Perceptual and Cortical Discrimination of Indiscriminable Odor Cues. *Science,* 319**,** 1842-1845.

Li, Y., Zhong, W., Wang, D., Feng, Q., Liu, Z., Zhou, J., Jia, C., Hu, F., Zeng, J., Guo, Q., Fu, L. & Luo, M. 2016. Serotonin neurons in the dorsal raphe nucleus encode reward signals. *Nature Communications,* 7**,** 10503.

Lin, D., Boyle, M. P., Dollar, P., Lee, H., Lein, E. S., Perona, P. & Anderson, D. J. 2011. Functional identification of an aggression locus in the mouse hypothalamus. *Nature,* 470**,** 221-226.

Liu, C., Cai, X., Ritzau-Jost, A., Kramer, P. F., Li, Y., Khaliq, Z. M., Hallermann, S. & Kaeser, P. S. 2022. An action potential initiation mechanism in distal axons for the control of dopamine release. *Science,* 375**,** 1378-1385.

Liu, C. M. & Kanoski, S. E. 2018. Homeostatic and non-homeostatic controls of feeding behavior: Distinct vs. common neural systems. *Physiology & Behavior,* 193**,** 223-231.

Lo, H., Tantirigama, M. L. S., Schoenherr, A., Moreno-Velasquez, L., Faiss, L., Rost, B. R., Larkum, M. E., Judkewitz, B., Stumpenhorst, K., Rivalan, M., Winter, Y.,

Schmitz, D. & Johenning, F. W. 2023. Binge Feeding Promotes Appetite via Modulating Olfactory Flavor Representation. bioRxiv.

Loos, R. J. F. & Yeo, G. S. H. 2022. The genetics of obesity: from discovery to biology. *Nature Reviews Genetics,* 23**,** 120-133.

Lopes, G. A., Bonacchi, N., Frazã£O, J. O., Neto, J. P., Atallah, B. V., Soares, S., Moreira, L. S., Matias, S., Itskov, P. M., Correia, P. C. A., Medina, R. E., Calcaterra, L., Dreosti, E., Paton, J. J. & Kampff, A. R. 2015. Bonsai: an event-based framework for processing and controlling data streams. *Frontiers in Neuroinformatics,* 9.

Lottem, E., Lorincz, M. L. & Mainen, Z. F. 2016. Optogenetic Activation of Dorsal Raphe Serotonin Neurons Rapidly Inhibits Spontaneous But Not Odor-Evoked Activity in Olfactory Cortex. *Journal of Neuroscience,* 36**,** 7-18.

Loureiro, M., Achargui, R., Flakowski, J., Van Zessen, R., Stefanelli, T., Pascoli, V. & Lüscher, C. 2019. Social transmission of food safety depends on synaptic plasticity in the prefrontal cortex. *Science,* 364**,** 991-995.

Lowe, G. & Gold, G. H. 1993. Nonlinear amplification by calcium-dependent chloride channels in olfactory receptor cells. *Nature,* 366**,** 283-286.

Luquet, S., Perez, F. A., Hnasko, T. S. & Palmiter, R. D. 2005. NPY/AgRP Neurons Are Essential for Feeding in Adult Mice but Can Be Ablated in Neonates. *Science,* 310**,** 683-685.

Ly, T., Oh, J. Y., Sivakumar, N., Shehata, S., La Santa Medina, N., Huang, H., Liu, Z., Fang, W., Barnes, C., Dundar, N., Jarvie, B. C., Ravi, A., Barnhill, O. K., Li, C., Lee, G. R., Choi, J., Jang, H. & Knight, Z. A. 2023. Sequential appetite suppression by oral and visceral feedback to the brainstem. *Nature*.

Maes, H. 1980. Time course of feeding induced by pentobarbital-injections into the rat's VMH. *Physiology & Behavior,* 24**,** 1107-1114.

Mahn, M., Saraf-Sinik, I., Patil, P., Pulin, M., Bitton, E., Karalis, N., Bruentgens, F., Palgi, S., Gat, A., Dine, J., Wietek, J., Davidi, I., Levy, R., Litvin, A., Zhou, F., Sauter, K., Soba, P., Schmitz, D., Lüthi, A., Rost, B. R., Wiegert, J. S. & Yizhar, O. 2021. Efficient optogenetic silencing of neurotransmitter release with a mosquito rhodopsin. *Neuron,* 109**,** 1621-1635.e8.

Maier, Joost x., Blankenship, Meredith l., Li, Jennifer x. & Katz, Donald b. 2015. A Multisensory Network for Olfactory Processing. *Current Biology,* 25**,** 2642-2650.

Maier, J. X., Wachowiak, M. & Katz, D. B. 2012. Chemosensory Convergence on Primary Olfactory Cortex. *Journal of Neuroscience,* 32**,** 17037-17047.

Malnic, B., Hirono, J., Sato, T. & Buck, L. B. 1999. Combinatorial Receptor Codes for Odors. *Cell,* 96**,** 713-723.

Mandelblat-Cerf, Y., Ramesh, R. N., Burgess, C. R., Patella, P., Yang, Z., Lowell, B. B. & Andermann, M. L. 2015. Arcuate hypothalamic AgRP and putative POMC neurons show opposite changes in spiking across multiple timescales. *eLife,* 4**,** e07122.

Mankin, E. A., Sparks, F. T., Slayyeh, B., Sutherland, R. J., Leutgeb, S. & Leutgeb, J. K. 2012. Neuronal code for extended time in the hippocampus. *Proceedings of the National Academy of Sciences,* 109**,** 19462-19467.

Marek, G. J. & Aghajanian, G. K. 1994. Excitation of interneurons in piriform cortex by 5-hydroxytryptamine: Blockade by MDL 100,907, a highly selective 5-HT2A receptor antagonist. *European Journal of Pharmacology,* 259**,** 137-141.

Margolis, D. J., Lütcke, H., Schulz, K., Haiss, F., Weber, B., Kügler, S., Hasan, M. T. & Helmchen, F. 2012. Reorganization of cortical population activity imaged throughout long-term sensory deprivation. *Nature Neuroscience,* 15**,** 1539-1546.

Margrie, T. W. & Schaefer, A. T. 2003. Theta oscillation coupled spike latencies yield computational vigour in a mammalian sensory system. *The Journal of Physiology,* 546**,** 363-374.

Markopoulos, F., Rokni, D., Gire, D. H. & Murthy, V. N. 2012. Functional Properties of Cortical Feedback Projections to the Olfactory Bulb. *Neuron,* 76**,** 1175-1188.

Marks, T. D. & Goard, M. J. 2021. Stimulus-dependent representational drift in primary visual cortex. *Nature Communications,* 12**,** 5169.

Marvin, J. S., Shimoda, Y., Magloire, V., Leite, M., Kawashima, T., Jensen, T. P., Kolb, I., Knott, E. L., Novak, O., Podgorski, K., Leidenheimer, N. J., Rusakov, D. A., Ahrens, M. B., Kullmann, D. M. & Looger, L. L. 2019. A genetically encoded fluorescent sensor for in vivo imaging of GABA. *Nature Methods,* 16**,** 763-770.

Mathis, A., Mamidanna, P., Cury, K. M., Abe, T., Murthy, V. N., Mathis, M. W. & Bethge, M. 2018. DeepLabCut: markerless pose estimation of user-defined body parts with deep learning. *Nature Neuroscience,* 21**,** 1281-1289.

Mattes, R. 2005. Soup and satiety. *Physiol. Behav.,* 83**,** 739-747.

Mayrhofer, J. M., Haiss, F., Helmchen, F. & Weber, B. 2015. Sparse, reliable, and long-term stable representation of periodic whisker deflections in the mouse barrel cortex. *NeuroImage,* 115**,** 52-63.

Mcgann, J. P. 2017. Poor human olfaction is a 19th-century myth. *Science,* 356**,** eaam7263.

Mei, L., Yan, R., Yin, L., Sullivan, R. M. & Lin, D. 2023. Antagonistic circuits mediating infanticide and maternal care in female mice. *Nature*.

Mena, W., Baker, K., Rubin, A., Kohli, S., Yoo, Y., Ziv, Y., Razaei-Mazinani, C. & Fleischmann, A. 2023. Differential encoding of odor and place in mouse piriform and entorhinal cortex. bioRxiv.

Miura, K., Mainen, Z. F. & Uchida, N. 2012. Odor Representations in Olfactory Cortex: Distributed Rate Coding and Decorrelated Population Activity. *Neuron,* 74**,** 1087-1098.

Miyamichi, K., Amat, F., Moussavi, F., Wang, C., Wickersham, I., Wall, N. R., Taniguchi, H., Tasic, B., Huang, Z. J., He, Z., Callaway, E. M., Horowitz, M. A. & Luo, L. 2011. Cortical representations of olfactory input by trans-synaptic tracing. *Nature,* 472**,** 191-196.

Moberg, S. & Takahashi, N. 2022. Neocortical layer 5 subclasses: From cellular properties to roles in behavior. *Frontiers in Synaptic Neuroscience,* 14.

Mohammad, H., Senol, E., Graf, M., Lee, C.-Y., Li, Q., Liu, Q., Yeo, X. Y., Wang, M., Laskaratos, A., Xu, F., Luo, S. X., Jung, S., Augustine, G. J. & Fu, Y. 2021. A neural circuit for excessive feeding driven by environmental context in mice. *Nature Neuroscience,* 24**,** 1132-1141.

Mombaerts, P., Wang, F., Dulac, C., Chao, S. K., Nemes, A., Mendelsohn, M., Edmondson, J. & Axel, R. 1996. Visualizing an Olfactory Sensory Map. *Cell,* 87**,** 675-686.

Moreno-Velasquez, L., Lo, H., Lenzi, S., Kaehne, M., Breustedt, J., Schmitz, D., Rüdiger, S. & Johenning, F. W. 2020. Circuit-Specific Dendritic Development in the Piriform Cortex. *eneuro,* 7**,** ENEURO.0083-20.2020.

Moss, E. H., Tantry, E. K., Le, E., Brandel-Ankrapp, K. & Arenkiel, B. R. 2022. Odor and reward-evoked GABAergic neuronal activity in the basal forebrain influences olfactory-guided behavior in mice. Neuroscience.

Murata, K., Kinoshita, T., Fukazawa, Y., Kobayashi, K., Kobayashi, K., Miyamichi, K., Okuno, H., Bito, H., Sakurai, Y., Yamaguchi, M., Mori, K. & Manabe, H. 2019. GABAergic neurons in the olfactory cortex projecting to the lateral hypothalamus in mice. *Scientific Reports,* 9**,** 7132.

Murthy, V. N. 2011. Olfactory Maps in the Brain. *Annual Review of Neuroscience,* 34**,** 233-258.

Musall, S., Kaufman, M. T., Juavinett, A. L., Gluf, S. & Churchland, A. K. 2019. Single-trial neural dynamics are dominated by richly varied movements. *Nature Neuroscience,* 22**,** 1677-1686.

Niimura, Y. 2009. Evolutionary dynamics of olfactory receptor genes in chordates: interaction between environments and genomic contents. *Human Genomics,* 4**,** 107.

Nyema, N. T., Mcknight, A. D., Vargas-Elvira, A. G., Schneps, H. M., Gold, E. G., Myers, K. P. & Alhadeff, A. L. 2023. AgRP neuron activity promotes associations between sensory and nutritive signals to guide flavor preference. *Molecular Metabolism,* 78**,** 101833.

O'connor, Eoin c., Kremer, Y., Lefort, S., Harada, M., Pascoli, V., Rohner, C. & Lüscher, C. 2015. Accumbal D1R Neurons Projecting to Lateral Hypothalamus Authorize Feeding. *Neuron,* 88**,** 553-564.

O'keefe, J. M., Nadel, L. & O'keefe, J. 1978. *The hippocampus as a cognitive map,* Oxford, Clarendon Press.

Ohkuma, T., Hirakawa, Y., Nakamura, U., Kiyohara, Y., Kitazono, T. & Ninomiya, T. 2015. Association between eating rate and obesity: a systematic review and meta-analysis. *Int. J. Obes.,* 39**,** 1589-1596.

Omoluabi, T., Torraville, S. E., Maziar, A., Ghosh, A., Power, K. D., Reinhardt, C., Harley, C. W. & Yuan, Q. 2021. Novelty-like activation of locus coeruleus protects against deleterious human pretangle tau effects while stress-inducing activation worsens its effects. *Alzheimer's & Dementia: Translational Research & Clinical Interventions,* 7**,** e12231.

Pachitariu, M., Stringer, C., Schröder, S., Dipoppa, M., Rossi, L. F., Carandini, M. & Harris, K. D. 2016. Suite2p: beyond 10,000 neurons with standard two-photon microscopy.

Paquelet, G. E., Carrion, K., Lacefield, C. O., Zhou, P., Hen, R. & Miller, B. R. 2022. Single-cell activity and network properties of dorsal raphe nucleus serotonin neurons during emotionally salient behaviors. *Neuron,* 110**,** 2664-2679.e8.

Parma, V., Ohla, K., Veldhuizen, M. G., Niv, M. Y., Kelly, C. E., Bakke, A. J., Cooper, K. W., Bouysset, C., Pirastu, N., Dibattista, M., Kaur, R., Liuzza, M. T., Pepino, M. Y., Schopf, V., Pereda-Loth, V., Olsson, S. B., Gerkin, R. C., Rohlfs Dominguez, P., Albayay, J., Farruggia, M. C., Bhutani, S., Fjaeldstad, A. W., Kumar, R., Menini, A., Bensafi, M., Sandell, M., Konstantinidis, I., Di Pizio, A., Genovese, F., Ozturk, L., Thomas-Danguin, T., Frasnelli, J., Boesveldt, S., Saatci, O., Saraiva, L. R., Lin, C., Golebiowski, J., Hwang, L. D., Ozdener, M. H., Guardia, M. D., Laudamiel, C., Ritchie, M., Havlicek, J., Pierron, D., Roura, E., Navarro, M., Nolden, A. A., Lim, J., Whitcroft, K. L., Colquitt, L. R., Ferdenzi, C., Brindha, E. V., Altundag, A., Macchi, A., Nunez-Parra, A., Patel, Z. M., Fiorucci, S., Philpott, C. M., Smith, B. C., Lundstrom, J. N., Mucignat, C., Parker, J. K., Van Den Brink, M., Schmuker, M., Fischmeister, F. P. S., Heinbockel, T., Shields, V. D. C., Faraji, F., Santamaria, E., Fredborg, W. E. A., Morini, G., Olofsson, J. K., Jalessi, M., Karni, N., D'errico, A., Alizadeh, R., Pellegrino, R., Meyer, P., Huart, C., Chen, B., Soler, G. M., Alwashahi, M. K., Welge-Lussen, A., Freiherr, J., De Groot, J. H. B., Klein, H., Okamoto, M., Singh, P. B., Hsieh, J. W., Author, G. G., Reed, D. R., Hummel, T., Munger, S. D. & Hayes, J. E. 2020. More Than Smell-COVID-19 Is Associated With Severe Impairment of Smell, Taste, and Chemesthesis. *Chem Senses,* 45**,** 609-622.

Pashkovski, S. L., Iurilli, G., Brann, D., Chicharro, D., Drummey, K., Franks, K. M., Panzeri, S. & Datta, S. R. 2020. Structure and flexibility in cortical representations of odour space. *Nature,* 583**,** 253-258.

Patriarchi, T., Cho, J. R., Merten, K., Howe, M. W., Marley, A., Xiong, W.-H., Folk, R. W., Broussard, G. J., Liang, R., Jang, M. J., Zhong, H., Dombeck, D., Zastrow, M. V., Nimmerjahn, A., Gradinaru, V., Williams, J. T. & Tian, L. 2018. Ultrafast neuronal imaging of dopamine dynamics with designed genetically encoded sensors. *Science,* 360.

Paxinos, G. & Keith B. J. Franklin, M. A. 2007. *The Mouse Brain in Stereotaxic Coordinates*, Elsevier Science.

Pedregosa, F., Varoquaux, G., Gramfort, A., Michel, V., Thirion, B., Grisel, O., Blondel, M., Prettenhofer, P., Weiss, R., Dubourg, V., Vanderplas, J., Passos, A. &

Cournapeau, D. Scikit-learn: Machine Learning in Python. *MACHINE LEARNING IN PYTHON*.

Peng, M., Coutts, D., Wang, T. & Cakmak, Y. O. 2019. Systematic review of olfactory shifts related to obesity. *Obesity Reviews,* 20**,** 325-338.

Peters, C., He, S., Fermani, F., Lim, H., Ding, W., Mayer, C. & Klein, R. 2023. Transcriptomics reveals amygdala neuron regulation by fasting and ghrelin thereby promoting feeding. *SCIENCE ADVANCES*.

Piszár, I. & Lőrincz, M. L. 2022. Differential Serotonergic Modulation of Principal Neurons and Interneurons in the Anterior Piriform Cortex. *Frontiers in Neuroanatomy,* 16**,** 821695.

Poessel, M., Breuer, N., Joshi, A., Pampel, A., Villringer, A., Hummel, T. & Horstmann, A. 2020a. Reduced Olfactory Bulb Volume in Obesity and Its Relation to Metabolic Health Status. *Frontiers in Human Neuroscience,* 14.

Poessel, M., Freiherr, J., Wiencke, K., Villringer, A. & Horstmann, A. 2020b. Insulin Resistance Is Associated with Reduced Food Odor Sensitivity across a Wide Range of Body Weights. *Nutrients,* 12**,** 2201.

Poo, C., Agarwal, G., Bonacchi, N. & Mainen, Z. F. 2021. Spatial maps in piriform cortex during olfactory navigation. *Nature*.

Poo, C. & Isaacson, J. S. 2009. Odor Representations in Olfactory Cortex: “Sparse” Coding, Global Inhibition, and Oscillations. *Neuron,* 62**,** 850-861.

Poo, C. & Isaacson, Jeffry s. 2011. A Major Role for Intracortical Circuits in the Strength and Tuning of Odor-Evoked Excitation in Olfactory Cortex. *Neuron,* 72**,** 41-48.

Pronier, É., Morici, J. F. & Girardeau, G. 2023. The role of the hippocampus in the consolidation of emotional memories during sleep. *Trends in Neurosciences,* 46**,** 912-925.

Prud'homme, M. J., Lacroix, M. C., Badonnel, K., Gougis, S., Baly, C., Salesse, R. & Caillol, M. 2009. Nutritional status modulates behavioural and olfactory bulb Fos responses to isoamyl acetate or food odour in rats: roles of orexins and leptin. *Neuroscience,* 162**,** 1287-1298.

Ragan, T., Kadiri, L. R., Venkataraju, K. U., Bahlmann, K., Sutin, J., Taranda, J., Arganda-Carreras, I., Kim, Y., Seung, H. S. & Osten, P. 2012. Serial two-photon tomography for automated ex vivo mouse brain imaging. *Nat. Methods,* 9**,** 255-258.

Reisert, J. & Matthews, H. R. 1999. Adaptation of the odour-induced response in frog olfactory receptor cells. *The Journal of Physiology,* 519**,** 801-813.

Ren, J., Friedmann, D., Xiong, J., Liu, C. D., Ferguson, B. R., Weerakkody, T., Deloach, K. E., Ran, C., Pun, A., Sun, Y., Weissbourd, B., Neve, R. L., Huguenard, J., Horowitz, M. A. & Luo, L. 2018. Anatomically Defined and Functionally Distinct Dorsal Raphe Serotonin Sub-systems. *Cell,* 175**,** 472-487.e20.

Rennaker, R. L., Chen, C.-F. F., Ruyle, A. M., Sloan, A. M. & Wilson, D. A. 2007. Spatial and Temporal Distribution of Odorant-Evoked Activity in the Piriform Cortex. *Journal of Neuroscience,* 27**,** 1534-1542.

Revusky, S. H. & Bedarf, E. W. 1967. Association of Illness with Prior Ingestion of Novel Foods. *Science,* 155**,** 219-220.

Richardson, B. E., Vander Woude, E. A., Sudan, R., Thompson, J. S. & Leopold, D. A. 2004. Altered Olfactory Acuity in the Morbidly Obese. *Obesity Surgery,* 14**,** 967-969.

Richman, E. B., Ticea, N., Allen, W. E., Deisseroth, K. & Luo, L. 2023. Neural landscape diffusion resolves conflicts between needs across time. *Nature,* 623**,** 571-579.

Riera, C. E., Tsaousidou, E., Halloran, J., Follett, P., Hahn, O., Pereira, M. M. A., Ruud, L. E., Alber, J., Tharp, K., Anderson, C. M., Brönneke, H., Hampel, B., Filho, C. D. D. M., Stahl, A., Brüning, J. C. & Dillin, A. 2017. The Sense of Smell Impacts Metabolic Health and Obesity. *Cell Metabolism,* 26**,** 198-211.e5.

Robinson, S. W. & Caron, M. G. 1997. Selective Inhibition of Adenylyl Cyclase Type V by the Dopamine D3 Receptor. *Molecular Pharmacology,* 52**,** 508-514.

Roesch, M. R., Stalnaker, T. A. & Schoenbaum, G. 2007. Associative Encoding in Anterior Piriform Cortex versus Orbitofrontal Cortex during Odor Discrimination and Reversal Learning. *Cerebral Cortex,* 17**,** 643-652.

Rokni, U., Richardson, A. G., Bizzi, E. & Seung, H. S. 2007. Motor Learning with Unstable Neural Representations. *Neuron,* 54**,** 653-666.

Roland, B., Deneux, T., Franks, K. M., Bathellier, B. & Fleischmann, A. 2017. Odor identity coding by distributed ensembles of neurons in the mouse olfactory cortex. *eLife,* 6**,** e26337.

Roman-Ortiz, C., Guevara, J. A. & Clem, R. L. 2021. GABAergic basal forebrain projections to the periaqueductal gray promote food consumption, reward and predation. *Scientific Reports,* 11**,** 22638.

Rose, T., Jaepel, J., Hübener, M. & Bonhoeffer, T. 2016. Cell-specific restoration of stimulus preference after monocular deprivation in the visual cortex. *Science,* 352**,** 1319-1322.

Rosen, J. B., Asok, A. & Chakraborty, T. 2015. The smell of fear: innate threat of 2,5-dihydro-2,4,5-trimethylthiazoline, a single molecule component of a predator odor. *Frontiers in Neuroscience,* 9.

Rubin, A., Geva, N., Sheintuch, L. & Ziv, Y. 2015. Hippocampal ensemble dynamics timestamp events in long-term memory. *eLife,* 4**,** e12247.

Russo, C., Russo, A., Pellitteri, R. & Stanzani, S. 2018. Ghrelin-containing neurons in the olfactory bulb send collateralized projections into medial amygdaloid and arcuate hypothalamic nuclei: neuroanatomical study. *Experimental Brain Research,* 236**,** 2223-2229.

Sagar, V., Shanahan, L. K., Zelano, C. M., Gottfried, J. A. & Kahnt, T. 2023. High-precision mapping reveals the structure of odor coding in the human brain. *Nature Neuroscience,* 26**,** 1595-1602.

Saito, H., Chi, Q., Zhuang, H., Matsunami, H. & Mainland, J. D. 2009. Odor coding by a Mammalian receptor repertoire. *Sci Signal,* 2**,** ra9.

Samakidou, G. E., Koliaki, C. C., Liberopoulos, E. N. & Katsilambros, N. L. 2023. Non-Classical Aspects of Obesity Pathogenesis and Their Relative Clinical Importance for Obesity Treatment. *Healthcare,* 11**,** 1310.

Samuelsen, C. L. & Fontanini, A. 2017. Processing of Intraoral Olfactory and Gustatory Signals in the Gustatory Cortex of Awake Rats. *Journal of Neuroscience,* 37**,** 244-257.

Schindelin, J., Arganda-Carreras, I., Frise, E., Kaynig, V., Longair, M., Pietzsch, T., Preibisch, S., Rueden, C., Saalfeld, S., Schmid, B., Tinevez, J.-Y., White, D. J., Hartenstein, V., Eliceiri, K., Tomancak, P. & Cardona, A. 2012. Fiji: an open-source platform for biological-image analysis. *Nature Methods,* 9**,** 676-682.

Schneider, C. A., Rasband, W. S. & Eliceiri, K. W. 2012. NIH Image to ImageJ: 25 years of image analysis. *Nat Methods,* 9**,** 671-5.

Schoonover, C. E., Ohashi, S. N., Axel, R. & Fink, A. J. P. 2021. Representational drift in primary olfactory cortex. *Nature,* 594**,** 541-546.

Schultz, W. 2016. Dopamine reward prediction error coding. *Dialogues in Clinical Neuroscience,* 18**,** 23-32.

Schultz, W., Dayan, P. & Montague, P. R. 1997. A Neural Substrate of Prediction and Reward. *Science,* 275**,** 1593-1599.

Sciolino, N. R., Hsiang, M., Mazzone, C. M., Wilson, L. R., Plummer, N. W., Amin, J., Smith, K. G., Mcgee, C. A., Fry, S. A., Yang, C. X., Powell, J. M., Bruchas, M. R., Kravitz, A. V., Cushman, J. D., Krashes, M. J., Cui, G. & Jensen, P. 2022. Natural locus coeruleus dynamics during feeding. *Science Advances,* 8**,** eabn9134.

Scisco, J. L., Muth, E. R., Dong, Y. & Hoover, A. W. 2011. Slowing bite-rate reduces energy intake: an application of the bite counter device. *J. Am. Diet. Assoc.,* 111**,** 1231-1235.

Sclafani, A. 2001. Post-ingestive positive controls of ingestive behavior. *Appetite,* 36**,** 79-83.

Seabold, S. & Perktold, J. Statsmodels: Econometric and Statistical Modeling with Python. Python in Science Conference, 2010 2010. Austin, Texas, 92-96.

Seo, C., Guru, A., Jin, M., Ito, B., Sleezer, B. J., Ho, Y.-Y., Wang, E., Boada, C., Krupa, N. A., Kullakanda, D. S., Shen, C. X. & Warden, M. R. 2019. Intense threat switches dorsal raphe serotonin neurons to a paradoxical operational mode. *Science,* 363**,** 538-542.

Shakhawat, A. M. D., Harley, C. W. & Yuan, Q. 2014. Arc Visualization of Odor Objects Reveals Experience-Dependent Ensemble Sharpening, Separation, and Merging in Anterior Piriform Cortex in Adult Rat. *Journal of Neuroscience,* 34**,** 10206-10210.

Sheldon, P. W. & Aghajanian, G. K. 1991. Excitatory responses to serotonin (5-HT) in neurons of the rat piriform cortex: Evidence for mediation by 5-HT1C receptors in pyramidal cells and 5-HT2 receptors in interneurons. *Synapse,* 9**,** 208-218.

Shepherd, G. M. 2006. Smell images and the flavour system in the human brain. *Nature,* 444**,** 316-321.

Slyper, A. 2021. Oral Processing, Satiation and Obesity: Overview and Hypotheses. *Diabetes, Metabolic Syndrome and Obesity: Targets and Therapy,* Volume 14**,** 3399-3415.

Small, D. M. 2012. Flavor is in the brain. *Physiology & Behavior,* 107**,** 540-552.

Soria-Gómez, E., Bellocchio, L., Reguero, L., Lepousez, G., Martin, C., Bendahmane, M., Ruehle, S., Remmers, F., Desprez, T., Matias, I., Wiesner, T., Cannich, A., Nissant, A., Wadleigh, A., Pape, H.-C., Chiarlone, A. P., Quarta, C., Verrier, D., Vincent, P., Massa, F., Lutz, B., Guzmán, M., Gurden, H., Ferreira, G., Lledo, P.-M., Grandes, P. & Marsicano, G. 2014. The endocannabinoid system controls food intake via olfactory processes. *Nature Neuroscience,* 17**,** 407-415.

Sosulski, D. L., Bloom, M. L., Cutforth, T., Axel, R. & Datta, S. R. 2011. Distinct representations of olfactory information in different cortical centres. *Nature,* 472**,** 213-216.

Spors, H. & Grinvald, A. 2002. Spatio-Temporal Dynamics of Odor Representations in the Mammalian Olfactory Bulb. *Neuron,* 34**,** 301-315.

Stachniak, T. J., Ghosh, A. & Sternson, S. M. 2014. Chemogenetic Synaptic Silencing of Neural Circuits Localizes a Hypothalamus→Midbrain Pathway for Feeding Behavior. *Neuron,* 82**,** 797-808.

Stafford, L. D. & Whittle, A. 2015. Obese Individuals Have Higher Preference and Sensitivity to Odor of Chocolate. *Chemical Senses,* 40**,** 279-284.

Steinmetz, N. A., Buetfering, C., Lecoq, J., Lee, C. R., Peters, A. J., Jacobs, E. a. K., Coen, P., Ollerenshaw, D. R., Valley, M. T., De Vries, S. E. J., Garrett, M., Zhuang, J., Groblewski, P. A., Manavi, S., Miles, J., White, C., Lee, E., Griffin, F., Larkin, J. D., Roll, K., Cross, S., Nguyen, T. V., Larsen, R., Pendergraft, J., Daigle, T., Tasic, B., Thompson, C. L., Waters, J., Olsen, S., Margolis, D. J., Zeng, H., Hausser, M., Carandini, M. & Harris, K. D. 2017. Aberrant Cortical Activity in Multiple GCaMP6-Expressing Transgenic Mouse Lines. *eneuro,* 4**,** ENEURO.0207-17.2017.

Steinmetz, N. A., Zatka-Haas, P., Carandini, M. & Harris, K. D. 2019. Distributed coding of choice, action and engagement across the mouse brain. *Nature,* 576**,** 266-273.

Sternson, S. M. & Eiselt, A.-K. 2017. Three Pillars for the Neural Control of Appetite. *Annual Review of Physiology,* 79**,** 401-423.

Stettler, D. D. & Axel, R. 2009. Representations of Odor in the Piriform Cortex. *Neuron,* 63**,** 854-864.

Stiebler, I., Neulist, R., Fichtel, I. & Ehret, G. 1997. The auditory cortex of the house mouse: left-right differences, tonotopic organization and quantitative analysis of frequency representation. *Journal of Comparative Physiology A,* 181**,** 559-571.

Storace, D. A. & Cohen, L. B. 2021. The Mammalian Olfactory Bulb Contributes to the Adaptation of Odor Responses: A Second Perceptual Computation Carried Out by the Bulb. *eneuro,* 8**,** ENEURO.0322-21.2021.

Stratton, R. J. & Elia, M. 1999. The effects of enteral tube feeding and parenteral nutrition on appetite sensations and food intake in health and disease. *Clin. Nutr.,* 18**,** 63-70.

Stringer, C., Pachitariu, M., Steinmetz, N., Reddy, C. B., Carandini, M. & Harris, K. D. 2019. Spontaneous behaviors drive multidimensional, brainwide activity. *Science,* 364**,** eaav7893.

Stringer, C., Wang, T., Michaelos, M. & Pachitariu, M. 2021. Cellpose: a generalist algorithm for cellular segmentation. *Nature Methods,* 18**,** 100-106.

Strupp, B. J. & Levitsky, D. A. 1984. Social transmission of food preferences in adult hooded rats (Rattus norvegicus). *Journal of Comparative Psychology,* 98**,** 257-266.

Su, Z., Alhadeff, A. L. & Betley, J. N. 2017. Nutritive, Post-ingestive Signals Are the Primary Regulators of AgRP Neuron Activity. *Cell Reports,* 21**,** 2724-2736.

Sun, C., Tang, K., Wu, J., Xu, H., Zhang, W., Cao, T., Zhou, Y., Yu, T. & Li, A. 2019. Leptin modulates olfactory discrimination and neural activity in the olfactory bulb. *Acta Physiologica,* 227**,** e13319.

Suzuki, N. & Bekkers, J. M. 2010. Distinctive Classes of GABAergic Interneurons Provide Layer-Specific Phasic Inhibition in the Anterior Piriform Cortex. *Cerebral Cortex,* 20**,** 2971-2984.

Suzuki, N. & Bekkers, J. M. 2011. Two Layers of Synaptic Processing by Principal Neurons in Piriform Cortex. *Journal of Neuroscience,* 31**,** 2156-2166.

Suzuki, N. & Bekkers, J. M. 2012. Microcircuits Mediating Feedforward and Feedback Synaptic Inhibition in the Piriform Cortex. *Journal of Neuroscience,* 32**,** 919-931.

Suzuki, N., Tantirigama, M. L. S., Aung, K. P., Huang, H. H. Y. & Bekkers, J. M. 2022. Fast and slow feedforward inhibitory circuits for cortical odor processing. *eLife,* 11**,** e73406.

Takase, K., Tsuneoka, Y., Oda, S., Kuroda, M. & Funato, H. 2016. High-fat diet feeding alters olfactory-, social-, and reward-related behaviors of mice independent of obesity. *Obesity,* 24**,** 886-894.

Talluri, B. C., Kang, I., Lazere, A., Quinn, K. R., Kaliss, N., Yates, J. L., Butts, D. A. & Nienborg, H. 2023. Activity in primate visual cortex is minimally driven by spontaneous movements. *Nature Neuroscience,* 26**,** 1953-1959.

Tan, H.-E., Sisti, A. C., Jin, H., Vignovich, M., Villavicencio, M., Tsang, K. S., Goffer, Y. & Zuker, C. S. 2020. The gut–brain axis mediates sugar preference. *Nature,* 580**,** 511-516.

Tan, K., Knight, Z. A. & Friedman, J. M. 2014. Ablation of AgRP neurons impairs adaption to restricted feeding. *Molecular Metabolism,* 3**,** 694-704.

Tantirigama, M. L. S., Huang, H. H. Y. & Bekkers, J. M. 2017. Spontaneous activity in the piriform cortex extends the dynamic range of cortical odor coding. *Proc. Natl. Acad. Sci. U. S. A.,* 114**,** 2407-2412.

Team, R. C. 2022. *R: A Language and Environment for Statistical Computing,* Vienna, Austria, R Foundation for Statistical Computing.

Team, R. S. 2020. *RStudio: Integrated Development Environment for R,* Boston, MA, RStudio, PBC.

Teo, P. S., Van Dam, R. M. & Forde, C. G. 2020. Combined Impact of a Faster Self-Reported Eating Rate and Higher Dietary Energy Intake Rate on Energy Intake and Adiposity. *Nutrients,* 12**,** 3264.

Teo, P. S., Van Dam, R. M., Whitton, C., Tan, L. W. L. & Forde, C. G. 2021. Consumption of Foods With Higher Energy Intake Rates is Associated With Greater Energy Intake, Adiposity, and Cardiovascular Risk Factors in Adults. *The Journal of Nutrition,* 151**,** 370-378.

Thiebaud, N., Johnson, M. C., Butler, J. L., Bell, G. A., Ferguson, K. L., Fadool, A. R., Fadool, J. C., Gale, A. M., Gale, D. S. & Fadool, D. A. 2014. Hyperlipidemic Diet Causes Loss of Olfactory Sensory Neurons, Reduces Olfactory Discrimination, and Disrupts Odor-Reversal Learning. *Journal of Neuroscience,* 34**,** 6970-6984.

Tindell, A. J., Smith, K. S., Peciña, S., Berridge, K. C. & Aldridge, J. W. 2006. Ventral Pallidum Firing Codes Hedonic Reward: When a Bad Taste Turns Good. *Journal of Neurophysiology,* 96**,** 2399-2409.

Tong, J., Mannea, E., Aimé, P., Pfluger, P. T., Yi, C.-X., Castaneda, T. R., Davis, H. W., Ren, X., Pixley, S., Benoit, S., Julliard, K., Woods, S. C., Horvath, T. L., Sleeman, M. M., D'alessio, D., Obici, S., Frank, R. & Tschöp, M. H. 2011. Ghrelin Enhances Olfactory Sensitivity and Exploratory Sniffing in Rodents and Humans. *Journal of Neuroscience,* 31**,** 5841-5846.

Tsukahara, T., Brann, D. H., Pashkovski, S. L., Guitchounts, G., Bozza, T. & Datta, S. R. 2021. A transcriptional rheostat couples past activity to future sensory responses. *Cell,* 184**,** 6326-6343.e32.

Tsuneki, H., Sugiyama, M., Ito, T., Sato, K., Matsuda, H., Onishi, K., Yubune, K., Matsuoka, Y., Nagai, S., Yamagishi, T., Maeda, T., Honda, K., Okekawa, A., Watanabe, S., Yaku, K., Okuzaki, D., Otsubo, R., Nomoto, M., Inokuchi, K.,

Nakagawa, T., Wada, T., Yasui, T. & Sasaoka, T. 2022. Food odor perception promotes systemic lipid utilization. *Nature Metabolism,* 4**,** 1514-1531.

Tucker, K., Overton, J. M. & Fadool, D. A. 2012. Diet-Induced Obesity Resistance of Kv1.3−/− Mice is Olfactory Bulb Dependent: Olfactory bulb dependent obesity resistance. *Journal of Neuroendocrinology,* 24**,** 1087-1095.

Tyson, A. L., Rousseau, C. V., Niedworok, C. J., Keshavarzi, S., Tsitoura, C., Cossell, L., Strom, M. & Margrie, T. W. 2021. A deep learning algorithm for 3D cell detection in whole mouse brain image datasets. *PLOS Computational Biology,* 17**,** e1009074.

Tyson, A. L., Velez-Fort, M., Rousseau, C. V., Cossell, L., Tsitoura, C., Lenzi, S. C., Obenhaus, H. A., Claudi, F., Branco, T. & Margrie, T. W. 2022. Accurate determination of marker location within whole-brain microscopy images. *Sci Rep,* 12**,** 867.

Unger, E. K., Keller, J. P., Altermatt, M., Liang, R., Matsui, A., Dong, C., Hon, O. J., Yao, Z., Sun, J., Banala, S., Flanigan, M. E., Jaffe, D. A., Hartanto, S., Carlen, J., Mizuno, G. O., Borden, P. M., Shivange, A. V., Cameron, L. P., Sinning, S., Underhill, S. M., Olson, D. E., Amara, S. G., Temple Lang, D., Rudnick, G., Marvin, J. S., Lavis, L. D., Lester, H. A., Alvarez, V. A., Fisher, A. J., Prescher, J. A., Kash, T. L., Yarov-Yarovoy, V., Gradinaru, V., Looger, L. L. & Tian, L. 2020. Directed Evolution of a Selective and Sensitive Serotonin Sensor via Machine Learning. *Cell,* 183**,** 1986-2002.e26.

Uygun, B., Kiyici, S., Ozmen, S., Gul, Z., Sigirli, D. & Cavun, S. 2019. The Association Between Olfaction and Taste Functions with Serum Ghrelin and Leptin Levels in Obese Women. *Metabolic Syndrome and Related Disorders,* 17**,** 452-457.

Van Rossum, G. & De Boer, J. 1991. Interactively testing remote servers using the Python programming language. *CWI Quarterly,* 4**,** 283-304.

Vandecasteele, M., Varga, V., Berényi, A., Papp, E., Barthó, P., Venance, L., Freund, T. F. & Buzsáki, G. 2014. Optogenetic activation of septal cholinergic neurons suppresses sharp wave ripples and enhances theta oscillations in the hippocampus. *Proceedings of the National Academy of Sciences,* 111**,** 13535-13540.

Vardy, E., Robinson, J. E., Li, C., Olsen, R. H. J., Diberto, J. F., Giguere, P. M., Sassano, F. M., Huang, X.-P., Zhu, H., Urban, D. J., White, K. L., Rittiner, J. E., Crowley, N. A., Pleil, K. E., Mazzone, C. M., Mosier, P. D., Song, J., Kash, T. L., Malanga, C. J., Krashes, M. J. & Roth, B. L. 2015. A New DREADD Facilitates the Multiplexed Chemogenetic Interrogation of Behavior. *Neuron,* 86**,** 936-946.

Vestergaard, M., Carta, M., Güney, G. & Poulet, J. F. A. 2023. The cellular coding of temperature in the mammalian cortex. *Nature,* 614**,** 725-731.

Viejo, G., Levenstein, D., Carrasco, S. S., Mehrotra, D., Mahallati, S., Vite, G. R., Denny, H., Sjulson, L., Battaglia, F. P. & Peyrache, A. 2023. Pynapple, a toolbox for data analysis in neuroscience. *eLife,* 12.

Vincis, R. & Fontanini, A. 2016. Associative learning changes cross-modal representations in the gustatory cortex. *eLife,* 5**,** e16420.

Virtanen, P., Gommers, R., Oliphant, T. E., Haberland, M., Reddy, T., Cournapeau, D., Burovski, E., Peterson, P., Weckesser, W., Bright, J., Van Der Walt, S. J., Brett, M., Wilson, J., Millman, K. J., Mayorov, N., Nelson, A. R. J., Jones, E., Kern, R., Larson, E., Carey, C. J., Polat, I., Feng, Y., Moore, E. W., Vanderplas, J., Laxalde, D., Perktold, J., Cimrman, R., Henriksen, I., Quintero, E. A., Harris, C. R., Archibald, A. M., Ribeiro, A. H., Pedregosa, F., Van Mulbregt, P., Scipy, C., Vijaykumar, A., Bardelli, A. P., Rothberg, A., Hilboll, A., Kloeckner, A., Scopatz, A., Lee, A., Rokem, A., Woods, C. N., Fulton, C., Masson, C., Häggström, C., Fitzgerald, C., Nicholson, D. A., Hagen, D. R., Pasechnik, D. V., Olivetti, E., Martin, E., Wieser, E., Silva, F., Lenders, F., Wilhelm, F., Young, G., Price, G. A., Ingold, G.-L., Allen, G. E., Lee, G. R., Audren, H., Probst, I., Dietrich, J. P., Silterra, J., Webber, J. T., Slavič, J., Nothman, J., Buchner, J., Kulick, J., Schönberger, J. L., De Miranda Cardoso, J. V., Reimer, J., Harrington, J., Rodríguez, J. L. C., Nunez-Iglesias, J., Kuczynski, J., Tritz, K., Thoma, M., Newville, M., Kümmerer, M., Bolingbroke, M., Tartre, M., Pak, M., Smith, N. J., Nowaczyk, N., Shebanov, N., Pavlyk, O., Brodtkorb, P. A., Lee, P., Mcgibbon, R. T., Feldbauer, R., Lewis, S., Tygier, S., Sievert, S., Vigna, S., Peterson, S., More, S., Pudlik, T., et al. 2020. SciPy 1.0: fundamental algorithms for scientific computing in Python. *Nature Methods,* 17**,** 261-272.

Viskaitis, P., Irvine, E. E., Smith, M. A., Choudhury, A. I., Alvarez-Curto, E., Glegola, J. A., Hardy, D. G., Pedroni, S. M. A., Paiva Pessoa, M. R., Fernando, A. B. P., Katsouri, L., Sardini, A., Ungless, M. A., Milligan, G. & Withers, D. J. 2017. Modulation of SF1 Neuron Activity Coordinately Regulates Both Feeding Behavior and Associated Emotional States. *Cell Reports,* 21**,** 3559-3572.

Waisman, A., Norris, A. M., Elías Costa, M. & Kopinke, D. 2021. Automatic and unbiased segmentation and quantification of myofibers in skeletal muscle. *Scientific Reports,* 11**,** 11793.

Wang, D., Wang, X., Liu, P., Jing, S., Du, H., Zhang, L., Jia, F. & Li, A. 2020a. Serotonergic afferents from the dorsal raphe decrease the excitability of pyramidal neurons in the anterior piriform cortex. *Proceedings of the National Academy of Sciences,* 117**,** 3239-3247.

Wang, L., Zhang, Z., Chen, J., Manyande, A., Haddad, R., Liu, Q. & Xu, F. 2020b. Cell-Type-Specific Whole-Brain Direct Inputs to the Anterior and Posterior Piriform Cortex. *Frontiers in Neural Circuits,* 14**,** 4.

Wang, P. Y., Boboila, C., Chin, M., Higashi-Howard, A., Shamash, P., Wu, Z., Stein, N. P., Abbott, L. F. & Axel, R. 2020c. Transient and Persistent Representations of Odor Value in Prefrontal Cortex. *Neuron,* 108**,** 209-224.e6.

Waskom, M. 2021. seaborn: statistical data visualization. *Journal of Open Source Software,* 6**,** 3021.

Wee, R. W. S., Mishchanchuk, K., Alsubaie, R., Church, T. W., Gold, M. G. & Macaskill, A. F. 2023. Internal-state-dependent control of feeding behavior via hippocampal ghrelin signaling. *Neuron*.

Wei, Q., Krolewski, D. M., Moore, S., Kumar, V., Li, F., Martin, B., Tomer, R., Murphy, G. G., Deisseroth, K., Watson, S. J. & Akil, H. 2018. Uneven balance of power between hypothalamic peptidergic neurons in the control of feeding. *Proceedings of the National Academy of Sciences,* 115**,** E9489-E9498.

Weinberger, N. M., Javid, R. & Lepan, B. 1993. Long-term retention of learning-induced receptive-field plasticity in the auditory cortex. *Proceedings of the National Academy of Sciences,* 90**,** 2394-2398.

Wiegand, H. F., Beed, P., Bendels, M. H. K., Leibold, C., Schmitz, D. & Johenning, F. W. 2011. Complementary Sensory and Associative Microcircuitry in Primary Olfactory Cortex. *The Journal of Neuroscience,* 31**,** 12149-12158.

Williams, E. K., Chang, R. B., Strochlic, D. E., Umans, B. D., Lowell, B. B. & Liberles, S. D. 2016. Sensory Neurons that Detect Stretch and Nutrients in the Digestive System. *Cell,* 166**,** 209-221.

Williams, K. W., Margatho, L. O., Lee, C. E., Choi, M., Lee, S., Scott, M. M., Elias, C. F. & Elmquist, J. K. 2010. Segregation of Acute Leptin and Insulin Effects in Distinct Populations of Arcuate Proopiomelanocortin Neurons. *Journal of Neuroscience,* 30**,** 2472-2479.

Wilson, D. A. 1998. Habituation of Odor Responses in the Rat Anterior Piriform Cortex. *Journal of Neurophysiology,* 79**,** 1425-1440.

Wilson, D. A. & Sullivan, R. M. 2011. Cortical processing of odor objects. *Neuron,* 72**,** 506-519.

Wu, Q., Howell, M. P., Cowley, M. A. & Palmiter, R. D. 2008a. Starvation after AgRP neuron ablation is independent of melanocortin signaling. *Proceedings of the National Academy of Sciences,* 105**,** 2687-2692.

Wu, Q., Howell, M. P. & Palmiter, R. D. 2008b. Ablation of Neurons Expressing Agouti-Related Protein Activates Fos and Gliosis in Postsynaptic Target Regions. *Journal of Neuroscience,* 28**,** 9218-9226.

Wu, Y., Chen, C., Chen, M., Qian, K., Lv, X., Wang, H., Jiang, L., Yu, L., Zhuo, M. & Qiu, S. 2020. The anterior insular cortex unilaterally controls feeding in response to aversive visceral stimuli in mice. *Nature Communications,* 11**,** 640.

Xie, Z., Zhang, X., Zhao, M., Huo, L., Huang, M., Li, D., Zhang, S., Cheng, X., Gu, H., Zhang, C., Zhan, C., Wang, F., Shang, C. & Cao, P. 2022. The gut-to-brain axis for toxin-induced defensive responses. *Cell,* 185**,** 4298-4316.e21.

Xu, A. W., Kaelin, C. B., Morton, G. J., Ogimoto, K., Stanhope, K., Graham, J., Baskin, D. G., Havel, P., Schwartz, M. W. & Barsh, G. S. 2005. Effects of Hypothalamic Neurodegeneration on Energy Balance. *PLOS Biology,* 3**,** e415.

Yamamoto, T., Inui, T. & Tsuji, T. 2013. The odor of Osmanthus fragrans attenuates food intake. *Scientific Reports,* 3**,** 1-8.

Yamamoto, T., Yuyama, N., Kato, T. & Kawamura, Y. 1985. Gustatory responses of cortical neurons in rats. III. Neural and behavioral measures compared. *Journal of Neurophysiology,* 53**,** 1370-1386.

Yaswen, L., Diehl, N., Brennan, M. B. & Hochgeschwender, U. 1999. Obesity in the mouse model of pro-opiomelanocortin deficiency responds to peripheral melanocortin. *Nature Medicine,* 5**,** 1066-1070.

Ye, Q., Nunez, J. & Zhang, X. 2023. Zona incerta dopamine neurons encode motivational vigor in food seeking. *Sci Adv,* 9**,** eadi5326.

Yu, X.-D., Zhu, Y., Sun, Q.-X., Deng, F., Wan, J., Zheng, D., Gong, W., Xie, S.-Z., Shen, C.-J., Fu, J.-Y., Huang, H., Lai, H.-Y., Jin, J., Li, Y. & Li, X.-M. 2022. Distinct serotonergic pathways to the amygdala underlie separate behavioral features of anxiety. *Nature Neuroscience,* 25**,** 1651-1663.

Zeng, X., Cai, L., Ma, J., Ma, Y., Jing, J. & Chen, Y. 2018. Eating fast is positively associated with general and abdominal obesity among Chinese children: A national survey. *Scientific Reports,* 8**,** 14362.

Zhan, C. & Luo, M. 2010. Diverse Patterns of Odor Representation by Neurons in the Anterior Piriform Cortex of Awake Mice. *Journal of Neuroscience,* 30**,** 16662-16672.

Zhan, C., Zhou, J., Feng, Q., Zhang, J.-E., Lin, S., Bao, J., Wu, P. & Luo, M. 2013. Acute and Long-Term Suppression of Feeding Behavior by POMC Neurons in the Brainstem and Hypothalamus, Respectively. *Journal of Neuroscience,* 33**,** 3624-3632.

Zhang, C., Kaye, J. A., Cai, Z., Wang, Y., Prescott, S. L. & Liberles, S. D. 2021a. Area Postrema Cell Types that Mediate Nausea-Associated Behaviors. *Neuron,* 109**,** 461-472.e5.

Zhang, J., Chen, D., Sweeney, P. & Yang, Y. 2020. An excitatory ventromedial hypothalamus to paraventricular thalamus circuit that suppresses food intake. *Nature Communications,* 11**,** 6326.

Zhang, X. & Van Den Pol, A. N. 2017. Rapid binge-like eating and body weight gain driven by zona incerta GABA neuron activation. *Science,* 356**,** 853-859.

Zhang, Y.-F., Vargas Cifuentes, L., Wright, K. N., Bhattarai, J. P., Mohrhardt, J., Fleck, D., Janke, E., Jiang, C., Cranfill, S. L., Goldstein, N., Schreck, M., Moberly, A. H., Yu, Y., Arenkiel, B. R., Betley, J. N., Luo, W., Stegmaier, J., Wesson, D. W., Spehr, M., Fuccillo, M. V. & Ma, M. 2021b. Ventral striatal islands of Calleja neurons control grooming in mice. *Nature Neuroscience,* 24**,** 1699-1710.

Zhong, W., Li, Y., Feng, Q. & Luo, M. 2017. Learning and Stress Shape the Reward Response Patterns of Serotonin Neurons. *Journal of Neuroscience,* 37**,** 8863-8875.

Zhou, P., Resendez, S. L., Rodriguez-Romaguera, J., Jimenez, J. C., Neufeld, S. Q., Giovannucci, A., Friedrich, J., Pnevmatikakis, E. A., Stuber, G. D., Hen, R., Kheirbek, M. A., Sabatini, B. L., Kass, R. E. & Paninski, L. 2018. Efficient and

accurate extraction of in vivo calcium signals from microendoscopic video data. *eLife,* 7**,** e28728.

Zhu, C., Yao, Y., Xiong, Y., Cheng, M., Chen, J., Zhao, R., Liao, F., Shi, R. & Song, S. 2017. Somatostatin Neurons in the Basal Forebrain Promote High-Calorie Food Intake. *Cell Reports,* 20**,** 112-123.

Zimmerman, C. A., Pan-Vazquez, A., Wu, B., Keppler, E. F., Guthman, E. M., Fetcho, R. N., Bolkan, S. S., Mcmannon, B., Lee, J., Hoag, A. T., Lynch, L. A., Janarthanan, S. N., López Luna, J. F., Bondy, A. G., Falkner, A. L., Wang, S. S. H. & Witten, I. B. 2023. A neural mechanism for learning from delayed postingestive feedback. Neuroscience.

Ziv, Y., Burns, L. D., Cocker, E. D., Hamel, E. O., Ghosh, K. K., Kitch, L. J., Gamal, A. E. & Schnitzer, M. J. 2013. Long-term dynamics of CA1 hippocampal place codes. *Nature Neuroscience,* 16**,** 264-266.

Zoon, H. F. A., De Graaf, C. & Boesveldt, S. 2016. Food Odours Direct Specific Appetite. *Foods,* 5**,** 12.

Zutshi, I., Brandon, M. P., Fu, M. L., Donegan, M. L., Leutgeb, J. K. & Leutgeb, S. 2018. Hippocampal Neural Circuits Respond to Optogenetic Pacing of Theta Frequencies by Generating Accelerated Oscillation Frequencies. *Current Biology,* 28**,** 1179-1188.e3.

7. Statutory Declaration

“I, **Hung Lo**, by personally signing this document in lieu of an oath, hereby affirm that I prepared the submitted dissertation on the topic: **Odor representation in mouse olfactory cortex during food intake / Geruchsrepräsentation im olfaktorischen Cortex der Maus während der Nahrungsaufnahme**, independently and without the support of third parties, and that I used no other sources and aids than those stated.

All parts which are based on the publications or presentations of other authors, either in letter or in spirit, are specified as such in accordance with the citing guidelines. The sections on methodology (in particular regarding practical work, laboratory regulations, statistical processing) and results (in particular regarding figures, charts and tables) are exclusively my responsibility.

Furthermore, I declare that I have correctly marked all of the data, the analyses, and the conclusions generated from data obtained in collaboration with other persons, and that I have correctly marked my own contribution and the contributions of other persons (cf. declaration of contribution). I have correctly marked all texts or parts of texts that were generated in collaboration with other persons.

My contributions to any publications to this dissertation correspond to those stated in the below joint declaration made together with the supervisor. All publications created within the scope of the dissertation comply with the guidelines of the IME (International Committee of Medical Journal Editors; http://www.icmje.org) on authorship. In addition, I declare that I shall comply with the regulations of Charité – Universitätsmedizin Berlin on ensuring good scientific practice.

I declare that I have not yet submitted this dissertation in identical or similar form to another Faculty.

The significance of this statutory declaration and the consequences of a false statutory declaration under criminal law (Sections 156, 161 of the German Criminal Code) are known to me.”

Date Signature

8. Curriculum Vitae

My curriculum vitae does not appear in the electronic version of my paper for reasons of data protection.

My curriculum vitae does not appear in the electronic version of my paper for reasons of data protection.

9. Publication list

Related to this dissertation

(preprinted manuscript)

Lo, H., Tantirigama, M. L. S., Schoenherr, A., Moreno-Velasquez, L., Faiss, L., Rost, B. R., Larkum, M. E., Judkewitz, B., Stumpenhorst, K., Rivalan, M., Winter, Y., Schmitz, D., & Johenning, F. W. (2023). Binge Feeding Promotes Appetite via Modulating Olfactory Flavor Representation
bioRxiv preprint. https://doi.org/10.1101/2023.10.17.562714
(Currently under revision in *Neuron*)

Not related to this dissertation

Moreno-Velasquez, L., **Lo, H.**, Lenzi, S., Kaehne, M., Breustedt, J., Schmitz, D., Rüdiger, S., & Johenning, F. W. (2020). Circuit-Specific Dendritic Development in the Piriform Cortex.
Eneuro, 7(3), ENEURO.0083-20.2020. https://doi.org/10.1523/ENEURO.0083-20.2020

Jambor, H., Antonietti, A., Alicea, B., Audisio, T. L., Auer, S., Bhardwaj, V., Burgess, S. J., Ferling, I., Gazda, M. A., Hoeppner, L. H., Ilangovan, V., **Lo, H.**, Olson, M., Mohamed, S. Y., Sarabipour, S., Varma, A., Walavalkar, K., Wissink, E. M., & Weissgerber, T. L. (2021). Creating clear and informative image-based figures for scientific publications.
PLoS Biology, 19(3), e3001161. https://doi.org/10.1371/journal.pbio.3001161

Kent, B.A., Holman, C., Amoako, E., Antonietti, A., Azam, J.M., Ballhausen, H., Bediako, Y., Belasen, A.M., Carneiro, C.F.D., Chen, Y.-C., Compeer, E.B., Connor, C.A.C., Crüwell, S., Debat, H., Dorris, E., Ebrahimi, H., Erlich, J.C., Fernández-Chiappe, F., Fischer, F., Gazda, M.A., Glatz, T., Grabitz, P., Heise, V., Kent, D.G., **Lo, H.**, McDowell, G., Mehta, D., Neumann, W.-J., Neves, K., Patterson, M., Penfold, N.C., Piper, S.K., Puebla, I., Quashie, P.K., Quezada, C.P., Riley, J.L., Rohmann, J.L., Saladi, S., Schwessinger, B., Siegerink, B., Stehlik, P., Tzilivaki, A., Umbers, K.D.L., Varma, A., Walavalkar, K., de Winde,

C.M., Zaza, C., Weissgerber, T.L., (2022). Recommendations for empowering early career researchers to improve research culture and practice. PLoS Biology 20, e3001680. https://doi.org/10.1371/journal.pbio.3001680

Heise, V., Holman, C., **Lo, H.**, Lyras, E.M., Adkins, M.C., Aquino, M.R.J., Bougioukas, K.I., Bray, K.O., Gajos, M., Guo, X., Hartling, C., Huerta-Gutierrez, R., Jindrová, M., Kenney, J.P.M., Kępińska, A.P., Kneller, L., Lopez-Rodriguez, E., Mühlensiepen, F., Richards, A., Richards, G., Siebert, M., Smith, J.A., Smith, N., Stransky, N., Tarvainen, S., Valdes, D.S., Warrington, K.L., Wilpert, N.-M., Witkowska, D., Zaneva, M., Zanker, J., Weissgerber, T.L., (2023). Ten simple rules for implementing open and reproducible research practices after attending a training course. PLoS Computational Biology 19, e1010750. https://doi.org/10.1371/journal.pcbi.1010750

10. Acknowledgments

First and foremost, I extend my deepest gratitude to my supervisors, Friedrich Johenning and Dietmar Schmitz, for their invaluable mentorship throughout my Ph.D. journey. Without their unwavering support and guidance, this journey would not have been possible. I am particularly grateful to Friedrich for his close mentorship, patience, and constant availability to address even the most silly questions from me.

I extend my thanks to Matthew Larkum, David Owald, Rachel Lippert, and Benjamin Rost for serving on my Ph.D. thesis committee and providing invaluable feedback.

I wish to express my appreciation to every member of the Schmitz lab for their experimental, intellectual, and emotional support over the years, which has made the lab an enriching environment. Special thanks to Laura and Anne-Kathrin for their close mentorship, which helped me navigate through my early patch clamp challenges and mistakes. Thanks for patching support from Laura, Lukas, and Benni. Science and coffee chats with Daniel, Claire, Feli, Judith, Annie, Aarti, Alexandra T, Lukas, Verjinia, Katerina, Oliver, Andrea, Alexandra OF, Ze, Roberto, Marta, Rosie, and many others have been both enjoyable and enlightening. I am also grateful to the dedicated group, Aileen, and Amit, for their collaboration and insightful discussions. Furthermore, I extend my thanks to our technicians, especially Anke, Suse, Monika, and Anny, for their role in maintaining the lab's functionality.

I am indebted to my science friends around the lab, particularly Tim, Mostafa, and Naoya, for their unwavering support. I would like to thank members of AG Larkum, AG Winter, and AG Judkewitz for supporting my Ph.D. projects. I would like to further thank the Franks lab for sharing details on experimental protocols.

I am grateful to the Einstein Center for Neurosciences Berlin for supporting my Ph.D. Fellowship and providing me with the opportunity to be part of the awesome ECN OG cohort.

This Ph.D. journey would not have been possible without the support of my best friends in Berlin: Hsiang-Jung, Cindy, Irene, Rafa, Natalie, Sara, and Meng; my beach volleyball teammates Tim, Eduardo, Moritz, Rita, Oded, and many others; and my longstanding friends Yen-Chung, Shirley, Sih-Rong, Chi-Yu, Yi and many more. I am thankful for the friendships forged through Twitter and conferences, including Nicole, Ana, Elisa, Chloe, Robin, Laura, and Steve, as well as the camaraderie shared with my teaching friends Constance, Ahmed, and Karina, and my eLife and meta-research friends Tracey, Alberto, Verena, and Iulia.

To my family, who have supported my decisions and endured my absence over the years, I extend my deepest gratitude.

Lastly, I am immensely grateful to Chi for her unwavering support throughout the past 13+ years. Without her unconditional encouragement, none of this would have been possible.

I am happy to say, finally, it's Ph.Done! This journey has been fun.

Hung Lo 羅鴻

> "…Until one day, the boundary gives way. And, that dent you've made is called a Ph.D. Of course, the world looks different to you now. So, don't forget the bigger picture. Keep pushing." – Matt Might "The Illustrated Guide to a Ph.D."

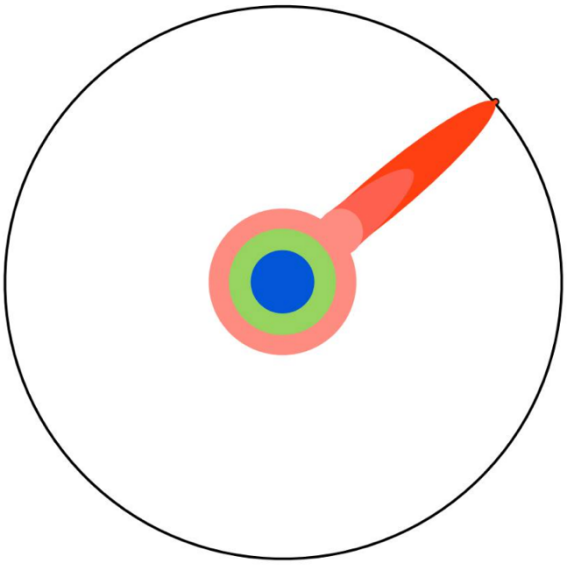

11. Certificate of The Accredited Statistician

CHARITÉ

CharitéCentrum für Human- und Gesundheitswissenschaften

Charité | Campus Charité Mitte | 10117 Berlin

Institut für Biometrie und klinische Epidemiologie (iBikE)

Direktor: Prof. Dr. Frank Konietschke

Postanschrift:
Charitéplatz 1 | 10117 Berlin
Besucheranschrift:
Reinhardtstr. 58 | 10117 Berlin

Tel. +49 (0)30 450 562171
frank.konietschke@charite.de
https://biometrie.charite.de/

Name, Vorname: Lo, Hung
Emailadresse: hung.lo@charite.de
Matrikelnummer: 225994
PromotionsbetreuerIn: PD Dr. Friedrich Johenning
Promotionsinstitution / Klinik: Neurowissenschaftliches Forschungszentrum (NWFZ), CCM

Bescheinigung

Hiermit bescheinige ich, dass Herr Hung Lo innerhalb der Service Unit Biometrie des Instituts für Biometrie und klinische Epidemiologie (iBikE) bei mir eine statistische Beratung zu einem Promotionsvorhaben wahrgenommen hat. Folgende Beratungstermine wurden wahrgenommen:

- 29.01.2023

Folgende wesentliche Ratschläge hinsichtlich einer sinnvollen Auswertung und Interpretation der Daten wurden während der Beratung erteilt:

- Lineare gemischte Modelle
- T-Test und Multiple Tests Korrektur
- Cohens D als Effektgröße

Diese Bescheinigung garantiert nicht die richtige Umsetzung der in der Beratung gemachten Vorschläge, die korrekte Durchführung der empfohlenen statistischen Verfahren und die richtige Darstellung und Interpretation der Ergebnisse. Die Verantwortung hierfür obliegt allein dem Promovierenden. Das Institut für Biometrie und klinische Epidemiologie übernimmt hierfür keine Haftung.

Datum:
06.02.2024

Name des Beraters\ der Beraterin:
Camilo J. Hernandez-Toro

Unterschrift BeraterIn, Institutsstempel

CHARITÉ
UNIVERSITÄTSMEDIZIN BERLIN
Institut für Biometrie und
Klinische Epidemiologie
Campus Charité Mitte
Charitéplatz 1 | D-10117 Berlin
Sitz: Reinhardtstr. 58